

Chapter 12: Long-term Climate Change: Projections, Commitments and Irreversibility

Coordinating Lead Authors: Matthew Collins (UK), Reto Knutti (Switzerland)

Lead Authors: Julie Arblaster (Australia), Jean-Louis Dufresne (France), Thierry Fichefet (Belgium), Pierre Friedlingstein (UK), Xuejie Gao (China), William Gutowski (USA), Tim Johns (UK), Gerhard Krinner (France), Mxolisi Shongwe (South Africa), Claudia Tebaldi (USA), Andrew Weaver (Canada), Michael Wehner (USA)

Contributing Authors: Myles R. Allen, Tim Andrews, Urs Beyerle, Cecilia Bitz, Sandrine Bony, Ben Booth, Oliver Brown, Victor Brovkin, Claire Brutel-Vuilmet, Mark Cane, Robin Chadwick, Ed Cook, Kerry H. Cook, Sébastien Denvil, Michael Eby, John Fasullo, Erich M. Fischer, Piers Forster, Peter Good, Hugues Goosse, Kevin I. Hodges, Marika Holland, Philippe Huybrechts, Manoj Joshi, Viatcheslav Kharin, Yochanan Kushnir, David Lawrence, Robert W. Lee, Spencer Liddicoat, Wolfgang Lucht, Damon Matthews, François Massonnet, Malte Meinshausen, Christina M. Patricola, Gwenaëlle Philippon-Berthier, Prabhat, Stefan Rahmstorf, William J. Riley, Joeri Rogelj, Oleg Saenko, Richard Seager, Jan Sedlacek, Len Shaffrey, Drew Shindell, Jana Sillmann, Andrew Slater, Robert Webb, Giuseppe Zappa, Kirsten Zickfeld

Review Editors: Sylvie Joussaume (France), Abdalah Mokssit (Morocco), Karl Taylor (USA), Simon Tett (UK)

Date of Draft: 5 October 2012

Notes: TSU Compiled Version

Table of Contents

Executive Summary	3
12.1 Introduction	9
12.2 Climate Model Ensembles and Sources of Uncertainty from Emissions to Projections	10
12.2.1 <i>The Coupled Model Intercomparison Project Phase 5 and Other Tools</i>	10
12.2.2 <i>General Concepts: Sources of Uncertainties</i>	10
12.2.3 <i>From Ensembles to Uncertainty Quantification</i>	13
Box 12.1: Methods to Qualify Multi-Model Result in Maps	13
12.2.4 <i>Joint Projections of Multiple Variables</i>	16
12.3 Projected Changes in Forcing Agents, including Emissions and Concentrations	17
12.3.1 <i>Description of Scenarios</i>	18
12.3.2 <i>Implementation of Forcings in CMIP5 Experiments</i>	20
12.3.3 <i>Projected Radiative Forcing for the 21st Century</i>	23
12.4 Projected Climate Change over the 21st Century	24
12.4.1 <i>Time-Evolving Global Quantities</i>	24
12.4.2 <i>Pattern Scaling</i>	28
12.4.3 <i>Changes in Temperature and Energy Budget</i>	30
12.4.4 <i>Changes in Atmospheric Circulation</i>	37
12.4.5 <i>Changes in the Water Cycle</i>	41
12.4.6 <i>Changes in Cryosphere</i>	48
12.4.7 <i>Changes in the Ocean</i>	52
12.4.8 <i>Changes Associated with Carbon Cycle Feedbacks and Vegetation Cover</i>	54
12.4.9 <i>Consistency and Main Differences Between CMIP3/CMIP5 and SRES/RCPs</i>	56
12.5 Climate Change Beyond 2100, Commitment, Stabilization and Irreversibility	58
12.5.1 <i>RCP Extensions</i>	58
12.5.2 <i>Climate Change Commitment</i>	59
12.5.3 <i>Global Measures of Climate Sensitivity and Transient Response</i>	61
12.5.4 <i>Climate Stabilization and Long-Term Climate Targets</i>	62
Box 12.2: Equilibrium Climate Sensitivity and Transient Climate Response	64

1 12.5.5 Potentially Abrupt or Irreversible Changes.....67

2 **FAQ 12.1: Why are so Many Models and Scenarios Used to Project Climate Change?73**

3 **FAQ 12.2: How will the Earth’s Water Cycle Change?74**

4 **FAQ 12.3: What would Happen to Future Climate if We Stopped Emissions Today?76**

5 **References.....78**

6 **Tables102**

7 **Figures106**

8

Executive Summary

Global Mean Projections

- Global-mean surface temperatures are projected to rise over the century under all of the GHG concentration pathways represented by the RCPs. Around the mid-21st century, the rate of global warming begins to be more strongly dependent on the scenario. By 2100, the best estimate global-mean temperature change relative to 1986–2005 in the non-mitigation RCP8.5 is about a factor of 3 higher than in the lowest RCP2.6 (*high confidence*), where warming stabilizes in the second half of this century.
- It is *very likely* that global-mean surface temperatures at the end of the 21st century will be greater than present-day under the specified RCPs. Global-mean surface temperatures for 2081–2100 (relative to 1986–2005) for the CO₂ concentration driven RCPs will *likely* be in the 5–95% range of the CMIP5 models, i.e., 0.2–1.8°C (RCP2.6), 1.0–2.6°C (RCP4.5), 1.3–3.2°C (RCP6.0), 2.6–4.8°C (RCP8.5).
- For RCP4.5, 6.0 and 8.5, global temperatures are projected to *likely* exceed 2°C warming with respect to preindustrial by 2100, and about *as likely as not* to be above 2°C warming for RCP2.6
- It is *virtually certain* that global precipitation will increase with global mean surface temperature in the next century, with an increase per °C smaller than that of atmospheric water vapour. It is *likely* that the rate of increase of precipitation with temperature will be in the range 1–3% °C⁻¹, for scenarios other than RCP2.6. For RCP2.6 the range of sensitivities in the CMIP5 models is 0.5–4% °C⁻¹ at the end of the 21st century.

Projections in Temperature and Energy Budget

- Future changes in global land surface air temperature exceed changes in global average ocean-area surface air temperature by a factor of $\sim 1.5 \pm 0.2$ (one standard deviation), as was found in AR4 (*very high confidence*).
- The Arctic region is projected to warm most rapidly (*very high confidence*). This polar amplification is not found in Antarctic regions due to deep ocean mixing, strong ocean heat uptake and to the persistence of the vast Antarctic ice sheet.
- Projected regional surface air temperature warming has minima in the North Atlantic and Southern Oceans in all scenarios. Some models exhibit regional cooling in 2081–2100 over the North Atlantic Ocean under RCP4.5 forcing.
- As global mean surface temperature rises, the pattern of atmospheric zonal-mean temperatures show warming throughout the troposphere and cooling in the stratosphere, consistent with previous assessments. The consistency is especially clear in the tropical upper troposphere and the northern high latitudes, indicating that the greatest atmospheric warming is *very likely* to occur in these regions.
- It is *virtually certain* that, in most places, there will be more hot and fewer cold temperature extremes as global temperature increases. These changes are expected for events defined as extremes on both daily and seasonal time scales. Since AR4, the understanding of mechanisms and feedbacks leading to projected changes in extremes has been improved. Increases in the frequency, duration and magnitude of hot extremes along with heat stress are expected, however occasional cold winter extremes will continue to occur.
- Projected changes in 20-year return values of high and low temperature events experience greater increases than mean temperatures in many regions, with the largest changes in the return values of low temperatures at high latitudes. Under RCP8.5 it is *likely* that, in most regions, a 20 year maximum temperature event will occur more frequently (at least doubling its frequency, but in

many regions becoming an annual or two-year event) and that a 20 year minimum temperature event will become exceedingly rare by the end of the 21st century under RCP8.5.

- Models simulate a decrease in cloud amount in the future over most of the tropics and mid-latitudes, due mostly to reductions in low cloud. Changes in marine boundary layer clouds are most uncertain. Increases in cloud fraction and cloud optical depth and therefore cloud reflection are simulated in high latitudes, poleward of 50° (*medium confidence*).
- The top of atmosphere (TOA) net flux into the climate system is positive in 21st century under all RCP scenarios, but the trajectory is very dependent on scenario, with increases over the 21st century under RCP8.5 and increases followed by stabilization, and even decreases for the other scenarios.

Changes in Atmospheric Circulation

- A robust feature of the pattern of mean sea level pressure change is a decrease in high latitudes and increases in the mid-latitudes as global temperatures rise. Poleward shifts in the mid-latitude jets of 1–2 degrees are *likely* at the end of the 21st Century under RCP8.5. In austral summer, the additional influence of stratospheric ozone recovery in the Southern Hemisphere opposes changes due to greenhouse gases there, though the net response varies strongly across models and scenarios.
- A poleward shift of several degrees in Southern Hemisphere storm tracks is *likely* by the end of the 21st century under the RCP8.5 scenario. There is some uncertainty in the degree of shift but the consistency of behaviour with observation-based trends, consistency between CMIP5 and CMIP3 projections and the physical consistency of the storm response with other climatic changes provides *high confidence* in this response.
- Substantial uncertainty and thus *low confidence* remains in projecting changes in Northern Hemisphere storm tracks, especially for the North Atlantic basin.
- As the climate warms, the projected Hadley and Walker circulations are *likely* to slow down. The weakening is linked to changes in moisture transport from the boundary layer to the free atmosphere associated with changes in precipitation. The Hadley cell is *likely* to widen, which translates to broader tropical regions and a poleward encroachment of subtropical dry zones.
- In the stratosphere, the Brewer-Dobson circulation is *likely* to strengthen as global temperatures increase.

Changes in the Water Cycle

- On the planetary scale, relative humidity is projected to remain roughly constant, but specific humidity increases in warmer climates. A projected differential warming of land and ocean promotes changes in atmospheric circulation and resulting moisture transport that lead to decreases in near-surface relative humidity over most land areas with the notable exceptions of tropical Africa and polar regions (*medium confidence*).
- It is *virtually certain* that changes in average precipitation in a much warmer world will not be uniform, with regions experiencing increases, or decreases or no significant change at all. The high latitudes are *very likely* to experience greater amounts of precipitation due to the additional water carrying capacity of the warmer troposphere as well as increased transport of water vapour from the tropics. Many mid-latitude arid and semi-arid regions will *likely* experience less precipitation and many moist mid-latitude regions will *likely* experience more precipitation. The largest precipitation changes over northern Eurasia and North America are projected to occur during the winter.
- Regional to global-scale projections of soil moisture and drought remain relatively uncertain compared to other aspects of the hydrological cycle. Drying in the Mediterranean, southwestern U.S. and southern African regions is consistent with projected changes in Hadley circulation and

increased surface temperatures, so surface drying in these regions as global temperatures increase is *likely*. Despite *high confidence* of projected precipitation increases in certain regions, there are no regions of confident projected increases in surface soil moisture.

- Decreases in runoff are *likely* in southern Europe, the Middle East, and southwestern U.S. The CMIP5 models project consistent increases in high latitude runoff, consistent with AR4, but confidence in this projection is tempered by large biases in their simulation of present-day snow cover.
- Annual surface evaporation is projected to increase as global temperatures rise over most of the ocean and is projected to change over land following a similar pattern as precipitation. Prominent areas of projected decreases in evaporation include the southwestern U.S./northwestern Mexico, southern Africa and land bordering the Mediterranean. Evaporation increases over land in the northern high latitudes, consistent with the increase in precipitation and an overall warming, increasing potential evaporation. There is *high confidence* in patterns of these change but there is *low confidence* in the magnitude.
- The frequency distribution of precipitation events is projected to *very likely* undergo changes. For short-duration events, a shift to more intense individual storms and fewer weak storms is *likely*. In moist and some arid and semi-arid regions, extreme precipitation events will *very likely* be more intense and more frequent. Over land areas where increased evapotranspiration is projected, the evidence indicates that soil moisture will decrease over many land areas over the 21st century with *medium confidence* of decrease in dry regions despite an increase in the likelihood of more intense individual storms.

Changes in the Cryosphere

- It is *very likely* that the Arctic sea ice cover will continue shrinking and thinning in the course of the 21st century as global temperature rises. The CMIP5 multi-model projections give average reductions in sea ice extent ranging from 39% for RCP2.6 to 94% for RCP8.5 in September and from 9% to 35% in February by the end of the century. It is *very likely* that the September Arctic sea ice will nearly vanish (ice extent less than 1×10^6 km²) before the end of the century under RCP8.5 forcing. There is also a *high confidence* that an increase in annual mean global surface temperature greater than 2°C above present will eventually lead to a nearly ice-free Arctic Ocean in late summer. A seasonally ice-free Arctic Ocean within the next 50 years is a very distinct possibility, even though later dates cannot be excluded.
- The CMIP5 multi-model mean projects, for the end of the 21st century, a decrease in Southern Hemisphere sea ice extent from 14% for RCP2.6 to 57% for RCP8.5 in February and from 9% to 29% in September, with a large inter-model scatter.
- Some climate change projections exhibit 5–10 year periods of very rapid summer Arctic sea ice decline – greater than has occurred in the period 2008–2012. Nonetheless, there is little evidence in global climate models of a critical threshold in the transition from a perennial ice-covered to a seasonally ice-free Arctic Ocean beyond which further sea ice loss is unstoppable and irreversible. While instances of rapid summer Arctic sea ice loss are *likely* to occur in the future, it appears *unlikely* that these result from a tipping point in the system.
- Snow cover changes result from precipitation and ablation changes, which are sometimes opposite. It is very likely that Northern Hemisphere snow cover will reduce as global temperatures rise over the coming century. Projections of the Northern Hemisphere spring snow covered area by the end of the 21st century vary between 7% (RCP2.6) and 25% (RCP8.5) and are fairly coherent among models.
- The projected changes in permafrost are a response not only to warming, but also to changes in snow cover, which exerts a control on the underlying soil. A retreat of permafrost extent with rising global

temperatures is virtually certain. By the end of the 21st century, diagnosed near-surface permafrost area is projected to decrease by between 37% (RCP2.6) to 81% (RCP8.5).

Changes in the Ocean

- Based on the available models and the literature, it remains *very likely* that the AMOC will weaken over the 21st century with a best estimate decrease in 2100 of about 20–30% for the RCP4.5 scenario and 36–44% for the RCP8.5 scenario. Based on the range of models and scenarios considered, it also remains *very unlikely* that the AMOC will undergo an abrupt transition or collapse in the 21st century and it is *unlikely* that the AMOC will collapse beyond the end of the 21st century.

Carbon Cycle

- When forced with RCP8.5 CO₂ emissions, as opposed to the RCP8.5 CO₂ concentrations, CMIP5 Earth System Models with interactive carbon cycle simulate, on average, a 60 ppm larger atmospheric CO₂ concentration and 0.2°C larger global surface temperature increase by 2100. The value of 60 ppm is uncertain with a range of ±70 ppm in the small number of models available.

Long-Term Climate Change Beyond 2100

- Continuing greenhouse gas emissions beyond 2100 as in the RCP8.5 extension induces a total radiative forcing above 12 W m⁻² by 2300 that would lead to a warming of 8.7°C (range 5.0–11.6) by 2300 (relative to 1986–2005). Continuously reducing emissions beyond 2100, inducing a total radiative forcing below 2 W m⁻² by 2300 as in the RCP2.6 extension would reduce the warming to 0.6°C (range 0.3–1.0) by 2300.
- If radiative forcing were stabilized, the fraction of realized warming at that point would be between 40 and 90% of the total equilibrium warming. It is strongly dependent on the history of the forcing. Equilibrium would be reached only after centuries to millennia.
- The persistence of warming is substantially longer than the lifetime of anthropogenic greenhouse gases themselves, as a result of non-linear absorption effects as well as the slow heat transfer into and out of the ocean. In much the same way as the warming to a rapid increase of forcing is delayed, the cooling after a decrease of radiative forcing is also delayed.
- For high climate sensitivities, and in particular if sulfate aerosol emissions are eliminated at the same time as greenhouse gas emissions, the commitment from past emission can be strongly positive, and is a superposition of a fast response to reduced aerosols emissions and a slow response to reduced CO₂.
- Processes related to vegetation change, changes in the ice sheets, deep ocean warming and associated sea level rise and potential feedbacks linking for example ocean and the ice sheets have their own intrinsic long timescales. Those may result in significant changes hundreds to thousands of years after global temperature is stabilized.
- Analysis of a range of multi-gas emission pathways from integrated assessment models shows that pathways that *likely* limit warming below 2°C (above pre-industrial) by 2100 consist of emissions of about 31–46 GtCO₂eq yr⁻¹ and 17–23 GtCO₂eq yr⁻¹ by 2020 and 2050, respectively. Median 2010 emissions of all models are 48 GtCO₂eq yr⁻¹. In cumulative terms, the 2°C temperature target implies cumulative carbon emissions by 2100 of about 1000–1300 GtC in the set of scenarios considered, of which about 520 GtC were emitted by 2011.

Abrupt Change and Irreversibility

- For scenarios driven by carbon dioxide alone, global average temperature is projected to remain approximately constant for many centuries following a complete cessation of emissions. Thus a large fraction of climate change is largely irreversible on human time scales, except if net anthropogenic

GHGs emissions were strongly negative over a sustained period. The positive commitment from CO₂ may be enhanced by the effect of an abrupt cessation of aerosol emissions, which will cause warming. By contrast cessation of emission of short-lived greenhouse gases will contribute a cooling.

- Several components or phenomena in the climate system could potentially exhibit abrupt or nonlinear changes, and some are known to have done so in the past. Examples include the Atlantic Meridional Overturning Circulation, sea ice, the Greenland ice sheet, the Amazon forest and monsoonal circulations. For some events, there is information on potential consequences, but in general there is *low confidence* and little consensus on the likelihood of such events over the 21st century.

Equilibrium Climate Sensitivity, Transient Climate Response and Transient Climate Response to Cumulative Carbon Emission

- Despite considerable advances in climate models and in understanding and quantifying climate feedbacks, the assessed literature still supports the conclusion from AR4 that climate sensitivity is *likely* in the range 2–4.5°C, and *very likely* above 1.5°C. The most likely value remains near 3°C. An ECS greater than about 6–7°C is *very unlikely*, based on combination of multiple lines of evidence
- The transient climate response (TCR) is *very likely* in the range 1–3°C, *likely* in the range 1.2–2.6°C estimated from CMIP5 (5–95%), with a most likely value near 1.8°C. An Earth system sensitivity (ESS) over millennia timescales including long-term feedbacks not typically included in models could be significantly higher than ECS.
- The ratio of global temperature change to total cumulative anthropogenic carbon emissions is relatively constant and independent of the scenario, but is model dependent, as it is a function of the model airborne fraction and climate sensitivity. For any given temperature target, higher emissions in earlier decades therefore imply lower emissions by about the same amount later on. The transient climate response to cumulative carbon emission (TCRE) is *very likely* between 0.8–3°C PgC⁻¹ (10¹² metric tons of carbon), with a best estimate in the range of 1.5–2.0°C PgC⁻¹, for cumulative emissions less than 2 PgC until the time at which temperatures peak. Under these conditions, and for low to medium estimates of climate sensitivity, the TCRE is near identical to the peak climate response to cumulated carbon emissions.

Scenarios, Ensembles and Uncertainties

- The Coupled Model Intercomparison Project Phase 5 (CMIP5) presents an unprecedented level of information on which to base projections including new Earth Systems Models, new model experiments and a more diagnostics output.
- New scenarios called Representative Concentration Pathways (RCPs) have been collected and analysed as part of CMIP5, with a general increase in the number of forcing agents commonly represented in CMIP5, with respect to aerosols and land use particularly. Black carbon aerosol is now a commonly included forcing agent.
- Considering CO₂, both “concentrations-driven” projections and “emissions-driven” projections are assessed from CMIP5. These allow quantification of the physical response uncertainties as well as climate-carbon cycle interactions. For the first time a strong mitigation scenario (RCP2.6) is assessed in CMIP5.
- Understanding of the sources and means of characterizing uncertainties in long-term projections of climate change has not changed significantly since AR4, but new experiments and studies have continued to work towards a more complete and rigorous characterization.
- The well-established stability of geographical patterns of change during a transient experiment remains valid in the CMIP models. There remain limitations to the validity of the technique when it

is applied to strong mitigation scenarios, to scenarios where localized forcing (e.g., aerosols) are significant and vary in time and for variables other than average temperature and precipitation. Robustness of the results varies across regions, with high latitudes showing larger variations in temperature patterns and subtropical areas showing larger variations for precipitation patterns across models and scenarios

- It is *unlikely* that the assessment of the mean values and ranges of global mean temperature changes in AR4 would have been substantially different if the CMIP5 models had been used in that report. There is remarkable consistency between the projections based on CMIP3 and CMIP5, for both large-scale patterns and magnitudes of change, providing increased confidence in projections overall. Model agreement and confidence in projections depends on the variable and spatial and temporal averaging, with better agreement for larger scales. Confidence is higher for temperature than for those quantities related to the water cycle or circulation. Improved methods to quantify and display model robustness have been developed to indicate where lack of agreement across models on local trends is a result of internal variability, rather than models actually disagreeing on their forced response.

12.1 Introduction

Projections of future climate change are not like weather forecasts. It is not possible to make deterministic, definitive predictions of how climate will evolve over the next century and beyond as it is with short-term weather forecasts. It is not even possible to make projections of the frequency of occurrence of all possible outcomes in the way that it might be possible with a calibrated probabilistic medium-range weather forecast. Projections of climate change are uncertain, firstly because they are primarily dependent on scenarios of future anthropogenic and natural forcings, secondly because of incomplete understanding and inadequate models of the climate system and finally because of the existence of natural climate variability. The term climate projection tacitly implies these uncertainties and dependencies. Nevertheless, as greenhouse gas concentrations continue to rise, we expect to see future changes to the climate system that are greater than those already observed and attributed to human activities. It is possible to understand future climate change using models and to use models to quantify likely outcomes and uncertainties dependent on assumptions about future forcing scenarios.

This chapter assesses climate projections on time scales beyond those covered in Chapter 11, approximately from the mid-point of the 21st century. Information from a range of different modelling tools is used here; from simple energy balance models, through Earth System Models of Intermediate Complexity (EMICs) to complex dynamical climate and Earth System Models (ESMs). These tools are evaluated in Chapter 9 and, where possible, the evaluation is used in assessing the validity of the projections. This chapter also summarises some of the information on leading-order measures of the sensitivity of the climate system from other chapters and discusses the relevance of these for climate projections, commitments and irreversibility.

Since the AR4 (Meehl et al., 2007b) there have been a number of advances:

- New scenarios of future forcings have been developed to replace the SRES scenarios. The Representative Concentration Pathways (RCPs, see Section 12.3) (Moss et al., 2010), have been designed to cover a wide range of possible magnitudes of climate change in models rather than being derived sequentially from storylines of socio-economic possibilities. The aim is to provide a range of climate responses from which individual socio-economic scenarios may be derived, scaled and interpolated (some including explicit climate policy). Nevertheless, many studies that have been performed since AR4 have used SRES and, where appropriate, these are assessed. Simplified scenarios of future change, developed for understanding, are also synthesised and the understanding of leading-order measures of climate response such as the Equilibrium Climate Sensitivity (ECS) and the Transient Climate Response (TCR) are assessed.
- New models have been developed with higher spatial resolution, with better representation of processes and with the inclusion of more processes, in particular processes that are important in simulating the carbon cycle of the Earth. In these models, emissions of greenhouse gases may be specified and these gases may be chemically active in the atmosphere or be exchanged with pools in terrestrial and oceanic systems before ending up as an airborne concentration (see Figure 10.1 of AR4).
- New types of model experiments have been performed, many coordinated by the Coupled Model Intercomparison Project version 5 (CMIP5) (Taylor et al., 2012), which exploit the addition of these new processes. Models may be driven by emissions of greenhouse gases, or driven by their concentrations with different Earth system feedback loops cut. This allows the separate assessment of different feedbacks in the system and of projections of physical climate variables and future emissions.
- Techniques to assess and quantify uncertainties in projections have been further developed and, where possible, projections are presented in the form of probability density functions (PDFs) that quantify the uncertainty. We make the distinction between the spread of a multi-model, an *ad hoc*, measure of the possible range of projections, and the quantification of uncertainty that combines information from models and observations using statistical algorithms. Just like climate models, different techniques for quantifying uncertainty exist and produce different outcomes. Where possible, different estimates of uncertainty are compared.

While not an advance, as time has moved on, the baseline period from which climate change is expressed has also moved on (a common baseline period of 1986–2005 is used throughout, consistent with the 2006 start-point for the RCP scenarios). Hence climate change is expressed as a change with respect to a recent period of history, rather than a time before significant anthropogenic influence. It should be born in mind that some climate change has already occurred by the time of the 1986-2005 baseline period.

The focus of this chapter is on global and continental/ocean basin-scale features of climate. For many aspects of future climate change, it is possible to discuss generic features of projections and the processes that underpin them for such large scales. Where interesting or unique changes have been investigated at smaller scales, and there is a level of agreement between different studies of those smaller-scale changes, these may also be assessed in this chapter, although where changes are linked to phenomena such as El Niño, the reader is referred to Chapter 14. An innovation for AR5 is Annex I, a collection of global and regional maps of projected climate changes derived from model output. A detailed commentary on each of the maps presented in Annex I is not provided here, but some discussion of generic features will be found.

Projections from regional models driven by boundary conditions from global models are not extensively assessed but may be mentioned in the chapter. More detailed regional information may be found in Chapter 14 and is also now assessed in the Working Group II report where it can more easily be linked to impacts.

12.2 Climate Model Ensembles and Sources of Uncertainty from Emissions to Projections

12.2.1 The Coupled Model Intercomparison Project Phase 5 and Other Tools

Many of the figures presented in this chapter and in others draw on data collected as part of the Coupled Model Intercomparison Project Phase 5, CMIP5 (Taylor et al., 2012). The project involves the worldwide coordination of Earth System Model (ESM) experiments including the coordination of input forcing fields, diagnostic output and the hosting of data in a distributed archive. CMIP5 has been unprecedented in terms of the number of modelling groups and models used, the number of experiments performed and the number of diagnostics collected. The archive of model simulations began being populated in the summer of 2011 and continued to grow during the writing of AR5, hence the production of figures for this and other chapters do not draw on a fixed database of simulations or variables. Different figures may use different subsets of models and there are unequal numbers of models that have produced output for the different RCP scenarios. Figure 12.1 gives a summary of which output was available from which model for which scenario. Where multiple runs are performed with exactly the same model but with different initial conditions, we choose only one ensemble member (usually the first but in cases where that was not available, the first available member is chosen). Rather than give an exhaustive account of which models were used to make which figures, this summary information is presented as a guide to readers.

[INSERT FIGURE 12.1 HERE]

Figure 12.1: A summary of the output used to make the CMIP5 figures in this chapter (and some figures in Chapter 11). The climate variable names run along the horizontal axis and use the standard abbreviations. The climate model names run along the vertical axis. In each box the shading indicates the number of ensemble members available for historical, RCP2.6, RCP4.5, RCP6.0, RCP8.5 and pre-industrial control experiments, although only one ensemble member per model is used in the relevant figures.

In addition to output from CMIP5, information from a coordinated set of simulations with Earth System Models of intermediate complexity (EMICs) is also used (Zickfeld et al., 2012) to investigate long-term climate change beyond 2100. Even more simplified energy balance models or emulation techniques are also used, mostly to estimate responses where ESM experiments are not available (Good et al., 2011b; Meinshausen et al., 2011b).

12.2.2 General Concepts: Sources of Uncertainties

The understanding of the sources of uncertainty affecting future climate change projections has not substantially changed since AR4, but many experiments and studies since then have proceeded to characterize them further. A full characterization, qualitative and even more so quantitative, involves much more than a measure of the range of model outcomes, because additional sources of information (e.g.,

observational constraints, model evaluation) lead us to expect that the uncertainty around the future climate state does not coincide straightforwardly with those ranges. In fact, in this chapter we will highlight wherever relevant the distinction between model uncertainty evaluation, which encompasses the notion that models have intrinsic shortcoming in fully and accurately representing the real system, and simple quantification of model spread and ranges.

Uncertainty affecting mid- to long-term projections of climatic changes stems from distinct but not necessarily independent sources. Figure 12.2 shows a schematic of the chain from scenarios, through Earth Systems Models to projections.

[INSERT FIGURE 12.2 HERE]

Figure 12.2: Links in the chain from scenarios, through models to climate projections. The Representative Concentration Pathways (RCPs) are designed to sample a range of radiative forcing of the climate system at 2100. The RCPs are translated into both concentrations and emissions of greenhouse gases using Integrated Assessment Models (IAMs). These are then used as inputs to dynamical Earth System Models (ESMs) in simulations that are either concentration-driven (the majority of projection experiments) or emissions-driven (only run for RCP8.5). Aerosols and other forcing factors are implemented in subtly different ways in each ESM. The ESM projections each have a potentially different radiative forcing, which may be viewed as an output of the model and which may not correspond to precisely the level of radiative forcing indicated by the RCP nomenclature. Similarly, for concentration-driven experiments, the emissions consistent with those concentrations diagnosed from the ESM may be different from those specified in the RCP (diagnosed from the IAM). Different models would produce different responses even under the same radiative forcing. Uncertainty propagates through the chain and results in a spread of ESM projections. This spread is only one way of assessing uncertainty in projections and alternative methods, which combine information from simple and complex models and observations through statistical models or expert judgment are also used to quantify that uncertainty.

Future anthropogenic emissions of greenhouse gases, aerosol particles and other forcing agents such as land use change are dependent on socio-economic factors including global geopolitical agreements to control those emissions. Systematic studies that attempt to quantify the likely ranges of anthropogenic emission have been undertaken (Sokolov et al., 2010b) but it is more common to use a scenario approach of different but plausible pathways, leading to the concept of *scenario uncertainty*. AR4 made extensive use of the SRES scenarios (Nakicenovic et al., 2000) developed using a sequential approach, i.e., socio-economic factors feed into emissions scenarios which are then used either to directly force the climate models or to determine concentrations of greenhouse gases and other agents required to drive these models. This report also assesses outcomes of simulations that use the new RCP scenarios, developed using a parallel process (Moss et al., 2010) whereby different targets in terms of radiative forcing at 2100 were selected (2.6, 4.5, 6.0 and 8.5 W m⁻²) and greenhouse gas and aerosol emissions consistent with those targets, and their corresponding socio-economic drivers were developed simultaneously. Rather than being identified with one socio-economic storyline, RCP scenarios are consistent with many possible economic futures. Their development was driven by the need to produce scenarios more efficiently and to produce a wide range of model responses that may be scaled and interpolated to estimate the response under other scenarios involving different measures of adaptation and mitigation.

In terms of the uncertainties related to the RCP emissions scenarios, the following issues can be identified:

- No probabilities or likelihoods have been attached to the alternative RCP scenarios (as it was the case for SRES scenarios). Each of them should be considered plausible (see Chapter 1).
- Despite the naming of the RCPs in terms of their 2100 radiative forcing, models translate concentrations of forcing agents into forcing in different ways. Hence a model simulation of RCP6.0 may not attain exactly a radiative forcing of 6 W m⁻². Thus, in addition to the scenario uncertainty there is *radiative forcing uncertainty* in the way the RCP scenarios are implemented in the models.
- Some model simulations are *concentration-driven* (greenhouse gas concentrations are specified) whereas some models, which have Earth Systems components, convert emission scenarios into concentrations and are termed *emissions-driven*. Different Earth System models driven by emissions may produce different concentrations of greenhouse gases and aerosols because of

differences in the representation and/or parameterization of the processes responsible for the conversion of emissions into concentrations. This aspect may be considered a facet of forcing uncertainty, or may be compounded in the category of model uncertainty, which we discuss below. Also, aerosols loading, as is the case for land-use changes, are not dictated intrinsically by the RCP specification. Rather, they are a result of the integrated assessment model that created the emission pathway for a given RCP.

- SRES and RCPs only account for future changes in anthropogenic forcings. With regard to solar forcing, the 1985–2005 solar cycle is repeated. Neither projections of future deviations from this solar cycle, nor future volcanic radiative forcing and their uncertainties are considered.

Any climate projection is subject to uncertainties that arise because of *internal variability*. In this chapter, the prediction of e.g., the amplitude or phase of some mode of variability that may be important on long time scales is not addressed (see Sections 11.2 and 11.3). Any climate variable projection from a single simulation of an individual climate model will be affected by internal variability (stemming from the chaotic nature of the system), whether it be a variable which involves a long time average (e.g., 20 years), a snapshot in time or some more complex diagnostic such as the variance computed from a time series over many years. No amount of time averaging can reduce internal variability to zero, although for some EMICs and simplified models, which may be used to reproduce the results of more complex model simulations, the representation of internal variability is excluded from the model specification. For different variables, and different spatial and time scale averages, the relative importance of internal variability in comparison with other sources of uncertainty will be different. In general, internal variability becomes more important on shorter time scales and for smaller scale variables (see Section 11.3 and Figure 11.4). The concept of signal-to-noise ratio may be used to quantify the relative magnitude of the forced response (signal) versus internal variability (noise). Internal variability may be sampled explicitly by running ensembles of simulations with slightly different initial conditions, or can be estimated on the basis of long control runs where external forcings are held constant. In the case of both multi-model and perturbed physics ensembles (see below), there is an implicit perturbation in the initial state of each run considered, which means that these ensembles sample both modelling uncertainty and internal variability jointly.

The ability of models to mimic nature is achieved by simplification choices that are non-unique in terms of the fundamental numeric and algorithmic structures, forms and values of parameterizations, and number and kinds of coupled processes included. Simplifications and the interactions between parameterised and resolved processes induce ‘errors’ in models, which can have a leading-order impact on projections. It is possible to characterise the choices made when building and running models into structural -- indicating the numerical techniques used for solving the dynamical equations, the analytic form of parameterisation schemes and the choices of inputs for fixed or varying boundary conditions -- and parametric -- indicating the choices made in setting the parameters which control the various components of the model. The community of climate modellers has regularly collaborated in producing coordinated experiments forming multiple model ensembles, MMEs from now on, (using both global and regional model families – e.g., CMIP3/5 - (Meehl et al., 2007a), ENSEMBLES - (Johns et al., 2011)), through which structural uncertainty can be at least in part explored, and perturbed physics ensembles (PPEs - with e.g., HadCM3 (Murphy et al., 2004), MIROC (Yokohata et al., 2012), CCSM3 (Jackson et al., 2008; Sanderson, 2011)), through which uncertainties in parameterization choices can be assessed. As noted below, neither MMEs nor PPEs represent an adequate sample of all the possible choices one could make in building a climate model. Also, current models may exclude some processes that could turn out to be important for projections (e.g., methane hydrate release) or produce a common error in the representation of a particular process. For this reason, it is of critical importance to distinguish two different senses in which this terminology is used or mis-used in the literature (see also Sections 1.4.2; 9.2.2; 9.2.3; 11.2.1, 11.2.1). A narrow interpretation of the concept of model uncertainty often identifies it with the range of responses of a model ensemble. In this chapter this type of characterization will be referred as *model range* or *model spread*. A broader concept entails the recognition of a fundamental uncertainty in the representation of the real system that these models can achieve, given their necessary approximations and given the limits in the scientific understanding of the real system that they encapsulate. When addressing this aspect and characterizing it this chapter will use the term *model uncertainty*.

The relative role of the different sources of uncertainty as one moves from short- to mid- to long term projections and considers different variables at different spatial scales has to be recognized (see section 11.3). The three sources exchange relevance as the time horizon, the spatial scale and the variable change. In absolute terms, internal variability is generally estimated to remain approximately constant across the forecast horizon, with model ranges and scenario/forcing variability increasing over time. For forecasts of global temperatures after mid-century, scenario and model ranges dominate the amount of variation due to internally-generated variability, with scenario uncertainty accounting for the largest source of uncertainty in projections by the end of the century. For global average precipitation projections, scenario uncertainty has a much smaller role even by the end of the century and model range has the lion share across all projection horizons. For temperature and precipitation projections at smaller spatial scales, internal variability may remain a significant source of uncertainty up until middle of the century in some regions (Hawkins and Sutton, 2011; Knutti and Sedláček, 2012; Rowell, 2012). Within single model experiments, the persistently significant role of internally generated variability for regional projections even beyond short- and mid-term horizons has been documented thanks to relatively large ensembles sampling initial conditions (Deser et al., 2012a; Deser et al., 2012b).

12.2.3 From Ensembles to Uncertainty Quantification

The opportunistic nature of the MME has been discussed for example in Tebaldi and Knutti (2007) and Knutti et al. (2010a), highlighting how it does not represent a systematically sampled family of models, but relies on self-selection by the modelling groups. The models are therefore not designed to explore uncertainty in a coordinated manner, and the range of their results cannot be straightforwardly interpreted as an exhaustive range of plausible outcomes, even if some studies have shown how they appear to behave as well calibrated probabilistic forecasts for some large-scale quantities (Annan and Hargreaves, 2010). Other studies have argued instead that the tail of distributions is by construction undersampled (Raisanen, 2007). In general, the difficulty in producing quantitative estimates of uncertainty based on multiple model output originates in their peculiarities as a statistical sample, neither random nor systematic, with possible dependencies among the members and of spurious nature, i.e., often counting among their members models with different degrees of complexities (different number of processes explicitly represented or parameterized) even within the category of general circulation models.

Agreement between multiple models can be source of information in an uncertainty assessment or confidence statement. Various methods have been proposed to indicate regions where models agree on the projected changes, agree on no change, or disagree. Several of those methods are compared Box 12.1. Many figures use stippling or hatching to display such information, but it is important that confidence cannot be inferred from model agreement alone

[START BOX 12.1 HERE]

Box 12.1: Methods to Qualify Multi-Model Result in Maps

The climate change projections in this report are based on ensembles of climate models. The ensemble mean is a useful quantity to characterize the average response, but does not convey any information on model robustness, uncertainty, likelihood of change, or magnitude relative to unforced climate variability. In the IPCC AR4 WGI contribution (IPCC, 2007) several criteria were used to indicate robustness of change, most prominently in Fig. SPM7. In that figure showing projected precipitation changes, stippling marked regions where at least 90% of the models agree on the sign of the change. Regions where less than 66% of the models agreed on the sign were masked white. This large white area was often misinterpreted as indicating large uncertainties in the different models' response to external forcings, but recent studies show that, for the most part, the disagreement in sign among models is found where projected changes are still within the modeled range of internal variability, i.e., where a response to the greenhouse gas increase has not yet been locally detected (Power et al., 2012; Tebaldi et al., 2011).

A number of methods to indicate model robustness, involving an assessment of the significance of the change when compared to internal variability have been proposed. The different methods have in common that they all identify regions with large, significant or robust changes, regions with small changes, regions where models disagree, or a combination of those. They do however use different assumptions about the

statistical properties of the model ensemble, and therefore different criteria for synthesizing the information from it. Different methods include different approaches to estimate internal variability. We briefly describe and compare several of these methods here.

Method (a): The default method used in Chapters 11, 12, and 14 as well as in the Atlas, is shown in Figure 1a, and is based on relating the climate change signal to internal variability in twenty-year means of the models as a reference¹. Regions where the multi model mean exceeds two standard deviations of internal variability and where at least 90% of the models agree on the sign of change are stippled and interpreted as “large change with high model agreement”. Regions where the model mean is less than one standard deviation of internal variability are hatched and interpreted as “small signal or low agreement of models”. This can have various reasons: (i) changes in individual models are smaller than internal variability, or (ii) while changes in individual models are significant, they disagree about the sign and the multi-model mean remains small. Using this method, the case where all models scatter widely around zero and the case where all models agree on near zero change therefore are both hatched (e.g., the Amazon which the following methods mark as “inconsistent model response”).

Method (b): A modification of methods (a) is to restrict hatching to regions where there is high agreement among the models that the change will be “small”, thus eliminating the ambiguous interpretation “small or low agreement” in (a). In contrast to method (a) where the model mean is compared to variability, this case (b) marks regions where at least 80% of the individual models show a change smaller than two standard deviations of variability with hatching. Grid points where many models show significant change but don’t agree are no longer hatched.

Method (c): Knutti and Sedláček (2012) define a dimensionless robustness measure R which is inspired by the signal-to-noise ratio and the ranked probability skill score. It considers the natural variability and agreement on magnitude and sign of change. A value of $R=1$ implies perfect model agreement, low or negative values imply poor model agreement. Any level of R can be chosen for the stippling. For illustration, regions with $R>0.8$ are marked with small dots, regions with $R>0.9$ with larger dots and are interpreted as “robust large change”. This yields similar results to the first method for the end of the century, but with some areas of moderate model robustness ($R>0.8$) already for the short term projections, even though the signal is still within the noise. Regions where at least 80% of the models individually show no significant change are hatched and interpreted as “changes unlikely to emerge from variability”². There is less hatching in this method than method (a), because it requires 80% of the models to be within variability, not just the model average. Regions where at least 50% of the models show significant change but $R<0.5$ are masked as white to indicate “models disagreeing on the projected change projections”.

Method (d): Tebaldi et al. (2011) start from IPCC AR4 SPM7 but separate lack of model agreement from lack of signal. Grid points are stippled and interpreted as “robust large change” when more than 50% of the models show significant change (as in (b)) and at least 80% of those agree on the sign of change. Grid points where more than 50% of the models show significant change but less than 80% of those agree on the sign of change are masked as white and interpreted as “unreliable”. The results are again similar to the methods above. No hatching was defined in that method.

Method (e): Power et al. (2012) and Power and Delage (2012) identify three distinct regions using various methods in which projections can be very loosely described as either: “statistically significant”, “small (relative to temporal variability) or zero, but not statistically significant” or “uncertain”. Power and Delage (2012), for example, estimate confidence intervals for projected changes under the assumption of model independence and stipple where the 95% confidence interval for the projected change does not include zero. Hatching indicates where the projected change is statistically significant below a given level (66% in Figure

¹ The internal variability in this method is estimated using pre-industrial control runs for each of the models which are at least 500 years long. The first 200 years of the pre-industrial are ignored. Variability is calculated for every grid point as the standard deviation of non-overlapping 20 years means, multiplied by the square root of 2. A quadratic fit as a function of time is subtracted from these at every grid point to eliminate model drift. This is by definition the standard deviation of the difference between two independent 20 years averages having the same variance and estimates the variation of that difference that would be expected due to unforced internal variability. The median across all models of that quantity is used.

² Variability in methods b-d is estimated from interannual variations in the base period within each model.

1d), and the 95% confidence interval for standardized change lies entirely within $[-0.2, +0.2]$. The “uncertain” region is comprised of all remaining areas, i.e., areas that are neither stippled nor hatched. The emphasis with this approach is to identify robust signals taking the models at face value and to address the questions: (1) What will change? (2) By how much? and (3) What will not change? The underlying consideration here is that statistical testing under the assumption of model independence provides a worthwhile, albeit imperfect, line of evidence that needs to be considered in conjunction with other evidence (e.g., degree of interdependence, ability of models to simulate the past), in order to assess the degree of confidence one has in a projected change.

The examples given here are not exhaustive but illustrate the main ideas. Other methods include counting the number of models indicating significant increase, significant decrease, or no significant change (McSweeney and Jones, 2012), simply counting the number of models agreeing on the sign (Christensen et al., 2007), or varying hue and saturation to indicate magnitude of change and robustness of change separately (Kaye et al., 2012). In summary, there is a variety of ways to characterize magnitude or significance of change, and agreement between models. There is also a compromise to make between clarity and richness of information. Different methods serve different purposes and a variety of criteria can be justified to highlight specific properties of multi model ensembles. Clearly only a subset of information regarding robust and uncertain change can be conveyed in a single plot. The methods above convey some of the more important parts of this information, but obviously more information could be provided if more maps with additional statistics were provided. In fact Annex II provides more explicit information on the range of projected changes evident in the models (e.g. the median, and the upper and lower quartiles). For most of the methods there is a necessity to choose thresholds for the level of agreement that cannot be identified objectively, but could be the result of individual, application-specific evaluations. Note also that all of the above methods measure model agreement in an ensemble of opportunity, and without considering consistency with observations, model dependence, the degree to which the relevant processes are understood and reflected in the models, it is impossible to derive a confidence or likelihood statement from the model agreement or model spread alone.

The methods Power et al. (2012) and Power and Delage (2012) differ from the other methods in that they test the statistical significance of the ensemble mean rather than a single simulation. As a result, the area where changes are significant increases with an increasing number of models. Already for the period centered around 2025, most of the grid points when using this method show significant change in the ensemble mean whereas in the other methods projections for this time period are classified as changes not exceeding internal variability. The reason is that the former produces a statement about the mean of the distribution being significantly different from zero, equivalent to treating the ensemble as “truth plus error”, i.e., assuming that the models are independent and randomly distributed around reality. Methods b-d on the hand are using an “indistinguishable” interpretation, in which each model and reality are drawn from the same distribution. In that case, the stippling and hatching characterize the likelihood of a single member being significant or not, rather than the ensemble mean. There is some debate in the literature on how the multi model ensembles should be interpreted statistically. This and past IPCC reports treat the model spread as some measure of uncertainty, irrespective of the number of models, which implies an “indistinguishable” interpretation. For a detailed discussion the reader is referred to the literature (Annan and Hargreaves, 2010; Annan and Hargreaves, 2011b; Knutti et al., 2010a; Knutti et al., 2010b; Sanderson and Knutti, 2012; Tebaldi and Knutti, 2007).

[INSERT BOX 12.1 FIGURE 1 HERE]

Box 12.1, Figure 1: Projected relative change in December to February precipitation for 2016–2035 and 2081–2100, relative to 1986–2005 from CMIP5. The choice of the variable is just for illustration on how the different methods compare in cases with low and high signal-to-noise situations (left and right column, respectively). The color maps are identical in all cases. Stippling and hatching are shown as determined a) from relating the model mean to internal variability, b) as a but hatching indicating high agreement for “small change” (see text), c) the robustness measure by Knutti and Sedlacek (2012), d) the method proposed by Tebaldi et al. (2011) and e) the method by Power et al.(2012) and Power and Delage (2012) (but using 66% rather than 95% for the hatched area). Detailed technical explanations for each method are given in the text. The number of CMIP5 models used is indicated in the upper right corner of each panel.

[END BOX 12.1 HERE]

Perturbed physics experiments (PPEs) differ radically in their output interpretability for they can be, and have been, systematically constructed and as such lend themselves to a more straightforward treatment through statistical modelling (Rougier, 2007; Sanso and Forest, 2009). Uncertain parameters in a single model to whose values the output is known to be sensitive are targeted for perturbations. More often it is the parameters in the atmospheric component of the model to be varied (Collins et al., 2006a; Sanderson et al., 2008), and to-date, those have in fact shown to be the source of the largest uncertainties in large-scale response, but lately, and more expensively, also parameters within the ocean component have been perturbed (Brierley et al., 2010; Collins et al., 2007). Parameters in the land-surface schemes have also been subject to perturbation studies (Fischer et al., 2011). Ranges of possible values are explored and often statistical models that fit the relationship between parameters values and model output are trained on the ensemble and used to predict the outcome for unsampled parameter value combinations, in order to explore the parameter space more thoroughly that would otherwise be computationally affordable. The space of a single model simulations (even when filtered through observational constraints) can show a large range of outcomes for a given scenario (Jackson et al., 2008). However, multi-model ensembles and perturbed physics ensembles produce modes and distributions of climate responses that can be different from one another, demonstrating how one type of ensemble cannot be used as an analogue for the other (Collins et al., 2011; Murphy et al., 2007; Sanderson et al., 2010; Yokohata et al., 2010).

Many studies have made use of results from these ensembles to characterize uncertainty in future projections, and these will be assessed and their results incorporated when describing specific aspects of future climate responses. PPEs have been uniformly treated across the different studies through the statistical framework of analysis of computer experiments (Harris et al., 2010; Rougier et al., 2009; Sanso et al., 2008) or, more plainly, as a thorough exploration of alternative responses reweighted by observational constraints (Forest et al., 2008; Piani et al., 2005; Sexton et al., 2012). In all cases the construction of a probability distribution is facilitated by the systematic nature of the experiments. MMEs have generated a much more diversified treatment, (i) according to the choice of applying weights to the different models on the basis of past performance or not (Weigel et al., 2010), and (ii) according to the fundamental notion of treating the different models as exchangeable among themselves or as a version of the truth to which each model adds an error (Annan and Hargreaves, 2010; Sanderson and Knutti, 2012). Many studies can be classified according to these two criteria and their combination, but even within each of the four resulting categories different studies produce different estimates of uncertainty, due to the preponderance of a-priori assumptions, explicitly in those studies that approach the problem through a Bayesian perspective, or only implicit in the choice of likelihood models, or weighting. This makes the use of probabilistic and other results produced through statistical inference necessarily dependent on agreeing with a particular set of assumptions (Sansom et al., 2012), in the lack of a full exploration of the robustness of probabilistic estimates to varying these assumptions.

In summary, there does not exist at present a single agreed upon and robust formal methodology to deliver uncertainty quantification estimates of future changes in climate variables. As a consequence, in this chapter, statements using the calibrated uncertainty language are a result of the expert judgment of the authors, combining assessed literature results with an evaluation of models demonstrated ability (or lack thereof) in simulating the relevant processes (see Chapter 9) and model consensus (or lack thereof) over future projections. In some cases when a significant relation is detected between model performance and reliability of its future projections, some models may be excluded (e.g. Arctic sea ice, Section 12.4.6) but in general it remains an open research question to find significant connections of this kind that justify some form of weighting across the ensemble of models and produce aggregated future projections that are significantly different from straightforward one model-one vote (Knutti, 2010) ensemble results. Therefore, most of the analyses performed for this chapter make use of all available models in the ensembles, with equal weight given to each of them unless otherwise stated.

12.2.4 Joint Projections of Multiple Variables

While many of the key processes relevant to the simulation of single variables are understood, studies are only starting to focus on assessing projections of joint variables, especially when extremes or variability in the individual quantities are of concern. A few studies have addressed projected changes in joint variables, e.g., by combining mean temperature and precipitation (Sexton et al., 2012; Tebaldi and Lobell, 2008; Tebaldi and Sanso, 2009; Watterson, 2011; Watterson and Whetton, 2011; Williams et al., 2007), linking

soil moisture, precipitation and temperature mean and variability (Fischer and Schar, 2009; Koster et al., 2009b; Koster et al., 2009c; Seneviratne et al., 2006), combining temperature and humidity (Diffenbaugh et al., 2007; Fischer and Schar, 2010; Willett and Sherwood, 2012), linking summertime temperature and soil moisture to prior winter snowpack (Hall et al., 2008) or linking precipitation change to circulation, moisture and moist static energy budget changes (Chou and Neelin, 2004; Chou et al., 2006; Chou et al., 2009; Neelin et al., 2003). Models may have difficulties simulating all relevant interactions between atmosphere and land surface and the water cycle that determine the joint response, observations to evaluate models are often limited (Seneviratne et al., 2010), and model uncertainties are therefore large (Boe and Terray, 2008; Fischer et al., 2011; Koster et al., 2006; Notaro, 2008). In some cases, correlations between e.g., temperature and precipitation or accumulated precipitation and temperature have found to be too strong in climate models (Hirschi et al., 2011; Trenberth and Shea, 2005). The situation is further complicated by the fact that model biases in one variable affect other variables. The standard method for model projections is to subtract model biases derived from control integrations (under an assumption of so called ‘constant bias’). Several studies note that this may be problematic when a consistent treatment of biases in multiple variables is required (Buser et al., 2009; Christensen et al., 2008), but there is no consensus at this stage for a methodology addressing this problem. A more general aspect of models’ shortcoming, that of an unavoidable discrepancy (Rougier, 2007) between models and reality due to structural errors is relevant here as well as for univariate projections, and starts to be addressed in the recent literature through the use of MMEs, where a measure distance between a single model and the other models of the ensemble is used to estimate the distance between a model and the real world (Sanderson, 2012; Sexton and Murphy, 2012; Sexton et al., 2012). Statistical frameworks to deal with multivariate projections are challenging even for just two variables, since they have to address a trade-off between modeling the joint behavior at scales that are relevant for impacts – i.e., fine spatial and temporal scales, often requiring complex spatio-temporal models – and maintaining computational feasibility. In one instance (Tebaldi and Sanso, 2009) scales were investigated at the seasonal and subcontinental level, and projections of the forced response of temperature and precipitation at those scales did not show significant correlations, likely because of the heterogeneity of the relation between the variables within those large averaged regions and seasons. In Sexton et al. (2012) the spatial scale focused on regions of Great Britain and correlation, for example, between summer temperatures and precipitation amounts shaped significantly the bivariate distribution of the two variables instead.

Even while recognizing the need for joint multivariate projections, the above limitations at this stage prevent a quantitative assessment for most cases. A few robust qualitative relationships nonetheless emerge from the literature and these are assessed, where appropriate, in the rest of the chapter. For applications that are sensitive to relationships between variables, but still choose to use the multi-model framework to determine possible ranges for projections, sampling from univariate ranges may lead to unrealistic results when significant correlations exist. IPCC assessments often show model averages as best estimates, but such averages can underestimate spatial variability, and more in general they neither represent any of the actual model states (Knutti et al., 2010a) nor do they necessarily represent the joint best estimate in a multivariate sense. For impact studies that need dynamically coherent multivariate input from climate model simulations, using each climate model output individually as a realization of joint variables to feed into the impact model is likely to be more consistent, at least as far as the model captures the spatial covariance, the temporal co-evolution and the relevant feedbacks.

12.3 Projected Changes in Forcing Agents, including Emissions and Concentrations

The experiments at the basis of global future projections discussed in this chapter are extensions of the simulations of the observational record discussed in Chapters 9 and 10. The scenarios assessed in AR5, introduced in Chapter 1, include four new scenarios designed to explore a wide range of future climate characterised by representative trajectories of long lived greenhouse gas (LLGHG) concentrations and other anthropogenic forcing agents. These are described further in Section 12.3.1. The implementation of forcing agents in model projections, including natural and anthropogenic aerosols, ozone, and land-use change are discussed in Section 12.3.2, with a strong focus on CMIP5 experiments. Global mean emissions, concentrations and radiative forcings applicable to the historical record simulations assessed in Chapters 8, 9 and 10, and the future scenario simulations assessed here, are illustrated in Annex II. Radiative forcing for the 21st century consistent with these scenarios, derived from CMIP5 and other climate model studies, is discussed in Section 12.3.3.

12.3.1 Description of Scenarios

Long-term climate change projections reflect how human activities or natural effects could alter the climate over decades and centuries. In this context, defined scenarios are important, as assuming specific time series of emissions, land-use, atmospheric concentrations or radiative forcing across multiple models allows for coherent climate model intercomparisons and synthesis. Some scenarios are academic, they present an idealized future, not accompanied by a socio-economic storyline and are used for process understanding. More comprehensive scenarios are produced by Integrated Assessment Models (IAMs) as internally consistent sets of emissions and socio-economic assumptions (e.g., regarding population and socio-economic development) with the aim of presenting several plausible future worlds (see Chapter 1 for more details). Often, it is these scenarios that are used for policy relevant climate change, impact, adaptation and mitigation analysis. Here, we focus on the RCP scenarios used within the CMIP5 intercomparison exercise (Taylor et al., 2012) along with the SRES scenarios (IPCC, 2000) developed for the IPCC TAR but still widely used by the community.

12.3.1.1 Idealized Concentration Scenarios

A 1%-per-annum compound increase of atmospheric CO₂ concentration until a doubling or a quadrupling of its initial value has been widely used since the second phase of CMIP (Meehl et al., 2000) and the SAR (Kattenberg et al., 1996). This idealized scenario is a useful benchmark for comparing coupled model climate sensitivity, climate feedback and transient climate response. The exponential increase of CO₂ concentrations induces approximately a linear increase in radiative forcing (Myhre et al., 1998) due to a ‘saturation effect’ of the strong absorbing bands. Thus, a linear ramp function results from these idealized pathways, adding to their suitability for comparative diagnostics of the models’ climate feedbacks and inertia. The CMIP5 intercomparison project again includes such an idealized pathway up to a quadrupling of CO₂ concentrations. In this experiment, the initial CO₂ concentration is doubled after 70 years and quadrupled after 140 years. The corresponding radiative forcings are about 3.9 W m⁻² and 7.8 W m⁻² respectively (see Chapter 8), and these values are in the range of the radiative forcings at the end of the 21st century for the future scenarios presented below. The CMIP5 project also includes a second idealized experiment where the CO₂ concentration is quadrupled pathway instantaneously, which allows a distinction between adjusted forcings and longer-term feedbacks.

12.3.1.2 The Socio-Economic Driven SRES Scenarios

The climate change projections undertaken as part of CMIP3 and discussed in AR4 were based on the SRES A2, A1B and B2 scenarios (IPCC, 2000). These scenarios were developed using IAMs and resulted from specific socio-economic scenarios, i.e., from storylines about future demographic and economic development, regionalization, energy production and use, technology, agriculture, forestry, and land-use. All SRES scenarios assumed that no climate mitigation policy would be undertaken. Based on these SRES scenarios, global climate models were then forced with corresponding LLGHG and aerosol concentrations, although the degree to which models implemented these forcings differed (Meehl et al., 2007b, Table 10.1). The resulting climate projections, together with the socio-economic scenarios, were then the basis for further analysis by the impact, adaptation and vulnerability research community.

12.3.1.3 The New Concentration Driven RCPs Scenarios, and their Extensions

As already detailed in Chapter 1, a new parallel process for scenario development was proposed in order to facilitate the interactions between the scientific communities working on climate change, adaptation and mitigation (Moss et al., 2010; Moss et al., 2008; van Vuuren et al., 2011). These new scenarios, named "Representative Concentration Pathways" (RCPs), are referred to as pathways in order to emphasize that their primary purpose is to provide time-dependent projections of atmospheric greenhouse gas (GHG) concentrations. They are representative in that they are one of several different scenarios that have similar radiative forcing and emissions characteristics. The scenarios are identified by the stabilization value of the radiative forcing relative to the pre-industrial period (in W m⁻²) (Figure 12.3): the lowest RCP, RCP2.6 (also referred to as RCP3-PD), which peaks at 3 W m⁻² and then declines to approximately 2.6 W m⁻² by 2100; the medium-low RCP4.5 and the medium-high RCP6.0 aiming for stabilization at 4.5 and 6.0 W m⁻² respectively around 2100; and the highest one, RCP8.5, which implies a radiative forcing of 8.5 W m⁻² by

2100. The primary objective of these scenarios is to provide all the input variables necessary to run comprehensive climate models in order to reach a target radiative forcing (Figure 12.2). These scenarios were developed using IAMs that provide the time evolution of a large ensemble of anthropogenic forcings (concentration and emission of gas and aerosols, land use changes, etc.) and their individual radiative forcing values (Moss et al., 2010; Moss et al., 2008; van Vuuren et al., 2011). Note that due to the substantial uncertainties in radiative forcing, these forcing values should be understood as comparative ‘labels’, not as exact definitions of the forcing that is effective in climate models. This is because concentrations or emissions, rather than the radiative forcing itself, are prescribed in the CMIP5 climate model runs. The forcing as manifested in climate models is discussed in Section 12.3.3.

[INSERT FIGURE 12.3 HERE]

Figure 12.3: (a) Time evolution of the total anthropogenic and anthropogenic aerosol radiative forcing relative to preindustrial (~1765) between 2000 and 2300 for RCP scenarios and their extensions (continuous lines), and SRES scenarios (dashed lines) as computed by the integrated assessment models (IAMs) used to develop those scenarios. The four RCP scenarios used in CMIP5 are: RCP2.6 (dark blue), RCP4.5 (light blue), RCP6.0 (orange) and RCP8.5 (red). The three SRES scenarios used in CMIP3 are: B1 (light blue, dashed), A1B (orange, dashed) and A2 (red, dashed). Positive values correspond to the total anthropogenic radiative forcing. Negative values correspond to the forcing from all anthropogenic aerosol-radiation interactions. (b) Contribution of the individual anthropogenic forcings to the total radiative forcing in year 2100 for the four RCP scenarios. The individual forcings are gathered into five groups: CO₂, CH₄, ozone, other GHGs, aerosol (all effects, i.e. aerosols-radiation and aerosol-cloud interactions, aerosol deposition on snow, unlike in (a)) and land use. (c) As in b, but the individual forcings are relative to the total radiative forcing (i.e., RF_x/RF_{tot} , in %, with RF_x individual radiative forcings and RF_{tot} total radiative forcing). The total radiative forcing of the two families of scenarios, SRES and RCP, differ in 2000 as the number of forcings and our knowledge about them have changed since the TAR. The values shown here are summarised in Annex II.

Various steps were necessary to turn the selected ‘raw’ RCP emission scenarios from the IAMs into datasets usable by the climate modelling community, including the extension with historical emissions (Granier et al., 2011; Smith et al., 2011), the harmonization and gridding of land-use datasets (Hurtt et al., 2011), the provision of atmospheric chemistry runs, particular for tropospheric ozone, and the harmonization of 2000–2005 GHG emission levels, extension of GHG concentrations with historical GHG concentrations and harmonization of 2000–2005 GHG concentrations levels (Meinshausen et al., 2011c). A single carbon cycle model with a representation of carbon-climate feedbacks has been used in order to provide consistent values of both concentration and emission of CO₂ for all the scenarios. After these processing steps, the final RCP datasets comprise land-use data, harmonized GHG emissions and concentrations, gridded reactive gas and aerosol emissions, as well as ozone and aerosol abundance fields. Only some of these data are used as forcings in individual climate models, depending on the experiment and model configuration (Section 12.3.2), and for instance on whether the carbon cycle uncertainties will affect temperature or compatible CO₂ emissions (Section 12.3.2.1).

During this development process, the total radiative forcing and the radiative forcing of individual forcing agents have been estimated by the IAMs and made available via the RCP database (Meinshausen et al., 2011c). Each individual anthropogenic forcing varies from one scenario to another and all of them have been gathered in a few groups in Figure 12.3b and c. The change in CO₂ concentration is the main cause of difference in the total radiative forcing among the scenarios (Figure 12.3b). The contribution of CO₂ to the total anthropogenic forcing is currently about 90% and does not vary much across the scenarios (Figure 12.3c), as was also the case for SRES scenarios (Ramaswamy et al., 2001). Aerosols have a large negative contribution to the total forcing at the end of the 20th century (about –60%), but this contribution decreases (in absolute value) in the future for all the RCPs scenarios. This means that while anthropogenic aerosols have had a cooling effect in the past, they are expected to have a warming effect in the future with respect to their current values in the RCP scenarios (Levy II et al., 2012). This decrease in aerosol forcing was not as large and as fast in the SRES scenarios (Figure 12.3a). However, even in the SRES scenarios, aerosol effect was expected to have a smaller role in the future compared to GHG forcings, mainly because of the accumulation of GHG in the atmosphere (Dufresne et al., 2005). Other forcings do not change much in the future, except CH₄ which increases in the RCP8.5 scenario. Note that the estimates of all of these individual radiative forcings are subject to many uncertainties (see Chapters 6, 7, 8 and 11).

The Four Representative Concentration Pathways (RCPs) are based through the end of the 21st century on the IAMs. In order to investigate longer-term climate change implications, these RCPs were extended until

2300 (Meinshausen et al., 2011c). These extensions, formally named Extended Concentration Pathways (ECPs;) but often simply referred to as RCP extensions, use simple assumptions about GHG and aerosol emissions and concentrations beyond 2100 and were designed as hypothetical ‘what-if’ scenarios, not as results of socio-economic considerations beyond 2100. In order to continue to investigate a broad range of possible climate futures, the two outer RCPs, RCP2.6 and RCP8.5 assume constant emissions after 2100, while the two middle RCPs aim for a smooth stabilization of concentrations by 2150. RCP8.5 stabilizes concentrations only by 2250, with CO₂ concentrations of approximately 2000 ppm, nearly 7 times the pre-industrial levels. As the RCP2.6 implies net negative CO₂ emissions after around 2070 and throughout the extension, CO₂ concentrations are slowly reduced towards 360 ppm by 2300.

12.3.1.4 *Comparison of SRES and RCP Scenarios*

The four RCP scenarios used in CMIP5 lead to radiative forcing values that span a range larger than that of the three SRES scenarios used in CMIP3 (Figure 12.3). RCP4.5 is close to SRES B1, RCP6.0 is in between SRES B1 and SRES A1B and RCP8.5 is higher than SRES A2. RCP2.6 is lower than any SRES scenario and very close to the ENSEMBLES E1 scenario (Johns et al., 2011). Results obtained with one GCM confirm that the only two SRES and RCP scenarios that are close are RCP4.5 and SRES B1, and that the temperature increase with RCP8.5 is larger than that with SRES A2 (Dufresne et al., 2011). Results obtained with a reduced-complexity model and six SRES scenarios (and not only the three SRES scenarios used in CMIP3) show that RCP4.5 yield a temperature increase close to SRES B1, RCP6.0 close to SRES B2 and RCP8.5 close to SRES A1FI, although the transient trajectories may be different (Rogelj et al., 2012). Scenarios RCP2.6 that assumes strong mitigation action yield to a smaller temperature increase of any SRES scenarios. The spread of projected global warming with the RCP scenarios is much larger than with SRES scenarios, especially if only the three SRES scenarios used in CMIP3 are considered.

12.3.1.5 *Range of Other Scenarios Used in the Literature*

Aside from the pathways and scenarios investigated as part of the CMIP5 experiments, there is a broad range of scenarios and pathways in the literature. Some of these investigate emission implications of various temperature or concentration-based climate targets, some are designed to investigate the climatic effect of peaking or overshoot profile, yet others are meant to provide best-estimate predictions over the next decades. Aside from this distinction regarding their purpose, the literature scenarios and pathways can be distinguished regarding the coverage of gases, sectors and regions. For example, very specific emission scenarios exist for single sectors, like transport sector scenarios (Skeie et al., 2009) or aviation sector scenarios (Vedantham and Oppenheimer, 1998).

12.3.2 *Implementation of Forcings in CMIP5 Experiments*

The CMIP5 experimental protocol for long term transient climate experiments prescribes a common basis for a comprehensive set of anthropogenic forcing agents acting as boundary conditions in three experimental phases – historical, RCPs and ECPs (Taylor et al., 2012). To permit common implementations of this set of forcing agents in CMIP5 models, self-consistent forcing data time series have been computed and provided to participating models (see Sections 9.3.2.2 and 12.3.1.3) comprising emissions or concentrations of GHGs and related compounds, ozone and atmospheric aerosols and their chemical precursors, and land use change.

The forcing agents implemented in AOGCMs and ESMs used to make long term climate projections in CMIP5 are summarised in Table 12.1. The number of CMIP5 models listed here is about double the number of CMIP3 models listed in Table 10.1 of AR4 (Meehl et al., 2007b).

Natural forcings (arising from solar variability and aerosol emissions via volcanic activity) are also specified elements in the CMIP5 experimental protocol, but their future time evolutions are not prescribed very precisely. A repeated 11-year cycle for total solar irradiance (Lean and Rind, 2009) is suggested for future projections but the periodicity is not specified precisely as solar cycles vary in length. A few models include the effect of orbital variations as well, but most do not. For volcanic eruptions, no specific CMIP5 prescription is given for future emissions or concentration data, the general recommendation being that volcanic aerosols should either be omitted entirely both from the control experiment and future projections or the same background aerosols should be prescribed in both. This provides a consistent framework for

model intercomparison given a lack of knowledge of when future large eruptions will occur. In general models have adhered to this guidance, but there are variations in the background aerosol levels chosen and some cases, e.g. ACCESS1.0 and ACCESS1.3 (Dix et al., 2012), where the background volcanic aerosol in future differs significantly from that in the control experiment, with a small effect on future radiative forcing.

For the other natural aerosols (dust, sea-salt, etc.), no emission or concentration data is recommended. The emissions are potentially computed interactively by the models themselves and may change with climate, or prescribed from separate model simulations carried out in the implementation of CMIP5 experiments. Natural aerosols (mineral dust and sea salt) are in a few cases prescribed with no year-to-year variation (giving no transient forcing effect), in some cases prescribed from datasets computed off-line as described above, and in other cases calculated interactively via prognostic or diagnostic calculations.

[INSERT TABLE 12.1 HERE]

Table 12.1: Radiative forcing agents in the CMIP5 multi-model global climate projections. See Table 9.1 for descriptions of the models and main model references. ESMs are highlighted in bold. Numeric superscripts indicate model-specific references that document forcing implementations. Forcing agents are mostly implemented in close conformance with standard prescriptions (Taylor et al., 2012) and recommended datasets (Cionni et al., 2011; Lamarque et al., 2011; Lamarque et al., 2010; Meinshausen et al., 2011c) provided for CMIP5. Variations in forcing implementations are highlighted with superscripts and expanded in the table footnotes. Entries mean: n.a.: Forcing agent is not included in either the historical or future scenario simulations; Y: Forcing agent included (via prescribed concentrations, distributions or time series data); E: Concentrations of forcing agent calculated interactively driven by prescribed emissions or precursor emissions; Es: Concentrations of forcing agent calculated interactively driven by prescribed surface concentrations. For a more detailed classification of ozone chemistry and ozone forcing implementations in CMIP5 models see Eyring et al. (2012).

12.3.2.1 “Emissions-Driven” versus “Concentrations-Driven” Experiments

A novel feature within the CMIP5 experimental design is that experiments with prescribed anthropogenic emissions are included in addition to classical experiments with prescribed concentration pathways for LLGHGs (Taylor et al., 2012) are included. The CMIP5 protocol includes experiments in which “ESMs” (models possessing an interactive carbon cycle) and AOGCMs (that do not possess an interactive carbon cycle) are both forced with LLGHG concentration pathways to derive a consistent range of climate responses from the two types of model. The range of climate responses including climate-carbon cycle feedbacks can additionally be explored in ESMs driven with emissions rather than concentrations, analogous to C⁴MIP experiments (Friedlingstein et al., 2006). Results from the two types of experiment cannot be compared directly, but they provide complementary information. Firstly, uncertainties in the forward climate response driven with specified emissions or concentrations can be derived from all participating models, while concentrations-driven ESM experiments also permit a policy-relevant diagnosis of the range of anthropogenic carbon emissions compatible with the imposed concentration pathways (Hibbard et al., 2007; Moss et al., 2010).

LLGHG forcing implementations in CMIP5 concentrations-driven experiments conform closely in almost all cases to the standard protocol (Table 12.1; CO₂, CH₄, N₂O, CFCs), imposing an effective control over the radiative forcing due to LLGHGs across the multi-model ensemble, apart from the uncertainty arising from radiative transfer code (Collins et al., 2006b; Meehl et al., 2007b). The ability of ESMs to determine their own LLGHG concentrations in “emissions-driven” experiments means that radiative forcing due to LLGHGs is less tightly controlled in such experiments. Even in “concentrations-driven” experiments, many models implement some emissions-driven forcing agents (more often aerosols, but also ozone in some cases) leading to a potentially greater spread in both the concentrations and hence radiative forcing of those emissions-driven agents.

12.3.2.2 Variations Between Model Forcing Implementations

Apart from the distinction between concentrations-driven and emissions-driven protocols, a number of variations are present in the implementation of forcing agents listed in Table 12.1, which generally arise due to constraining characteristics of the model formulations, computational efficiency considerations, or local implementation decisions (e.g., rescaling of prescribed data). In a number of models, off-line modelling using an aerosol chemistry climate model has been used to convert emissions into concentrations compatible

with the specific model formulation or characteristics. As a result, although detailed prescriptions are given for the forcing agents in CMIP5 experiments in emissions terms, individual modelling approaches lead to considerable variations in their implementations and consequential radiative forcings. This was also the case in the ENSEMBLES multi-model projections, in which similar forcing agents to CMIP5 models were applied but again with variations in the implementation of aerosol, ozone and land-use forcings, prescribing the SRES A1B and E1 scenarios in a “concentrations-driven” protocol (Johns et al., 2011) akin to the CMIP5 protocol.

Methane, nitrous oxide and CFCs (typically with some aggregation of the multiple gases) are generally prescribed with standard well-mixed concentrations in CMIP5 models, but in a number of models (CESM1 (WACCM), GFDL-CM3, GISS-E2 (TCAD, TCADI) and HadGEM2-ES) surface concentrations are prescribed along with prescribed emissions. In the emissions-driven models, the 3-dimensional concentrations in the atmosphere that are passed to the radiation scheme vary interactively.

Eyring et al. (2012) document, in greater detail than Table 12.1, the implementations of tropospheric and stratospheric ozone in CMIP5 models, including their ozone chemistry schemes and modifications applied to reference datasets in models driven by concentrations. In most models that prescribe ozone, concentrations are based on the original or slightly modified CMIP5 standard ozone dataset computed as part of the IGAC/SPARC activity (Cionni et al., 2011). In the stratosphere, this dataset is based on observations of the past (Randel and Wu, 2007) continued into the future with the multi-model mean of 13 chemistry-climate models (CCMs) projections following the SRES A1B GHG (IPCC, 2000) and A1 adjusted halogen scenario (WMO, 2007). The stratospheric zonal mean ozone field is merged with a 3-D tropospheric ozone timeseries generated as mean of two CCMs in the past and continued by one CCM in the future. Some models prescribe ozone concentrations using different datasets, MIROC-ESM, MIROC4h, MIROC5, GISS-E2-H p1 and GISS-E2-R p1, but again following just one GHG scenario in the future for the projection of stratospheric ozone. In other models (e.g., IPSL-CM5, CCSM4) ozone is again prescribed, but supplied as concentrations from off-line computations using a related CCM. Some models determine ozone interactively from specified emissions via on-line atmospheric chemistry (CESM1(FASTCHEM), CESM1(WACCM), CNRM-CM5, GFDL-CM3, GISS-E2-H-p2, GISS-E2-H-p3, GISS-E2-R-p2, GISS-E2-R-p3, and MIROC-ESM-CHEM, and HadGEM2-ES for tropospheric ozone only). Computing ozone concentrations interactively allows the fast coupling between chemistry and climate to be captured, but modelling of chemistry processes is sometimes simplified (CNRM-CM5, CESM(FASTCHEM)) in comparison with full complexity CCMs to reduce the computational cost. Compared to CMIP3, in which all models prescribed ozone and around half of them used a fixed ozone climatology, this leads to substantial improvement to ozone forcings in CMIP5, although differences remain among the models with interactive chemistry.

For atmospheric aerosols, either aerosol precursor emissions-driven or concentrations-driven forcings are applied depending on individual model characteristics. A larger fraction of models in CMIP5 than CMIP3 prescribe aerosol precursor emissions rather than concentrations. Many still prescribe concentrations pre-computed either using a directly related aerosol CCM or from output of another, complex, emissions-driven aerosol chemistry model within the CMIP5 process. As for ozone, aerosol concentrations provided from off-line simulations help to reduce the computational burden of the projections themselves. For several of the concentrations-driven models (CCSM4, IPSL-CM5A variants, MPI-ESM-LR, MPI-ESM-MR), additional emissions-driven simulations have been undertaken so as to tailor the prescribed concentrations closely to the model’s individual aerosol-climate characteristics. Lamarque et al. (2011; 2010) provided the recommended CMIP5 aerosols dataset which has been used in several of the models driven by concentrations. Compared with the CMIP3 models in AR4, a much larger fraction of CMIP5 models now incorporate black and organic carbon aerosol forcings. Also, a larger fraction of CMIP5 than CMIP3 models include aerosol indirect effects, although in several of those models that include the cloud albedo effect it only includes the effect of sulphate aerosol, and the majority of models still exclude the cloud lifetime effect completely. No CMIP5 models represent urban aerosol pollution explicitly so that is not listed in Table 12.1. Only one centre’s model (GISS-E2) explicitly includes nitrate aerosol as a forcing.

Land-use change is typically applied by blending anthropogenic land surface disturbance via crop and pasture fraction changes with underlying land cover maps of natural vegetation, but model variations in the underlying land cover maps and biome modelling mean that the land-use forcing agent is impossible to impose in a completely common way at present (Pitman et al., 2009). Most CMIP5 models represent crop

and pasture disturbance separately, while some (CanESM2, MIROC4h, MIROC5) represent crop but not pasture. Some models allow a dynamical representation of natural vegetation changes alongside anthropogenic disturbance.

Treatment of the CO₂ emissions associated with land cover changes is also model-dependent. Some models do not account for land cover changes at all, some simulate the biophysical effects but are still forced externally by land cover change induced CO₂ emissions (in emission driven simulations), while the most advanced ESMs simulate both the biophysical effects of land cover changes and their associated CO₂ emissions.

12.3.3 Projected Radiative Forcing for the 21st Century

This section presents the projected radiative forcing estimated from the CMIP5 model projections and discusses the consistency with radiative forcing (RF) estimates determined using other methods in Chapter 8. Quantification of future radiative forcing is of interest here as it is directly related to changes in the global energy balance of the climate system and resultant climate change. Chapter 8 defines RF concepts in general and considers the methodology for computing adjusted radiative forcing (AF) directly from output of model projections (Forster and Taylor, 2006) which is used here.

Figure 12.4 illustrates the total AF estimated from CMIP5 models through the 21st century for the four RCPs (Forster et al., 2012). The multi-model ensemble mean AF at 2100 (relative to pre-industrial control experiments for circa-1850 conditions) is 2.4, 3.9, 4.6 and 7.9 W m⁻² respectively for RCP2.6, RCP4.5, RCP6.0 and RCP8.5 concentrations-driven projections, with a 1-sigma uncertainty of ±0.6 to 0.9 W m⁻² depending on scenario (lowest for RCP2.6 and highest for RCP8.5). For three out of the four RCPs these are remarkably close to the indicative RCP total RF at 2100 (relative to the mean of 1850 to 1859) of 2.4, 4.0, 5.2 and 8.0 W m⁻² respectively, the exception being RCP6.0 for which the CMIP5 multi-model mean estimate is 0.6 W m⁻² lower than the indicative value. Note that indicative RCP total RF values are here based on Meinshausen et al. (2011c) but computed using an estimate of *total anthropogenic AF* combined with natural RF rather than the RF basis used to label the RCPs. The difference from using AF versus RF varies with RCP and over time but is in the range 0.1 to 0.2 W m⁻² over the 21st century.

The range of forcing uncertainty indicated from CMIP5 models results with specified GHG concentration pathways is broadly consistent with that found for CMIP3 models for the A1B scenario using the corresponding method (Forster and Taylor, 2006). As for CMIP3 models, part of the forcing spread in CMIP5 models (Forster et al., 2012) is consistent with differences in GHG forcings arising from the radiative transfer codes (Collins et al., 2006b). Aerosol forcing implementations in CMIP5 models also vary considerably however (Section 12.3.2), leading to a spread in aerosol concentrations and forcings which contributes to the overall uncertainty.

CMIP5-based projected AF at 2030 and 2100 is systematically lower than that estimated from ACCMIP models, in which different techniques are used to estimate forcings (Shindell et al., 2012b). CMIP5 and ACCMIP multi-model ensembles comprise different sets of models, but the discrepancy in forcings from the two methods appears to be unrelated to different model samples as confining the analysis to a common subset of models also gives higher forcing estimates from ACCMIP compared to CMIP5. The reasons for this discrepancy are not yet understood.

The evidence available, from the GISS-E2 CMIP5 simulations (Shindell et al., 2012a) and an earlier study with a version of the HadGEM2-ES model related to that used in CMIP5 (Bellouin et al., 2011) suggests that, in contrast to the projected decrease in aerosol forcing in RCP scenarios, ammonium nitrate aerosol will increase over the 21st century, tending to increase total aerosol-related RF throughout the 21st century and slow its decline at 2100. Bellouin et al. (2011) find that inclusion of nitrate aerosol would increase the aerosol-related RF at 2100 (relative to pre-industrial) by a factor of 2 to 4 (dependent on RCP scenario).

Natural radiative forcing variations are, by their nature, difficult to project (Section 8.5.3), but on the assumption that forcing from episodic volcanic activity remains of a similar magnitude and character to that since pre-industrial it is *virtually certain* that (independent of RCP scenario) on decadal time scales total

anthropogenic forcing at 2100 (relative to pre-industrial) will remain larger than total natural (solar plus volcanic) forcing.

In summary, the multi-model CMIP5 average of future forcing is consistent with the indicative RCP values and the climate model-based uncertainty range in future forcing for a given RCP scenario is substantial for the CMIP5 experiments assessed here, even for concentrations-driven experiments.

[INSERT FIGURE 12.4 HERE]

Figure 12.4: Global mean radiative forcing (W m^{-2}) between 1980 and 2100, relative to 1850, estimated by alternative methods. Dashed lines indicate the indicative total anthropogenic plus natural forcing from Meinshausen et al. (2011c), using adjusted forcing values for anthropogenic combined with solar and volcanic RF, normalised by the mean between 1850 and 1859. Solid lines are multi-model mean adjusted forcing relative to the pre-industrial control simulations realised in a subset of CMIP5 models for the historical experiment and RCP scenarios (Forster et al., 2012) driven by concentrations, with a 1-sigma uncertainty range about each line shaded in light colour. This assumes each model has an invariant climate feedback parameter, calculated from abrupt $4 \times \text{CO}_2$ experiments using the method of Gregory et al. (2004). Grey or coloured vertical bars illustrate the 5–95% uncertainty range of anthropogenic forcing estimated in ACCMIP models (Shindell et al., 2012b) for time slice experiments at 1980, 2000, 2030 (RCP8.5 only) and 2100 (all RCPs). Note that the ACCMIP bars at 1980 and 2100 are shifted slightly to aid clarity. The mean adjusted forcing diagnosed from 21 CMIP3 models for the SRES A1B scenario, as in Forster and Taylor (2006), is also shown with a 1-sigma uncertainty range.

12.4 Projected Climate Change over the 21st Century

12.4.1 Time-Evolving Global Quantities

12.4.1.1 Projected Changes in Global Mean Temperature and Precipitation

A consistent and robust feature across climate models is a continuation of global warming in the 21st century for all the RCP scenarios (Figure 12.5 – showing changes in concentrations-driven model simulations). Temperature increases are almost the same for all the RCP scenarios during the first two decades after 2005. At longer time scales, the warming rate begins to depend strongly on the specified GHG concentration pathway, being highest ($>0.3^\circ\text{C}$ per decade) in the highest RCP8.5 and significantly lower in RCP2.6, particularly after ~ 2050 when global surface temperature response stabilizes (and declines thereafter). The dependence of global temperature rise on GHG forcing at longer timescales has been confirmed by several studies (Meehl et al., 2007b). In the CMIP5 ensemble mean, global warming under RCP2.6 stays below 2°C above pre-industrial levels throughout the 21st century, clearly demonstrating the result of mitigation policies (assuming 0.60°C of observed warming as discussed in Chapter 11), added to the anomalies in Figure 12.5). This is in agreement with previous studies of aggressive mitigation scenarios (Johns et al., 2011; Meehl et al., 2012a). Under the non-mitigation pathways, global warming exceeds 2°C within the 21st century in RCP4.5, RCP6.0 and RCP8.5, in qualitative agreement with previous studies using the SRES A1B and A2 scenarios (Joshi et al., 2011). Global mean temperature increase exceeds 4°C in RCP8.5 by 2100. The CMIP5 concentration-driven global temperature projections are broadly similar to CMIP3 SRES scenarios discussed in AR4 (Meehl et al., 2007b) although the overall range of the former is larger primarily because of the low-emission mitigation pathway (RCP2.6; Knutti and Sedláček, 2012).

[INSERT FIGURE 12.5 HERE]

Figure 12.5: Time series of global and annual mean surface air temperature anomalies (relative to 1986–2005) from CMIP5 concentration-driven experiments. Projections are shown for each RCP for the multimodel mean (solid lines) and ± 1 standard deviation across the distribution of individual models (shading). Discontinuities at 2100 are due to different numbers of models performing the extension runs beyond the 21st century and have no physical meaning. Numbers in the figure indicate the number of different models contributing to the different time periods.

The multimodel global mean temperature changes under different radiative concentration pathways are summarized in Table 12.2. The relationship between cumulative anthropogenic carbon emissions and global temperature is assessed in Section 12.5 and only concentration-driven models are included here. Warming in 2046–2065 is slightly larger under RCP4.5 compared to RCP6.0, consistent with its greater total anthropogenic forcing then (see Annex II Table A.II.6.12). For all other periods the magnitude of global temperature change increases with the RCP. Also shown in Table 12.2 are projected changes at 2081–2100 for land and ocean points separately as well as area-weighted averages over the Tropics (30°S – 30°N), Arctic

(67.5°N–90°N) and Antarctic (90°S–55°S) regions. Surface air temperatures over land warm more than over the ocean and northern polar regions warm more than the tropics. The excess of land mass in the Northern Hemisphere in comparison with the Southern Hemisphere, coupled with the greater uptake of heat by the Southern Ocean in comparison with northern ocean basins means that the Northern Hemisphere generally warms more than the Southern. Arctic warming is much greater than in the Antarctic, due to the presence of the Antarctic ice sheet and differences in local responses in snow and ice. Mechanisms behind these features of warming are discussed in Section 12.4.3. Maps and timeseries of regional temperature changes are displayed in the Annex I Atlas and regional averages are presented in Chapter 14.

Table 12.2: CMIP5 annual mean surface air temperature anomalies from the 1986–2005 reference period for selected time slices, regions and RCPs. The multimodel mean ± 1 standard deviation range across the individual models are listed and the minimum and maximum values from the model distribution are given in brackets

	RCP2.6	RCP4.5	RCP6.0	RCP8.5
Global: 2016–2035	0.7 ± 0.2 (0.4,1.2)	0.7 ± 0.2 (0.4,1.2)	0.7 ± 0.2 (0.3,1.4)	0.8 ± 0.2 (0.5,1.2)
2046–2065	1.0 ± 0.4 (0.4,1.7)	1.4 ± 0.4 (0.8,2.2)	1.3 ± 0.4 (0.8,2.2)	2.0 ± 0.4 (1.3,2.7)
2081–2100	1.0 ± 0.5 (0.0,2.0)	1.8 ± 0.5 (1.0,2.8)	2.3 ± 0.6 (1.5,3.2)	3.7 ± 0.7 (2.5,5.0)
2181–2200	0.8 ± 0.4 (0.3,1.5)	2.3 ± 0.6 (1.5,3.3)	3.7 ± 0.7 (3.2,4.1)	7.0 ± 2.1 (4.4,10.5)
2281–2300	0.7 ± 0.4 (0.3,1.4)	2.6 ± 0.6 (1.7,3.9)	4.2 ± 0.9 (3.6,4.9)	8.6 ± 3.1 (5.0,14.1)
Land: 2081–2100	1.3 ± 0.6 (-0.3,2.7)	2.4 ± 0.7 (1.0,3.8)	3.0 ± 0.7 (1.7,4.4)	4.9 ± 0.9 (3.4,6.6)
Ocean: 2081–2100	0.9 ± 0.4 (0.1,1.6)	1.6 ± 0.4 (0.8,2.2)	1.9 ± 0.5 (1.2,2.7)	3.1 ± 0.6 (2.1,4.2)
Tropics: 2081–2100	0.9 ± 0.4 (0.3,1.7)	1.6 ± 0.4 (1.0,2.5)	2.0 ± 0.5 (1.5,2.9)	3.3 ± 0.7 (2.2,4.5)
Polar: Arctic: 2081–2100	2.3 ± 1.9 (-4.0,6.0)	4.3 ± 1.8 (-0.8,8.3)	5.2 ± 2.0 (0.6,9.6)	8.3 ± 1.9 (4.7,13.2)
Polar: Antarctic: 2081–2100	0.9 ± 0.7 (-0.7,2.1)	1.6 ± 0.8 (-0.5,3.0)	1.9 ± 1.1 (-0.2,3.9)	3.2 ± 1.3 (0.7,5.5)

CMIP5 models on average project a gradual increase in global precipitation over the 21st century: change exceeds 0.05 mm day^{-1} ($\sim 2\%$ of global precipitation) and 0.15 mm day^{-1} ($\sim 5\%$ of global precipitation) by 2100 in RCP2.6 and RCP8.5, respectively. The relationship between global precipitation and global temperature is approximately linear (Figure 12.6). The precipitation sensitivity, i.e., the change of global precipitation with temperature, is about $1\text{--}3\% \text{ }^{\circ}\text{C}^{-1}$ in most models, tending to be highest for RCP2.6 and RCP4.5 (Figure 12.7; Note that only global values are discussed in this section, ocean and land changes are discussed section 12.4.5.2). These behaviours are consistent with previous studies, including CMIP3 model projections for SRES scenarios and AR4 constant composition commitment experiments (Meehl et al., 2007b), and ENSEMBLES multi-model results for SRES A1B and E1 scenarios (Johns et al., 2011).

[INSERT FIGURE 12.6 HERE]

Figure 12.6: Global mean precipitation (mm day^{-1}) versus temperature ($^{\circ}\text{C}$) changes relative to 1986–2005 for CMIP5 model projections for the four RCPs scenarios. a) Ensemble means for individual models averaged over successive decadal periods (2006–2015 up to 2086–2095), each line representing a different model. b) The corresponding multi-model means for each RCP.

The main characteristics of global precipitation changes are now well understood (see also Section 7.6). The precipitation sensitivity (about $\sim 1\text{--}3\% \text{ }^{\circ}\text{C}^{-1}$) is very different from the water vapour sensitivity ($\sim 7\% \text{ }^{\circ}\text{C}^{-1}$) as the main physical laws that drive these changes also differ. Water vapor increases are primarily a consequence of the Clausius-Claperyon relationship associated with increasing temperatures in the lower troposphere (where most atmospheric water vapor resides). In contrast, future precipitation changes are primarily the result of changes in the energy balance of the atmosphere and the way that these later interact with circulation, moisture and temperature (Boer, 1993; Mitchell, 1983; O’Gorman et al., 2012; Vecchi and Soden, 2007). Indeed, the radiative cooling of the atmosphere is balanced by latent heating (associated with precipitation) and sensible heating. Since AR4, the changes in heat balance and their effects on precipitation have been analyzed in detail for a large variety of forcings, simulations and models (Andrews et al., 2010; Bala et al., 2010; Bony et al., 2012; Ming et al., 2010; O’Gorman et al., 2012; Takahashi, 2009b).

An increase of CO₂ decreases the radiative cooling of the troposphere and reduces precipitations (Andrews et al., 2010; Bala et al., 2010). The inferred hydrological adjustment for zero warming under an instantaneous 4 × CO₂ forcing perturbation is in the range –0.20 to –0.008 mm day^{–1} (or –6.8 to –2.9%) for CMIP5 models using the same method as (Andrews et al., 2009). On longer time scales, the increase of CO₂ induces a slow increase of temperature and water vapour, thereby enhancing the radiative cooling of atmosphere and increasing global precipitation (Allen and Ingram, 2002; Held and Soden, 2006). When the CO₂ forcing stabilises or decreases, the effect of temperature continues to rise due to the thermal inertia of the ocean. This presumably explains the steepening of the precipitation versus temperature relationship in RCP2.6 and RCP4.5 scenario (Figure 12.6), as radiative forcing stabilises and/or declines from the mid-century (Figure 12.4). In idealized CO₂ ramp-up/ramp-down experiments, this effect produces an hydrological response overshoot (Wu et al., 2010). An increase of absorbing aerosols warms the atmosphere and reduces precipitation, and the surface temperature response may be too small to compensate this decrease (Andrews et al., 2010; Ming et al., 2010; Shiogama et al., 2010a). Change in scattering aerosols or incoming solar radiation modify global precipitation mainly via the response of the surface temperature (Andrews et al., 2009; Bala et al., 2010).

The main reasons for the inter-model spread of the precipitation sensitivity estimate amongst GCMs have not been fully understood. Nevertheless, spread in the changes of the cloud radiative effect have been shown to have an impact (Previdi, 2010), although the effect is less dominant for precipitation than it is for the climate sensitivity estimate (Lambert and Webb, 2008). The lapse rate plus water vapour feedback and the response of the surface heat flux (O’Gorman et al., 2012; Previdi, 2010), the shortwave absorption by water vapor (Takahashi, 2009a) or by aerosols have been also identified as important factors.

Global precipitation sensitivity estimates from observation are very sensitive to the data and the time period considered. Some observational studies suggest precipitation sensitivity values higher than model estimates (Wentz et al., 2007; Zhang et al., 2007) although more recent studies suggest consistent values (Adler et al., 2008; Li et al., 2011b).

[INSERT FIGURE 12.7 HERE]

Figure 12.7: Percentage changes in global, land and ocean precipitation per °C of global warming for CMIP5 model projections for the four RCPs, over the period 2006–2100. Changes are calculated relative to the mean precipitation and temperature for 1986–2005 and the gradient of a least-squares fit through annual mean data for each model ensemble mean is computed. Land and ocean values use global mean temperature in the denominator. Each coloured symbol represents the ensemble mean for a single model, and black squares are multi-model means. Also shown are corresponding results for ENSEMBLES model projections for the E1 and A1B scenarios (Johns et al., 2011), in this case using a least-squares fit calculated over the period 2000–2099 and for percentage change relative to the period 1980–1999. The change of precipitation over land and ocean are discussed in Section 12.4.5.2.

12.4.1.2 Uncertainties in Global Quantities

Uncertainties in global mean quantities arise from variations in internal natural variability, model response and forcing pathways. Table 12.2 gives two measures of uncertainty in the CMIP5 model projections, the standard deviation and range (min/max) across the model distribution. Because CMIP5 was not designed to explore to fully the uncertainty range in projections (see Section 12.2), neither the standard deviation nor its range can be interpreted directly as a statement about probability, and other techniques and arguments to assess uncertainty in future projections must be considered. Figure 12.8 summarises the uncertainty ranges in global mean temperature changes at the end of the 21st century under the various scenarios for various methods. Individual CMIP5 models are shown in red. Red bars indicate mean and 5–95% percentiles based on assuming a normal distribution for the CMIP5 sample (i.e., samples 1.64 its standard deviations). Estimates from the MAGICC model (Meinshausen et al., 2011a; Meinshausen et al., 2011b) calibrated to C⁴MIP (Friedlingstein et al., 2006) and the climate sensitivity assessment of AR4 are given as yellow bars (Rogelj et al., 2011). Not all models have simulated all scenarios. To test the effect of that, and to generate a consistent set of uncertainties across scenarios, a pulse response method (Good et al., 2011a) is used to emulate 23 CMIP5 model under the different scenarios (those 23 models that supplied the necessary simulations to compute the emulators, i.e., CO₂ step change experiments). This provides means and ranges (5–95%) that are comparable across scenarios (blue).

For the CO₂ concentration driven simulations (Figure 12.8a), the dominant driver of uncertainty in projections of global temperature for the higher RCPs beyond 2050 is the transient climate response (TCR), for RCP2.6, which is closer to equilibrium, it is the equilibrium climate sensitivity (ECS). In a transient situation, the ratio of temperature to forcing is approximately constant and scenario independent (Gregory and Forster, 2008; Knutti et al., 2008b). Therefore, the uncertainty in TCR maps directly into the uncertainty in global temperature projections for the RCPs other than RCP2.6. The assessed *likely* range of TCR based on various lines of evidence, including constraints from the observed warming (see Box 12.2) is almost identical to the 5–95% percentile range of TCR in CMIP5. In addition, the assessed *likely* range of ECS is also close to the CMIP5 range (see Box 12.2). There is no evidence that the CMIP5 models are significantly over- or underestimating the radiative forcing and ocean heat uptake. Therefore, for global mean temperature projections only, the 5–95% range (estimated as 1.64 standard deviation) of the CMIP5 projections can also be interpreted as a *likely* range for future temperature change between about 2050 and 2100. Global-mean surface temperatures for 2081–2100 (relative to 1986–2005) for the CO₂ concentration driven RCPs will therefore likely fall in the range 0.2°C–1.8°C (RCP2.6), 1.0°C–2.6°C (RCP4.5), 1.3°C–3.2°C (RCP6.0), and 2.6°C–4.8°C (RCP8.5). Beyond 2100, the number of CMIP5 simulations is insufficient to estimate a *likely* range. Uncertainties before 2050 are assessed in chapter 11. The assessed *likely* range is very similar to the range estimated by the pulse response model, suggesting that the different sample of models for the different RCPs are not strongly affecting the result, and providing further support that this pulse response technique can be used to emulate temperature and thermal expansion in Chapter 13 and Section 12.4.9 below. The results are consistent with the probabilistic results from MAGICC, which are slightly smaller due to the lack of internal variability and the fact that non-CO₂ forcings are treated more homogeneously than in CMIP5. This is particularly pronounced for RCP2.6 where the CMIP5 range is substantially larger, partly due to the larger fraction of non-CO₂ forcings in that scenario. The uncertainty estimate in AR4 for the SRES scenarios was –40% to +60% around the CMIP3 means (shown here in grey for comparison). That range is asymmetric and wider for the higher scenarios because it included the uncertainty in carbon cycle climate feedbacks. For scenarios that stabilize (RCP2.6) that approach of constant fractional uncertainty underestimates the uncertainty and is no longer applicable.

Simulations with prescribed CO₂ emissions rather than concentrations are only available for RCP8.5 (Figure 12.8b) and from MAGICC. The projected temperature change in 2100 is slightly higher and the uncertainty range is wider as a result of uncertainties in the carbon cycle climate feedbacks. The CMIP5 range is consistent with the uncertainty range given in AR4 for SRES A2 in 2100. Further details are given in Section 12.4.8.

In summary, the projected changes in global temperature for 2100 in the RCP scenarios are very consistent with those obtained by CMIP3 for SRES in IPCC AR4. The *likely* uncertainty ranges provided here are similar for RCP4.5 and RCP6.0 but smaller for RCP8.5. RCP2.6 did not have an equivalent scenario in AR4. The main reason is that uncertainties in carbon cycle feedbacks are not considered in the concentration driven RCPs. In contrast, the *likely* range in AR4 included those. The assessed *likely* ranges are therefore smaller for the high RCPs. The differences in the projected warming are largely attributable to the difference in scenarios (Knutti and Sedláček, 2012), and the change in the future and reference period. A detailed comparison between the SRES and RCP scenarios and the CMIP3 and CMIP5 models is given in Section 12.4.9.

Figure 12.9 shows maps of surface air temperature from each of the CMIP5 models highlighting both similarities and differences between the responses of different models. The similarities may be exploited to estimate temperature changes under different scenarios using pattern scaling (see next section).

[INSERT FIGURE 12.8 HERE]

Figure 12.8: Uncertainty estimates for global mean temperature change in 2081–2100 with respect to 1986–2005. Red crosses mark projections from individual CMIP5 models. Red bars indicate mean and 5–95% ranges based on CMIP5 (1.64 standard deviations), which are considered as a *likely* range. Blue bars indicate 5–95% ranges from the pulse response emulation of 23 models (Good et al., 2011a). Grey bars mark the range from the mean of CMIP5 minus 40% mean to the mean +60%, assessed as *likely* in AR4 for the SRES scenarios. The yellow bars show the median, 33–66% range and 10–90% range based on Rogelj et al. (2012).

[INSERT FIGURE 12.9 HERE]

Figure 12.9: Surface air temperature change in 2081–2100 displayed as anomalies with respect to 1986–2005 for RCP4.5 from one ensemble member of each of the concentration-driven models available in the CMIP5 archive.

12.4.2 Pattern Scaling

12.4.2.1 Definition and Use

“Pattern scaling” is an approximation that has been explicitly suggested in the description of the new RCPs (Moss et al., 2010) as a method for deriving impact-relevant regional projections for scenarios that have not been simulated by global and regional climate models. It was first proposed by Santer et al. (1990) and relies on the existence of robust geographical patterns of change. The robustness of temperature change pattern has been amply documented from the original paper onward. The precipitation pattern was shown to scale linearly with global average temperature to a sufficient accuracy in CMIP3 models (Neelin et al., 2006) for this to be useful for projections related to the hydrological cycle. (Shiogama et al., 2010b) find similar results with the caution that in the early stages of warming aerosols modify the pattern. The pattern remains approximately constant along the length of the simulation and across different scenarios and models, once it is scaled by the corresponding global average temperature change. It is in the latter quantity that the dependence of the evolution of the change in time on the model (e.g., its climate sensitivity) and the forcing (e.g., the emission scenario) is encapsulated.

In analytical terms, it is assumed that the following relation approximately holds

$$C(t, \xi) = T_G(t) \chi(\xi)$$

where the symbol ξ identifies the geographic location (model grid point or other spatial coordinates) and possibly the time of year (for example a June-July-August average). The index t runs along the length of the forcing scenario of interest. $T_G(t)$ indicates global average temperature change at time t under this scenario; $\chi(\xi)$ is the time-invariant geographic pattern of change for the variable of interest (that by construction has a spatial mean of unity) and $C(t, \xi)$ is the actual field of change for that variable at the specific time t under this scenario. This way, regionally and temporally differentiated results under different scenarios or climate sensitivities can be approximated by the product of a spatial pattern constant over time and a time evolving global mean change in temperature. Characterizing the sensitivity to model and scenario is thus reduced to obtaining the global mean temperature response, which can be done inexpensively, by simple climate models calibrated against fully coupled climate models. The spatial pattern can be estimated through the available coupled models simulations and, by assumption, won’t depend on the actual scenario(s) under which those models were run.

The choice of the pattern in the studies available in the literature can be as simple as the ensemble average field of change (across models and/or across scenarios, for the coupled experiments available), normalized by the corresponding change in global average temperature, choosing a segment of the simulations when the signal has emerged from the noise of natural variability from a baseline of reference (e.g., the last 20 years of the 21st century compared to pre-industrial or current climate). Similar properties and results have been obtained using more sophisticated multivariate procedures that optimize the variance explained by the pattern (Holden and Edwards, 2010).

Pattern scaling and its applications have been documented in IPCC WG1 Reports before (IPCC WG1 TAR, Section 13.5.2.1; AR4 Section 10.3.2). It has been used extensively for regional temperature and precipitation change projections, e.g., Murphy et al. (2007), Watterson (2008), Giorgi (2008), Harris et al. (2006) and Harris et al. (2010), May (2008a), Ruosteenoja et al. (2007), Raisanen and Ruokolainen (2006), Cabre et al. (2010) and impacts studies, e.g., as described in Dessai et al. (2005) and Fowler et al. (2007b). Recent studies have focused on patterns linked to warming at certain global average temperature change thresholds (e.g., May, 2008a; Sanderson et al., 2011) and patterns derived under the new RCPs (Ishizaki et al., 2012).

There are basic limitations to this approach because the assumption holds only approximately and there exist in fact differences between the patterns generated by different GCMs, but uncertainty can be characterized, for example, by the inter-model spread in the pattern $\chi(\xi)$. The validity of this approximation is discussed by

Mitchell et al. (1999) and Mitchell (2003). Recent applications of the methodology to probabilistic future projections have in fact sought to fully quantify errors introduced by the approximation, on the basis of the available coupled model runs (Harris et al., 2006). Pattern scaling has been shown to be more accurate for temperature than for precipitation projections. In fact, recent work with MIROC3.2 has revealed a dependence of the precipitation sensitivity (global average precipitation change per 1°C of global warming – see Figure 12.6) on the scenario, and identified the reason for it in the fact that precipitation is more sensitive to carbon aerosols than well-mixed greenhouse gases and there are significant differences in black and organic carbon aerosol forcing between the emission scenarios investigated (Shiogama et al., 2010a). Levy II et al. (2012) confirm that patterns of precipitation change are spatially correlated with the sources of aerosol emissions, in simulations where the indirect effect is represented. This is a behaviour that is linked to a more general limitation of pattern scaling, which breaks down if aerosol forcing is significant, because the effects of aerosols have a regional nature and are thus dependent on the future sources of pollution which are likely to vary geographically in the future and be difficult to predict (May, 2008a). For example, Asian and North American aerosol production are likely to have different time histories going forward. Schlesinger et al. (2000) extended the methodology of pattern scaling by isolating and recombining patterns derived by dedicated experiments with a coupled climate model where sulfate aerosols were increased for various regions in turn. More recently, in an extension of pattern scaling into a fully probabilistic treatment of model, scenario and initial condition uncertainties, Frieler et al. (2012) derived joint probability distributions for regionally averaged temperature and precipitation changes as linear functions of global average temperature and additional predictors including regionally specific SO_x and black carbon emissions.

Pattern scaling is less accurate for strongly mitigated stabilization scenarios. It has been shown recently by May (2012), comparing patterns of temperature change under a scenario limiting global warming since pre-industrial times to 2 degrees and patterns produced by a scenario that reaches 4.5 degrees of global average temperature change. Already Manabe and Wetherald (1980) and Mitchell et al. (1999), however, pointed out that as the temperatures of the deep oceans reach equilibrium (over multiple centuries) patterns of temperature change as well, one effect being that the warming of high latitudes in the Southern hemisphere is much larger, relative to the global mean warming, than in the earlier periods. More recently Held et al. (2010) showed how this slow warming pattern is in fact present during the initial transient response of the system as well, albeit with much smaller amplitude. Further, Gillett et al. (2011) show how in a simulation in which emissions cease, regional temperatures and precipitation patterns exhibit ongoing changes, even though global mean temperature remains almost constant. It has also been shown (Wu et al., 2010) that the precipitation response shows a non-linear response to strong mitigation scenarios, with the hydrological cycle continuing to intensify even after atmospheric CO₂ concentration, and thus global average temperature, start decreasing.

Other areas where pattern scaling shows a lack of robustness are the edges of polar ice caps and sea ice extent, where at an earlier time in the simulation ice melts and regions of sharp gradient surface, while later in the simulation, in the absence of ice, the gradient will become less steep. Different models' ice representations also make these regions' location much less robust across the model ensembles and the scenarios.

Pattern scaling has been shown to have limited use for quantities other than average temperature and precipitation. For example, temperature extremes have been shown not to scale linearly with the mean of the distribution (Hegerl et al., 2004; Kharin et al., 2007).

12.4.2.2 CMIP5 Patterns

On the basis of CMIP5 simulations, we show geographical patterns (Figure 12.10) of warming and precipitation change and indicate measures of their variability across models and across RCPs. The patterns scaled to 1°C of warming above the reference period 1986–2005 for 2081–2100 (first row) and for the commitment runs (thus excluding RCP8.5) at a time of stabilization, 2181–2200 (second row). Spatial correlation of fields of temperature and precipitation change range from 0.93 to 0.99 when considering ensemble means under different RCPs. The lower values are found when computing correlation between RCP2.6 and the higher RCPs, and may be related to the fact that under RCP2.6 the climate is actually on a stabilization path due to the high mitigation scenario that the low RCP represents. Pattern correlation varies between 0.91 and 0.98 for temperature and between 0.91 and 0.96 for precipitation when comparing patterns

computed by averaging and normalizing changes at the end of the 21st, 22nd and 23rd century, with the largest value representing the correlation between the patterns at the end of the 22nd and 23rd century, the lowest representing the correlation between the pattern at the end of the 21st and the pattern at the end of the 23rd century. The zonal means shown to the side of each plot represent each model by one line, colour coding the four different scenarios. They show good agreement of models and scenarios over low and mid latitudes for temperature, but higher variability across models and especially across scenarios for the areas subject to polar amplification, consistently with the previous discussion of the role of the sea-ice edge. A comparison of the mean of the line to their spread indicates overall the presence of a strong mean signal with respect to the spread of the ensemble. Precipitation shows an opposite pattern of inter-model variability, with larger variations in the low latitudes and around the equator, and smaller around the high latitudes. Precipitation has also a lower signal-to-noise ratio (measured as above by comparing the ensemble mean change magnitude to the spread across models and scenarios of these zonal mean averages). While we do not explicitly use pattern scaling in the sections that follow, it should be borne in mind when trying to interpolate or extrapolate results to different scenarios or time periods, noting the possibility that the scaling may break down at higher levels of global warming.

[INSERT FIGURE 12.10 HERE]

Figure 12.10: Temperature (left) and precipitation (right) change patterns derived from transient simulations from the CMIP5 ensembles, scaled to 1°C of global average warming. The patterns have been calculated by computing 20-year averages at the end of the 21st (top) and 22nd (bottom) Century and over the period 1986–2005 for the available simulations under all RCPs, taking their difference (percentage difference in the case of precipitation) and normalizing it, grid-point by grid-point, by the corresponding value of global average temperature change for each model and scenario. The normalized patterns have then been averaged across models and scenarios. The colour scale represents °C (in the case of temperature) and % (in the case of precipitation) per 1°C of global average warming and stippling indicates the mean change averaged over all realisations is larger than the 95% percentile of the distribution of models. Zonal means of the geographical patterns are shown for each individual model for RCP2.6 (blue), 4.5 (light blue), 6.0 (orange) and 8.5 (red). RCP8.5 is excluded from the stabilisation figures.

12.4.3 Changes in Temperature and Energy Budget

12.4.3.1 Patterns of Surface Warming: Land-Sea Contrast, Polar Amplification and SSTs

Patterns of surface air temperature change for various RCPs show widespread warming during the 21st century (Figure 12.11; see Annex I: Atlas for seasonal patterns). A key feature that has been present throughout the history of coupled modelling is the larger warming over land compared to oceans, which occurs in both transient and equilibrium climate change (e.g., Manabe et al., 1990). The degree to which warming is larger over land than ocean is remarkably constant over time under transient warming due to well-mixed greenhouse gases (Boer, 2011; Lambert and Chiang, 2007; Lambert et al., 2011) and is predominantly a feature of the surface and lower atmosphere (Joshi et al., 2008). Somewhat counter intuitively, heat capacity differences between land and ocean do not play a major role in the land-sea warming contrast (Joshi et al., 2012). Indeed, studies have found it occurs due to contrasts in surface sensible and latent fluxes over land (Sutton et al., 2007) and boundary layer relative humidity (Joshi et al., 2008) which are amplified by changes to cloudiness (Doutriaux-Boucher et al., 2009; Fasullo, 2010) and due to soil moisture reductions (Clark et al., 2010; Dong et al., 2009) under climate change. The land-sea warming contrast is also sensitive to aerosol forcing (Allen and Sherwood, 2010; Joshi et al., 2012). Globally averaged warming over land and ocean is identified separately in Table 12.2 for the CMIP5 models and the ratio of land to ocean warming of $\sim 1.5 \pm 0.2$ is consistent with previous studies (Lambert et al., 2011). The CMIP5 multimodel mean ratio is approximately constant from 2020 through to 2300 (based on an update of Joshi et al., 2008 from available CMIP5 models).

[INSERT FIGURE 12.11 HERE]

Figure 12.11: Multimodel ensemble average of surface air temperature change (compared to 1986–2005 base period) for 2046–2065, 2081–2100, 2181–2200 for RCP2.6, 4.5 and 8.5. Hatching indicates regions where the multi model mean is less than one standard deviation of internal variability. Stippling indicates regions where the multi model mean is greater than two standard deviations of internal variability and where 90% of the models agree on the sign of change (see Box 12.1). The number of CMIP5 models used is indicated in the upper right corner of each panel.

Amplified surface warming in Arctic latitudes is also a consistent feature in climate model integrations (e.g., Manabe and Stouffer, 1980). This is often referred to as polar amplification, although as numerous studies have shown in transient forcing integrations this is primarily an Arctic phenomenon (Manabe et al., 1991; Meehl et al., 2007b). The lack of an amplified warming response in high Southern latitudes has been associated with deep ocean mixing, strong ocean heat uptake and the persistence of the vast Antarctic ice sheet. In equilibrium simulations, amplified warming occurs in both polar regions.

On an annual average, the CMIP5 models currently available show a mean Arctic (70°N–90°N) warming approximately 2.7 times the global average warming for 2081–2100 compared to 1986–2005 (for the RCP4.5 scenario). Similar polar amplification factors occur in the other RCPs and in earlier coupled model simulations (e.g., Holland and Bitz, 2003; Winton, 2006b). This factor in models is a bit higher than the observed central value, but it is within the uncertainty of the best estimate from observations of the recent past (Bekryaev et al., 2010). The uncertainty is large in the observed factor because station records are short and sparse (Serreze and Francis, 2006) and the forced signal is contaminated by the noise of internal variability. By contrast, model trends in surface air temperature are 2.5 to 5 times higher than observed over Antarctica, but here also the observational estimates have a very large uncertainty, so, for example, the CMIP3 ensemble mean is consistent with observations within error estimates (Monaghan et al., 2008). While, in general, the ability of models to reproduce observed trends is no indication of the confidence in the projection of future trends, a couple of studies have related historical to future trends in CMIP3 and CMIP5 models (Bracegirdle and Stephenson, 2012a; Bracegirdle and Stephenson, 2012b).

The amplified Arctic warming in models has a distinct seasonal character (Holland and Bitz, 2003; Lu and Cai, 2009; Manabe and Stouffer, 1980; Rind, 1987). Arctic amplification (defined as the 70–90N warming compared to the global average warming for 2081–2100 versus 1986–2005) peaks in early winter (November–December) with a CMIP5 RCP4.5 multi-model mean warming for 70°N–90N exceeding the global average by a factor of more than 4. The warming is smallest in summer when excess heat at the Arctic surface goes into melting ice and warming the surface ocean. Simulated Arctic warming also has a consistent vertical structure that is largest in the lower troposphere (e.g., Kay et al., 2012; Manabe et al., 1991). This is in agreement with recent observations (Screen and Simmonds, 2010; Serreze et al., 2009) but contrary to an earlier study which suggested a larger warming aloft (Graversen et al., 2008). The discrepancy in observed vertical structure may reflect inadequacies in datasets (Bitz and Fu, 2008; Grant et al., 2008; Thorne, 2008) and sensitivity to the time period used for averaging (see Chapters 9 and 10).

There are many mechanisms that contribute to Arctic amplification, some of which were identified in early modelling studies (Manabe and Stouffer, 1980). Feedbacks associated with changes in sea ice and snow amplify surface warming near the poles (Graversen and Wang, 2009; Hall, 2004; Soden et al., 2008). The longwave radiation changes in the top of the atmosphere associated with surface warming opposes surface warming at all latitudes, but less so in the Arctic (Soden et al., 2008; Winton, 2006b). Rising temperature globally is expected to increase the latent heat transport by the atmosphere into the Arctic (Kug et al., 2010), which warms primarily the lower troposphere. On average, CMIP3 models simulate enhanced latent heat transport (Held and Soden, 2006), but north of about 65°N, the sensible heat transport declines enough to more than offset the latent heat transport increase (Hwang et al., 2011). Ocean heat transport also plays a role in the simulated Arctic amplification, with both large late 20th century transport (Mahlstein and Knutti, 2011) and increases over the 21st century (Bitz et al., 2012) associated with higher amplification. As noted by Hwang et al. (2011) and Kay et al. (2012), diagnosing the role of various factors in amplified warming is complicated by coupling in the system in which local feedbacks interact with poleward heat transports.

While models consistently exhibit Arctic amplification as global mean temperatures rise, they differ considerably in the magnitude. Previous work has implicated variations across climate models in numerous factors including inversion strength (Boe et al., 2009b), ocean heat transport (Holland and Bitz, 2003; Mahlstein and Knutti, 2011), albedo feedback (Winton, 2006b), shortwave cloud feedback (Crook et al., 2011; Kay et al., 2012) as playing a role in the across-model scatter in polar amplification. In the CMIP5 models analyzed, amplification (defined as the 70°N–90N warming compared to the global average warming for 2081–2100 versus 1986–2005) varies from 1.8 to 3.3 for the RCP4.5 scenario. The magnitude of amplification is generally higher in models with less extensive late 20th century sea ice in June suggesting that the initial ice state influences the 21st century Arctic amplification. The pattern of simulated Arctic warming is also associated with the initial ice state, and in particular with the location of the winter sea ice

edge (Bracegirdle and Stephenson, 2012a; Holland and Bitz, 2003; Raisanen, 2007). This relationship has been suggested as a constraint on projected Arctic warming (Bracegirdle and Stephenson, 2012a; Bracegirdle and Stephenson, 2012b). In turn, higher amplification models tend to simulate larger June ice loss.

Minima in warming occur in the North Atlantic and Southern Oceans under transient forcing in part due to deep ocean mixed layers in those regions (Manabe et al., 1990; Xie et al., 2010). Trenberth and Fasullo (2010) find that the large biases in the Southern Ocean energy budget in CMIP3 coupled models are negatively correlated with equilibrium climate sensitivity (see Section 12.5.3), suggesting that an improved mean state in the Southern Ocean is needed before warming there can be understood. In the equatorial Pacific, warming is enhanced in a narrow band which previous assessments have described as ‘El Niño-like’, as may be expected from the projected decrease in atmospheric tropical circulations (see Section 12.4.4). However, DiNezio et al. (2009) highlight that the tropical Pacific warming in the CMIP3 models is not ‘El Niño-like’ as the pattern of warming and associated teleconnections is quite distinct from that of an El Niño event. They attribute the enhanced equatorial warming to ocean dynamical changes that can be decoupled from atmospheric changes. See also further discussion in Section 12.4.7.

In summary, there is much evidence, robust agreement over multiple generations of models and high confidence in these large scale warming patterns. They are *very likely* to persist in all scenarios but with different magnitudes as discussed in Section 12.4.2.

12.4.3.2 Zonal Average Atmospheric Temperature

Zonal temperature changes at the end of the 21st century show warming throughout the troposphere and, depending on the scenario, a mix of warming and cooling in the stratosphere (Figure 12.12). The maximum warming in the tropical upper troposphere is consistent with theoretical explanations and associated with a decline in the moist adiabatic lapse rate of temperature in the tropics as the climate warms (Bony et al., 2006). The northern polar regions also experience large warming in the lower atmosphere, consistent with the mechanisms discussed in the previous section (12.4.3.1). The tropospheric patterns are similar to those in the TAR and AR4 with the RCP8.5 changes being up to several degrees warmer in the tropics compared to the A1B changes appearing in the AR4. Similar tropospheric patterns appear in the RCP2.6 and 4.5 changes, but with reduced magnitudes, suggesting some degree of scaling with forcing change in the troposphere, similar to behaviour discussed in the AR4 and Section 12.4.2. The consistency of tropospheric patterns over multiple generations of models indicates robust changes.

In the stratosphere, the models show similar tropical patterns of change, with magnitudes differing according to degree of climate forcing. Substantial differences appear in polar regions. In the north, RCP8.5 and 4.5 yield cooling, though it is more significant in the RCP8.5 ensemble. In contrast, RCP2.6 shows warming, albeit weak and with little significance. In the southern polar region, RCP2.6 and 4.5 both show significant warming, and RCP8.5 is the outlier, with significant cooling. The polar stratospheric warming, especially in the southern hemisphere, is similar to that found by Butchart et al. (2010) and Meehl et al. (2012a) in GCM simulations that showed effects of ozone recovery in determining the patterns (Baldwin et al., 2007; Son et al., 2010). Eyring et al. (2012) find behaviour in the CMIP5 ensemble both for models with and without interactive chemistry that supports the contention that the polar stratospheric changes in Figure 12.12 are strongly influenced by ozone recovery. Overall, the stratospheric temperature changes do not exhibit pattern scaling with global temperature change and are dependent on ozone recovery.

Away from the polar stratosphere, there is physical and pattern consistency in temperature changes between different generations of models. The consistency is especially clear in the tropical upper troposphere and the northern high latitudes and, coupled with physical understanding, indicates that the greatest warming is *very likely* to occur in these regions. However, there remains uncertainty about the magnitude of warming simulated in the tropical upper troposphere because large observational uncertainties and contradictory analyses prevent confident assessment of model accuracy in simulating temperature trends in the tropical upper troposphere (see Sections 9.4.1.3 and 10.3.1.2.1).

[INSERT FIGURE 12.12 HERE]

Figure 12.12: CMIP5 multi-model changes in annual mean zonal mean temperature relative to 1986–2005 for 2081–2100 under the RCP2.6 (left), RCP4.5 (centre) and RCP8.5 (right) forcing scenarios. Hatching indicates regions where

the multi model mean is less than one standard deviation of internal variability. Stippling indicates regions where the multi model mean is greater than two standard deviations of internal variability and where 90% of the models agree on the sign of change (see Box 12.1).

12.4.3.3 Temperature Extremes

As the climate continues to warm, changes in several types of extremes in temperature are being observed (Seneviratne et al., 2012), and are expected to continue in the future in concert with global warming. Extremes occur on multiple time scales, from a single day or a few consecutive days (a heat spell or wave) to monthly and seasonal events and can be defined by indices e.g., percentage of days in a year when maximum temperature is above the 90th percentile of a present day distribution or by return periods or other measures. While changes in temperature extremes are a very robust signature of anthropogenic climate change, the magnitude of change and consensus among models varies with the characteristics of the event being considered (e.g., timescale, magnitude, duration and spatial extent) as well as the definition used to describe the extreme.

Since the AR4 many advances have been made in establishing global observed records of extremes (Alexander et al., 2006; Donat et al., 2012) against which models can be evaluated to give context to future projections (Alexander and Arblaster, 2009; Sillmann and Roeckner, 2008). Numerous regional assessments of future changes in extremes have also been performed and a comprehensive summary of these is given in IPCC Special Report on Extremes (Seneviratne et al., 2012). Here we summarise the key findings from this report and assess updates since then.

It is *virtually certain* that there will be more hot and fewer cold extremes as global temperature increases (Caesar and Lowe, 2012; Orłowsky and Seneviratne, 2012; Sillmann and Roeckner, 2008), consistent with previous assessments (Seneviratne and Nicholls, 2012; Seneviratne et al., 2012; Solomon et al., 2007). Figure 12.13 shows multimodel mean changes in the absolute temperature indices of the coldest day of the year and the hottest day of the year and the threshold-based indices of frost days and tropical nights from the CMIP5 ensemble (Sillmann et al., 2012). A robust increase in warm temperature extremes and decrease in cold temperature extremes is found at the end of the 21st Century, with the magnitude of the changes increasing with increased anthropogenic forcing. The coldest day of the year undergoes larger increases than the hottest day for all three RCPs and increases of more than 12°C are projected in the high latitudes of the Northern Hemisphere (Figure 12.13a). Similarly, increases in the frequency of warm nights are greater than increases in the frequency of warm days. The subtropics and mid-latitudes exhibit the greatest projected changes in the hottest day of the year, whereas changes in tropical nights and the frequency of warm days and warm nights are largest in the tropics (Sillmann et al., 2012). The number of frost days declines in all regions while significant increases in tropical nights are seen in south-eastern North America, the Mediterranean and central Asia.

It is *very likely* that, on average, there will be more record high than record cold temperatures in a warmer average climate. For example, Meehl et al. (2009) find that the current ratio of 2 to 1 for record daily high maxima to low minima over the United States becomes approximately 20 to 1 by the mid 21st century and 50 to 1 by late century in their model simulation. However, even at the end of the century daily record low minima continue to be broken, if in a small number, consistent with Kodra et al. (2011) who conclude that cold extremes will continue to occur in a warmer climate, even though their frequency declines.

It is also *very likely* that heat waves, defined as spells of days with temperature above a threshold determined from historical climatology, will occur with a higher frequency and duration, mainly as a direct consequence of the increase in seasonal mean temperatures (Ballester et al., 2010a; Ballester et al., 2010b; Barnett et al., 2006; Fischer and Schar, 2010). Changes in the absolute value of temperature extremes are also *very likely* and expected to regionally exceed global temperature increases by far, with substantial changes in hot extremes projected even for moderate average warming levels (Clark et al., 2010; Diffenbaugh and Ashfaq, 2010). These changes often differ from the mean temperature increase, as a result of changes in variability and shape of the temperature distribution (Clark et al., 2006; Hegerl et al., 2004; Meehl and Tebaldi, 2004). For example, summer temperature extremes over central and southern Europe are projected to warm substantially more than the corresponding mean local temperatures as a result of enhanced temperature variability at interannual to intraseasonal time scales (Clark et al., 2006; Fischer and Schar, 2009, 2010;

Fischer et al., 2012b; Kjellstrom et al., 2007; Nikulin et al., 2011; Schar et al., 2004; Vidale et al., 2007). Several recent studies have also argued that the probability of occurrence of a Russian heat wave at least as severe as the one in 2010 increases substantially (by a factor of 5 to 10 by the mid-century) along with increasing mean temperatures and enhanced temperature variability (Barriopedro et al., 2011; Dole et al., 2011).

[INSERT FIGURE 12.13 HERE]

Figure 12.13: CMIP5 multimodel mean geographical changes at RCP8.5 and 20-year smoothed timeseries for RCP2.6, RCP4.5 and RCP8.5 in the (a,b) annual minimum of minimum daily temperature, (c,d) annual maximum of maximum daily temperature, (e,f) frost days (number of days below 0°C) and (g,h) tropical nights (number of days above 20°C). Shading in the timeseries represents the interquartile ensemble spread (25th and 75th quantiles). The box-and-whisker plots show the interquartile ensemble spread (box) and outliers (whiskers) for 11 CMIP3 model simulations of the SRES scenarios A2 (orange), A1B (cyan), and B1 (purple) globally averaged over the respective future time periods (2046–2065 and 2081–2100) as anomalies from the CMIP3 reference period 1981–2000. Stippling indicates grid points with changes that are significant at the 5% level. Adapted from Sillmann et al. (2012).

Since the AR4, an increased understanding of mechanisms and feedbacks leading to projected changes in extremes has been gained (Seneviratne et al., 2012). Climate models suggest that hot extremes are amplified by soil moisture-temperature feedbacks (Diffenbaugh et al., 2007; Fischer and Schar, 2009; Fischer et al., 2012b; Lenderink et al., 2007; Seneviratne et al., 2006; Vidale et al., 2007) in certain regions as the climate warms, consistent with previous assessments. Changes in the temperature of hot extremes may also be amplified over the mean due to anomalous temperature advection from continental interiors in response to an increased land-sea contrast (Watterson et al., 2008). The largest increases in the magnitude of warm extremes are simulated over mid-latitude continental areas, consistent with the drier conditions, and the associated reduction in evaporative cooling from the land surface projected over these areas (Kharin et al., 2007). The representation of the latter constitutes a major source of model uncertainty for projections of the absolute magnitude of temperature extremes (Clark et al., 2010; Fischer et al., 2011).

Winter cold extremes also warm more than the local mean temperature over northern high latitudes (Orlowsky and Seneviratne, 2012) as a result of reduced temperature variability related to declining snow cover (Fischer et al., 2011; Gregory and Mitchell, 1995; Kjellstrom et al., 2007) and decreases in land-sea contrast. Changes in atmospheric circulation, induced by remote surface heating can also modify the temperature distribution (Haarsma et al., 2009). Sillmann and Croci-Maspoli (2009) note that cold winter extremes over Europe are in part driven by atmospheric blocking and changes to these blocking patterns in the future lead to changes in the frequency and spatial distribution of cold temperature extremes as global temperatures increase (Raisanen and Ylhaisi, 2011).

Human discomfort, morbidity and mortality during heat waves depend not only on temperature but also humidity. Heat stress, defined as the combined effect of temperature and humidity, is expected to increase along with warming temperatures and dominates the local decrease in summer relative humidity due to soil drying (Diffenbaugh et al., 2007; Fischer et al., 2012a). Areas with abundant atmospheric moisture availability and high present-day temperatures such as Mediterranean coastal regions are expected to experience the greatest heat stress changes because the heat stress response scales with humidity which thus becomes increasingly important to heat stress at higher temperatures (Fischer and Schar, 2010; Sherwood and Huber, 2010; Willett and Sherwood, 2012). For some regions, simulated heat stress indicators are remarkably robust, because those models with stronger warming simulate a stronger decrease in atmospheric relative humidity (Fischer and Knutti, 2012).

Changes in rare temperature extremes can be assessed using extreme value theory based techniques (Seneviratne et al., 2012). Kharin et al. (2007), in an analysis of CMIP3 models, found large increases in the 20 year return values of the annual maximum and minimum daily averaged surface air temperatures (i.e., the size of an event that would be expected on average once every 20 years, or with a 5% chance every year) with larger changes over land than ocean. Figure 12.14 displays the end of 21st century change in the magnitude of these rare events from the CMIP5 models in the RCP2.6, 4.5 and 8.5 scenarios (Kharin et al., 2012). Comparison to the changes in mean temperature shown in Figure 12.11 reveals that rare high temperature events are projected to change at similar rates to the mean in many land areas but rare low temperature events are projected to experience significantly larger increases than the mean in most regions, particularly at high latitudes. Kharin et al. (2012) concluded from the CMIP5 models that it is *likely* that in

most regions a current 20 year maximum temperature event is projected to become a one-in-two year event by the end of the 21st century under the RCP4.5 and RCP8.5 scenarios, except for some regions of the high latitudes of the Northern Hemisphere where it is *likely* to become a one-in-five year event (see also SREX Figure 3-5). Current 20 year minimum temperature events are projected to become exceedingly rare, with waiting times *likely* increasing to more than 100 years in almost all locations (Kharin et al., 2012). The SREX also notes that the limited number of detection and attribution studies suggest that the model changes may tend to be too large and these likelihood statements are somewhat less strongly stated than a direct interpretation of model output and its ranges. The CMIP5 analysis shown in Figure 12.14 reinforces this assessment of large changes in the frequency of rare events, particularly in the RCP8.5 scenario.

[INSERT FIGURE 12.14 HERE]

Figure 12.14: The CMIP5 multi-model median change in 20-year return values of annual warm temperature extremes (left hand panels) and cold temperature extremes (right hand panels) as simulated by CMIP5 models in 2081–2100 relative to 1986–2005 in the RCP2.6 (top panels), RCP4.5 (middle panels), and RCP8.5 (bottom panels) experiments.

There is high consensus amongst models in the sign of the future change in temperature extremes, with recent studies confirming this conclusion from the previous assessment (Meehl et al., 2007b; Orłowsky and Seneviratne, 2012; Seneviratne et al., 2012; Sillmann et al., 2012; Tebaldi et al., 2006). However, the magnitude of the change remains uncertain due to scenario and model (both structural and parameter) uncertainty (Clark et al., 2010) as well as internal variability. These uncertainties are much larger than corresponding uncertainties in the magnitude of mean temperature change (Barnett et al., 2006; Clark et al., 2006; Fischer and Schar, 2010; Fischer et al., 2011).

12.4.3.4 Energy Budget

The change of top of atmosphere (TOA) energy budget is the sum of the radiative forcings and the climate response and can be analysed separately in the shortwave (SW) and longwave (LW) domains. In the SW, the net flux at TOA represents the SW flux that is absorbed by the Earth's atmosphere, ocean, ice, and land surface. Anthropogenic or natural perturbations to the climate system produce radiative forcings that result in an imbalance in the global energy budget and affect the global mean temperature. The climate responds to a change in radiative forcing on multiple timescales and at longer timescales, the energy imbalance (i.e., the energy heating or cooling the Earth) is very close to the ocean heat uptake due to the much lower thermal inertia of the atmosphere and the continental surfaces (Hansen et al., 2011; Knutti et al., 2008a; Levitus et al., 2005; Murphy et al., 2009). The radiative responses of the fluxes at TOA are generally analysed using the forcing-feedback framework and are presented in Chapter 9.

CMIP5 models simulate a small increase of the energy imbalance at the TOA over the 20th century (see Chapters 3, 9 and 13). The future evolution of the imbalance is very different depending on the scenario (Figure 12.15a): for RCP8.5 it continues to increase rapidly, much less for RCP6.0, is almost constant for RCP4.5 and decreases for RCP2.6. This latter negative trend reveals the quasi-stabilisation characteristic of RCP2.6.

The rapid fluctuations that are simulated during the 20th century originate from volcanic eruptions that are prescribed in the models (see Section 12.3.2). These aerosols reflect solar radiation and thus decrease the amount of SW radiation absorbed by the Earth (Figure 12.15c). The minimum of SW radiation absorbed by the Earth during the period 1960–2000 is mainly due to two factors: a sequence of volcanic eruptions and an increase of the reflecting aerosol burden due to human activities (see Chapter's 7 and 9). During the 21st century, the absorbed SW radiation monotonically increases for the RCP8.5 scenario, and increases and subsequently stabilizes for the other scenarios, consistent with what has been previously obtained with CMIP3 models and SRES scenarios (Trenberth and Fasullo, 2009). The two main contributions to the SW changes are the change of clouds (see Section 12.4.3.5) and the change of the cryosphere (see Section 12.4.6) at high latitudes. During the 21st century, the amount of anthropogenic aerosols is reduced which leads to an increase in the amount of SW radiation that is absorbed by the surface. In the LW domain (Figure 12.15b), the net flux at TOA represent the opposite of the flux that is emitted by the Earth's surface and atmosphere toward space, i.e., a negative anomaly represents an increase of the emitted LW radiation. The LW net flux depends mainly on two factors: the surface temperature and the magnitude of the greenhouse effect of the atmosphere. The latter is driven mainly by the concentration of greenhouse gases (including water vapour),

the vertical temperature profile and the cloud properties. During the 20th century, the rapid fluctuations of LW radiation are driven by volcanic forcings, which decrease the absorbed SW radiation, surface temperature, and the LW radiation emitted by the Earth toward space. During the period 1960–2000, the fast increase of greenhouse gas concentrations also decreases the radiation emitted by the Earth. In response to this net heating of Earth, temperatures warm and thereby increase emitted LW radiation although the change of the temperature vertical profile, water vapour, and cloud properties modulate this response (e.g., Bony et al., 2006; Randall et al., 2007).

[INSERT FIGURE 12.15 HERE]

Figure 12.15: Time evolution of the global mean (a) net total radiation anomaly at the TOA, (b) net longwave radiation anomaly at the TOA and (c) net shortwave radiation anomaly at the TOA for the historical period and three RCP scenarios from available models. All the fluxes are positive downward and units are W m^{-2} . The anomalies are computed with respect to the 1900–1950 base period.

[INSERT FIGURE 12.16 HERE]

Figure 12.16: CMIP multi-model changes in annual mean net radiation (R_T , left) net longwave radiation ($-OLR$, centre) and absorbed solar radiation (ASR, bottom) at the TOA for the RCP4.5 scenario from the available models. All fluxes are positive downward, units are W m^{-2} and $R_T = ASR - OLR$. The net radiation anomalies are computed with respect to the 1900–1950 base period.

Since AR4, increased attention has been given to the energetics of the climate system, both at TOA and within the atmosphere (e.g., Andrews et al., 2009; Trenberth and Fasullo, 2010). An increased number of models now consider a larger variety forcings, such as more types of aerosols and varying concentrations of ozone which impact the energy budget. The relationship between changes in the energy budget and precipitation is discussed in Section 12.4.5.

12.4.3.5 Clouds

Clouds are a major component of the climate system and play an important role in climate sensitivity (Cess et al., 1990; Randall et al., 2007), the diurnal temperature range (DTR) over land (Zhou et al., 2009), and land-sea contrast (see Section 12.4.3.1 and Chapter 7). The observed global mean cloud radiative forcing is about -20 W m^{-2} (Loeb et al., 2009), i.e., clouds have a net cooling effect. Current GCMs simulate clouds through various complex parameterizations (see Section 7.2.3), and cloud feedback is a major source of the spread of the climate sensitivity estimate (Dufresne and Bony, 2008; Randall et al., 2007; Soden and Held, 2006) (see Chapter 9).

Under future projections the multimodel pattern of total cloud amount shows consistent decreases in the subtropics, in conjunction with a decrease of the relative humidity there, and increases at high latitudes. Another robust pattern is an increase in cloud cover at all latitudes in the vicinity of the tropopause, a signature of the increase of the altitude of high level clouds in convective regions (Meehl et al., 2007b; Soden and Vecchi, 2011; Wetherald and Manabe, 1988; Zelinka et al., 2012). Marine boundary layer clouds in subtropical regions were identified as a primary cause of inter-model spread in cloud feedbacks in CMIP3 models (Bony and Dufresne, 2005; Webb et al., 2006; Wyant et al., 2006). Since AR4, these results have been confirmed along with the positive feedbacks due to high level clouds (Soden and Vecchi, 2011; Zelinka and Hartmann, 2010). The radiative effect of clouds mainly depends on their fraction, optical depth and temperature. The contribution of these variables to the cloud feedback has been quantified for the multi-model CMIP3 (Soden and Vecchi, 2011) and CFMIP1 database (Zelinka et al., 2012). These findings may be summarized as follows (see Section 7.2.4 for more details) and are consistent with the results with the CMIP5 models (Figure 12.17).

The dominant contributor to the SW cloud feedback is the change in cloud fraction. The reduction of cloud fraction between 50°S and 50°N , except along the equator and the eastern part of the ocean basins (Figure 12.17), contributes to an increase in the absorbed solar radiation (Figure 12.16c). Physical mechanisms and the role of different parameterizations have been proposed to explain this reduction of low level clouds (Brient and Bony, 2012; Caldwell and Bretherton, 2009; Zhang and Bretherton, 2008). Poleward of 50°S , the cloud fraction and the cloud optical depth increases, thereby increasing cloud reflectance. This leads to a decrease of solar absorption around Antarctica where the ocean is ice free in summer (Figure 12.16c).

However, Trenberth and Fasullo (2010) show that this negative feedback could be an artefact since the observed storm tracks are already near 100% covered by clouds.

In the LW domain, the tropical high cloud changes exert the dominant effect. A lifting of the cloud top with warming is simulated consistently across models (Meehl et al., 2007b) which leads to a positive feedback whereby the LW emissions from high clouds decrease as they cool (Figure 12.16b). The dominant driver of this effect is the increase of tropopause height and physical explanations have been proposed (Hartmann and Larson, 2002; Lorenz and DeWeaver, 2007; Zelinka and Hartmann, 2010). In contrast, the decrease in cloudiness generally increases OLR and offsets the effect of cloud rising somewhat resulting in a consistent positive global-mean LW cloud feedback across CMIP and CFMIP models. Global-mean SW cloud feedbacks range from slightly negative to strongly positive (Soden and Vecchi, 2011; Zelinka et al., 2012), with an inter-model spread being mainly attributable to low-level cloud feedbacks.

[INSERT FIGURE 12.17 HERE]

Figure 12.17: CMIP5 multi-model changes in annual mean total cloud amount relative to 1986–2005 for 2081–2100 under the RCP2.6 (left), RCP4.5 (centre) and RCP8.5 (right) forcing scenarios. Hatching indicates regions where the multi model mean is less than one standard deviation of internal variability. Stippling indicates regions where the multi model mean is greater than two standard deviations of internal variability and where 90% of the models agree on the sign of change (see Box 12.1). The number of CMIP5 models used is indicated in the upper right corner of each panel.

12.4.4 Changes in Atmospheric Circulation

Projected changes in energy and water cycles couple with changes in atmospheric circulation and mass distribution. Understanding this coupling is necessary to assess physical behaviour underlying projected changes, revealing why changes occur and the realism of the changes. The focus in this section is on behaviour that CMIP5 GCMs resolve well. Thus, the section includes discussion of extratropical cyclones but not tropical cyclones: extratropical cyclones are fairly well resolved by CMIP5 GCMs, whereas tropical cyclones are not, except at resolutions finer than used by the large majority of CMIP5 GCMs (see Chapter 9, Section 9.5.4.3). Detailed discussion of tropical cyclones appears in Box 14.2 (see also Chapter 11, Section 11.4.2.5.3 and Seneviratne et al. (2012), Section 3.4.4). Regional detail concerning extratropical storm tracks, including causal processes, appears in Box 14.3 (see also Chapter 11, Section 11.4.2.4 for near-term changes and Seneviratne et al. (2012) for an assessment of projected changes related to weather and climate extremes).

12.4.4.1 Mean Sea Level Pressure and Upper-Air Winds

Sea level pressure gives an indication of surface changes in atmospheric circulation (Figure 12.18). As in previous assessments, a robust feature of the pattern of change is a decrease in high latitudes and increases in the mid latitudes, associated with poleward shifts in the mid latitude storm tracks (Section 12.4.4.3) and positive trends in the annular modes (Section 14.2.10) as well as an expansion of the Hadley Cell (Section 12.4.4.2). Similar patterns of sea level pressure change are found in observed trends over recent decades, suggesting an already detectable change (Gillett and Stott, 2009; Chapter 10), although the observed patterns are influenced by both natural and anthropogenic forcing as well as internal variability and the relative importance of these influences is likely to change in the future. Internal variability has been found to play a large role in uncertainties of future sea level pressure projections, particularly at higher latitudes (Deser et al., 2012a).

In boreal winter, decreases of sea level pressure over NH high latitudes are slightly weaker in the CMIP5 ensemble compared to previous assessments (Manzini et al., 2012), consistent with Scaife et al. (2012) and Karpechko and Manzini (2012) who suggest that improvements in the representation of the stratosphere can influence this pattern. However, Manzini et al. (2012) caution that processes outside the stratosphere likely explain this difference between the CMIP5 and CMIP3 multimodel mean. In austral summer, the SH projections are impacted by the additional influence of stratospheric ozone recovery (see Chapter 11) which opposes changes due to greenhouse gases. Under the weaker GHG emissions of RCP2.6, decreases in sea level pressure over the SH mid-latitudes and increases over SH high latitudes are consistent with expected changes from ozone recovery (Arblaster et al., 2011; McLandress et al., 2011; Polvani et al., 2011). For all other RCPs, the magnitude of SH extratropical changes scales with the radiative forcing, as found in previous model ensembles (Paeth and Pollinger, 2010; Simpkins and Karpechko, 2012).

Large increases in seasonal sea level pressure are also found in regions of sub-tropical drying such as the Mediterranean and northern Africa in DJF and Australia in JJA. Projected changes in the tropics are less consistent across the models, however a decrease in the eastern equatorial Pacific and increase over the maritime continent, associated with a weakening of the Walker Circulation (Power and Kociuba, 2011b; Vecchi and Soden, 2007), is found in all RCPs.

[INSERT FIGURE 12.18 HERE]

Figure 12.18: CMIP5 multimodel ensemble average of DJF and JJA mean sea level pressure change (2081–2100 minus 1986–2005) for RCP2.6, 4.5 and 8.5. Hatching indicates regions where the multi model mean is less than one standard deviation of internal. Stippling indicates regions where the multi model mean is greater than two standard deviations of internal variability and where 90% of models agree on the sign of change (see Box 12.1). The number of CMIP5 models used is indicated in the upper right corner of each panel.

Future changes in zonal and annual mean zonal winds (Figure 12.19) are seen throughout the atmosphere with stronger changes in higher RCPs. Large increases in winds are evident in the tropical stratosphere and a poleward shift and intensification of the SH tropospheric jet is seen under RCP4.5 and RCP8.5, associated with an increase in the SH meridional temperature gradient (Figure 12.12) (Wilcox et al., 2012). In the NH, the response of the tropospheric jet is weaker and complicated by the additional thermal forcing of polar amplification (Woollings, 2008). Barnes and Polvani (2012) evaluate changes in the annual mean mid-latitude jets in the CMIP5 ensemble, finding consistent poleward shifts in both hemispheres under RCP8.5 for the end of the 21st Century. In the NH, the poleward shift is $\sim 1^\circ$, similar to that found for the CMIP3 ensemble (Woollings and Blackburn, 2012). Some stratosphere-resolving models have been found to reduce or reverse this poleward shift, however no such dependence on the height of the model top is found in the CMIP5 analysis of Manzini et al. (2012). They examine projected changes in the NH wintertime circulation under RCP8.5 and attribute the weakening of the high latitude NH zonal mean winds at the end of the 21st Century to a strengthening of the Brewer-Dobson circulation (e.g., Butchart et al., 2010). In the SH, the annual mean mid-latitude jet shifts poleward by $\sim 2^\circ$ under RCP8.5 at the end of the 21st Century in the CMIP5 multimodel mean (Barnes and Polvani, 2012), with a similar shift of 1.5° in the surface westerlies (Swart and Fyfe, 2012). A strengthening of the SH surface westerlies is also found under all RCPs except RCP2.6 (Swart and Fyfe, 2012), with largest changes in the Pacific basin (Bracegirdle et al., 2012). In austral summer, ozone recovery offsets changes in GHGs to some extent, with a weak reversal of the jet shift found under the low emissions scenario of RCP2.6 (Eyring et al., 2012). CMIP5 models with interactive chemistry are found to have slightly stronger equatorward shifts in the SH jet at the end of the 21st century under RCP2.6 and weaker poleward shifts under RCP4.5, 6.0 and 8.5, compared to models with prescribed ozone (Eyring et al., 2012), consistent with their larger stratospheric ozone forcing.

While the poleward shift of the tropospheric jets are robust across models and *likely* under increased GHGs, the dynamical mechanisms behind these projections are still not completely understood and have been explored in both simple and complex models (Butler et al., 2010; Chen et al., 2008; Lim and Simmonds, 2009). The shifts are associated with a strengthening in the meridional temperature gradient (Wilcox et al., 2012) and hypotheses for associated changes in planetary wave activity and/or synoptic eddy characteristics that impact on the position of the jet have been put forward (Gerber et al., 2012). Equatorward biases in the position of the SH jet, while somewhat improved over similar biases in the CMIP3 models (Kidston and Gerber, 2010) still remain, limiting our confidence in the magnitude of future changes.

In summary, significant poleward shifts in the extratropical tropospheric circulation are *likely* at the end of the 21st century under RCP8.5 with weaker or non-significant shifts under lower emission scenarios. Ozone recovery will *likely* weaken the GHG-induced changes in the SH extratropical circulation in austral summer.

[INSERT FIGURE 12.19 HERE]

Figure 12.19: CMIP5 multimodel ensemble average of zonal and annual mean wind change (2081–2100 minus 1986–2005) for RCP2.6, 4.5 and 8.5. Black contours represent the multimodel mean average for the 1986–2005 base period. Hatching indicates regions where the multi model mean is less than one standard deviation of internal variability. Stippling indicates regions where the multi model mean is greater than two standard deviations of internal variability and where 90% of model agree on the sign of change (see Box 12.1).

12.4.4.2 Planetary-Scale Overturning Circulations

Large-scale atmospheric overturning circulations and their interaction with other atmospheric mechanisms are significant in determining tropical climate and regional changes in response to enhanced radiative forcing. Observed changes in tropical atmospheric circulation are assessed Chapter 2 (Section 2.6.5), while Chapter 10 (Section 10.3.3) discusses attribution of observed changes to anthropogenic forcing. Evidence is inconclusive on recent trends in the strength of the Hadley and Walker circulations, though there is medium confidence of an anthropogenic influence on the observed widening of the Hadley circulation. In the projections, there are indications of a weakening of tropical overturning of air as the climate warms (Bony et al., 2012; Chou and Chen, 2010; Gastineau et al., 2008; Gastineau et al., 2009; Held and Soden, 2006; Vecchi and Soden, 2007). In the SRESA1b scenario, AR4 models show a remarkable agreement in simulating a weakening of the tropical atmospheric overturning circulation (Vecchi and Soden, 2007). Along the ascending branches of tropical overturning cells, a reduction in convective mass flux from the boundary layer to the free atmosphere is implied by the differential response to global warming of the boundary-layer moisture content and surface evaporation. This weakening of vertical motion along the ascending regions of both the tropical meridional and near-equatorial zonal cells is associated with an imbalance in the rate of atmospheric moisture increase and that of global mean precipitation (Held and Soden, 2006). A reduction in the compensating climatological subsidence along the downward branches of overturning circulations, where the rate of increase of static stability exceeds radiative cooling, is implied.

The weakening of low-level convective mass flux along ascending regions of tropical overturning cells has been ascribed to changes in the hydrologic cycle (Held and Soden, 2006; Vecchi and Soden, 2007). Advection of dry air from subsidence regions towards the ascending branches of large-scale tropical circulation has been suggested to be a feasible mechanism weakening ascent along the edges of convection regions (Chou et al., 2009). Enhanced atmospheric stability associated with an increase in the vertical extent of convection resulting from a deepening of the tropical troposphere in response to global warming has been demonstrated to contribute to the slowdown of the overturning cells (Chou and Chen, 2010). An imbalance between the increase in diabatic heating of the troposphere and in static stability whereby the latter increases more rapidly has also been thought to play a role in weakening tropical ascent (Lu et al., 2008). The latest findings using CMIP5 models reveal that an increase in greenhouse gases (particularly CO₂) contributes significantly to weakening tropical overturning cells by reducing radiative cooling in the upper atmosphere (Bony et al., 2012).

Apart from changes in Hadley circulation strength, a robust feature in twenty-first century climate model simulations is an increase in the cell's depth and width (Frierson et al., 2007; Lu et al., 2007; Lu et al., 2008; Mitas and Clement, 2006), with the latter change translating to a broadening of tropical regions (Seidel and Randel, 2007; Seidel et al., 2008) and a poleward displacement of subtropical dry zones (Lu et al., 2007; Scheff and Frierson, 2012). The increase in the cell's depth is consistent with a tropical tropopause rise. The projected increase in the height of the tropical tropopause and the associated increase in meridional temperature gradients close to the tropopause slope have been proposed to be an important mechanism behind the Hadley cell expansion and the poleward displacement of the subtropical westerly jet (Johanson and Fu, 2009; Lu et al., 2008). An increase in subtropical and mid-latitude static stability has been found to be an important factor widening the Hadley cell by shifting baroclinic eddy activity and the associated eddy-driven jet and subsidence poleward (Lu et al., 2008; Mitas and Clement, 2006). The projected widening of the Hadley cell, albeit weaker, is consistent with late twentieth century observations, where ~2°–5° expansion was found (Fu et al., 2006; Johanson and Fu, 2009).

The zonally asymmetric Walker Circulation is projected to weaken under global warming (Power and Kociuba, 2011a; Power and Kociuba, 2011b), more than the Hadley circulation (Lu et al., 2007; Vecchi and Soden, 2007). Almost everywhere around the equatorial belt, changes in the 500hPa pressure velocity oppose the climatological background motion, notably over the maritime continent (Shongwe et al., 2011; Vecchi and Soden, 2007). Over the equatorial Pacific Ocean, where mid-tropospheric ascent is projected to strengthen, changes in zonal SST hence sea-level pressure gradients induce low-level westerly wind anomalies which act to weaken the low-level branch of the Pacific Walker circulation. These projected changes in the tropical Pacific circulation, towards a more El-Niño-like state, are already occurring (Zhang and Song, 2006). However, the projected weakening of the Pacific Walker cell does not imply an increase in the frequency and/or magnitude of El-Niño events (Collins et al., 2010).

In the upper atmosphere, a robust feature of projected stratospheric circulation change is that the Brewer-Dobson circulation will *likely* strengthen in the 21st century (Butchart et al., 2006; Butchart et al., 2010; Li et al., 2008; McLandress and Shepherd, 2009; Shepherd and McLandress, 2011). This is attributed to an increase in the propagation of resolved planetary and parameterized orographic waves into the lower stratosphere in response to changes in temperature and zonal wind structure. In a majority of chemistry-climate models (CCMs), the projected changes in the large-scale overturning circulation in the stratosphere feature an intensification of tropical upward mass flux, which extends to the upper stratosphere. It is to a large extent driven by parameterized orographic gravity waves which result from strengthening of subtropical westerly jets and cause more waves to propagate into the lower stratosphere (Butchart et al., 2006; Sigmond et al., 2004). The projected intensification in tropical upwelling is counteracted by enhanced mean extra-tropical/polar lower stratospheric subsidence. In the Northern Hemisphere high latitudes, the enhanced downwelling is associated with an increase in stationary planetary wave activities (McLandress and Shepherd, 2009). The intensification of the stratospheric meridional residual circulation has already been observed during the last decades of the 20th century (Li et al., 2008). The projected increase in troposphere-to-stratosphere mass exchange rate (Butchart et al., 2006) and stratospheric mixing associated with the strengthening of the Brewer-Dobson circulation will *likely* result in a decrease in the mean age of air in the lower stratosphere. In the mid-latitude lower stratosphere, quasi-horizontal mixing is a significant contributor to reducing the lifetimes of air.

12.4.4.3 Extratropical Storms: Tracks and Influences on Planetary-Scale Circulation and Transports

Since the AR4, there has been continued evaluation of changes in extratropical storm tracks under projected warming using both CMIP3 and, more recently, CMIP5 simulations, as well as supporting studies using single models or idealized simulations. These analyses use a variety of methods for diagnosing storm tracks and, for Southern Hemisphere storm tracks, generally agree with earlier studies, showing that extratropical storm tracks will tend to shift poleward (Bengtsson et al., 2009; Chang et al., 2012b; Gastineau and Soden, 2009; Gastineau et al., 2009; Perrie et al., 2010; Schuenemann and Cassano, 2010). The behaviour is consistent with a trend in reanalysis output (Chapter 2) associated with a *likely* anthropogenic contribution to the Southern Annular Mode (Chapter 10). Similar behaviour appears in CMIP5 simulations for the Southern Hemisphere (Figure 12.20). In Southern Hemisphere winter there is a clear poleward shift in storm tracks of several degrees and a small overall reduction in the frequency of storms. The poleward shift at the end of the century is consistent with a poleward shift in the Southern Hemisphere of the latitudes with strongest tropospheric jets (Figure 12.19), though the degree of jet shift appears to be sensitive to bias in a model's contemporary-climate storm tracks (Chang et al., 2012a; Chang et al., 2012b). Although there is thus some uncertainty in the degree of shift, the consistency of behaviour with observation-based trends, consistency between CMIP5 and CMIP3 projections under a variety of diagnostics and the physical consistency of the storm response with other climatic changes gives *high confidence* that a poleward shift of several degrees in Southern Hemisphere storm tracks is *likely* by the end of the 21st century under the RCP8.5 scenario.

In the Northern Hemisphere winter (Figure 12.20), the CMIP5 multi-model ensemble shows an overall reduced frequency of storms and less indication of a poleward shift in the tracks. Although observations indicate a poleward shift of storm tracks over the last half of the 20th century (Chapter 2), there is only *medium confidence* that there is an anthropogenic influence on the behaviour (Chapter 10). The clearest poleward shift in the Northern Hemisphere at the end of the 21st century occurs in the Asia-Pacific storm track, where intensification of the westerly jet promotes more intense cyclones in an ensemble of CMIP5 models (Mizuta, 2012). Otherwise, changes in storm-track magnitude, as measured by band-pass sea-level pressure fluctuations, show only small change relative to interannual and interdecadal variability by the end of the 21st century in SRES A1B and RCP4.5 simulations for several land areas over the Northern Hemisphere (Harvey et al., 2012). Consistency in CMIP3 and CMIP5 changes seen in the Southern Hemisphere are absent in the Northern Hemisphere (Chang et al., 2012a). Factors identified that affect changes in the North Atlantic basin's storm track include horizontal resolution (Colle et al., 2012) and how models simulate changes in modal behaviour (Chapter 14), the Atlantic's meridional overturning circulation (Catto et al., 2011; Woollings et al., 2012), the zonal jet and Hadley circulation (Mizuta, 2012; Zappa et al., 2012) and subtropical upper troposphere temperature (Haarsma et al., 2012). Substantial uncertainty and thus *low confidence* remains in projecting changes in Northern Hemisphere storm tracks, especially for the North Atlantic basin.

[INSERT 12.20 HERE]

Figure 12.20: Change in winter, extratropical storm track density for end of the century (2081–2100) – Historical Control (1986–2005) in the CMIP5 multi-model ensembles: (a) RCP4.5 Northern Hemisphere DJF and (b) RCP8.5 Northern Hemisphere DJF (c) RCP4.5 Southern Hemisphere JJA and (d) RCP8.5 Southern Hemisphere JJA. Storm-track computation uses the method of Bengtsson et al. (2006, their Figure 13a) applied to 850 hPa vorticity. Densities have units (number density/month/unit area), where the unit area is equivalent to a 5° spherical cap (~106 km²).

Additional analyses of CMIP3 GCMs have determined other changes in properties of extratropical storms. Most analyses find that the frequency of storms decreases in projected climates (Favre and Gershunov, 2009; Finnis et al., 2007), though the occurrence of strong storms may increase (Albrecht et al., 2009; Ulbrich et al., 2009; Ulbrich et al., 2008). Many studies focus on behaviour of specific regions, and results of these studies are detailed in Box 14.3.

Changes in extratropical storms in turn may influence other large-scale climatic changes. Kug et al. (2010) in a set of time-slice simulations show that a poleward shift of storm tracks in the Northern Hemisphere could enhance polar warming and moistening. The Arctic Oscillation is sensitive to synoptic eddy vorticity flux, so that projected changes in storm tracks can alter the Arctic Oscillation (Choi et al., 2010). The net result is that changes in extratropical storms alter the climate in which they are embedded, so that links between surface warming, extratropical storms and their influence on climate are more complex than simple responses to changes in baroclinicity (O’Gorman, 2010). Conclusive results on projected changes await further analysis.

12.4.5 Changes in the Water Cycle

The water cycle consists of water stored on the Earth in all its phases, along with the movement of water through the Earth’s climate system. In the atmosphere, water occurs primarily as gaseous water vapour, but it also occurs as solid ice and liquid water in clouds. The ocean is primarily liquid water, but is partly covered by ice in polar regions. Terrestrial water in liquid form appears as surface water (lakes, rivers), soil moisture and groundwater. Solid terrestrial water occurs in ice sheets, glaciers, frozen lakes, snow and ice on the surface and permafrost. Projections of future changes in the water cycle are inextricably connected to changes in the energy cycle (Section 12.4.3) and atmospheric circulation (Section 12.4.4).

Warmer air can contain more water vapour, but projected future changes in the water cycle are far more complex than projected temperature changes. Some regions of the world will be subject to decreases in hydrologic activity while others will be subject to increases. There are important local seasonal differences among the responses of the water cycle to climate change as well.

At first sight, the CMIP3/5 models may appear to be inconsistent amongst each other, particularly at regional scales. Anthropogenic changes to the water cycle are superimposed on complex naturally varying modes of the climate (such as ENSO, AO, PDO, etc.) which further increase the differences between model projections as the timing of these natural modes is not same in each simulation. However, by careful consideration of the interaction of the water cycle with changes in other aspects of the climate system, the mechanisms of change are revealed, increasing confidence in projections.

12.4.5.1 Atmospheric Humidity

Atmospheric water vapour is the primary greenhouse gas in the atmosphere. Its changes affect all parts of the water cycle. However, the amount of water vapour is controlled by naturally occurring processes rather than directly through water vapour emissions from human activities. A common experience from past modelling studies is that relative humidity (RH) remains approximately constant on climatological time scales and planetary space scales, implying a strong constraint by the Clausius-Clapeyron relationship on how specific humidity will change. However, underlying this fairly straight-forward behaviour are changes in RH that can influence changes in cloud cover and atmospheric convection (Sherwood, 2010). Analysis of CMIP3 and CMIP5 models shows near-surface RH decreasing over most land areas as temperatures increase with the notable exception of tropical Africa (O’Gorman and Muller, 2010). A prominent contributor to changes in RH is the land-ocean difference in temperature change during a warming scenario (Fasullo, 2010; Joshi et al., 2008; O’Gorman and Muller, 2010), which controls RH over land by a last-saturation-temperature

constraint. Moisture originating over more slowly warming oceans will have its specific humidity level governed by saturation temperatures of oceanic air (Sherwood et al., 2010). As this air moves over land and is warmed, its relative humidity drops as any further moistening of the air over land is insufficient to maintain constant RH. The differential warming of land and ocean can promote changes in atmospheric circulation and moisture transports. Figure 12.21 shows projected CMIP5 changes in near surface relative humidity under RCP8.5 forcing for various time periods. Confidence in projected humidity changes over land is somewhat lower than in many of the following figures describing changes in the water cycle. The CMIP5 models project with *medium confidence* large RH reductions in northern polar regions in contrast to the CMIP3 models. Land-ocean differences in warming are projected to continue through the twenty-first century, and the CMIP5 projections are consistent with a last-saturation constraint, indicating that reductions in near-surface RH over many land areas is *likely*.

[INSERT FIGURE 12.21 HERE]

Figure 12.21: Projected changes in near-surface relative humidity from the CMIP5 models under RCP8.5 for the DJF (left), JJA (middle) and annual mean (left) averages relative to 1986–2005 for the periods 2046–2065 (top row), 2081–2100 (bottom row). Hatching indicates regions where the multi model mean is less than one standard deviation of internal variability. Stippling indicates regions where the multi model mean is greater than two standard deviations of internal variability and where 90% of models agree on the sign of change (see Box 12.1). The number of CMIP5 models used is indicated in the upper right corner of each panel.

12.4.5.2 Patterns of Projected Average Precipitation Changes

Patterns of projected large scale precipitation changes exhibit strong seasonal characteristics in many regions of the Earth. Combining projections into an annual quantity can hide regions where confidence may be high for individual seasons by mixing different mechanisms of change. Figure 12.22 shows CMIP5 multi-model mean projections of percent changes in seasonal average precipitation for the RCP8.5 scenario at the middle of the 21st century, the end of the 21st century and the end of the 22nd century.

Projected zonally averaged precipitation changes exhibit the typical wet-get-wetter and dry-get-drier type of response. This simple response has a robust explanation for the precipitation-evaporation over ocean (Chou et al., 2009; Held and Soden, 2006; Vecchi and Soden, 2007).

As seen in Section 12.4.5.1, water vapour increases are primarily a consequence of the Clausius-Clapeyron relationship associated with increasing temperatures in the lower troposphere (where most atmospheric water vapour resides) which has been observed to warm slightly less than the surface temperatures (Chou and Neelin, 2004; Held and Soden, 2006). The radiative cooling of the atmosphere is balanced by latent heating (coming from precipitation) and sensible heating. Relatively small changes in radiative fluxes are *likely* to cause substantial changes to the global circulation (see Section 12.4.4.2) and water cycle. Since AR4, these changes have been analyzed in detail for a large variety of forcings, simulations and models. Over tropical oceans, in the absence of atmospheric circulation change, an increase of water vapour in the boundary layer leads to additional moisture convergence within tropical convergence zones and to additional moisture divergence in the descent zones, increasing the contrast in precipitation minus evaporation between wet and dry regions (Chou et al., 2009; Held and Soden, 2006). The pattern of increases and decreases in projected average precipitation is less robust than that of precipitation minus evaporation, owing to the competing effects of increased evaporation and increased moisture divergence in subsidence regions (Bony et al., 2012). The net effect is an increase in the tropical precipitation together with a suppression in the subtropics (Allan, 2012; Chou et al., 2009).

Causes of large scale changes in precipitation may be decomposed into those resulting from atmospheric circulation changes (dynamical) and those resulting from water vapour changes (thermodynamical) (see also Section 7.6). The thermodynamical components explain almost all of the projected increased precipitation in the mid and high latitudes (Emori and Brown, 2005), a common feature across recent generations of climate models. This is entirely consistent with theoretical explanations that anticipate an increase of poleward moisture flux with increasing temperature of about $5\%K^{-1}$ (Held and Soden, 2006). For CO_2 forcing, the modelled ratio between the relative change of precipitation (dP/P) and the temperature change (dT) is in the range $dP/P/dT = 2\text{--}3\%K^{-1}$ (Allen and Ingram, 2002; Held and Soden, 2006). Several observational studies suggest that this ratio may actually be higher (e.g., Allan and Soden, 2007; Wentz et al., 2007; Zhang et al., 2007). The inter-model spread may be due to differences in modelled shortwave absorption by water vapour

(Takahashi, 2009a) but not the large uncertainty in shortwave cloud feedbacks (Lambert and Webb, 2008). An increase of absorbing aerosols induces similar fast and slow responses in precipitation, but with a smaller impact on the global mean temperature than greenhouse gases and hence a smaller impact on the slow response of global precipitation (Andrews et al., 2010; Ming et al., 2010). Overall, the global-mean precipitation change may be estimated from a simple relationship between the global-mean temperature change, the tropospheric greenhouse gas forcing and the black carbon emissions (Frieler et al., 2011) and it is *virtually certain* that its rate of increase per °C global warming will be less than that of atmospheric water vapour .

A general slowing down of the global circulation of the atmosphere (see Section 12.4.4.2) and an enhancement of the patterns of evaporation minus precipitation are robust features across the CMIP3 models in a warmer world (Held and Soden, 2006). It is *likely* that many arid and semi-arid regions will experience less precipitation and that many moist regions will experience more precipitation simply because the increased water vapour leads to additional moisture convergence within tropical convergence zones and additional moisture divergence in the descent zones (Chou and Neelin, 2004; Held and Soden, 2006). However, the reaction of the tropical circulation to this basic effect includes strong local convergence feedback that can yield much stronger precipitation changes at the regional scale (Chou et al., 2006), especially seasonally. These regional changes can differ considerably from model to model, especially along the margins of the convection zones (Neelin et al., 2006) where spatial inhomogeneities, including the rate at which air masses tend to flow into the convection zone from dry regions, can yield considerable sensitivity in precipitation response. Such is the case, for instance, in the Sahel region, West Africa, where the spread of model projections are large in both the CMIP3 and CMIP5 multi-model data base (Roehrig et al., 2012). However, verification of the muted response in global precipitation relative to water vapour, as described by the physical mechanism detailed above and projected by all CMIP3/5 models and the relatively short satellite observational record, is mixed (Li et al., 2011b; Wentz et al., 2007). Due to the intermittent and highly variable nature of precipitation in most parts of the world, changes to average regional precipitation may not be easily detected either in the recent past (see Chapter 10) or in the near future. Nonetheless, it is *virtually certain* that changes in average precipitation in a much warmer world will be mixed, with regions experiencing increases, or decreases or not much change at all.

The patterns of multi-model precipitation changes displayed in Figure 12.22 tend to smooth and decrease the spatial contrast of precipitation changes. In regions where models tend to put precipitation changes in slightly different locations, these changes are washed out in the multi-model ensemble average. The amplitude of the multi-model ensemble mean precipitation response thus significantly under predicts the median amplitude calculated from each individual model (Knutti, 2010; Neelin et al., 2006). The CMIP3/5 multi-model ensemble precipitation projections must be interpreted in this context of uncertainty. Multi-model projections are not probabilistic statements about the likelihood of changes. Maps of multi-model projected changes are smoothly varying but observed changes are and will continue to be much more granular. Projected precipitation changes vary greatly between models, much more so than for temperature projections. Part of this variance is due to genuine differences between the models including their ability to replicate observed precipitation patterns (see Chapter 9). However, a large part of it is also the result of the small ensemble size from each model (Rowell, 2012). This is especially true for regions of small projected change situated between two other regions, one experiencing significant increases while the other experiences significant decreases. Individual climate model realizations may differ in their projection of future precipitation changes in these regions due simply to their internal variability (Deser et al., 2012a; Deser et al., 2012b). Multi-model projections containing large numbers of realizations would tend to average to small changes in these regions. However, due to a limited number of available realizations this may not always be the case. As a result, confidence in projections in regions of limited or no change in precipitation may be more difficult to obtain than confidence in regions of large projected changes. However, Power et al. (2012) indicate that certain of these regions of small multi-model average projected changes but large differences in sign between models are more confidently described as regions of small projected change than in the AR4.

The patterns of projected precipitation change shown in Figure 12.22 become more confident as temperature increases. Projected changes in precipitation under different scenarios or at different times exhibit the pattern scaling behavior and limitations described in Section 12.4.2. These patterns of projected change and the associated uncertainties are very similar between the SRES scenarios discussed in the AR4 and the RCP

scenarios with the CMIP5 projections slightly more robust over land than those from CMIP3 (Knutti and Sedláček, 2012). The high latitudes are *very likely* to experience greater amounts of precipitation due to the additional water carrying capacity of the warmer troposphere. The largest changes over northern Eurasia and North America are projected to occur during the winter and are *likely* manifested as increases in snowfall at the highest latitudes and in rainfall in the southern extents of these regions (Raisanen, 2008).

Recent studies suggest that CO₂ increase has a significant direct influence on global and tropical precipitation changes (Andrews et al., 2010; Bala et al., 2010; Bony et al., 2012). Over oceans, the positive radiative forcing from increased atmospheric CO₂ reduces the radiative cooling of the upper troposphere and the large scale rising motion and hence reduces precipitation in the convective regions (Bony et al., 2012). On longer time scales, the increase of CO₂ increases the ocean surface temperature, water vapour and therefore increases precipitation as explained above. Over large land masses, the direct effect of CO₂ on precipitation is the opposite owing to the small thermal inertia of land surfaces. As a result, global temperature increases lead to increases in precipitation, but with a smaller amplitude than over ocean. These differences in behavior presumably explain the large land-sea difference between the precipitation sensitivity of the RCP2.6 scenario, which is close to equilibrium by the end of the 21st century, and that of the other scenarios that are not (Figure 12.7).

In general, areas that are currently wet tend to become wetter, while areas that are currently dry tend to become dryer. This holds well in the seasonal averages for the multi-model ensemble mean (Figure 12.22), but it is important to note that significant exceptions can occur in particular regions. In the tropics, an increase of water vapour leads to additional moisture convergence within tropical convergence zones and to additional moisture divergence in the descent zones, increasing the contrast in precipitation between wet and dry regions (Chou and Neelin, 2004; Held and Soden, 2006). This increase in contrast is partly compensated by the slowdown of the tropical circulation due to the water vapour increase (see Section 12.4.4) and the net effect is an increase in tropical precipitation together with a simultaneous suppression in the subtropics (Allan, 2012; Chou et al., 2009).

The predominant pattern of tropical and subtropical precipitation change detailed in the AR4 is reinforced in the CMIP5 models. Subtropical drying is more pronounced in the CMIP5 projections than in CMIP3, with the largest declines between subtropical minima and midlatitude precipitation maxima indicating that dynamical effects are greater than thermodynamic effects in this region (Scheff and Frierson, 2012).

[INSERT FIGURE 12.22 HERE]

Figure 12.22: Multi-model CMIP5 average percent change in seasonal mean precipitation relative to the reference period 1985–2005 averaged over the periods 2045–2065, 2081–2100 and 2181–2200 under the RCP8.5 forcing scenarios. Hatching indicates regions where the multi model mean is less than one standard deviation of internal variability. Stippling indicates regions where the multi model mean is greater than two standard deviations of internal variability and where 90% of models agree on the sign of change (see Box 12.1).

12.4.5.3 Soil Moisture

Near-surface soil moisture is the net result of a suite of complex processes (e.g., precipitation evapotranspiration, drainage, overland flow, infiltration), and heterogeneous and difficult-to-characterize aboveground and belowground system properties (e.g., slope, soil texture). As a result, regional to global-scale simulations of soil moisture and drought remain relatively uncertain (Burke and Brown, 2008; Henderson-Sellers et al., 2008). The AR4 (Section 8.2.3.2) discussed the lack of assessments of global-scale models in their ability to simulate soil moisture, and this problem appears to have persisted. Furthermore, consistent multi-model projections of total soil moisture are difficult to make due to substantial differences between climate models in the depth of their soil. However, Koster et al. (2009a) argued that once climatological statistics affecting soil moisture were accounted for, different models tend to agree on soil moisture predictions. The AR4 summarized multi-model projections of 21st century annual mean soil moisture changes as decreasing in the subtropics and Mediterranean region, and increasing in east Africa and central Asia. Figure 12.23 shows projected changes in surface soil moisture (upper 10 cm) in the CMIP5 ensemble at the end of the 21st century under the RCPs 2.6, 4.5, 6.0 and 8.5. We focus on this variable because it describes soil moisture at a consistent depth across all CMIP5 models. The patterns are consistent across the RCPs, with the changes tending to become stronger as the strength of the forcing change increases. The agreement among CMIP5 models and the consistency with other physical features of climate

change indicate high confidence in certain regions where surface soils are projected to dry. There is little to no confidence anywhere in projections of moister surface soils. Under RCP8.5, where the largest change is expected, individual ensemble members (not shown), show consistency across the ensemble for drying in the Mediterranean region, northeast and southwest South America, southern Africa, and southwestern USA. However, ensemble members do not show large regions of agreement on the sign of the change in central Asia or the high northern latitudes. The Mediterranean, southwestern USA, northeast South America and southern African drying regions are consistent with projected increases in the Hadley circulation downwelling that inhibit precipitation in these regions and have continued to appear across generations of projections and climate models. The large scale drying in the Mediterranean, southwest USA, and southern Africa is *likely*. Additionally, an analysis of CMIP3 and CMIP5 projections of soil moisture in five drought-prone regions indicates that the differences in future forcing scenarios are the largest source of uncertainty in such regions rather than differences between model responses (Orlowsky and Seneviratne, 2012).

Other recent assessments include multi-model ensemble approaches, dynamical downscaling, and regional climate models applied around the globe. Kolomyts and Surova (2010), using projections from the CMIP3 models, GISS and HadCM2, under the SRES A2 forcing, show that vegetation type has substantial influence on the development of pronounced drying over the 21st century in Middle Volga Region forests. Analyses of the southwestern USA using CMIP3 models (Christensen and Lettenmaier, 2007; Seager et al., 2007) show consistent projections of drying, primarily due to a decrease in winter precipitation. In contrast, Kellomaki et al. (2010) find that SRES A2 projections for Finland yield decreased snow depth, but soil moisture generally increasing, consistent with the general increase in precipitation occurring in high northern latitudes.

Projected changes in soil moisture from the CMIP3/5 models show substantial seasonal variation. For the Cline River watershed in western Canada, Kienzle et al. (2012) find annual mean soil moisture increases 2.6% by the 2080s, but summer decreases. Sato et al. (2007), using dynamical downscaling, find summer soil moisture decreases in Mongolia of up to 6% due to increased potential evaporation in a warming climate and decreased precipitation and decreased precipitation.

Soil moisture projections in high latitude permafrost regions are critically important for assessing future climate feedbacks from trace-gas emissions (Riley et al., 2011; Zhuang et al., 2004) and vegetation changes (Chapin et al., 2005). In addition to changes in precipitation, snow cover and evapotranspiration, future changes in high latitude soil moisture also will depend on permafrost degradation, thermokarst evolution, rapid changes in drainage (Smith et al., 2005), and changes in plant communities and their water demands. Current understanding of these interacting processes at scales relevant to climate is poor, so that full incorporation in current GCMs is lacking.

[INSERT FIGURE 12.23 HERE]

Figure 12.23: Change in annual mean soil moisture (mass of water in all phases in the uppermost 10 cm of the soil) (mm) relative to the reference period 1985–2005 projected for 2081–2100 from the CMIP5 ensemble for (a) RCP2.6, (b) RCP4.5, (c) RCP6.0 and (d) RCP8.5. Hatching indicates regions where the multi model mean is less than one standard deviation of internal variability. Stippling indicates regions where the multi model mean is greater than two standard deviations of internal variability and where 90% of models agree on the sign of change (see Box 12.1). The number of CMIP5 models used is indicated in the upper right corner of each panel.

12.4.5.4 Runoff and Evaporation

In the AR4, 21st century runoff projections consistently (across models) decreased in southern Europe, the Middle East, and southwestern U.S. and increased in Southeast Asia, tropical East Africa, and at high northern latitudes. The same general features appear in the CMIP5 ensemble of GCMs for all four RCPs shown in Figure 12.24. with the areas of most robust change typically increasing with magnitude of forcing change. The large decreases in runoff in southern Europe and the southwestern USA are consistent with changes in the Hadley circulation and related precipitation decreases and warming-induced evapotranspiration increases. The high northern latitude runoff increases are consistent with the projected precipitation increases. The consistency of changes across different generations of models and different forcing scenarios, together with the physical consistency of change indicates that decreases are *likely* in runoff in southern Europe, the Middle East, and southwestern USA. The models project consistent increases in high latitude runoff but confidence in this projection is tempered by large biases in their current snow cover.

A number of reports since the AR4 have updated findings from CMIP3 models and analyzed a large set of mechanisms affecting runoff. Several studies have focused on the Colorado River basin in the United States (Barnett and Pierce, 2008; Barnett et al., 2008; Christensen and Lettenmaier, 2007; McCabe and Wolock, 2007) showing that runoff reductions under global warming occur through a combination of evapotranspiration increases and precipitation decreases, with the overall reduction in river flow exacerbated by human water demands on the basin's supply.

CMIP3 analyses also showed seasonal shifts. Kienzie et al. (2012) studied climate change scenarios over the Cline River watershed and projected (1) spring runoff and peak streamflow up to four weeks earlier than in 1961–1990; (2) significantly higher streamflow between October and June; and (3) lower streamflow between July and September.

[INSERT FIGURE 12.24 HERE]

Figure 12.24: Change in annual mean runoff (mm) relative to the reference period 1985–2005 projected for 2081–2100 from the CMIP5 ensemble for (a) RCP2.6, (b) RCP4.5, and (c) RCP6.0 and (d) RCP8.5. Hatching indicates regions where the multi model mean is less than one standard deviation of internal variability. Stippling indicates regions where the multi model mean is greater than two standard deviations of internal variability and where 90% of models agree on the sign of change (see Box 12.1). The number of CMIP5 models used is indicated in the upper right corner of each panel.

Annual mean surface evaporation in the AR4 increased over most of the ocean and increased or decreased over land with largely the same pattern as increases and decreases in precipitation. Similar behaviour occurs in an ensemble of CMIP5 models (Figure 12.25). Evaporation increases over most of the ocean and land, with prominent areas of decrease over land occurring in the southwestern USA/northwestern Mexico, southern Africa and land bordering the Mediterranean. The areas of decrease correspond to areas with reduced precipitation. There is some uncertainty about storm-track changes over Europe (see Box 14.4). However, the consistency of the decreases across different generations of models and different forcing scenarios along with the physical basis for the precipitation decrease indicates that these decreases in annual mean evaporation are *likely*. Annual mean evaporation increases over land in the northern high latitudes are consistent with the increase in precipitation and the overall warming that would increase potential evaporation. For the northern high latitudes, the physical consistency and the similar behaviour across multiple generations and forcing scenarios indicates that annual mean evaporation increases there are *likely*.

Evapotranspiration changes partly reflect changes in precipitation. However, some changes might come from altered biological processes. For example, increased atmospheric CO₂ promotes stomatal closure and reduced evapotranspiration (Betts et al., 2007; Cruz et al., 2010) which potentially can yield increased runoff. There is potential for substantial feedback between vegetation changes and regional water cycles, though the impact of such feedback remains uncertain at this point due to uncertainties in plant response, ecosystem shifts, and land management changes.

[INSERT FIGURE 12.25 HERE]

Figure 12.25: Change in annual mean evaporation (mm) relative to the reference period 1985–2005 projected for 2081–2100 from the CMIP5 ensemble for (a) RCP2.6, (b) RCP4.5, and (c) RCP6.0 and (d) RCP8.5. Hatching indicates regions where the multi model mean is less than one standard deviation of internal variability. Stippling indicates regions where the multi model mean is greater than two standard deviations of internal variability and where 90% of models agree on the sign of change (see Box 12.1). The number of CMIP5 models used is indicated in the upper right corner of each panel.

12.4.5.5 Extreme Events in the Water Cycle

In addition to the changes in the seasonal pattern of mean precipitation described above, the distribution of precipitation events is projected to *very likely* undergo profound changes (Boberg et al., 2010; Gutowski et al., 2007; Sun et al., 2007). At daily to weekly scales, a shift to more intense individual storms and fewer weak storms is projected (Seneviratne et al., 2012). At seasonal or longer time scales, increased evapotranspiration over land can lead to more frequent and more intense periods of agricultural drought.

A general relationship between changes in total precipitation and extreme precipitation does not exist (Seneviratne et al., 2012). Two possible mechanisms controlling short term extreme precipitation amounts are discussed at length in the literature and are similar to the thermodynamic and dynamical mechanisms detailed above for changes in average precipitation. The first considers that extreme precipitation events occur when most of the available atmospheric water vapour rapidly precipitates out in a single storm. If the maximum amount of water vapour air control is controlled by the Clausius-Clapeyron relationship, as air temperature increases, this amount of water also increases (Allan and Soden, 2008; Allen and Ingram, 2002; Kendon et al., 2010; Pall et al., 2007). Kunkel et al. (2012) examined the CMIP5 model RCP4.5 and 8.5 projections for changes in maximum water vapour concentrations, a principal factor controlling the probable bound on maximum precipitation, concluding that maximum water vapour changes are comparable to mean water vapour changes but that the potential for changes in dynamical factors are less compelling. Such increases in atmospheric water vapour are expected to increase the intensity of individual precipitation events, but have less impact on their occurrence. As a result projected increases in extreme precipitation may be more reliable than similar projections in mean precipitation in some regions (Kendon et al., 2010). A second mechanism for extreme precipitation put forth by O’Gorman and Schneider (2009a, 2009b) is that such events are controlled by anomalous horizontal moisture flux convergence and associated convective updrafts which would change in a more complicated fashion in a warmer world (Sugiyama et al., 2010). Emori and Brown (2005) showed that the thermodynamic mechanism dominated nearly everywhere outside the tropical warm pool. However, Li et al (2011a) found that both mechanisms contribute to extreme precipitation in a high-resolution aquaplanet model with updrafts as the controlling element in the tropics and air temperature controlling the mid latitudes consistent with (Chou et al., 2012). Additionally, Lenderink and Van Meijgaard (2008) found that very short extreme precipitation events increase at a rate twice the amount predicted by Clausius-Clapeyron scaling in a very high-resolution model over Europe suggesting that both mechanisms can interact jointly. Gastineau and Soden (2009) found in the CMIP3 models that the updrafts associated with the most extreme tropical precipitation events actually weaken despite an increase in the frequency of the heaviest rain rates further complicating simple mechanistic explanations. Mechanisms of natural variability are a large factor in assessing the robustness of these projections (Kendon et al., 2008). Projections of changes in future extreme precipitation may be larger at the regional scales than for future mean precipitation, but natural variability is also larger causing a tendency for signal-to-noise ratios to decrease when considering increasingly extreme metrics. However, mechanisms of natural variability still are a large factor in assessing the robustness of these projections (Kendon et al., 2008). In addition, large-scale circulation changes, which are uncertain, could dominate over the above mechanisms depending on the rarity and type of events considered. However, analysis of CMIP3 models suggests circulation changes are unlikely to be sufficient to offset the influence of increasing atmospheric water vapour on extreme precipitation change over Europe at least on large spatial scales (Kendon et al., 2010). An additional shift of the storm track has been shown in models with a better representation of the stratosphere, and this is found to lead to an enhanced increase in extreme rainfall over Europe in winter (Scaife et al., 2012).

What is considered extreme precipitation in one season at a particular place could be normal during a different season or in a different location. The term “extreme” depends very much on context and is often used in discussion of particular climate-related impacts (SREX, 2011, Box 3.1). Commonly used indices to address precipitation extremes summarize daily measurements into annual mean or seasonal quantities, like SDII, the simple daily intensity index, R95p, the annual mean total precipitation falling in wet days with amounts larger than the 95th quantile of the climatology, R5dmax, the annual maximum total precipitation in a pentad and CDD, the longest spell of consecutive dry days in the year. The definition of these indices aims for statistical robustness, applicability to a wide range of climates and a high signal-to-noise ratio together with a longer decorrelation scale in the spatial domain when compared to daily extremes definitions (Alexander et al., 2006). Consistently, climate models project future episodes of more intense precipitation in the wet seasons for most of the land areas, especially in the Northern Hemisphere and its higher latitudes, and the monsoon regions of the world, and at a global average scale. It is the case that the actual magnitude of the change is dependent on the model used, but there is strong agreement across the models over the direction of change (Chen and Knutson, 2008; Goubanova and Li, 2007; Haugen and Iversen, 2008; Kamiguchi et al., 2006; Kysely and Beranova, 2009; May, 2008b; Sillmann et al., 2012; Tebaldi et al., 2006). Regional details are less robust in terms of the relative magnitude of changes but remain in good accord across models in terms of the sign of the change and the large scale geographical patterns (CCSP_3.3, 2008; Meehl et al., 2005a). In semi-arid regions of the mid latitudes and subtropics like the Mediterranean, the southwest USA, south-western Australia, southern Africa and a large portion of South America, the

tendency manifested in the majority of model simulations is for longer dry periods and is consistent with the average decreases shown in Figure 12.22. Figure 12.26 shows projected percent changes in R5dmax, the annual maximum five-day precipitation accumulation over land regions obtained from the CMIP5 models. Globally averaged end of 21st century changes over land range from 5% (RCP2.6) to 20% (RCP8.5) more precipitation during very wet five day periods. Locally, the few regions where this index of extreme precipitation decreases in the late 21st century RCP8.5 projection coincide with areas of robust decreases in the mean precipitation of Figure 12.22.

[INSERT FIGURE 12.26 HERE]

Figure 12.26: Projected percent changes (relative to the AR4 1981–2000 baseline period) from the CMIP5 models in R5dmax, the annual maximum five-day precipitation accumulation a) Global average percent change over land regions for the RCP2.6, 4.5 and 8.5 scenarios. b) Percent change over the 2081–2100 period in the RCP8.5. Equal model weighting.

Truly rare precipitation events can cause very significant impacts. The statistics of these events at the tails of the precipitation distribution are well described by Extreme Value (EV) Theory although there are significant biases in the direct comparison of gridded model output and actual station data (Smith et al., 2009). There is also strong evidence that model resolution plays a key role in replicating EV quantities estimated from gridded observational data, suggesting that high-resolution models may provide somewhat more confident projection of changes in rare precipitation events (Fowler et al., 2007a; Wehner et al., 2011). Figure 12.27 shows the late 21st century changes per Kelvin (K) in local warming in twenty-year return values of annual maximum daily precipitation relative to the late 20th century (left) and the associated return periods of late 20th century twenty year return values at the end of the 21st century from the CMIP5 models. The global average of the CMIP5 multi-model median return value sensitivity is an increase of 5.3% per K (Kharin et al., 2012). The CMIP5 land average is close to the CMIP3 value of 4% per K reported by (Min et al., 2011) for a subset of CMIP3 models. The global average of return periods of late 20th century twenty year return values is reduced from 20 years to 14 years with reductions of 10–20% per K are projected over the large land masses of North America and larger reductions over wet tropical regions (Kharin et al., 2012). Reductions in return values (or equivalently, increases in return period) are confined to convergent oceanic regions where circulation changes have reduced the available water vapour.

[INSERT FIGURE 12.27 HERE]

Figure 10.27: Left: The average 2081–2100 CMIP5 multi-model ensemble median percent change in twenty year return values of annual maximum daily precipitation per 1 K of local warming relative to the 1986–2005 reference period. Right: The average 2081–2100 CMIP5 multi-model ensemble median of the return periods (years) of 1986–2005 twenty year return values of annual maximum daily precipitation corresponding to 1 K of local warming. Regions of no change would have return periods of twenty years.

12.4.6 Changes in Cryosphere

12.4.6.1 Changes in Sea Ice Cover

Based on the analysis of CMIP3 climate change simulations (e.g., Arzel et al., 2006; Zhang and Walsh, 2006), the AR4 concludes that the Arctic and Antarctic sea ice covers are projected to shrink in the 21st century under all SRES scenarios, with a rather large range of model responses (Meehl et al., 2007b). It also stresses that, in some projections, the Arctic Ocean becomes almost entirely ice-free in late summer during the second half of the 21st century. Those conclusions were confirmed by further analyses of the CMIP3 archives (e.g., Bracegirdle et al., 2008; Körper et al., 2012; Lefebvre and Goosse, 2008; NRC, 2011; Stroeve et al., 2007). Figures 12.28 and 12.29 and the studies of Stroeve et al. (2012), Wang and Overland (2012) and Massonnet et al. (2012) show that the CMIP5 AOGCMs and ESMs as a group also project long-term decreases in sea ice extent in both hemispheres under all RCPs. However, as for CMIP3, the inter-model spread is considerable.

[INSERT FIGURE 12.28 HERE]

Figure 12.28: Anomalies in sea ice extent (5-year running mean) as simulated by CMIP5 models over the late 20th century and the whole 21st century under RCP2.6, RCP4.5, RCP6.0 and RCP8.5 for (a) Northern Hemisphere February, (b) Northern Hemisphere September, (c) Southern Hemisphere February and (d) Southern Hemisphere September. The solid curves show the multi-model means and the shading denotes the 5–95% range of the ensemble. The vertical bar

marks the end of CMIP5 historical climate change simulations. One ensemble member per model is taken into account in the analysis. Sea ice extent is defined as the total oceanic area where sea ice concentration exceeds 15% and is calculated on the original model grids. Anomalies are relative to the reference period 1986–2005. The number of models is given in the legend. Also plotted (solid pink curves) are the satellite data of Comiso and Nishio (2008) over 1979–2011.

[INSERT FIGURE 12.29 HERE]

Figure 12.29: February and September CMIP5 multi-model mean sea ice concentrations (%) in the Northern and Southern Hemispheres for the periods (a) 1986–2005, (b) 2081–2100 under RCP4.5 and (c) 2081–2100 under RCP8.5. The model ice concentrations are interpolated onto a $1^\circ \times 1^\circ$ regular grid. One ensemble member per model is taken into account in the analysis. The number of models is given in parentheses. The pink lines show the observed 15% sea ice concentration limits averaged over 1986–2005 (Comiso and Nishio, 2008).

In the Northern Hemisphere, consistently with CMIP3 results, the absolute rate of decrease of the CMIP5 multi-model mean sea ice areal coverage is greatest in September. The reduction in sea ice extent between the time periods 2081–2100 and 1986–2005 for the CMIP5 multi-model average ranges from 39% for RCP2.6 to 94% for RCP8.5 in September and from 9% to 35% in February. About 90% (45%) of the CMIP5 models analysed reach nearly ice-free conditions (sea ice extent less than $1 \times 10^6 \text{ km}^2$) at the end of summer in the Arctic before 2100 under RCP8.5 (RCP4.5). By the end of the 21st century, the decrease in multi-model mean sea ice volume ranges from 58% for RCP2.6 to 97% for RCP8.5 in September and from 32% to 74% in February. These percentages are always much higher than the corresponding ones for ice extent in February, which is indicative of a substantial sea ice thinning.

A frequent criticism of the CMIP3 models is that, as a group, they strongly underestimate the fast decline in summer Arctic sea ice observed during the past few decades (e.g., Stroeve et al., 2007; Winton, 2011), which suggests that the CMIP3 Arctic sea ice projections might be too conservative. As shown in Chapter 9, although still underestimated, the magnitude of the CMIP5 multi-model mean trend in September Arctic sea ice extent over the satellite era is more consistent with the observed one (see also Massonnet et al., 2012; Stroeve et al., 2012; Wang and Overland, 2012). The too slow retreat of the summer Arctic sea ice in most CMIP3 and CMIP5 simulations may partly result from an underestimation of the sea ice sensitivity to global surface temperature (Mahlstein and Knutti, 2012). In a global warming context, this sensitivity seems to be critical for determining future ice losses because of the almost linear relationship that exists in climate change simulations between the annual mean or September mean Arctic sea ice extent and the annual mean global surface temperature change for ice extents larger than $\sim 1 \times 10^6 \text{ km}^2$ (e.g., Mahlstein and Knutti, 2012; NRC, 2011; Ridley et al., 2007; Winton, 2011; Zhang, 2010b). This relationship is illustrated in Figure 12.30 for both CMIP3 and CMIP5 models. From this figure, it can be seen that the sea ice sensitivity varies significantly from model to model and is generally larger and less scattered for CMIP5 models.

[INSERT FIGURE 12.30 HERE]

Figure 12.30: September Arctic sea ice extent as a function of the annual mean global surface temperature change with respect to the period 1986–2005 for (left) CMIP3 models (all SRES scenarios) and (right) CMIP5 models (all RCPs). The ice extents and global temperatures are computed on a common latitude-longitude grid for CMIP3 and on the original model grids for CMIP5. One ensemble member per model is taken into account in the analysis. A 21-year running mean is applied to the model output. The black circle on the y-axis shows the mean observed September Arctic sea ice extent over 1986–2005 (Comiso and Nishio, 2008).

A complete and detailed explanation for what controls the range of Arctic sea ice responses in models over the 21st century remains elusive, but the Arctic sea ice study provides an example where process-based constraints can be applied to model simulations (Collins et al., 2012; Overland et al., 2011). For CMIP3 models, results indicate that the changes in Arctic sea ice mass budget over the 21st century are linearly related to the mean late 20th century sea ice thickness distribution (Holland et al., 2010), average sea ice thickness (Bitz, 2008), fraction of thin ice cover (Boe et al., 2009a) and oceanic heat transport to the Arctic (Mahlstein and Knutti, 2011). For CMIP5 models, Massonnet et al. (2012) showed that the time needed for the September Arctic sea ice areal coverage to drop below a certain threshold is highly correlated with the September sea ice extent and annual mean ice volume averaged over the past several decades (12.31a-b). The timing of a seasonally ice-free Arctic Ocean or the fraction of remaining sea ice in September at any time during the 21st century were also found to be correlated with the past trend in September Arctic sea ice extent and the amplitude of the mean seasonal cycle of sea ice extent (Boe et al., 2009a; Collins et al., 2012;

Massonnet et al., 2012) (Figure 12.31c-d). All those empirical relationships can be understood on simple physical grounds (see the aforementioned references for details).

[INSERT FIGURE 12.31 HERE]

Figure 12.31: (a-d) First year during which the September Arctic sea ice extent falls below $1 \times 10^6 \text{ km}^2$ in CMIP5 climate projections (29 models, RCP8.5) as a function of (a) the September Arctic sea ice extent averaged over 1979–2010, (b) the annual mean Arctic sea ice volume averaged over 1979–2010, (c) the amplitude of the seasonal cycle of Arctic sea ice extent averaged over 1979–2010 and (d) the trend in September Arctic sea ice extent over 1979–2010. The sea ice variables shown are calculated on the original model grids. The correlations and one-tailed p -values are computed from the multi-member means for models with several ensemble members (coloured crosses), but the ensemble members of individual models are also depicted (coloured dots). (e) Time series of September Arctic sea ice extent (5-year running mean) as simulated by all CMIP5 models and their ensemble members under RCP8.5 (thin curves). The thick curves correspond to a subset of six CMIP5 models that meet criteria based on panels a-d and defined in Massonnet et al. (2012). Note that each of these selected models only provides one ensemble member.

These results lend support for weighting/recalibrating the models based on their present-day Arctic sea ice simulations. Today, the optimal approach for sea ice projections is not clear, although one notes that these methods should have a credible underlying physical basis in order to increase their reliability. In addition, they should account for the potentially large imprint of natural variability on both observations and model simulations when these two sources of information are to be compared (see Chapter 9). This latter point is particularly critical if the past sea ice trend or sensitivity is used as a metric given the relatively short observational period (Kay et al., 2011; Mahlstein and Knutti, 2012; Massonnet et al., 2012; Notz, 2012; Overland et al., 2011; Stroeve et al., 2012). A number of studies have applied such metrics to the CMIP3 and CMIP5 models. Stroeve et al. (2007) and Stroeve et al. (2012) rejected several CMIP3 and CMIP5 models, respectively, on the basis of their simulated mean late 20th century September Arctic sea ice extent. Wang and Overland (2009) selected a subset of CMIP3 models (and Wang and Overland (2012) did the same for the CMIP5 models) based on their fidelity to the observed mean seasonal cycle of Arctic sea ice extent in the late 20th century and then scaled the chosen models to the recently observed September sea ice extent. Zhang (2010b) retained a number of CMIP3 models based on the regression between summer sea ice loss and Arctic surface temperature change. Massonnet et al. (2012) selected a subset of CMIP5 models on the basis of the four relationships shown in Figure 12.31a-d. The outcome of their study is illustrated, as an example, in Figure 12.31e for RCP8.5. Boe et al. (2009a) and Mahlstein and Knutti (2012) did not perform a model selection but rather recalibrated the CMIP3 Arctic sea ice projections on available observations of September Arctic sea ice trend and sensitivity to global surface temperature change, respectively.

These various methods all suggest a faster rate of summer Arctic sea ice decline than the multi-model mean. However, they also lead to different timings for when the Arctic Ocean might become nearly ice-free in September. The following time intervals are obtained when combining all available studies: 2020–2100⁺ (2100⁺ = sometime after 2100) for the SRESA1B scenario and RCP4.5, with a best estimate in the range of 2035–2065 (Boe et al., 2009a; Massonnet et al., 2012; Stroeve et al., 2012; Wang and Overland, 2009; Wang and Overland, 2012; Zhang, 2010b), and 2020–2060 for RCP8.5, with a best estimate in the range of 2035–2050 (Massonnet et al., 2012; Wang and Overland, 2012). Mahlstein and Knutti (2012) encompassed the dependence on the forcing scenario by determining the annual mean global surface warming threshold for nearly ice-free conditions in September (see Chapter 9). Their best estimate of 2°C above present derived from both CMIP3 models and observations lies within the range of all CMIP5 projections (see right panel of Figure 12.30). This range is 1.9–2.5°C if only the models that satisfy at the same time the criteria of Massonnet et al. (2012), Stroeve et al. (2012) and Wang and Overland (2012) are considered.

In light of all those results, it is *very likely* that the Arctic sea ice cover will continue to shrink and thin during the 21st century. It is also *very likely* that the Arctic Ocean will become nearly ice-free in September before the end of the century for high greenhouse gas emissions such as those corresponding to RCP8.5. There is *high confidence* that the September Arctic sea ice will not survive a global warming larger than 2°C above present. A seasonally ice-free Arctic Ocean within the next 50 years is a very distinct possibility, although later dates cannot be ruled out. The potential irreversibility of the Arctic sea ice loss and the possibility of a rapid, nonlinear transition toward an ice-free Arctic Ocean are discussed in Section 12.5.5.7.

In the Southern Hemisphere, the decrease in sea ice extent between 2081–2100 and 1986–2005 projected by the CMIP5 models as a group varies from 14% for RCP2.6 to 57% for RCP8.5 in February and from 9% to

29% in September, with a large inter-model spread. Contrary to the Northern Hemisphere, the absolute rate of decline is greatest in wintertime. Eisenman et al. (2011) argue that this hemispheric asymmetry in the seasonality of sea ice loss is fundamentally related to the geometry of coastlines. For each forcing scenario, the relative changes in multi-model mean February and September Antarctic sea ice volumes by the end of the century are very similar to the corresponding ones in ice extent. About 75% (50%) of the CMIP5 models analysed reach a nearly ice-free state in February within this century under RCP8.5 (RCP4.5). For RCP8.5, only small portions of the Weddell and Ross Seas stay ice-covered in February during 2081–2100 in those models that do not project a seasonally ice-free Southern Ocean (see Figure 12.29).

As their CMIP3 counterparts, the majority of CMIP5 models exhibit a decreasing trend in Antarctic sea ice extent over the satellite era, in contrast to the weak observed increase (see Chapters 9 and 10; Mahlstein et al., 2012; Zunz et al., 2012). A large variation in the modelled trends is present, and a comparison of multiple ensemble members from the same model suggests a strong imprint of natural variability during the late 20th century and the first decade of the 21st century (e.g., Landrum et al., 2012; Mahlstein et al., 2012; Zunz et al., 2012). Furthermore, the summer and winter mean sea ice extents for present-day conditions differ significantly from one model to another, the reasons for all these discrepancies being unclear (see Chapters 9 and 10; Mahlstein et al., 2012; Zunz et al., 2012). In view of this, future changes in Southern Hemisphere sea ice remain uncertain.

12.4.6.2 Changes in Snow Cover and Frozen Ground

Excluding ice sheets and glaciers, analyses of seasonal snow cover changes generally focus on the Northern Hemisphere, where the configuration of the continents on Earth induces a larger maximum seasonal snow cover extent (SCE) and a larger sensitivity of SCE to climate changes. Seasonal snow cover extent (SCE) and snow water equivalent (SWE) respond to both temperature and precipitation. At the beginning and the end of the snow season, SCE decreases are closely linked to a shortening of the seasonal snow cover duration, while SWE is more sensitive to snowfall amount (Brown and Mote, 2009). Future widespread reductions of SCE, particularly in spring, are simulated by the CMIP3 models (Brown and Mote, 2009; Roesch, 2006) and confirmed by the CMIP5 ensemble (Brutel-Vuilmet et al., 2012). Projections for the change in annual maximum SWE are more mixed. Warming decreases SWE both by reducing the fraction of precipitation that falls as snow and by increasing snowmelt, but projected increases in precipitation over much of the northern high latitudes during winter months act to increase snow amounts. Whether snow covering the ground will become thicker or thinner depends on the balance between these competing factors. Both in the CMIP3 (Raisanen, 2008) and in the CMIP5 models (Brutel-Vuilmet et al., 2012), annual maximum SWE tends to increase or only marginally decrease in the coldest regions, while SWE decreases are strong closer to the southern limit of the seasonally snow-covered area. The Northern Hemisphere spring (March–April average) snow cover area changes are very coherent in the CMIP5 MMD. Relative to the 1986–2005 reference period, (Brutel-Vuilmet et al., 2012) report a weak decrease of about $7 \pm 4\%$ (one sigma inter-model dispersion) for RCP2.6 during the last two decades of the 21st century, while SCA decreases of about $13 \pm 4\%$ are simulated for RCP4.5, $15 \pm 6\%$ for RCP6.0, and $25 \pm 7\%$ for RCP8.5 (Figure 12.32).

[INSERT FIGURE 12.32 HERE]

Figure 12.32: Northern Hemisphere spring (March to April average) relative snow covered area (RSCA) in the CMIP5 MMD, obtained through dividing the simulated 5-year box smoothed spring snow covered area (SCA) by the simulated average spring SCA of 1986–2005 reference period. Blue: RCP2.6; Light blue: RCP4.5; Orange: RCP6.0; Red: RCP8.5. Thick lines: MMD average. Shading and thin dotted lines indicate the inter-model spread (one standard deviation).

The strong projected warming across the northern high latitudes in climate model simulations has implications for frozen ground. Recent projections of the extent of permafrost degradation continue to vary widely depending on the underlying climate forcing scenario and model physics, but virtually all of them indicate that a substantial amount of near-surface permafrost degradation and thaw depth deepening over much of the permafrost area will occur (Koven and Riley, 2012; Koven et al., 2011; Lawrence et al., 2012; Lawrence et al., 2008a; Saito et al., 2007; Slater and Lawrence, 2012). Permafrost degradation at greater depths naturally occurs much more slowly (Delisle, 2007), but very deep permafrost is less relevant as a component of the climate system. Climate models are beginning to represent permafrost physical processes and properties more accurately (Alexeev et al., 2007; Gouttevin et al., 2012; Koven et al., 2009; Lawrence et

al., 2008a; Nicolsky et al., 2007; Rinke et al., 2008). The projected changes in permafrost are a response not only to warming, but also to changes in snow conditions because snow properties and their seasonal evolution exert significant control on soil thermal state (Koven and Riley, 2012; Lawrence and Slater, 2010; Shkolnik et al., 2010; Zhang, 2005). Applying the surface frost index method (Nelson and Outcalt, 1987) to coupled climate model anomalies from the CMIP5 models (Slater and Lawrence, 2012) yields a reduction of the diagnosed 2080–2099 near-surface permafrost area (continuous plus discontinuous permafrost) by $37 \pm 11\%$ (RCP2.6), $51 \pm 13\%$ (RCP4.5), $58 \pm 13\%$ (RCP6.0), and $81 \pm 12\%$ (RCP8.5), compared to the 1986–2005 diagnosed near-surface permafrost area (Figure 12.33). The uncertainty range given here is the 1 sigma inter-model dispersion. Applying directly the model output to diagnose permafrost extent and its changes over the 21st century yields similar relative changes (Koven and Riley, 2012). In summary, there is a high agreement across CMIP5 and older model projections indicating substantial future near-surface permafrost degradation, with amplitude depending on the emission scenario and on the processes taken into account.

[INSERT FIGURE 12.33 HERE]

Figure 12.33: Northern hemisphere diagnosed near-surface permafrost area in the CMIP5 MMD following Nelson and Outcalt (1987) and using 20-year average monthly surface air temperatures and snow depths. Blue: RCP2.6; Light blue: RCP4.5; Orange: RCP6.0; Red: RCP8.5. Thick lines: MMD average. Shading and thin lines indicate the inter-model spread (one standard deviation).

12.4.7 Changes in the Ocean

12.4.7.1 Surface Temperature, Salinity and Ocean Heat Content

Projected increase of sea surface temperature (SST) over the next two decades is relatively insensitive to the emissions trajectory. However, projected outcomes diverge as the 21st century progresses. Changes in globally-averaged upper ocean heat content reflect changes in net global ocean surface heat fluxes. Recent observations compiled by Levitus et al. (2009) indicate that ocean heat content (OHC) has increased at a rate of $0.40 \times 10^{22} \text{ J yr}^{-1}$ since 1955 (see Sections 3.2.3 and 10.4.1), thereby accounting for upwards of 90% of the global energy change inventory since 1970 (see Box 3.1). As in the case for SST, the differences in projected OHC for different RCPs manifest themselves most profoundly as the century progresses. Subsurface warming is most pronounced where North Atlantic Deep Water forms in the Northern Hemisphere and Antarctic Intermediate Water forms in the Southern Hemisphere.

Durack and Wijffels (2010) examined trends in global sea surface salinity (SSS) changes over the period 1950–2008. Their analysis revealed strong, spatially-coherent, trends in SSS over much of the global ocean, with a pattern that bears “striking” resemblance to the climatological SSS field (see Sections 3.3.2.1 and 10.4.2). The CMIP5 climate model projections available suggest that high SSS subtropical regions that are dominated by net evaporation are typically getting more saline; lower SSS regions at high latitudes are typically getting fresher. They also suggest a continuation of this trend in the Atlantic where subtropical surface waters become more saline as the century progresses (Figure 12.34) (see also Terray et al., 2012).

[INSERT FIGURE 12.34 HERE]

Figure 12.34: Projected sea surface salinity differences 2081–2100 for RCP8.5 relative to 1986–2005 from CMIP5 models. Hatching indicates regions where the multi model mean is less than one standard deviation of internal variability. Stippling indicates regions where the multi model mean is greater than two standard deviations of internal variability and where 90% of the models agree on the sign of change (see Box 12.1). The number of CMIP5 models used is indicated in the upper right corner of each panel.

12.4.7.2 Atlantic Meridional Overturning

Almost all climate model projections reveal an increase of high latitude temperature and high latitude precipitation (Meehl et al., 2007b). Both of these effects tend to make the high latitude surface waters lighter and hence increase their stability. As seen in Figure 12.35, all models show a weakening of the Atlantic meridional overturning circulation (AMOC) over the course of the 21st century (see Section 12.5.5.2 for further analysis). Projected changes in the strength of the AMOC at high latitudes appear stronger in GFDL CM2.1 when density is used as a vertical coordinate instead of depth (Zhang, 2010a). Once the radiative forcing is stabilized, the AMOC recovers, but in some models to less than its preindustrial level. The recovery may include a significant overshoot if the anthropogenic radiative forcing is eliminated (Wu et al.,

2011). Gregory et al. (2005) found that for all eleven models analysed (six from CMIP2/3 and five EMICs), the AMOC reduction was caused more by changes in surface heat flux than changes in surface freshwater flux.

[INSERT FIGURE 12.35 HERE]

Figure 12.35: Multi model projections of Atlantic meridional overturning circulation (AMOC) strength at 30°N from 1850 through to the end of the RCP extensions. a) RCP2.6; b) RCP4.5; c) RCP6.0; d) RCP8.5. Results are based on a small number of CMIP5 models available. Curves show results from only the first member (r1i1p1) of the submitted ensemble of experiments.

12.4.7.3 Southern Ocean

A dominant and robust feature of the CMIP3 climate projections assessed in AR4 is the weaker surface warming at the end of the 21st century in the Southern Ocean area than at global scale. Furthermore, in response to the simulated southward shift and strengthening of the Southern Hemisphere mid-latitude westerlies, the Antarctic Circumpolar Current (ACC) moves southward in most of the climate projections analysed (Meehl et al., 2007b).

The additional analyses of the CMIP3 model output performed since the release of AR4 confirm and refine the earlier findings. The above-mentioned displacement and intensification of the mid-latitude westerlies enhances the warming between 40°S and 60°S from the surface to mid-depths (Fyfe et al., 2007; Sen Gupta et al., 2009). Part of this warming has been attributed to the southward translation of the Southern Ocean current system (Sen Gupta et al., 2009). Moreover, the wind changes influence the surface temperature through modifications of the latent and sensible heat fluxes, and because of a larger northward Ekman transport of relatively cold polar surface water. They also lead to a stronger upwelling that brings warm and salty deep water southward and upward, resulting in a subsurface salinity increase at mid-depths south of 50°S (Screen et al., 2010; Sen Gupta et al., 2009). Additionally, changes in the Southern Hemisphere oceanic circulation projected for the end of the 21st century include, in many models, a strengthening of subtropical gyres (Sen Gupta et al., 2009) together with a reduced subduction of Subantarctic Mode Water and Antarctic Intermediate Water (Downes et al., 2010). All those circulation changes must however be taken with caution as a number of studies suggest that oceanic mesoscale eddies, which are not explicitly resolved in models used for climate projections, might noticeably affect the ACC response to changes in zonal wind stress (Böning et al., 2008; Downes et al., 2011; Farneti and Gent, 2011; Farneti et al., 2010).

Overall, CMIP3 climate projections exhibit a decrease in mixed layer depth at southern mid- and high latitudes by the end of the 21st century. This feature is a consequence of the enhanced stratification resulting from surface warming and freshening, the latter characteristic being mainly observed south of 45°S (Capotondi et al., 2012; Lefebvre and Goosse, 2008; Sen Gupta et al., 2009). Despite large inter-model differences, there is a robust weakening of Antarctic Bottom Water (AABW) production and its northward outflow, which is consistent with the decrease in surface density and which in turn is manifest as a warming signal close to the Antarctic margin that reaches abyssal depths (Sen Gupta et al., 2009). However, mesoscale eddies may also be important in controlling the deep circulation of the Southern Ocean, bringing additional uncertainties in the changes of AABW circulation simulated by the non-eddy-resolving global climate models (Saenko et al., 2012). In the vicinity of the Antarctic ice sheet, CMIP3 models predict over the course of the 21st century an average warming of ~0.5°C at depths of 200–500 m for a mid-range increase in atmospheric greenhouse gas concentrations, which might seriously impact on the mass balance of ice shelves (Yin et al., 2011). In a recent study, Hellmer et al. (2012) showed with a regional model of the Southern Ocean driven by a range of climate projections conducted with HadCM3 that a redirection of the coastal current into the Filchner Trough and underneath the Filchner-Ronne Ice Shelf during the second half of the 21st century might yield a ~2°C warming in the deep southern ice shelf cavity that would enhance the average basal melting rate from 0.2 m yr⁻¹ to almost 4 m yr⁻¹.

So far, there have been very few analyses of CMIP5 climate projections focusing on the Southern Ocean. Ridley et al. (2012b) confirmed with the HadGEM2-ES ESM the large heat uptake by the Southern Ocean present in CMIP3 simulations (Sen Gupta et al., 2009). Meijers et al. (2012) found no dramatic change between CMIP5 and CMIP3 in the ACC response to warming scenarios. The CMIP5 inter-model range is reduced compared to the CMIP3 one, but the westerly winds appear less directly correlated with the ACC

response under climate warming, particularly the ACC core position. There is a strong correlation between the changes in ACC strength and position, with those models in which the ACC gets stronger (weaker) shifting their core southward (northward). In agreement with the CMIP3 assessment, subtropical gyres generally strengthen under RCP4.5 and RCP8.5, and all expand southward. The trend in ACC transport is highly correlated with the change in the northern and southern ACC boundaries, especially the southern one, with an increase in subpolar gyre northern extent very strongly correlated with reduced ACC transport. As in CMIP3 climate projections, an overall thinning of the Southern Ocean mixed layer is observed (Sallée et al., 2012b). Finally, Sallée et al. (2012a) reported a warming of all mode, intermediate and deep water masses down to below 2000 m in the Southern Ocean.

None of the CMIP3 and CMIP5 models include an interactive ice sheet component. When climate–ice sheet interactions are accounted for in an Earth system model of intermediate complexity under a $4 \times \text{CO}_2$ scenario, the melt water flux from the Antarctic ice sheet further reduces the surface density close to Antarctica and the AABW formation rate, which ultimately moderates the surface warming at high southern latitudes (Swingedouw et al., 2008). Nevertheless, in this study, this effect becomes significant only after more than one century

12.4.8 Changes Associated with Carbon Cycle Feedbacks and Vegetation Cover

Climate change may affect the global biogeochemical cycles changing the magnitude of the natural sources and sinks of major greenhouse gases. Numerous studies investigated the interactions between climate change and the carbon cycle (e.g., Friedlingstein et al., 2006), methane cycle (e.g., O'Connor et al., 2010), ozone (Cionni et al., 2011) or aerosols (e.g., Carslaw et al., 2010). Many CMIP5 ESMs now include a representation of the carbon cycle as well as atmospheric chemistry, allowing interactive projections of greenhouse gases (mainly CO_2 and O_3) and aerosols. With such models, projections account for the imposed changes in anthropogenic emissions, but also for changes in natural sources and sinks as they respond to changes in climate and atmospheric composition. If included in ESMs, the impact on projected concentration, radiative forcing and hence on climate can be quantified. Climate induced changes on the carbon cycle are assessed below, while changes in natural emissions of CH_4 and changes in chemistry are assessed in Chapter 6 and 11 respectively, and climate-aerosols interactions are assessed in Chapter 7.

12.4.8.1 Carbon Dioxide

As presented in Section 12.3, the CMIP5 experimental design includes, for the RCP8.5 scenario, experiments driven either by prescribed anthropogenic CO_2 emissions (E-driven) or concentration (C-driven). The historical and 21st century E-driven simulations allow evaluating the climate response of the Earth system when atmospheric CO_2 and the climate response are interactively being calculated by the ESMs. In such ESMs, the atmospheric CO_2 is calculated as the difference between the imposed anthropogenic emissions and the sum of land and ocean carbon uptakes. As most of these ESMs accounts for land use changes and their CO_2 emissions, the only external forcing is fossil fuel CO_2 emissions (along with all non- CO_2 forcings as in the C-driven RCP8.5 simulations). For a given ESM, the E-driven and C-driven simulations would show different climate projections if the simulated atmospheric CO_2 in the E-driven run is significantly different from the one prescribed for the C-driven runs. This would happen if the ESMs carbon cycle is different from the one simulated by MAGICC6, the model used to calculate the CMIP5 GHGs concentrations from the emissions for the four RCPs (Meinshausen et al., 2011c). Likewise, when driven by CO_2 concentration, the ESMs can calculate the fossil fuel CO_2 emissions that would be compatible with the prescribed atmospheric CO_2 trajectory, allowing comparison with the set of emissions initially estimated by the IAMs (Arora et al., 2011; Jones et al., 2012) (see Chapter 6).

Seven models (bcc-ccsm1, CanESM2, GFDL-ESM2, HadGem2-ES, IPSL-CM5A-LR, MPI-ESM-LR, and MIROC-ESM) reported the emission driven RCP85 simulation. Figure 12.36 shows the simulated atmospheric CO_2 and global average surface air temperature warming (relative to the 1986–2005 reference period) for the RCP8.5 E-driven simulations, compared to the C-driven simulations from the same seven models. Six of the seven models estimate a larger CO_2 concentration than the prescribed one. The multi models average CO_2 concentration by 2100 is 1002 ± 70 ppm, while the CO_2 concentration prescribed for the C-driven RCP8.5 is 941 ppm. Figure 12.36 also shows the range of atmospheric CO_2 projections when the MAGICC6 model, used to provide the RCP concentrations, is tuned to emulate combinations of climate

sensitivity uncertainty taken from 19 CMIP3 models and carbon cycle feedbacks uncertainty taken from 10 C⁴MIP models, generating 190 model simulations (Friedlingstein et al., 2012; Meinshausen et al., 2011a; Meinshausen et al., 2011b). The emulation of the CMIP3/C⁴MIP models shows an upper range of simulated CO₂ concentrations that is comparable to what obtained with the CMIP5 ESMs, with atmospheric concentration as high as 1150 ppm by 2100, i.e., more than 200 ppm above the prescribed CO₂ concentration. However, the lower estimates are significantly below the CMIP5 ESMs estimates.

Global warming simulated by the E-driven runs show higher upper ends than when atmospheric CO₂ is prescribed. For the seven models assessed here, the global surface temperature change (2081–2100 average relative to 1986–2005 average) ranges between 2.7°C and 4.7°C, with a multi-model average of 4.0°C ± 0.7°C for the C-driven simulations, while the E-driven simulations give a range of 2.7 to 5.6°C, with a multi-model average of 4.2°C ± 0.9°C, i.e., 5% larger than for the concentration driven runs. Two models CanESM2 and MIROC-ESM, have a strong warming amplification in the E-driven simulations, with an additional warming of 0.45°C (10%) and 0.9°C (19%) respectively (Friedlingstein et al., 2012).

[INSERT FIGURE 12.36 HERE]

Figure 12.36: Comparison between CMIP5 ESMs simulations for RCP8.5 with CO₂ emissions (black) or CO₂ concentration (red) as external forcing for a) atmospheric CO₂ concentration (ppm), and b) global average surface air temperature difference (°C). Range of c) CO₂ concentrations and d) global average surface air temperature difference (°C) simulated by the MAGICC6 model when emulating the CMIP3 models climate sensitivity range and the C⁴MIP models carbon cycle feedbacks.

Comparing the relative contribution of carbon-cycle processes with other contributions such as climate sensitivity uncertainty is not straightforward. Huntingford et al. (2009) used a simple model to characterize the relative role of carbon cycle and climate sensitivity uncertainties in contributing to the range of future temperature changes, concluding that the range of carbon cycle processes represent about 40% of the physical feedbacks. Perturbed parameter ensembles systematically explore land carbon cycle parameter uncertainty and illustrate that a wide range of carbon cycle responses are consistent with the same underlying model structures and plausible parameter ranges (Booth et al., 2012). Figure 12.37 shows how the comparable range of future climate change (SRES A1B) arises from parametric uncertainty in land carbon cycle and atmospheric feedbacks. The same ensemble shows that the range of atmospheric CO₂ in the land carbon cycle ensemble is wider than the range of business as usual concentrations when carbon cycle uncertainties are neglected.

[INSERT FIGURE 12.37 HERE]

Figure 12.37: Uncertainty in global mean temperature from HadCM3 results exploring atmospheric physics and terrestrial carbon cycle parameter perturbations (Booth et al., 2012; Murphy et al., 2004). Relative uncertainties in the Perturbed Carbon Cycle (PCC, green plume) and Perturbed Atmospheric Processes (PAP, blue) on global mean anomalies of temperature (plotted with respect to the 1980–1999 period). The green/blue hatching illustrates where these two ensembles overlap. The standard simulations from the two ensembles, HadCM3 (black solid) and HadCM3C (black dashed) are also shown. Four bars are shown on the right illustrating the 2100 temperature anomalies associated with the CMIP3/AR4 ensemble (black) the PAP ensemble (blue) the land carbon cycle (PCC) and the weighted land carbon ensemble wPCC (both green). The range (thin line), 10th–90th (medium line) and 25th–75th (thick line) and 50th percentiles (central bar) are all shown.

12.4.8.2 Changes in Vegetation Cover

Vegetation cover can also be affected by climate change, with forest cover potentially being decreasing (e.g., in the tropics) or increasing (e.g., in high latitudes). In particular, the Amazon forest has been the subject of several studies, generally agreeing that future climate change would increase the risk tropical Amazon forest being replaced by seasonal forest or even savannah (Huntingford et al., 2008; Jones et al., 2009; Malhi et al., 2009). Increase in atmospheric CO₂ would only partly reduce such risk, through increase in water efficiency under elevated CO₂ (Malhi et al., 2009).

CMIP5 ESMs also include human induced land cover changes (deforestation, reforestation) affecting the climate system through changes in land surface physical properties (Hurtt et al., 2011). Future changes in land cover will have an impact on the climate system through biophysical and biogeochemical processes (e.g., Pongratz et al., 2010). Biophysical processes include change in surface albedo and changes in

partitioning between latent and sensible heat, while biogeochemical feedbacks essentially include change in CO₂ sources and sinks but could potentially also include changes in N₂O or CH₄ emissions. The biophysical response to future land cover changes has been investigated within the SRES scenarios. Using the SRES A2 2100 land cover, (Davin et al., 2007) simulated a global cooling of 0.14 K largely driven by change in albedo. Regional analyses have been performed in order to quantify the biophysical impact of biofuels plantation generally finding a local to regional cooling when annual crops are being replaced by bioenergy crops (such as sugar cane) (Georgescu et al., 2011; Loarie et al., 2011).

In the context of the LUCID activity (Pitman et al., 2009) ESMs performed additional simulations in order to separate the biophysical from the biogeochemical effects of land-use changes in the RCP scenarios. The LUCID-CMIP5 experiments were designed to complement RCP8.5 and RCP2.6 simulations of CMIP5. The analysis was focused on a difference in climate and land-atmosphere fluxes between the average of ensemble of simulations with- and without land-use changes by the end of 21st century (Brovkin et al., 2012). Due to different interpretation of land-use classes, areas of crops and pastures were specific for each ESM (Figure 12.38, left). On the global scale, simulated biogeophysical effects of land-use changes projected in the CMIP5 experiments with prescribed CO₂ concentrations were not significant. However, these effects were significant for regions with land-use changes >10%. Two out of five participated models, MIROC and HadGEM2, reveal statistically significant changes in regional mean annual mean surface air temperature for the RCP2.6 scenario (Figure 12.38, right). Changes in land surface albedo, available energy, latent and sensible heat fluxes were small but significant in most of ESMs for regions with substantial land-use changes. The scale of climatic effects reflects a small magnitude of land-use changes in the RCP2.6 and 8.5 scenarios and their limitation mainly to the tropical and subtropical regions where differences between biogeophysical effects of forests and grasslands are less pronounced than in mid- and high latitudes. The importance of climatic effect of land-use changes is higher for the RCP2.6 scenario with low CO₂ forcing which considers expansion of biofuel croplands as a climate mitigation option.

[INSERT FIGURE 12.38 HERE]

Figure 12.38: Impact of land-use change on surface temperature. LUCID experiments where 4 ESMs (MPI-ESM-LR, CanESM2, MIROC-ESM and HadGEM2-ES) were forced with and without land-use change beyond 2005 under the RCP2.6 scenario. Left maps show the change in crop and pasture fractions due to the absence of future land-use as implemented in the four ESMs. Right maps show the difference in near surface temperature difference between the simulation with- and without land use change beyond 2005 (Brovkin et al., 2012). The differences are averaged for years 2071–2100; only statistically significant changes ($p < 0.05$) are plotted

12.4.9 Consistency and Main Differences Between CMIP3/CMIP5 and SRES/RCPs

In the experiments collected under CMIP5, both models and scenario have changed with respect to CMIP3 making a comparison with earlier results and the scientific literature they generated (on which some of this chapter's content is still based) complex. The set of models used in AR4 (the CMIP3 models) have been superseded by the new CMIP5 models (Table 12.1, Chapter 9) and the SRES scenarios have been replaced by four RCPs (Section 12.3.1). In addition, the baseline period used to compute anomalies has advanced 6 years, from 1980–1999 to 1986–2005.

It would be extremely costly computationally to rerun the full CMIP3 ensemble under the new RCPs and/or the full CMIP5 ensemble under the old SRES scenarios in order to separate model and scenario effects. In the absence of a direct comparison, we rely on simplified modelling frameworks to emulate CMIP3/5 SRES/RCP model behavior and compare them. Figure 12.39 shows an emulation of the global mean temperature response at the end of the 21st century that we would expect from the CMIP5 models if they were run under SRES A1B. In this case, anomalies are computed with respect to 1980–1999 for direct comparison with the values reported in AR4, which used that baseline. The method used to emulate the SRES A1B response of the CMIP5 is documented in (Good et al., 2011a; Good et al., 2011b). Ensemble-mean A1B radiative forcing was computed from CMIP3 projections using the (Forster and Taylor, 2006) method, scaled to ensure consistency with the forcing required by the method. The scaling factor was derived linear regression of forcing from the two methods calculated for RCP4.5 and RCP8.5. The simple model is only used to predict the temperature difference between A1B and RCP8.5, and between A1B and RCP4.5 separately for each model. These differences are then added to CMIP5 GCM simulations of RCP8.5 and RCP4.5 respectively, and averaged to give a single A1B estimate. The emulated CMIP5 SRES A1B results show a slightly larger mean response than the actual CMIP3 models, with a similar spread (± 1 standard

deviation in this case). The main reasons for this is the slightly larger mean Transient Climate Response (TCR) in the subset of CMIP5 models available in comparison with the AR4 CMIP3 models. An alternative emulation is presented by Knutti and Sedláček (2012) who use the simplified MAGICC models with parameters chosen to emulate the response of the CMIP3 models to RCP6.0 forcing, with anomalies expressed with respect to the 1986–2005 baseline period (Figure 12.39). They too find a slightly large mean response in the CMIP5 case but also a larger spread (± 1 standard deviation) in CMIP5. Uncertainties in the different approaches to emulating climate model simulations, for example estimating the non-greenhouse gas radiative forcing, and the small sample sizes of CMIP3 and CMIP5 make it difficult to draw conclusions on the statistical significance of the differences displayed in Figure 12.39, but the same uncertainties leads us to conclude that on the basis of these analyses there appears to be no fundamental difference between the behaviour of the CMIP5 ensemble, in comparison with CMIP3.

[INSERT FIGURE 12.39 HERE]

Figure 12.39: Global mean temperature anomalies at the end of the 21st century (2080–2099) from GCM experiments and emulators comparing CMIP3/CMIP5 responses under SRES A1B and RCP6.0. The boxes and whiskers indicate minimum, mean value – 1 standard deviation, mean, mean value + 1 standard deviation and maximum values. The emulated SRES A1B projections of CMIP5 are obtained by the method of Good et al. (2011b) and are expressed with respect to the AR4 baseline period of 1980–1999. (Because of the method, the subset of CMIP5 that are emulated are restricted to those with preindustrial control, abrupt $4 \times \text{CO}_2$, historical, RCP4.5 and RCP8.5 simulations). The emulated RCP6.0 projections of CMIP3 are from Knutti and Sedláček (2012) obtained using the method of Meinshausen et al. (2011a; 2011c) and are expressed with respect to the AR5 baseline period of 1986–2005.

Meinshausen et al. (2011a; 2011b) tuned MAGICC6 to emulate 19 GCMs from CMIP3. The results are temperature projections and their uncertainties (based on the empirical distribution of the ensemble) under each of the RCPs, extended to year 2500 (under constant emissions for the lowest RCP and constant concentrations for the remaining three). In the same paper, an ensemble produced by combining carbon cycle parameter calibration to nine C⁴MIP models with the 19 CMIP3 model parameter calibrations is also used to estimate the emissions implied by the various concentration pathways had the CMIP3 models included a carbon cycle component. Rogelj et al., (2012) use the same tool but perform a fully probabilistic analysis of the SRES and RCP scenarios using a parameter space that is consistent with CMIP3/C⁴MIP but a more general uncertainty characterization for key quantities like equilibrium climate sensitivity, similarly to the approach utilized in (Meinshausen et al., 2009). Observational or other historical constraints are also used in this study and the analysis is consistent with the overall assessment of sources and ranges of uncertainties for relevant quantities (equilibrium climate sensitivity above all) stemming from the AR4. Figure 12.40 summarizes results of this probabilistic comparison for global temperature. The RCPs span a large range of stabilization, mitigation and non-mitigation pathways and the resulting range of temperature changes are larger than those produced under SRES scenarios, which do not consider mitigation options. Emissions under RCP8.5 are highest and the resulting temperature changes likely range from 4.0°C to 6.1°C by 2100. The lowest RCP2.6 assumes significant mitigation and the global temperature change likely remains below 2°C.

[INSERT FIGURE 12.40 HERE]

Figure 12.40: Temperature projections for SRES scenarios and the RCPs. (a) Time-evolving temperature distributions (66% range) for the four RCPs computed with this study's ECS distribution and a model setup representing closely the carbon-cycle and climate system uncertainty estimates of the AR4 (grey areas). Median paths are drawn in yellow. Red shaded areas indicate time periods referred to in panel b. (b) Ranges of estimated average temperature increase between 2090 and 2099 for SRES scenarios and the RCPs respectively. Note that results are given both relative to 1980–1999 (left scale) and relative to pre-industrial (right scale). Yellow ranges indicate results of this study; other ranges show the AR4 estimates. Colour-coding of AR4 ranges is chosen to be consistent with the AR4.

Similar temperature change projections by the end of the 21st century are obtained under RCP8.5 and SRES A1FI, RCP6 and SRES B2 and RCP4.5 and SRES B1. There remain large differences though in the transient trajectories, with rates of change slower or faster for the different pairs. These differences can be traced back to the interplay of the (negative) short-term effect of sulphate aerosols and the (positive) effect of long-lived GHGs. Impact studies may be sensitive to the differences in these temporal profiles so care should be taken in approximating SRES with RCPs and vice versa.

While simple models can separate the effect of the scenarios and the model response, no studies are currently available that allow an attribution of the CMIP3-CMIP5 differences to changes in the transient climate response, the carbon cycle, and the inclusion of new processes (chemistry, land surface, vegetation). The fact that these sets of CMIP3 and CMIP5 experiments does not include emission-driven runs would suggest that differences in the representation of the carbon cycle are very unlikely to explain differences in the simulations, since the only effect of changes in the carbon cycle representation would affect the land surface, and thus would have only a minor effect on the climate response at the global scale.

Figure 12.41 shows a comparison of the patterns of warming and precipitation change from CMIP3 (using 23 models and three SRES scenarios) and CMIP5 (using 27 models and four RCPs), utilizing the pattern scaling methodology (Section 12.4.2). The geographic patterns of mean change are very similar across the two ensembles of models, with pattern correlations of 0.98 for temperature and 0.87 for precipitation changes. However there exist significant differences in the absolute values of the patterns, if not in their geographic shapes. A simple bootstrapping exercise that pooled together all models and scenarios and resampled 500 times the same numbers of models/scenarios divided into two groups, but without distinguishing CMIP3 from CMIP5 (and thus SRES from RCPs) allows to compute a measure of significance of the actual differences in the patterns. Stippling in Figure 12.41 marks the large regions where the difference is significant for temperature and precipitation patterns. The temperature pattern from CMIP5 shows significantly larger warming per °C of global average temperature change in the Northern Hemisphere and less warming per °C in the Southern Hemisphere compared to the corresponding pattern from CMIP3. For precipitation patterns, CMIP5 shows significantly larger increases per °C in the Northern Hemisphere and significantly larger decreases per °C in the Southern Hemisphere compared to CMIP3. Even in this case we do not have studies that allow tracing the source of these differences to specific changes in models' configurations, processes represented or scenarios run.

Knutti and Sedlacek (2012), may be at this point the only study that attempts to identify or rule out at least some of these sources. In the study, differences in model projections spread or its counterpart, robustness, between CMIP3 and CMIP5 are discussed, and it is shown that by comparing the behaviour of only a subset of 11 models, contributed to the two CMIPs by the same group of institutions, the robustness of CMIP5 versus that of CMIP3 actually decreases. This would suggest that differences are not necessarily due to a more advanced understanding and modelling of the climate by a new generation of models and the presence in the full CMIP5 ensemble of duplicates of the same model may be responsible, rather, for the enhanced robustness of multimodel projections.

[INSERT FIGURE 12.41 HERE]

Figure 12.41: Patterns of temperature (left column) and percent precipitation change (right column) by the end of the 21st century (2081–2100 vs 1986–2005), for the CMIP3 models average (first row) and CMIP5 models average (second row), scaled by the corresponding global average temperature changes.

12.5 Climate Change Beyond 2100, Commitment, Stabilization and Irreversibility

12.5.1 RCP Extensions

The CMIP5 intercomparison project includes simulations extending the four RCPs to the year 2300 (see Section 12.3.1). This allows exploring the longer-term climate response to idealized GHG and aerosols forcings (Meinshausen et al., 2011c). By 2300, global warming reaches $8.7 \pm 2.4^\circ\text{C}$ relative to 1986–2005 (multi model average plus minus one standard deviation across models) under the RCP8.5 where radiative forcing continue to increase, only stabilizing after 2250; $2.3 \pm 0.4^\circ\text{C}$ under the RCP4.5 with a constant radiative forcing beyond 2100; and 0.6 ± 0.4 under the RCP2.6. with a decrease in radiative forcing beyond 2100 (Figures 12.3 and 12.5).

EMICs simulations have been performed following the same CMIP5 protocol for historical and RCPs extended to 2300 (Zickfeld et al., 2012). These scenarios have been prolonged beyond 2300 to investigate longer-term commitment and irreversibility (see below). Projected warming and the reduction of the AMOC up to 2300 as simulated by the EMICs is comparable to the one simulated by the CMIP5 ESMs (Figure 12.42).

[INSERT FIGURE 12.42 HERE]

Figure 12.42: Atmospheric CO₂ forcing, b) projected global mean surface temperature warming and c) projected change in meridional overturning circulation, as simulated by 12 EMICs (Bern3D, CLIMBER 2, CLIMBER 3-a, DCESS, GENIE, IAPRASC, IGSM, LOVECLIM, MICOC3-LGM, MESMO, UMD and UVic) for the four RCPs up to 2300 (Zickfeld et al., 2012). A ten-year smoothing was applied.

12.5.2 Climate Change Commitment

Climate change commitment, the idea that the climate will change further after the forcing or emissions have been eliminated or held constant, has caught the attention of scientists and policy makers shortly before the completion of IPCC AR4 (Hansen et al., 2005a; Meehl et al., 2005b; Meehl et al., 2006; Wigley, 2005) (AR4 Section 10.7.1). However, the argument that the surface response would lag the radiative forcing due to the large thermal reservoir of the ocean in fact goes back much longer (Hansen et al., 1985; Hansen et al., 1984; Mitchell et al., 2000; Schlesinger, 1986; Siegenthaler and Oeschger, 1984; Wetherald et al., 2001). The discussion in this section is framed largely in terms of temperature change, but other changes in the climate system (e.g., precipitation) are closely related to changes in temperature (see Section 12.4.2). A summary of how past emissions relate to future warming is also given in FAQ 12.3.

The Earth system has multiple response timescales related to different thermal reservoirs. For a step change in forcing (instantaneous increase in the magnitude of the forcing and constant forcing after that), a large fraction of the total of the surface temperature response will be realized within years to a few decades (Brasseur and Roeckner, 2005; Knutti et al., 2008a; Murphy et al., 2009). The remaining response over centuries is controlled by the slow mixing of the energy perturbation into the ocean (Stouffer, 2004). The response timescale depends on the amount of ocean mixing and the strength of climate feedbacks, and is longer for higher climate sensitivity (Hansen et al., 1985; Knutti et al., 2005). The transient climate response is therefore smaller than the equilibrium response, in particular for high climate sensitivities. Delayed responses can also occur due to processes other than ocean warming, e.g., vegetation change (Jones et al., 2009) or ice sheet melt that continues long after the forcing has been stabilized (see Section 12.5.3.1).

Several forms of commitment are often discussed in the literature. The most common is the “constant composition commitment”, the warming that would occur after stabilizing all radiative constituents at a given year (for example 2000) levels. AOGCMs estimated a most likely value of about 0.6°C for 2100 (relative to 1980–1999, AR4 Section 12.7.1) or 0.3°C (range 0.1–0.7°C across CMIP3) relative to the year 2000 (Knutti et al., 2008a). A present-day composition commitment simulation is not part of CMIP5, so direct comparison with CMIP3 is not possible, however, the available CMIP5 results based on the RCP4.5 extension with constant radiative forcing (see Section 12.5.1) are consistent with those numbers, with an additional warming of about 0.5°C 200 years after stabilization of the forcing (Figure 12.5).

A measure of constant composition commitment is the fraction of realized warming which can be estimated as the ratio of the warming at a given time to the long-term equilibrium warming (e.g., Solomon et al., 2009; Stouffer, 2004) (see also Meehl et al., 2007b, Section 10.7.2). EMICs simulations have been performed with RCPs forcing up to 2300 prolonged until the end of the millennium with a constant forcing set at the value reached by 2300. When the forcing stabilizes, the fraction of realized warming is significantly below 1. However, the fraction of realized warming depends on the history of the forcing. For the RCP4.5 and 6.0 extension scenarios with stabilization early on in the future, it is about 75%; for the RCP2.6 and 8.5, with later on stabilization, it is about 85%; but for a 1% yr⁻¹ CO₂ increase to 2 × or 4 × CO₂ and constant forcing thereafter, or for an instantaneous forcing change, the fraction of realized warming is much smaller, about 40–70% at the time when the forcing is kept constant. It rises typically by 10% over the following century with stable forcing. Due to the long timescales in the deep ocean, full equilibrium is reached only after hundreds to thousands of years (Danabasoglu and Gent, 2009; Gregory et al., 2004; Hansen et al., 2011; Hansen et al., 1985; Held et al., 2010; Knutti et al., 2008a; Li et al., 2012a; Stouffer, 2004) (see also Meehl et al., 2007b, Section 10.7.2).

[INSERT FIGURE 12.43 HERE]

Figure 12.43: Atmospheric CO₂ forcing, b) projected global mean surface temperature warming and c) fraction of realized warming calculate as the ratio of global temperature change at a given time to the change averaged over the 2980–2999 time period, as simulated by 12 EMICs (Bern3D, CLIMBER 2, CLIMBER 3-a, DCESS, GENIE,

IAPRASC, IGSM, LOVECLIM, MICOC3-LGM, MESMO, UMD and UVic) for the 4 RCPs up to 2300 followed by a constant (2300 level) radiative forcing up to the year 3000 (Zickfeld et al., 2012). A ten-year smoothing was applied.

“Constant emission commitment” is the warming that would result from keeping anthropogenic emissions constant and is estimated for example at about 1–2.5°C by 2100 assuming constant (year 2010) emissions in the future, based on the MAGICC model calibrated to CMIP3 and C⁴MIP (Meinshausen et al., 2011a; Meinshausen et al., 2011b) (see FAQ 12.3).

Another form of commitment involves climate change when anthropogenic emissions are set to zero (“zero emission commitment”). Results from a variety of models ranging from EMICs (Eby et al., 2009; Friedlingstein et al., 2011; Matthews and Caldeira, 2008; Meehl et al., 2007b; Plattner et al., 2008; Solomon et al., 2009; Weaver et al., 2007) to ESMs (Frolicher and Joos, 2010; Gillett et al., 2011) show that abruptly switching CO₂ emissions to zero (keeping other forcings constant) results in approximately constant global temperature for several centuries onward. Those results indicate that past emissions commit us for hundreds of years to approximately the amount of warming that has already been realized. On near equilibrium timescales of a few centuries to about a millennium, the temperature response to CO₂ emissions is controlled by climate sensitivity (see Box 12.2) and the airborne fraction of CO₂ on these time-scales. After about a thousand years (i.e., near thermal equilibrium), approximately 20–30% of the cumulative anthropogenic carbon emissions still remain in the atmosphere (Archer et al., 2009; Frolicher and Joos, 2010; Montenegro et al., 2007; Plattner et al., 2008) and maintain a substantial temperature response long after emissions have ceased (Eby et al., 2009; Friedlingstein and Solomon, 2005; Frolicher and Joos, 2010; Hare and Meinshausen, 2006; Lowe et al., 2009; Matthews and Caldeira, 2008; Plattner et al., 2008; Solomon et al., 2009; Solomon et al., 2010; Weaver et al., 2007). In the transient phase, on a hundred to thousand year time scale, the approximately constant temperature results from a compensation of delayed commitment warming (Meehl et al., 2005b; Wigley, 2005) with the reduction in atmospheric CO₂ resulting mainly from deep ocean carbon uptake as well as the nonlinear dependence of radiative forcing on atmospheric CO₂ (Meehl et al., 2007b; Plattner et al., 2008; Solomon et al., 2009; Solomon et al., 2010). The commitment associated with past emissions depends, as mentioned above, on the value of climate sensitivity and CO₂ airborne fraction, but it also depends on the choices made for other radiative forcing constituents. In a CO₂ only case and for sensitivities near the most likely value of 3°C, the warming commitment is near zero or slightly negative. For high climate sensitivities, and in particular if aerosol emissions are eliminated at the same time, the commitment from past emission can be strongly positive, and is a superposition of a fast response to reduced aerosols emissions and a slow response associated with high climate sensitivities (Armour and Roe, 2011; Brasseur and Roeckner, 2005; Hare and Meinshausen, 2006; Knutti and Plattner, 2011) (see FAQ 12.3). All of the above studies support the conclusion that temperatures would decrease only slowly even for strong reductions or complete elimination of CO₂ emissions, and might even increase temporarily for an abrupt reduction of the short-lived aerosols (FAQ 12.3). The implications of this fact for climate stabilization are discussed in Section 12.5.4.

New EMICs simulations with zero emissions beyond 2300 confirm this behaviour (Figure 12.44) seen in many earlier studies (see above). Switching off all anthropogenic emissions in 2300 leads to a continuous slow decline of atmospheric CO₂, to a significantly slower decline of global temperature and to a continuous increase in ocean thermal expansion over the course of the millennium. Larger forcings induce longer delays before the Earth system would reach equilibrium. For RCP8.5, by year 3000 (700 years after emissions have ceased) global temperature only decreases by 1–2°C (relative to its peak value by 2300) and ocean thermal expansion has almost doubled (relative to 2300) and is still increasing (Zickfeld et al., 2012).

[INSERT FIGURE 12.44 HERE]

Figure 12.44: a) compatible anthropogenic CO₂ emissions, b) projected atmospheric CO₂ concentration, c) global mean surface temperature change and d) ocean thermal expansion, as simulated by six EMICs (Bern3D, DCESS, GENIE, IGSM, MESMO and UVic) for the four RCPs with all forcings included, assuming zero anthropogenic emissions after 2300 (Zickfeld et al., 2012) A 10-year smoothing was applied. The drop in temperature in 2300 is a result of eliminating short-lived forcings along with CO₂.

The previous paragraph discussed climate change commitment from greenhouse gases that have already been emitted. Another form of commitment refers to climate change associated with heat and carbon that has gone into the land surface and oceans. This would be relevant to the consequences of a one-time removal of all of the excess CO₂ in the atmosphere and is computed by taking a transient simulation and instantaneously

setting atmospheric CO₂ concentrations to initial (pre-industrial) values (Cao and Caldeira, 2010). In such an extreme case, there would be a net flux of CO₂ from the ocean and land surface to the atmosphere, releasing an amount of CO₂ representing about 30% of what was removed from the atmosphere. A related form investigates the consequences of an initial complete removal followed by sustained removal of any CO₂ returned to the atmosphere from the land surface and oceans, and is computed by setting atmospheric CO₂ concentrations to pre-industrial values and maintaining this concentration (Cao and Caldeira, 2010). In this case, only about one-tenth of the pre-existing temperature perturbation persisted for more than half of a century. A similar study performed with a GFDL AOGCM where forcing was instantaneously returned to its preindustrial value, found larger residual warming, up to 30% of the pre-existing warming (Held et al., 2010).

Several studies on commitment to past emissions have demonstrated that the persistence of warming is substantially longer than the lifetime of anthropogenic greenhouse gases themselves, as a result of non-linear absorption effects as well as the slow heat transfer into and out of the ocean. In much the same way as the warming to a step increase of forcing is delayed, the cooling after setting radiative forcing to zero is also delayed. Loss of excess heat from the ocean will lead to a positive surface air temperature anomaly for decades to centuries (Held et al., 2010; Solomon et al., 2010).

Beside the commitments described above, due to inertia intrinsic to the climate system, there are a range of different sources of inertia and hence commitments related the time-scales for energy system transitions (Grubb, 1997). These sources of inertia in energy system transitions can be thought of as leading to commitments in climate change. For example, Davis et al. (2010) estimated climate commitment of 1.3°C (range 1.1°C–1.4°C, relative to preindustrial) from existing CO₂-emitting devices under the assumption that the lifetimes of these devices would not be extended beyond normal.

A more general form of commitment is therefore the question of how much can realistically be avoided and how much warming we are committed to (Washington et al., 2009). These forms of commitment however are strongly based on political, economic and social assumptions that are outside the domain of IPCC WGI and are not further considered here.

12.5.3 Global Measures of Climate Sensitivity and Transient Response

12.5.3.1 Forcing and Response, Timescales of Feedbacks

Equilibrium climate sensitivity, transient climate response and climate feedbacks are useful concepts to characterize the response of a model to an external forcing perturbation. However, there are limitations to the concept of radiative forcing (Hansen et al., 2005b; Joshi et al., 2003; Shine et al., 2003; Stuber et al., 2005), and the separation of forcings and fast (or rapid) responses (e.g., clouds changing almost instantaneously as a result of CO₂ induced heating rates rather than as a response to the slower surface warming) is sometimes difficult (Andrews and Forster, 2008; Gregory and Webb, 2008). Equilibrium warming also depends on the type of forcing (Davin et al., 2007; Hansen et al., 2005b; Stott et al., 2003). Climate sensitivity is time or state dependent in some models (Boer et al., 2005; Colman and McAvaney, 2009; Colman and Power, 2010; Gregory et al., 2004; Senior and Mitchell, 2000), and in some but not all models climate sensitivity from a slab ocean version differs from that of coupled models or the effective climate sensitivity (see glossary) diagnosed from a transient coupled integration (Danabasoglu and Gent, 2009; Gregory et al., 2004; Li et al., 2012a). The cost of coupled AOGCMs is often prohibitively large to run simulations to full equilibrium, and only a few models have performed those (Danabasoglu and Gent, 2009; Gregory et al., 2004; Li et al., 2012a; Manabe and Stouffer, 1994; Voss and Mikolajewicz, 2001). Because of the time dependence of effective climate sensitivity, fitting simple models to AOGCMs over the first few centuries may lead to errors in the response on multi-century timescales. In the HadCM3 case the long term warming would be underestimated by 30% if extrapolated from the first century (Gregory et al., 2004), in other models the warming of the slab and coupled model is almost identical (Danabasoglu and Gent, 2009). The assumption that the response to different forcings is approximately additive appears to be justified for large scale temperature changes but limited for other quantities (Boer and Yu, 2003; Gillett et al., 2004; Jones et al., 2007; Meehl et al., 2004; Schaller et al., 2012; Sexton et al., 2003). A more complete discussion of the concept of equilibrium climate sensitivity and the limitations is given in Knutti and Hegerl (2008).

A number of recent studies suggest that equilibrium sensitivities determined from AOGCMs and recent warming trends may significantly underestimate the true Earth System Sensitivity (ESS) if equilibration on millennial timescales is considered (Hansen et al., 2008; Lunt et al., 2010; Pagani et al., 2010; Rohling and Members, 2012; Rohling et al., 2009). The argument is that slow feedbacks associated with vegetation changes and ice sheets have their own intrinsic long timescales and are not represented in most models (Jones et al., 2009). Additional feedbacks are mostly thought to be positive but negative feedbacks of smaller magnitude are also simulated (Goelzer et al., 2011; Swingedouw et al., 2008). The climate sensitivity of a model may therefore not reflect the sensitivity of the full Earth system because those feedback processes are not considered. Feedbacks determined in very different base state (e.g., the Last Glacial Maximum) differ from those in the current warm period (Rohling and Members, 2012), and relationships between observables and climate sensitivity are model dependent (Crucifix, 2006; Edwards et al., 2007; Hargreaves et al., 2007; Schneider von Deimling et al., 2006). Estimates of climate sensitivity based on paleoclimate archives (Hansen et al., 2008; Lunt et al., 2010; Pagani et al., 2010; Rohling and Members, 2012; Rohling et al., 2009), most but not all based on climate states colder than present, are therefore not necessarily representative for an estimate of climate sensitivity today. Also it is uncertain on which timescale some of those Earth system feedbacks would become significant.

Equilibrium climate sensitivity undoubtedly remains a key quantity that is useful to relate a change in greenhouse gases or other forcings to a global temperature change. But the above caveats imply that estimates based on past climate states very different from today, based on timescales different than those relevant for climate stabilization (e.g., estimates based on the eruption of Pinatubo), or based on forcings other than greenhouse gases (e.g., spatially non-uniform land cover changes, volcanic eruptions or solar forcing) may differ from the climate sensitivity measuring the climate feedbacks of the Earth system today, and that again may be different from the sensitivity of the Earth in a much warmer state on timescales of millennia. The transient climate response (TCR) and the transient climate response to cumulative carbon emissions (TCRE) are often more directly relevant to short term changes and emission reductions needed for stabilization (see section 12.5.4)

12.5.4 Climate Stabilization and Long-Term Climate Targets

This section discusses the relation between emissions and climate targets, in the context of the uncertainties characterizing both the transient and the equilibrium climate responses to emissions. ‘Climate targets’ considered here are both stabilizing temperature at a specified value and avoiding a warming beyond a predefined threshold. The latter idea of limiting peak warming is a more general concept than stabilization of temperature or atmospheric CO₂, and one that is more realistic than an exact climate stabilization which would require perpetual non-zero positive emissions to counteract the otherwise ineluctable long-term slow decrease in global temperature (Figure 12.44).

12.5.4.1 Background

The concept of stabilization is strongly linked to the ultimate objective of the UNFCCC, which is “to achieve [...] stabilization of greenhouse gas concentrations in the atmosphere at a level that would prevent dangerous anthropogenic interference with the climate system.” Recent policy discussions focused on a global temperature increase, rather than on greenhouse gas concentrations. The most prominent target currently supported is the 2°C temperature target, i.e., to limit global temperature increase relative to preindustrial times to below 2°C. The 2°C target has been used first by the European Union as a policy target in 1996 but can be traced further back (Jaeger and Jaeger, 2011; Randalls, 2010). Climate impacts however are geographically diverse and sector specific, and no objective threshold separates dangerous from acceptable interference. Some changes may be delayed or irreversible, and some impacts are likely to be beneficial. It is thus not possible to define a single critical threshold without making value judgments and assumptions about cost and benefit and about aggregating and comparing values today and in the future. Targets other than 2°C have been proposed (e.g., 1.5°C relative to preindustrial), or 350 ppm (Hansen et al., 2008), and the rate of change may also be important (e.g., for adaptation). This section does not advocate or defend any threshold, nor does it judge the economic or political feasibility of such goals, but simply assesses the implications of different illustrative climate targets on allowed carbon emissions, based on our current understanding of climate and carbon cycle feedbacks.

12.5.4.2 Constraints on Cumulative Carbon Emissions

The current radiative forcing from greenhouse gases maintained indefinitely would correspond to approximately 2°C warming. That however does not imply that the commitment from past emissions has already exceeded 2°C. Part of the positive radiative forcing is compensated by negative aerosol forcing, and stopping emissions would lead to a decrease in the greenhouse gas forcing.

The total amount of anthropogenic CO₂ released in the atmosphere (often termed cumulative carbon emission) is a good indicator of the atmospheric CO₂ concentration and hence of the global warming response. The ratio of global temperature change to total cumulative anthropogenic CO₂ emissions (transient and equilibrium climate response to carbon emissions) is relatively constant and independent of the scenario, but is model dependent as it depends on the model airborne fraction and climate sensitivity (Allen et al., 2009; Bowerman et al., 2011; Knutti and Plattner, 2011; Matthews and Caldeira, 2008; Matthews et al., 2009; Meinshausen et al., 2009; Zickfeld et al., 2009). This is consistent with an earlier study indicating that the global warming potential is approximately independent of the scenario (Caldeira and Kasting, 1993).

Assuming constant climate sensitivity and given carbon cycle feedbacks, long-term (several centuries to millennium) stabilization of global temperatures requires eventually the stabilization of atmospheric concentrations. This requires decreasing emissions to the level of natural carbon sinks, and eventually to near-zero (Allen et al., 2009; Friedlingstein et al., 2011; Gillett et al., 2011; Jones et al., 2006; Knutti and Plattner, 2011; Matthews and Caldeira, 2008; Matthews et al., 2009; Meehl et al., 2007b; Meinshausen et al., 2009; Plattner et al., 2008; Weaver et al., 2007; Zickfeld et al., 2009).

The relationships between cumulative emissions and temperature for various studies is shown in Figure 12.45. Note that some lines mark the evolution of temperature as a function of emissions over time while other panels show peak temperatures for different simulations. Also some models prescribe only CO₂ emissions while others use multi gas scenarios, and the time horizons differ. Not all numbers are therefore comparable. Matthews et al. (2009) estimated the transient climate response to emission (TCRE) as 1°C–2.1°C PgC^{−1} (TtC, or 10¹² metric tons of carbon) (5–95%) based on the C⁴MIP model range (Figure 12.45a). The ENSEMBLES E1 show a range of 1°C–4°C PgC^{−1} (scaled from 0.5°C–2°C for 0.5PgC, Figure 12.45c) (Johns et al., 2011). Rogelj et al. (2012) estimate a 5–95% range of about 1°C–2°C PgC^{−1} (Figure 12.45d) based on the MAGICC model calibrated to the C⁴MIP model range and the likely range of 2°C–4.5°C for climate sensitivity given in AR4. Allen et al. (2009) used a simple model and found 1.3°C–3.9°C PgC^{−1} (5–95%) for peak warming (Figure 12.45f). The EMICs TCRE simulations so far suggest a range of about 2°C–3.5°C PgC^{−1} (Figure 12.45g). The results by Meinshausen et al. (2009) confirm the approximate linearity between temperature and CO₂ emissions. Their results are difficult to compare due to the shorter time period considered, but the model was found to be consistent with that of Allen et al. (2009). Zickfeld et al. (2009), using an EMIC, find a best estimate of about 1.5°C PgC^{−1}. Gillett et al. (2012) find a range of 0.8–2.4 K PgC^{−1} in 12 CMIP5 models and derive an observationally constrained range of 0.8–2.1 K PgC^{−1}.

Expert judgement based on the available evidence therefore suggest that the transient climate response to cumulative carbon emission (TCRE) is *very likely* between 0.8°C–3.0°C PgC^{−1}, with a best estimate in the range of 1.5°C–2.0°C PgC^{−1}, for cumulative emissions less than 2 PgC until the time at which temperature peaks. Under these conditions, and for low to medium estimates of climate sensitivity, the TCRE is near identical to the peak climate response to cumulated carbon emissions. For high climate sensitivity, strong carbon cycle climate feedback or large cumulative emissions the peak warming can be delayed and the peak response may be different from TCRE, but is often poorly constrained by models and observations. The best estimate for TCRE is similar to other recent attempts to synthesize the available evidence (Matthews et al., 2011; NRC, 2011). The upper bound is more uncertain and there is less agreement across studies, but in general the results from various methods and models are consistent. The results by Schwartz et al. (2010) imply a much larger warming for the carbon emitted over the historical period. Those results are not based on a climate model and, are inconsistent with the rest of the literature (see above), and are contested by Knutti and Plattner (2011) for neglecting the relevant response timescales and combining an transient airborne fraction with an equilibrium climate sensitivity. Schwartz et al. (2012) in their response maintain that their conclusions are correct.

The TCRE can be compared to the temperature response to emissions on a timescale of about 1000 years after emission cease. This can be estimated from the likely range of equilibrium climate sensitivity (2°C – 4.5°C) and an airborne fraction after about 1000 years of $25 \pm 5\%$ (Archer et al., 2009). Again combining the extreme values would suggest a range of 0.8°C – 2.7°C PgC^{-1} with a best estimate of 1.5°C . The most likely warming estimated after 1000 years is slightly lower than the transient warming, consistent with small decrease of temperature seen in many simple models and EMICs after zeroing emissions (Armour and Roe, 2011; Meehl et al., 2007b; Plattner et al., 2008; Solomon et al., 2009) (see also FAQ 12.3, Figure1). However, this equilibrium estimate is based on feedbacks estimated for the present day climate. Climate and carbon cycle feedbacks increase substantially on long timescales and for high cumulative emissions (see Section 12.5.3.2), introducing large uncertainties in particular on the upper bound. Based on paleoclimate data and an analytical model, Goodwin et al. (2009) estimate a long term radiative forcing of 1.5 W m^{-2} for an emission of 1 PgC . For a best estimate of climate sensitivity of 3°C this corresponds to a warming of 1.2°C on millennial timescales, consistent with the climate carbon cycle models results discussed above.

The uncertainty in TCRE is caused by the uncertainty in the physical feedbacks and ocean heat uptake (reflected in TCR) and uncertainties in carbon cycle climate feedbacks (affecting the airborne fraction). TCRE only characterizes the warming due to CO_2 emissions, and contributions from non- CO_2 gases need to be considered separately when estimating likelihoods to stay below a temperature limit.

[INSERT FIGURE 12.45 HERE]

Figure 12.45: Global temperature change vs. cumulative emissions for different scenarios and models. a) Transient global temperature increase vs. cumulative carbon emissions for C⁴MIP (Matthews et al., 2009), b) maximum temperature increase until 2100 vs. cumulative Kyoto-gas emissions (CO_2 equivalent) (Meinshausen et al., 2009), c) as in panel a but for the ENSEMBLES E1 scenario (Johns et al., 2011), d) transient temperature increase for the RCP scenarios based on the MAGICC model constrained to C⁴MIP, observed warming, and the IPCC AR4 climate sensitivity range (Rogelj et al., 2012), e) transient temperature change from the CMIP5 $1\% \text{ yr}^{-1}$ simulations, f) peak CO_2 induced warming vs. cumulative CO_2 emissions to 2200 (Allen et al., 2009; Bowerman et al., 2011), g) transient temperature increase from the new EMIC simulations (Eby et al., 2012) and g) transient temperature change from the CMIP5 RCP8.5 simulations (note that warming is higher in this case due to other forcings).

[START BOX 12.2 HERE]

Box 12.2: Equilibrium Climate Sensitivity and Transient Climate Response

Equilibrium climate sensitivity (defined as the equilibrium change in global surface temperature following a doubling of the atmospheric equivalent CO_2 concentration, see glossary) and the transient climate response (TCR, the change in global surface temperature in a global coupled climate model in a $1\% \text{ yr}^{-1}$ CO_2 increase experiment at the time of CO_2 doubling, see glossary) can be estimated based on feedback analysis in climate models (see Section 9.7.2.2), the patterns of mean climate and variability in models compared to observations (Section 9.7.3.3), and on the basis of the past behaviour of temperature fluctuations as reconstructed from paleoclimate archives, or observed and modelled short term perturbations of the energy balance like those caused by the Pinatubo eruption, and the observed surface and ocean temperature trends since preindustrial (see Section 10.9.3). Some studies estimate the “transient climate response” (Gregory and Forster, 2008; Padilla et al., 2011; Schwartz, 2012) as the ratio of global temperature change to radiative forcing. Those are scaled by the radiative forcing of $2 \times \text{CO}_2$ (3.7 W m^{-2}) to be comparable to TCR.

Newer studies of the observed 20th century warming, based on simple and intermediate complexity models, improved statistical methods, and several different and newer datasets, as assessed in detail in the sections listed above, largely confirm earlier studies showing that climate sensitivity is likely in the 2°C – 4.5°C range. Results based on shorter climate variations and paleoclimate evidence are consistent with those ranges, and sometimes more narrow, but make stronger structural assumptions. A few studies argued for low values of climate sensitivity, but almost all of them have received criticism in the literature (see Knutti and Hegerl (2008) and references therein). A summary of published ranges and PDFs of climate sensitivity is given in Box 12.2, Figure 1. Distributions and ranges for the transient climate response are shown in Box 12.2, Figure 2.

[INSERT BOX 12.2, FIGURE 1 HERE]

Box 12.2, Figure 1: Probability density functions, distributions and ranges for equilibrium climate sensitivity, based on Figure 10.19b plus climatological constraints shown in IPCC AR4 Box 12.2 Figure 1. See Figure 10.19b for details.

[INSERT BOX 12.2, FIGURE 2 HERE]

Box 12.2, Figure 2: Probability density functions, distributions and ranges (5–95%) for the transient climate response from different studies. See Figure 10.19a for details.

Combining information from different constraints from the observed warming trends, volcanic eruptions, model climatology, and paleoclimate, e.g., by using a distribution obtained from the Last Glacial Maximum as a prior for the 20th century analysis, yields a more narrow range for climate sensitivity (Annan and Hargreaves, 2006; Annan and Hargreaves, 2011a; Hegerl et al., 2006; Schmittner et al., 2011). However, those methods are sensitive to the assumptions on the independence of the various lines of evidence, the possibility of shared biases in models or feedback estimates (Lemoine, 2010), and the assumption that each individual line of evidence is unbiased. The assessed literature provides no consensus on a formal statistical method to combine different lines of evidence. All methods in general are sensitive to the assumed prior distributions (Annan and Hargreaves, 2011a; Frame et al., 2005; Hegerl et al., 2006; Tomassini et al., 2007). Annan and Hargreaves (2011a) criticize the use of uniform priors and argue that sensitivities above 4.5°C are extremely unlikely (<5%). Similar results have been obtained by other studies (Olson et al., 2012; Sokolov et al., 2010a; Urban and Keller, 2009). On the other hand fourteen experts in a recent expert elicitation on average allocate a probability of 22% to sensitivities above 4.5°C (Zickfeld et al., 2010), indicating still little consensus on the probability for high climate sensitivity.

Despite considerable advances in climate models and in understanding and quantifying climate feedbacks, the assessed literature still supports the conclusion from AR4 that climate sensitivity is *likely* in the range 2°C–4.5°C, and *very likely* above 1.5°C. The most likely value remains near 3°C. An ECS greater about 6°C–7°C is *very unlikely*. This last assessment is an expert judgment informed by several lines of evidence. First, the comprehensive climate models used in the CMIP exercises continue to produce an ECS range of 2.1°C–4.7°C (Section 9.7.2.1). Second, those perturbed-parameter model versions that show a very high ECS are generally less compelling in their representation of the present climate system (Section 9.7.3.3). Third, there is increasing evidence that the adjusted aerosol forcing of the twentieth century is not strongly negative (Chapter 7), which makes it unlikely that the observed warming was caused by a very small net forcing together with very large ECS. And fourth, multiple and at least partly independent observational constraints from the satellite period, instrumental period and palaeoclimate studies continue to yield very low probabilities for ECS beyond 7°C. On timescales of many centuries and longer, however, additional feedback with their own intrinsic timescales (e.g., vegetation, ice sheets) (Goelzer et al., 2011; Jones et al., 2009) may become important but are not usually modeled. The resulting Earth System Sensitivity (ESS) is less well constrained but likely to be larger than ECS (Hansen et al., 2008; Lunt et al., 2010; Pagani et al., 2010; Rohling and Members, 2012; Rohling et al., 2009), implying that lower atmospheric CO₂ concentrations are needed to meet a given temperature target. A number of caveats however apply to those studies (see Section 12.5.3.1). Those long-term feedbacks have their own intrinsic timescales, and are less likely to be proportional to global mean temperature change.

A number of papers (Frame et al., 2005; Held et al., 2010; Lorenz et al., 2012) have noted that for scenarios other than indefinite stabilisation of atmospheric greenhouse gas concentrations, TCR is a more accurate and hence useful indicator of future climate than ECS. The assessment suggests that the transient climate response (TCR) is very likely in the range 1°C–3°C, *likely* in the range 1.2°C–2.6°C estimated from CMIP5 (5–95%), with a most likely value near 1.8°C, based on the observed global changes in surface temperature, ocean heat uptake and radiative forcing, the detection/attribution studies identifying the response patterns to increasing greenhouse gas concentrations (Section 10.8.1), and the results of CMIP3/5 (Chapter 9). Estimating TCR is partly limited by the difficulty in accurately estimating the current disequilibrium of the Earth, but suffers from fewer difficulties in terms of time-dependent feedbacks (see Section 12.5.3.1). The assessment of both ECS and TCR is supported by several different and partly independent lines of evidence, each based on multiple studies, models and datasets.

For climate stabilization, the allowed cumulative carbon emissions are another useful metric relating directly CO₂ emissions to temperature. It considers carbon cycle feedbacks and uncertainties, but not additional feedbacks associated for example with the release of methane hydrates or large amounts of carbon from

permafrost (see Section 12.5.4, FAQ 12.3). The assessment suggests that the transient climate response to cumulative carbon emission (TCRE) is *very likely* between 0.8°C – 3°C PgC^{-1} (10^{12} metric tons of carbon), with a best estimate in the range of 1.5°C – 2.0°C PgC^{-1} , for cumulative emissions less than 2 PgC until the time at which temperatures peak. Under these conditions, and for low to medium estimates of climate sensitivity, the TCRE is near identical to the peak climate response to cumulated carbon emissions. TCRE has the advantage of directly relating temperature change to emissions, but as a result of combining the uncertainty in both TCR and the carbon cycle response, it is also similarly uncertain.

[END BOX 12.2 HERE]

12.5.4.3 Limitations and Conclusions

One general limitation is that stabilization of global temperature does not imply stabilization for all aspects of the climate system. For example, some models find significant hysteresis behaviour in the global water cycle, because global precipitation depends on both atmospheric CO_2 and temperature (Wu et al., 2010). Processes related to vegetation change (Jones et al., 2009) or changes in the ice sheets (Charbit et al., 2008; Ridley et al., 2010) as well as ocean acidification, deep ocean warming and associated sea level rise (Meehl et al., 2005b; Wigley, 2005) and potential feedbacks linking for example ocean and the ice sheets (Gillett et al., 2011; Goelzer et al., 2011) have their own intrinsic long timescales. Those may result in significant changes hundreds to thousands of years after global temperature is stabilized.

The simplicity of the concept of a cumulative carbon budget makes it attractive for policy (WBGU, 2009). Higher emissions in earlier decades simply imply lower emissions by the same amount later on. This is illustrated based on the RCP2.6 scenario in Figure 12.46a/b. Two idealized emission pathways with initially higher emissions (even sustained at high level for a decade in one case) lead to the same warming if emissions are then reduced much more rapidly. Even a step-wise emission pathway with levels constant at 2010 and zero near mid-century leads to a similar temperature evolution as they all have identical cumulative emissions. However, there are also limitations to the concept of a cumulative carbon budget. First, the ratio of global temperature and cumulative carbon is only approximately constant. It is the result of an interplay of several compensating carbon cycle and climate feedback processes, which operate at different timescales. Second, the ratio strongly depends on the model's climate sensitivity and carbon cycle feedbacks, thus the allowed emissions for a given temperature target are uncertain (see Figure 12.43) (Knutti and Plattner, 2011; Matthews et al., 2009). Third, non- CO_2 forcing constituents are important, which requires either assumptions on how CO_2 emission reductions are linked to changes in other forcings (Meinshausen et al., 2006; Meinshausen et al., 2009), or separate emission budgets for short lived and long lived gases. So far, most studies ignored non- CO_2 altogether. Those that consider them find non-negligible effects in particular for abrupt reductions in emissions of short-lived species (Armour and Roe, 2011; Brasseur and Roeckner, 2005; Hare and Meinshausen, 2006; Tanaka and Raddatz, 2011) (see also FAQ 12.3). Fourth, most models do not consider the possibility that long term feedbacks (Hansen et al., 2007; Knutti and Hegerl, 2008) may be different (see Section 12.5.3.1). Despite the fact that stabilization refers to equilibrium, the results assessed here are primarily relevant for the next few centuries and may differ for millennial scales. Finally, the concept of cumulative carbon implies that higher initial emissions can be compensated by a faster decline in emissions later or by negative emissions. However, in the real world short-term and long term goals are not independent and mitigation rates are limited by economic constraints and existing infrastructure (Davis et al., 2010; Friedlingstein et al., 2011; Meinshausen et al., 2009; Mignone et al., 2008; Rive et al., 2007). Likewise, assuming a cumulative carbon budget that requires negative emissions at a later stage will imply a temporary overshoot of a given target. An updated analysis of 193 published emission pathways with an energy balance model (Rogelj et al., 2011; UNEP, 2010) is shown in Figure 12.46c/d. Those emission pathways that likely limit warming below 2°C (above pre-industrial) by 2100 show emission of about 31–46 $\text{GtCO}_2\text{-eq yr}^{-1}$ and 17–23 $\text{GtCO}_2\text{-eq yr}^{-1}$ by 2020 and 2050, respectively. Median 2010 emissions of all models are 48 $\text{GtCO}_2\text{-eq/yr}$. Note that, as opposed to 12.47a/b, these scenarios still have positive emissions by 2100, implying that the warming would probably exceed the target in the longer-term. In cumulative terms, the best estimate for the transient climate response to cumulative carbon emissions (TCRE, 1.5°C – 2.0°C PgC^{-1}), implies a most likely value for the cumulative budget compatible with stabilization at 2°C of about 1000–1300 GtC , of which about 520 GtC have been emitted by 2011. It is important to note that the cumulative budget constraint does not consider non- CO_2 forcings. Also, since those ranges are based on a set of scenarios available in the literature the interpretation in terms of likelihood is difficult.

[INSERT FIGURE 12.46 HERE]

Figure 12.46: a) CO₂ emissions for the RCP3PD scenario (black) and three illustrative modified emission pathways leading to the same warming, b) global temperature change relative to preindustrial for the pathways shown in panel a. c) Coloured bands show IAM emission pathways over the twenty-first century. The pathways were grouped based on ranges of “likely” avoided temperature increase in the 21st century. Pathways in the yellow, orange and red bands likely stay below 2°C, 3°C, 4°C by 2100, respectively, while those in the purple band are higher than that. Emission corridors were defined by, at each year, identifying the 20th to 80th percentile range of emissions and drawing the corresponding coloured bands across the range. Individual scenarios that follow the upper edge of the bands early on tend to follow the lower edge of the band later on, d) global temperature relative to preindustrial for the pathways in panel a. Data in panels c,d based on Rogelj et al. (2011).

12.5.5 Potentially Abrupt or Irreversible Changes

12.5.5.1 Introduction

For the purposes of this section we adopt the definition of abrupt climate change used in Synthesis and Assessment Product 3.4 of the U.S. Climate Change Science Program CCSP (CCSP, 2008). We define *abrupt climate change* as a large-scale change in the climate system that takes place over a few decades or less, persists (or is anticipated to persist) for at least a few decades, and causes substantial disruptions in human and natural systems. Other definitions of abrupt climate change exist. For example, in the AR4 climate change was defined as abrupt if it occurred faster than the typical time scale of the responsible forcing.

A number of components or phenomena within the Earth system have been proposed as potentially possessing critical thresholds, or *tipping points* (Lenton et al., 2008), beyond which abrupt or non-linear transitions to a different state ensues. A change is said to be irreversible on a given time scale if the removal of the perturbation that caused the system to pass a tipping point does not lead to a recovery of the component or phenomenon within the Earth system due to natural processes within this time scale. In the context of interest here, the pertinent time scale is centennial (Boucher et al., 2012; Samanta et al., 2010).

In this section we examine the main components or phenomena within the Earth system that have been proposed in the literature as potentially being susceptible to abrupt or irreversible change (see Table 12.3). Abrupt changes that arise from nonlinearities within the climate system are inherently difficult to assess and their timing, if any, of future occurrence is very likely impossible to predict.

Table 12.3: Those components or phenomena within the Earth system that have been proposed in the literature as potentially being susceptible to abrupt or irreversible change. Columns 2 and 3 define whether or not a potential change can be considered to be abrupt under either the AR5 or AR4 definitions, respectively (see Section 12.5.5.1). Column 4 states whether or not the process is irreversible. Column 5 provides an assessment, if possible, of the likelihood of occurrence of abrupt change in the 21st century for the respective components or phenomena within the Earth system, for the scenarios considered in this chapter.

Phenomenon	Potentially Abrupt? (AR5 definition)	Potentially Abrupt? (AR4 definition)	Reversible?	Projected likelihood of 21st Century Change
Atlantic MOC	Yes	Yes	No	Very unlikely that MOC will undergo a rapid transition (High confidence)
Ice Sheets	No	Yes	No	Exceptionally unlikely that either Greenland or West Antarctic Ice sheets will suffer catastrophic near-complete disintegration mass loss (High confidence)
Permafrost Carbon	No	No	No	Irreversible but not an abrupt change (High confidence)
Atmospheric Methane	Yes	Yes	No	Very unlikely that methane release from clathrates will undergo catastrophic release (High confidence)

Tropical Forests	Yes	Yes	No	Cannot be ruled out (Low confidence)
Boreal Forests	Yes	Yes	No	Cannot be ruled out (Low confidence)
Arctic Sea Ice	Yes	Yes	Yes	Likely that the Arctic Ocean will become nearly ice-free at its September minimum (High confidence)
Antarctic Sea Ice	No	No	No	Irreversible but not an abrupt change (Low confidence)
Long-Term Droughts	Yes	No	Yes	Cannot be ruled out (Low confidence)
Monsoonal Circulation	Yes	No	Yes	Cannot be ruled out (Low confidence)

12.5.5.2 The Atlantic Meridional Overturning

EMICs for which the stability has been systematically assessed by suitably designed hysteresis experiments robustly show a threshold beyond which the Atlantic thermohaline circulation cannot be sustained (Rahmstorf et al., 2005). This is also the case for the FAMOUS AOGCM (Hawkins et al., 2011). However, proximity to this threshold is highly model-dependent and influenced by factors that are currently poorly understood. There is some indication that the CMIP3 climate models may generally overestimate the stability of the Atlantic Ocean circulation (Drijfhout et al., 2010; Hofmann and Rahmstorf, 2009). In particular, De Vries and Weber (2005), Dijkstra (2007), Weber et al. (2007), Huisman et al. (2010), Drijfhout et al. (2010) and Hawkins et al. (2011) suggest that the sign of net freshwater flux into the Atlantic transported through its southern boundary via the overturning circulation determines whether or not the AMOC is in a monostable or bistable regime. For the preindustrial control climate of most of the CMIP3 models, Drijfhout et al. (2010) found that the salt flux was negative (implying a positive freshwater flux), indicating that they were in a monostable regime. However, this is not the case in the CMIP5 models where Weaver et al. (2012) found that the majority of the models were in a bistable regime during RCP integrations. Observations suggest that the present day ocean is in a bistable regime, thereby allowing for multiple equilibria and a stable ‘off’ state of the AMOC (Hawkins et al., 2011).

In addition to the main threshold for a complete breakdown of the circulation, others may exist that involve more limited changes, such as a cessation of Labrador Sea deep water formation (Wood et al., 1999). Rapid melting of the Greenland ice sheet causes increases in freshwater runoff, potentially weakening the Atlantic meridional overturning circulation (AMOC). None of the CMIP5 simulations include an interactive ice sheet component. However, Jungclaus et al. (2006), Mikolajewicz et al. (2007), Driesschaert et al. (2007) and Hu et al. (2009) found only a slight temporary effect of increased melt water fluxes on the AMOC, that was either small compared to the effect of enhanced poleward atmospheric moisture transport or only noticeable in the most extreme scenarios.

While many more model simulations have been conducted since the AR4 under a wide range of forcing scenarios, projections of the AMOC behaviour have not changed. Based on the available CMIP5 models, EMICs and the literature, it remains very likely that the AMOC will weaken over the 21st century relative to preindustrial values with a best estimate decrease in 2100 of about 20–30% for the RCP4.5 scenario and 36–44% for the RCP8.5 scenario (Weaver et al., 2012). It also remains very unlikely that the AMOC will undergo an abrupt transition or collapse in the 21st century. No model exhibits an abrupt shutdown of the MOC after 2100 under any RCP simulation. Only one of the CMIP5 models revealed an eventual slowdown of the MOC to an off state. But this did not occur abruptly.

As assessed by Delworth et al. (2008), for an abrupt transition of the AMOC to occur, the sensitivity of the AMOC to forcing would have to be far greater than seen in current models. Alternatively, significant ablation of the Greenland ice sheet greatly exceeding even the most aggressive of current projections would be required (Hu et al., 2009; Swingedouw et al., 2007). While neither possibility can be excluded entirely, it is unlikely that the AMOC will collapse beyond the end of the 21st century because of global warming based on the models and range of scenarios considered.

12.5.5.3 Ice Sheets

As detailed in Section 13.5.3.1, all available modelling studies agree that the Greenland ice sheet will significantly decrease in area and volume in a warmer climate as a consequence of increased melt rates not compensated for by increased snowfall rates and amplified by positive feedbacks. Conversely, the surface mass balance of the Antarctic Ice Sheet is projected to increase in most projections because increased snowfall rates outweigh melt increase (see Section 13.5.3.3).

Irreversibility of ice sheet volume and extent changes can arise because of the surface-elevation feedback that operates when a decrease of the elevation of the ice sheet induces a decreased surface mass balance (generally through increased melting), and therefore essentially applies to Greenland. As detailed in Section 13.5.3.2, several stable states of the Greenland Ice Sheet might exist (Ridley et al., 2010; Robinson et al., 2012), and the ice sheet might irreversibly shrink to a stable smaller state once a warming threshold is crossed for a certain amount of time, with the critical duration depending on how far the temperature threshold has been exceeded. Based on the available evidence (see Section 13.5.3.2), an irreversible decrease of the Greenland Ice Sheet due to surface mass balance changes appears very unlikely in the 21st century and likely on multi-centennial to millennial time scales in the strongest forcing scenarios.

In theory (Schoof, 2007; Weertman, 1974) ice-sheet volume and extent changes can be abrupt because of the grounding line instability that can occur in coastal regions where bedrock is retrograde (that is, sloping towards the interior of the ice sheet) and below sea level (see Section 4.4.4 and Box 13.2). This essentially applies to West Antarctica, but also to parts of Greenland and East Antarctica. Furthermore, ice-shelf decay induced by oceanic or atmospheric warming might lead to abruptly accelerated ice flow further inland (De Angelis and Skvarca, 2003). Because ice sheet growth is usually a slow process, such changes could also be irreversible in the definition adopted here. The available evidence (see Section 13.5.4.4) suggests that it is exceptionally unlikely that either Greenland or West Antarctica will suffer a catastrophic abrupt and irreversible near -complete disintegration during the 21st century.

12.5.5.4 Permafrost Carbon Storage

Since the IPCC AR4, estimates of the amount of carbon stored in permafrost have been significantly revised upwards (Tarnocai et al., 2009), putting the permafrost carbon stock to an equivalent of twice the atmospheric carbon pool (Dolman et al., 2010). Because of low carbon input at high latitudes, permafrost carbon is to a large part of Pleistocene (Zimov et al., 2006) or Holocene (Smith et al., 2004) origin, and its potential vulnerability is dominated by decomposition (Eglin et al., 2010). The conjunction of a long carbon accumulation time scale on one hand and potential decomposition under climatic conditions leading to permafrost thaw (Kuhry et al., 2010; Schuur et al., 2009; Zimov et al., 2006) on the other hand suggests potential irreversibility of permafrost carbon decomposition (leading to an increase of atmospheric CO₂ and/or CH₄ concentrations) on timescales of hundreds to thousands of years in a warming climate. Indeed, recent observations (Dorrepaal et al., 2009; Kuhry et al., 2010) suggest that this process might be already occurring. However, the existing modelling studies of permafrost carbon balance under future warming that take into account at least some of the essential permafrost-related processes (Khvorostyanov et al., 2008; Koven et al., 2011; MacDougall et al., 2012; Schaefer et al., 2011; Schneider von Deimling et al., 2011; Wania et al., 2009) do not yield coherent results beyond the fact that present-day permafrost will become a net emitter of carbon during the 21st century under plausible future warming scenarios. This also reflects an insufficient understanding of the relevant soil processes during and after permafrost thaw, including processes leading to stabilization of unfrozen soil carbon (Schmidt et al., 2011), and precludes a firm assessment of the amplitude of irreversible changes in the climate system potentially related to permafrost degassing and associated global feedbacks at this stage.

12.5.5.5 Atmospheric Methane from Terrestrial and Oceanic Clathrates

Model simulations (Fyke and Weaver, 2006; Lamarque, 2008; Reagan and Moridis, 2007, 2009) suggest that clathrate deposits in shallow regions (in particular at high latitude regions and in the Gulf of Mexico) are susceptible to destabilization via ocean warming. However, concomitant sea level rise due to changes in ocean mass enhances clathrate stability in the ocean. A recent assessment of the potential for a future

catastrophic release of methane was undertaken by the U.S. Climate Change Science Program (Synthesis and Assessment Product 3.4 see Brooke et al. (2008)). They concluded that it was very unlikely that such a catastrophic release would occur this century. However, they argued that anthropogenic warming will very likely lead to enhanced methane emissions from both terrestrial and oceanic clathrates (Brooke et al., 2008). While difficult to formally assess, initial estimates of the 21st century feedback from methane clathrate destabilization are small but not insignificant (Archer, 2007; Fyke and Weaver, 2006; Lamarque, 2008). On multi-millennial timescales, such methane emissions provide a positive feedback to anthropogenic warming (Archer, 2007; Archer and Buffett, 2005; Brooke et al., 2008). Once more, due to the difference between release and accumulation timescales, such emissions are irreversible. See also FAQ 6.2.

12.5.5.6 *Tropical and Boreal Forests*

12.5.5.6.1 *Tropical forests*

In today's climate, the strongest growth in the Amazon rainforest occurs during the dry season when strong insolation is combined with water drawn from underground aquifers that store the previous wet season's rainfall. AOGCMs do not agree about how the dry season length in the Amazon may change in the future due to greenhouse gas increases (Bombardi and Carvalho, 2009), but simulations with coupled regional climate/potential vegetation models are consistent in simulating an increase in dry season length, a 70% reduction in the areal extent of the rainforest by the end of the 21st century using an A2 emissions scenario, and an eastward expansion of the caatinga vegetation (Cook and Vizzy, 2008; Sorensson et al., 2010). The transition could be abrupt when the dry season becomes too long for the vegetation to survive, although the resilience of the vegetation to a longer dry period may be increased by the CO₂ fertilization effect (Zelazowski et al., 2011). Deforestation may also increase dry season length (Costa and Pires, 2010) and drier conditions increase the likelihood of wildfires that, combined with fire ignition associated with human activity, can undermine the forest's resiliency to climate change. If climate change brings drier conditions closer to those supportive of seasonal forests rather than rainforest, fire can act as a trigger to abruptly and irreversibly change the ecosystem (Malhi et al., 2009). However the existence of refugia is an important determinant of the potential for the reemergence of the vegetation (Walker et al., 2009).

Analysis of projected change in the climate-biome space of current vegetation distributions suggest that the risk of Amazonian forest die-back is small (Malhi et al., 2009), a finding supported by modelling when strong carbon dioxide fertilization effects on Amazonian vegetation are assumed (Rammig et al., 2010). However, the strength of carbon dioxide fertilization on tropical vegetation is poorly known. Uncertainty concerning the existence tipping points in the Amazonian and other tropical rainforests purely driven by climate change therefore remains high, and so the possibility of a tipping point being crossed in precipitation volume cannot be ruled out (Good et al., 2011c; Good et al., 2011d; Nobre and Borma, 2009). The transitions of the Amazonian other tropical rainforests into a lower biomass state could however be the result of the combined effects of limits to carbon fertilization, climate warming, potential precipitation decline in interaction with the effects of human land-use.

12.5.5.6.2 *Boreal forest*

Evidence from field observations and biogeochemical modelling make it scientifically conceivable that regions of the boreal forest could tip into a different vegetation state under climate warming, but uncertainties on the likelihood of this occurring are very high (Allen et al., 2010; Lenton et al., 2008). This is mainly due to large gaps in knowledge concerning relevant ecosystemic and plant physiological responses to warming (Niinemets, 2010). The main response is a potential expansion of the boreal forest northward and the potential transition from a forest to a woodland or grassland state on its dry southern edges in the continental interiors, leading to an overall increase in herbaceous vegetation cover in the affected parts of the boreal zone (Lucht et al., 2006). The proposed potential mechanisms for decreased forest growth and/or increased forest mortality are: increased drought stress under warmer summer conditions in regions with low soil moisture (Barber et al., 2000; Dulamsuren et al., 2010; Dulamsuren et al., 2009); desiccation of saplings with shallow roots due to summer drought periods in the top soil layers, causing suppression of forest reproduction (Hogg and Schwarz, 1997); leaf tissue damage due to high leaf temperatures during peak summer temperatures under strong climate warming; increased insect, herbivory and subsequent fire damage in damaged or struggling stands (Dulamsuren et al., 2008). The balance of effects controlling standing biomass, fire type and frequency, permafrost thaw depth, snow volume and soil moisture remains uncertain.

While the existence of, and the thresholds controlling, a potential tipping point in the Boreal forest are highly uncertain, its existence cannot at present be ruled out.

12.5.5.7 Sea Ice

Several studies (e.g., Lenton et al., 2008; Lindsay and Zhang, 2005; Livina and Lenton, 2012; Serreze, 2011) have questioned whether the rapidly declining summer Arctic sea ice might reach a tipping point with a critical threshold beyond which sea ice loss is irreversible. In some climate projections, the decrease in summer Arctic sea ice areal coverage is not gradual but is instead punctuated by 5–10 year periods of rapid ice loss (Döscher and Koenigk, 2012; Holland et al., 2006). However, these events do not necessarily require a critical threshold or imply an irreversible behaviour (Amstrup et al., 2010). For example, the events discussed by Holland et al. (2006) seem to arise when large natural climate variability intrinsic to the Arctic reinforces the anthropogenically-forced change (Holland et al., 2008). Positive trends on the same time scale can also occur until the middle of the 21st century when internal variability counteracts the forced change (Holland et al., 2008; Kay et al., 2011).

Further work using single-column energy-balance models (Abbot et al., 2011; Eisenman and Wettlaufer, 2009; Merryfield et al., 2008) yielded mixed results about the possibility of abrupt thresholds in the transition from perennial to seasonal sea ice cover. Thin ice and snow covers promote strong longwave radiative loss to space and high ice growth rates (e.g., Bitz and Roe, 2004; Eisenman, 2012; Notz, 2009). These stabilizing negative feedbacks in the system can be large enough to overcome the surface albedo feedback and/or cloud feedback, which act to amplify the sea ice response. Nevertheless, Eisenman (2012) showed with a single-column energy-balance model that certain parameter choices causing thicker ice or warmer ocean under a given climate forcing make the model more prone to have a critical threshold in the transition from perennial to seasonal sea ice cover under warming conditions.

Identifying abrupt thresholds is difficult owing to internal variability and the long time scales inherent in the climate system. However, the reversibility of sea ice loss has been directly assessed in four AOGCMs or ESMs by first raising the CO₂ concentration until virtually all Arctic sea ice vanishes and then lowering the CO₂ level at the same rate as during the ramp-up phase until it reaches again the initial value (Armour et al., 2011; Li et al., 2012b; Ridley et al., 2012a). Three AOGCMs have also been used to test summer Arctic sea ice recovery after either sudden or very rapid artificial removal, and all had sea ice return within a few years (Schröder and Connolley, 2007; Sedláček et al., 2011; Tietsche et al., 2011). None of these studies with AOGCMs or ESMs show evidence of a critical irreversible change in Arctic sea ice at any point. By contrast, as a result of the strong coupling between the Southern Ocean's surface and the deep ocean, the Antarctic sea ice in the four models integrated with ramp-up and ramp-down atmospheric CO₂ concentration exhibits some asymmetric behaviour, so that its changes may be considered as irreversible on centennial time scales (Ridley et al., 2012b).

Diagnostic analyses of a few global climate models have shown very rapid sea ice loss with some evidence of an abrupt threshold in the transition from seasonal to year-round Arctic ice-free conditions after raising CO₂ to very high levels (Li et al., 2012b; Ridley et al., 2008; Winton, 2006a). Winton (2006a; 2008) hypothesize that the small ice cap instability (North, 1984) could cause such an abrupt transition. Eisenman and Wettlaufer (2009) also found that a critical threshold in the transition from seasonal ice to year-round ice-free conditions is plausible, but they concluded that the cause is a loss of the stabilizing effect of sea ice growth when the ice season shrinks in time.

Regardless of issues of reversibility or the cause, rapid sea ice losses have consequences throughout the climate system as noted by Vavrus et al. (2011) for cloud cover and Lawrence et al. (2008b) for the high-latitude ground state. Furthermore, the interannual-to-decadal variability in the summer Arctic sea ice extent is predicted to increase in response to global warming (Goosse et al., 2009; Holland et al., 2008). These studies suggest that large anomalies in Arctic sea ice areal coverage, like the one that occurred in 2007, might become increasingly frequent. Thus, while instances of rapid summer Arctic sea ice loss are *likely* to occur in the future, it appears *unlikely* that these result from a critical threshold in the system.

12.5.5.8 Hydrologic Variability: Long-Term Droughts and Monsoonal Circulation

12.5.5.8.1 Long Term Droughts

As noted in Sections 5.5.2.4 and 5.6.2, Long-term droughts (sometimes called megadroughts) are a recurring feature of Holocene paleoclimate records in North America, east and south Asia, Europe, Africa and India. The transitions into and out of the long-term droughts take many years and do not appear abrupt in the sense of indicating nonlinearity in the physical system. Since the long-term droughts all ended they are also not irreversible. Nonetheless transitions over years to a decade into a state of elevated aridity would have seriously stressed human populations and would do so again should a long-term drought reoccur.

While previous long term droughts in southwest North America arose from natural causes, climate models project that this region will undergo progressive aridification as part of a general drying and poleward expansion of the subtropical dry zones driven by rising greenhouse gases (Held and Soden, 2006; Seager and Vecchi, 2010; Seager et al., 2007). The models project the aridification to intensify steadily as radiative forcing and global warming progress without abrupt changes. Solomon et al. (2009), Frölicher and Joos (2010) and Gillett et al. (2011) considered the question of how precipitation will be changed in the future for the hypothetical case of increasing CO₂ emissions followed by immediate cessation of emissions. According to these studies, as well as Montenegro et al. (2007) and Eby et al (2009), the lifetime of the anthropogenic atmospheric CO₂ perturbation is on the multi-millennial timescale. For example, Solomon et al. (2009) show that if, for example, CO₂ rises to 600 ppm followed by zero emissions, the quasi-equilibrium CO₂ is about 400 ppm which, it is claimed on the basis of the climate models used in AR4, would reduce precipitation in key areas such as southwest North America, southern Europe and western Australia by as much as 15%. Multiyear droughts in the past that led to significant social crises (such as the U.S. Dust Bowl of the 1930s) had comparable precipitation reductions. Action to ensure a lower peak CO₂ or allowing CO₂ to peak even higher would lead to less or more aridification. If CO₂ concentrations are allowed to peak at around twice pre-industrial levels, hydrological changes of serious amplitude would be irreversible on the millennium timescale in the absence of carbon capture from the atmosphere.

12.5.5.8.2 Monsoonal circulation

Climate model simulations and paleo-reconstructions provide evidence of past abrupt changes in Saharan vegetation, with the “green Sahara” conditions (Hoelzmann et al., 1998) of the African Humid Period (AHP) during the mid-Holocene serving as the most recent example (see Section 5.6.2). However, Mitchell (1990) and Claussen et al. (2003) note that the mid-Holocene is not a direct analogue for future greenhouse gas-induced climate change since the forcings are different, with a maximum shortwave forcing in the Northern Hemisphere summer versus a globally and seasonally uniform longwave forcing, respectively. Paleoclimate examples suggest that a strong radiative or SST forcing is needed to achieve a rapid climate change, and that the rapid changes are reversible when the forcing is withdrawn. Both the abrupt onset and termination of the AHP were triggered when northern African summer insolation was 4.2% higher than present day, representing an increase of about 19 W m⁻² (deMenocal et al., 2000). The 1.66 W m⁻² greenhouse gas forcing from 1750 to 2005 estimated in the IPCC AR4 is much smaller. Indeed, a climate model of intermediate complexity simulates a rapid Saharan greening under very high levels (1000 ppm) but not under lower levels (560 ppm) of atmospheric CO₂ (Claussen et al., 2003). Abrupt Saharan vegetation changes of the Younger Dryas are linked with a rapid AMOC weakening which is considered very unlikely during the 21st century and unlikely beyond that as a consequence of global warming.

Climate model derived projections of changes in runoff by Milly et al. (2008) suggest widespread drying and drought across most of southwestern North America and many other subtropical regions by the middle of the 21st century. Some studies suggest that this subtropical drying may have already begun in southwestern North America (Barnett et al., 2008; Pierce et al., 2008; Seager et al., 2007; Seidel and Randel, 2007). More recent studies (Dai, 2011; Hoerling et al., 2010; Seager and Vecchi, 2010; Seager and Naik, 2012) suggest that regional reductions in precipitation are primarily due to internal variability and the anthropogenic forced trends remain currently weak compared to those caused by internal variability within the climate system.

Studies with conceptual models (Levermann et al., 2009; Zickfeld et al., 2005) have shown that the Indian summer monsoon can operate in two stable regimes: besides the “wet” summer monsoon, a stable state exists which is characterized by low precipitation over India. These studies suggest that any perturbation of the radiative budget which tends to weaken the driving pressure gradient has the potential to induce abrupt transitions between these two regimes.

Numerous studies with coupled ocean-atmosphere models have explored the potential impact of anthropogenic forcing on the Indian monsoon. When forced with anticipated increases in greenhouse gas concentrations, the majority of these studies show an intensification of the rainfall associated with the Indian summer monsoon (Cherchi et al., 2010; Douville et al., 2000; Hu et al., 2000; Kitoh et al., 1997; Kripalani et al., 2007; May, 2002; Meehl and Washington, 1993; Stowasser et al., 2009; Ueda et al., 2006). Despite the intensification of precipitation, several of these modeling studies show a weakening of the summer monsoon circulation (Cherchi et al., 2010; Kitoh et al., 1997; Kripalani et al., 2007; May, 2002; Stowasser et al., 2009; Ueda et al., 2006). The net effect is nevertheless an increase of precipitation due to enhanced moisture transport into the Asian monsoon region (Ueda et al., 2006). In recent years, studies with general circulation models have also explored the direct effect of aerosol forcing on the Indian monsoon (Collier and Zhang, 2009; Lau et al., 2006; Meehl et al., 2008; Randles and Ramaswamy, 2008). Considering absorbing aerosols (black carbon) only, Meehl et al. (2008) found an increase in pre-monsoonal precipitation, but a decrease in summer monsoon precipitation over parts of South Asia. In contrast, Lau et al. (2006) found an increase in May-June-July precipitation in that region. If an increase in scattering aerosols only is considered, the monsoon circulation weakens and precipitation is inhibited (Randles and Ramaswamy, 2008). Given that the effect of increased atmospheric regional loading of aerosols is opposed by the concomitant increases in greenhouse gas concentrations, it is unlikely that an abrupt transition to the dry summer monsoon regime will be triggered in the 21st century. However, a scenario is conceivable whereby aerosol control policies (meant to mitigate intolerable impacts on human health, food production and ecosystems reductions in air pollution in Asia) could, by reducing the damping effects of aerosols on the monsoon, result in sudden monsoon strengthening (Zickfeld et al., 2005).

[START FAQ 12.1 HERE]

FAQ 12.1: Why are so Many Models and Scenarios Used to Project Climate Change?

Future climate is partly determined by the magnitude of future emissions of greenhouse gases, aerosols and other natural and man-made forcings. These forcings are external to the climate system, but nevertheless modify how it behaves. Future climate is shaped by the Earth's response to those forcings, along with natural variability inherent in the climate system. A range of assumptions about the magnitude and pace of future emissions helps scientists develop different emission scenarios, upon which climate model projections are based. Different climate models, meanwhile, provide alternative representations of the Earth's response to those forcings, and of natural climate variability. Together, ensembles of models, simulating the response to a range of different scenarios, map out a range of possible futures, and help us understand these futures' uncertainties.

Predicting socio-economic development is arguably even more difficult than predicting the evolution of a physical system. It entails predicting human behaviour, policy choices, technological advances, international competition and cooperation. The common approach is to use scenarios of plausible future, socio-economic development, from which future emissions of greenhouse gases and other forcing agents are derived. It has not, in general, been possible to assign likelihoods to individual forcing scenarios. Rather, a set of alternatives is used to span a range of possibilities.

Natural fluctuations in climate are spontaneously generated by interactions between components such as the atmosphere and the ocean. In the case of near-term climate change, they may eclipse the effect of external perturbations, like greenhouse gas increases (see Chapter 11). Over the longer term, however, the effect of external forcings is likely to dominate instead. Climate model simulations project that, after a few decades, scenarios around future anthropogenic greenhouse gases and other forcing agents—and the climate system's response to them—become the main drivers of change in mean global temperature (FAQ 12.1, Figure 1, left panel). Therefore, evaluating the consequences of those various scenarios and responses is of paramount importance.

Climate models are built from physical and empirical understanding, and represent the complex, interacting processes needed to simulate climate and climate change, both past and future. Analogues from past observations, or extrapolations from recent trends, are inadequate strategies for producing projections, because the future won't necessarily be a simple continuation of what we have seen thus far.

While it is possible to write down the equations of fluid motion that determine the behaviour of the atmosphere and ocean, it is impossible to directly solve them without using numerical algorithms through computer model simulation. Also, many small-scale physical, biological and chemical processes, such as cloud processes, cannot be described by those equations, and need to be approximated instead by so-called parameterizations within those climate models.

There are various alternative and equally plausible numerical representations, solutions and approximations to the modelling of the climate system, given the limitations in computing and observations. This diversity is considered a healthy aspect of the climate modelling community, and results in a range of different, plausible climate change projections at global and regional scales. This range provides a basis for quantifying uncertainty in the projections, but because the number of models is relatively small, and the contribution of model output to public archives is voluntary, the sampling of possible futures is neither systematic nor comprehensive. Also, some inadequacies persist across all models.

Models of varying complexity are commonly used for different projection problems. A faster model with lower resolution, or a simplified description of the processes, may be used in cases where long multi-century simulations are required, or where multiple realisations are needed. Simplified models can adequately represent large scale average quantities, like global average temperature, but fine regional details can only be simulated by complex models.

The coordination of model experiments and output by groups such as the Coupled Model Intercomparison Project (CMIP) has seen the science community step up efforts to evaluate and inter-compare the ability of models to simulate past and current climate and climate change. The 'multi-model' approach is now a kind of industry-standard technique used to assess projections of a specific climate variable.

FAQ 12.2, Figure 1, right panels, shows the temperature response by the end of the 21st century for three illustrative models and the highest and lowest scenario.

Models agree on large-scale patterns of warming at the surface, for example, that the land is likely to warm faster than ocean, and the Arctic will warm faster than the tropics. But they differ both in the magnitude of their global response for the same scenario, and in small scale, regional aspects of their response. The magnitude of Arctic amplification, for instance, varies among different models, and a subset of models show a weaker warming or slight cooling in the North Atlantic as a result of the reduction in deepwater formation and shifts in ocean currents.

There are inevitable uncertainties around future external forcings, and the climate system's response to them, further complicated by internally-generated variability. These uncertainties make the use of multiple scenarios and models a standard choice if we are to assess and characterise them, describing a wide range of possible future evolutions of the Earth's climate.

[INSERT FAQ 12.1, FIGURE 1 HERE]

FAQ 12.1, Figure 1: Global mean temperature change (mean and one standard deviation, relative to 1986–2005) for the CMIP5 models, and the four RCP scenarios. For the highest (RCP8.5) and lowest (RCP2.6) scenario, illustrative maps of surface temperature change at the end of the 21st century (relative to 1986–2005) are shown for three CMIP5 models. These models are chosen to show a rather broad range of response, but this particular set is not representative of any measure of model response uncertainty.

[END FAQ 12.1 HERE]

[START FAQ 12.2 HERE]

FAQ 12.2: How will the Earth's Water Cycle Change?

The flow and storage of water in the Earth's climate system is highly variable, but changes beyond those due to natural variability are expected to occur by the end of the current century. In a warmer world, the water cycle will intensify, leading to overall increases in rainfall, surface evaporation and plant transpiration. In some locations, the more intense water cycle will yield an accumulation of water on land. In others, the amount of water will decrease, due to regional drying and loss of snow and ice cover.

The water cycle consists of water stored on the Earth in all its phases, along with the movement of water through the Earth's climate system. In the atmosphere, water occurs primarily as a gas—water vapour—but it also occurs as ice and liquid water in clouds. The ocean, of course, is primarily liquid water, but the ocean is also partly covered by ice in polar regions. Terrestrial water in liquid form appears as surface water—such as lakes and rivers—soil moisture and groundwater. Solid terrestrial water occurs in ice sheets, glaciers, snow and ice on the surface and in permafrost.

Statements about future climate sometimes say that the water cycle will accelerate, but this can be misleading, for strictly speaking, it implies that the cycling of water will occur more and more quickly with time and at all locations. Parts of the world will indeed experience intensification of the water cycle, with larger transports of water and more rapid movement of water into and out of storage reservoirs. However, other parts of the climate system will experience substantial depletion of water, and thus less movement of water. Some reservoirs may even vanish.

As the Earth warms, some general features of change should occur simply in response to a warmer climate. Those changes are governed by the amount of energy that global warming adds to the climate system. Ice in all forms should melt more rapidly, and be less pervasive. The atmosphere should have more water present, and observations and model results indicate that it already does. Water should evaporate more quickly from the surface. Sea level should rise, due to the slight expansion of warming ocean waters, and melting land ice flowing into the ocean.

These general changes are modified by the complexity of the climate system, so that they should not be expected to occur equally in all locations or at the same pace. For example, circulation of water in the atmosphere, on land and in the ocean can change as climate changes, concentrating water in some locations and depleting it in others. The changes also may vary throughout the year: some seasons tend to be wetter than others. Humans also intervene directly in the water cycle, through water management and changes in land-use. Changing population distributions and water practices would produce further changes in the water cycle.

Water cycle processes can occur over minutes, hours or days, and over distances from meters to kilometres. Variability on these scales is typically greater than for temperature, so climate changes in precipitation are harder to discern. Despite this complexity, projections of future climate show changes that are common across many models and climate forcing scenarios. This suggests some robust types of change, even if magnitudes vary with model and forcing. We focus here on changes over land, where changes in the water cycle have their largest impact on human and natural systems.

Projected climate changes (FAQ 12.2, Figure 1) generally show an increase in precipitation in the tropics, a decrease in the subtropics and increases at higher latitudes. In the tropics, these changes appear to be governed by increases in atmospheric water vapour and changes in atmospheric circulation that promote more tropical rainfall. In the subtropics, these circulation changes simultaneously promote less rainfall. Because the subtropics are home to most of the world's deserts, these changes imply increasing aridity in already dry areas, and possible expansion of deserts.

Increases at higher latitudes are governed by warmer temperatures, which allow more water in the atmosphere and thus, more water that can precipitate. The warmer climate also allows storm systems in the extratropics to transport more water vapour into the higher latitudes, without requiring substantial changes in typical wind strength. The high latitude changes are more pronounced during the colder seasons.

Whether land becomes drier or wetter depends partly on precipitation changes, but also on changes in surface evaporation and transpiration from plants (together called evapotranspiration). Because a warmer atmosphere can have more water vapour, it can induce greater evapotranspiration, given sufficient terrestrial water. In addition, increased carbon dioxide in the atmosphere reduces a plant's tendency to transpire, which can also restrict the flow of water from plants into the atmosphere.

In the tropics, increased evapotranspiration tends to mute the effects of increased precipitation, whereas in the subtropics, already relatively low amounts of soil moisture allow for little change in evapotranspiration.

At higher latitudes, the increased precipitation generally outweighs increased evapotranspiration in projected climates, yielding increased annual mean runoff, but mixed changes in soil moisture. As implied by circulation changes in FAQ 12.2, Figure 1, boundaries of high or low moisture regions may also shift.

A further complicating factor is the character of rainfall. Model projections show rainfall becoming more intense, in part because more moisture will be present in the atmosphere. The projections also show precipitation events will tend to occur less frequently. These changes produce two seemingly contradictory effects: more intense downpours, which might yield more floods, yet longer dry periods between rain events, which might yield more drought.

At high latitudes and at high elevation, further changes occur due to the loss of frozen water. Some of these are resolved by the present generation of global climate models (GCMs), and some changes can only be inferred because they involve features such as glaciers, which typically are not resolved or included in the models. The warmer climate means that snow tends to start accumulating later in the fall, and melt earlier in the spring. The earlier spring melt alters the timing of peak springtime flow in rivers receiving snowmelt. As a result, later flow rates will decrease, potentially affecting water resource management. These features appear in GCM simulations.

Loss of permafrost, a feature not included in current GCMs, will allow moisture to seep more deeply into the ground, but it will also allow the ground to warm, which could enhance evapotranspiration. In addition, even though current GCMs do not explicitly include glacier evolution, we can expect that glaciers will continue to recede, and the volume of water they provide to rivers in the summer may dwindle in some locations as they disappear. Glacier loss will also contribute to a reduction in springtime river flow. However, if overall annual mean precipitation increases—either as snow or rain—then these results do not necessarily mean that annual mean river flow will decrease.

[INSERT FAQ 12.2, FIGURE 1 HERE]

FAQ 12.2, Figure 1: Schematic diagram of projected changes in major components of the water cycle. The blue arrows indicate major types of water movement changes through the Earth's climate system: poleward water transport by extratropical winds, evaporation from the surface and runoff from the land to the oceans. The shaded regions denote areas more likely to become drier or wetter. Yellow arrows indicate an important atmospheric circulation change by the Hadley circulation, whose upward motion promotes tropical rainfall, while suppressing subtropical rainfall. Model projections indicate that the Hadley circulation will shift its downward branch poleward in both the Northern and Southern Hemispheres, with associated drying. Wetter conditions are projected at high latitudes, because a warmer atmosphere will allow greater precipitation, with greater movement of water into these regions.

[END FAQ 12.2 HERE]

[START FAQ 12.3 HERE]

FAQ 12.3: What would Happen to Future Climate if We Stopped Emissions Today?

Stopping emissions today is a scenario that is not plausible, but it is one of several idealized cases that provide insight into the response of the climate system and carbon cycle. As a result of the multiple timescales in the climate system, the relation between change in emissions and climate response is quite complex, with some changes still occurring long after emissions ceased. Models and process understanding show that as a result of the large ocean inertia and the long lifetime of many greenhouse gases, primarily carbon dioxide, much of the warming would persist for centuries after greenhouse gas emissions have stopped.

When emitted in the atmosphere, greenhouse gases get removed through chemical reactions with other reactive components or, in the case of carbon dioxide (CO₂), get exchanged with the ocean and the land. These processes characterize the lifetime of the gas in the atmosphere, defined as the time it takes for a concentration pulse to naturally decrease by a factor of e (2.71). How long greenhouse gases and aerosols persist in the atmosphere varies over a wide range, from days to thousands of years. For example, aerosols have a lifetime of weeks, methane (CH₄) of about 10 years, nitrous oxide (N₂O) of about 100 years and hexafluoroethane (C₂F₆) of about 10,000 years. CO₂ is more complicated as it is removed from the atmosphere through multiple physical and biogeochemical processes in the ocean and the land; all operating

at different time scales. About half of the anthropogenic CO₂ is removed within a few decades, but the remaining fraction stays in the atmosphere for much longer. About 20% of emitted CO₂ is still in the atmosphere after 1000 years.

As a result of the significant lifetimes of major anthropogenic greenhouse gases, the increased atmospheric concentration due to past emissions will persist long after emissions are ceased. Concentration of greenhouse gases would not return immediately to their pre-industrial levels if emissions were halted. Methane concentration would return to values close to pre-industrial level in about 50 years, N₂O concentrations would need several centuries, while CO₂ would essentially never come back to its preindustrial level on timescales relevant for our society. Changes in emissions of short-lived species like aerosols or tropospheric ozone on the other hand change the concentration nearly instantaneous.

The climate system response to the greenhouse gases and aerosols forcing is characterized by an inertia, mainly driven by the ocean. The ocean has a very large capacity of absorbing heat and a slow mixing between the surface and the deep ocean. This means that it will take several centuries for the whole ocean to warm up so to reach equilibrium with the altered radiative forcing. The surface ocean (and hence the continents) will continue to warm until it reaches a surface temperature in equilibrium with this new radiative forcing. The AR4 showed that if concentration of greenhouse gases were held constant at present day level, the Earth surface would still continue to warm of about 0.3°C over the 21st century relative to the year 2000. This is the climate commitment to current concentrations (or constant composition commitment), shown in grey in FAQ 12.3, Figure 1. Constant emissions at current levels would further increase the atmospheric concentration and result in much more warming than observed so far (FAQ 12.3, Figure 1, red lines).

Even if anthropogenic greenhouse gases emissions were halted now, the radiative forcing due to these long-lived greenhouse gases concentrations would only slowly decrease in the future. Moreover, the climate response of the Earth system to that radiative forcing would be even slower. Global temperature would not respond quickly to the greenhouse gas concentration changes. Eliminating short-lived negative forcings from sulphate aerosols at the same time (e.g., by air pollution measures) would cause a temporary warming of a few tenths of a degree, as shown in blue in FAQ 12.3, Figure 1. Setting all emissions to zero would therefore lead to a near stabilization of the climate for multiple centuries. This is called the commitment from past emissions (or zero future emission commitment). The concentration of GHG would decrease and hence the radiative forcing as well, but the inertia of the climate system would delay the temperature response.

As a consequence of the large inertia in the climate and carbon cycle, the long-term global temperature is largely controlled by total CO₂ emissions that have accumulated over time, irrespective of the time when they were emitted. Limiting global warming below a given level (e.g., 2°C above pre-industrial) requires peaking the atmospheric CO₂ concentration at a related level (defined by the climate sensitivity of the Earth system), requiring near zero CO₂ emissions eventually. A higher climate target allows for a higher CO₂ concentration peak, and hence larger cumulative CO₂ emissions (e.g., delaying the necessary emission reduction).

Global temperature is a useful aggregate number to describe the magnitude of climate change, but not all changes will scale linearly with global temperature. Changes in the water cycle for example also depend on the type of forcing (e.g., greenhouse gases, aerosols, land use change), slower components of the Earth System such as sea level rise and ice sheet would take even longer to respond, and there may be tipping points or irreversible changes in the climate system.

[INSERT FAQ 12.3, FIGURE 1 HERE]

FAQ 12.3, Figure 1: Projections based on the energy balance carbon cycle model MAGICC for constant atmospheric composition (constant forcing, grey), constant emissions (red) and zero future emissions (blue) starting in 2010, with estimates of uncertainty. Figure adapted from Hare and Meinshausen (2006) based on the MAGICC calibration to all CMIP3 and C⁴MIP models (Meinshausen et al., 2011a; Meinshausen et al., 2011b).

[END FAQ 12.3 HERE]

References

- Abbot, D. S., M. Silber, and R. T. Pierrehumbert, 2011: Bifurcations leading to summer Arctic sea ice loss. *J. Geophys. Res.*, **116**, D19120.
- Adler, R. F., G. J. Gu, J. J. Wang, G. J. Huffman, S. Curtis, and D. Bolvin, 2008: Relationships between global precipitation and surface temperature on interannual and longer timescales (1979-2006). *Journal of Geophysical Research-Atmospheres*, **113**, D22104.
- Albrecht, A., D. Schindler, K. Grebhan, U. Kohnle, and H. Mayer, 2009: Storminess over the North-Atlantic European region under climate change - a review. *Allgemeine Forst und Jagdzeitung*, **180**, 109-118.
- Alexander, L. V., and J. M. Arblaster, 2009: Assessing trends in observed and modelled climate extremes over Australia in relation to future projections. *International Journal of Climatology*, **29**, 417-435.
- Alexander, L. V., et al., 2006: Global observed changes in daily climate extremes of temperature and precipitation. *Journal of Geophysical Research-Atmospheres*, **111**, D05109.
- Alexeev, V., D. Nicolsky, V. Romanovsky, and D. Lawrence, 2007: An evaluation of deep soil configurations in the CLM3 for improved representation of permafrost. *Geophysical Research Letters*, **34**, L09502.
- Allan, R., and B. Soden, 2008: Atmospheric warming and the amplification of precipitation extremes. *Science*, **321**, 1481-1484.
- Allan, R. P., 2012: Regime dependent changes in global precipitation. *Climate Dynamics*. doi:10.1007/s00382-011-1134-x.
- Allan, R. P., and B. J. Soden, 2007: Large discrepancy between observed and simulated precipitation trends in the ascending and descending branches of the tropical circulation. *Geophysical Research Letters*, **34**.
- Allen, C., et al., 2010: A global overview of drought and heat-induced tree mortality reveals emerging climate change risks for forests. *Forest Ecology and Management*, **259**, 660-684.
- Allen, M., and W. Ingram, 2002: Constraints on future changes in climate and the hydrologic cycle. *Nature*, **419**, 224-232.
- Allen, M. R., D. J. Frame, C. Huntingford, C. D. Jones, J. A. Lowe, M. Meinshausen, and N. Meinshausen, 2009: Warming caused by cumulative carbon emissions towards the trillionth tonne. *Nature*, **458**, 1163-1166.
- Allen, R. J., and S. C. Sherwood, 2010: Aerosol-cloud semi-direct effect and land-sea temperature contrast in a GCM. *Geophysical Research Letters*, **37**, L07702.
- Amstrup, S., E. DeWeaver, D. Douglas, B. Marcot, G. Durner, C. Bitz, and D. Bailey, 2010: Greenhouse gas mitigation can reduce sea-ice loss and increase polar bear persistence. *Nature*, **468**, 955-958.
- Andrews, T., and P. Forster, 2008: CO2 forcing induces semi-direct effects with consequences for climate feedback interpretations. *Geophysical Research Letters*, **35**, L04802.
- Andrews, T., P. M. Forster, and J. M. Gregory, 2009: A Surface Energy Perspective on Climate Change. *Journal of Climate*, **22**, 2557-2570.
- Andrews, T., P. Forster, O. Boucher, N. Bellouin, and A. Jones, 2010: Precipitation, radiative forcing and global temperature change. *Geophysical Research Letters*, **37**, L14701.
- Annan, J., and J. Hargreaves, 2006: Using multiple observationally-based constraints to estimate climate sensitivity. *Geophysical Research Letters*, **33**, L06704.
- Annan, J. D., and J. C. Hargreaves, 2010: Reliability of the CMIP3 ensemble. *Geophysical Research Letters*, **37**, L02703.
- , 2011a: On the generation and interpretation of probabilistic estimates of climate sensitivity. *Climatic Change*, **104**, 423-436.
- Annan, J. D., and J. C. Hargreaves, 2011b: Understanding the CMIP3 multi-model ensemble. *Journal of Climate*, **24**, 4529-4538.
- Arblaster, J. M., G. A. Meehl, and D. J. Karoly, 2011: Future climate change in the Southern Hemisphere: Competing effects of ozone and greenhouse gases. *Geophys. Res. Lett.*, **38**, L02701.
- Archer, D., 2007: Methane hydrate stability and anthropogenic climate change. *Biogeosciences*, **4**, 521-544.
- Archer, D., and B. Buffett, 2005: Time-dependent response of the global ocean clathrate reservoir to climatic and anthropogenic forcing. *Geochemistry Geophysics Geosystems*, **6**, Q03002.
- Archer, D., et al., 2009: Atmospheric Lifetime of Fossil Fuel Carbon Dioxide. *Annual Review of Earth and Planetary Sciences*, **37**, 117-134.
- Armour, K., and G. Roe, 2011: Climate commitment in an uncertain world. *Geophysical Research Letters*, **38**, L01707.
- Armour, K., I. Eisenman, E. Blanchard-Wrigglesworth, K. McCusker, and C. Bitz, 2011: The reversibility of sea ice loss in a state-of-the-art climate model. *Geophysical Research Letters*, **38**, L16705.
- Arora, V. K., et al., 2011: Carbon emission limits required to satisfy future representative concentration pathways of greenhouse gases. *Geophysical Research Letters*, **38**, L05805.
- Arzel, O., T. Fichefet, and H. Goosse, 2006: Sea ice evolution over the 20th and 21st centuries as simulated by current AOGCMs. *Ocean Modelling*, **12**, 401-415.
- Bala, G., K. Caldeira, and R. Nemani, 2010: Fast versus slow response in climate change: implications for the global hydrological cycle. *Climate Dynamics*, **35**, 423-434.
- Baldwin, M. P., M. Dameris, and T. G. Shepherd, 2007: Atmosphere - How will the stratosphere affect climate change? *Science*, **316**, 1576-1577.

- Ballester, J., F. Giorgi, and X. Rodo, 2010a: Changes in European temperature extremes can be predicted from changes in PDF central statistics. *Climatic Change*, **98**, 277-284.
- Ballester, J., X. Rodo, and F. Giorgi, 2010b: Future changes in Central Europe heat waves expected to mostly follow summer mean warming. *Climate Dynamics*, **35**, 1191-1205.
- Bao, Q., et al., 2012: The Flexible Global Ocean-Atmosphere-Land System model Version: FGOALS-s2. *Advances in Atmospheric Sciences*, **submitted**.
- Barber, V., G. Juday, and B. Finney, 2000: Reduced growth of Alaskan white spruce in the twentieth century from temperature-induced drought stress. *Nature*, **405**, 668-673.
- Barnes, E. A., and L. M. Polvani, 2012: Response of the midlatitude jets and of their variability to increased greenhouse gases in the CMIP5 models, *Journal of Climate*, **submitted**.
- Barnett, D. N., S. J. Brown, J. M. Murphy, D. M. H. Sexton, and M. J. Webb, 2006: Quantifying uncertainty in changes in extreme event frequency in response to doubled CO₂ using a large ensemble of GCM simulations. *Climate Dynamics*, **26**, 489-511.
- Barnett, T., and D. Pierce, 2008: When will Lake Mead go dry? *Water Resources Research*, **44**, W03201.
- Barnett, T., et al., 2008: Human-induced changes in the hydrology of the western United States. *Science*, **319**, 1080-1083.
- Barriopedro, D., E. M. Fischer, J. Luterbacher, R. Trigo, and R. Garcia-Herrera, 2011: The Hot Summer of 2010: Redrawing the Temperature Record Map of Europe. *Science*, **332**, 220-224.
- Bekryaev, R. V., I. V. Polyakov, and V. A. Alexeev, 2010: Role of Polar Amplification in Long-Term Surface Air Temperature Variations and Modern Arctic Warming. *Journal of Climate*, **23**, 3888-3906.
- Bellouin, N., J. Rae, A. Jones, C. Johnson, J. Haywood, and O. Boucher, 2011: Aerosol forcing in the Hadley Centre CMIP5 simulations and the role of ammonium nitrate. *Journal of Geophysical Research*, **116**, D20206.
- Bengtsson, L., K. I. Hodges, and E. Roeckner, 2006: Storm tracks and climate change. *Journal of Climate*, **19**, 3518-3543.
- Bengtsson, L., K. I. Hodges, and N. Keenlyside, 2009: Will Extratropical Storms Intensify in a Warmer Climate? *Journal of Climate*, **22**, 2276-2301.
- Bentsen, M., et al., 2012: The Norwegian Earth System 1 Model, NorESM1-M. Part 1: Description and basic evaluation. *Geoscientific Model Development*, **submitted**.
- Betts, R., et al., 2007: Projected increase in continental runoff due to plant responses to increasing carbon dioxide. *Nature*, **448**, 1037-1041.
- Bitz, C., and G. Roe, 2004: A mechanism for the high rate of sea ice thinning in the Arctic Ocean. *Journal of Climate*, **17**, 3623-3632.
- Bitz, C., and Q. Fu, 2008: Arctic warming aloft is data set dependent. *Nature*, **455**, E3-E4.
- Bitz, C. M., 2008: Some aspects of uncertainty in predicting sea ice thinning. *Arctic Sea Ice Decline: Observations, Projections, Mechanisms, and Implications*, E. T. DeWeaver, C. M. Bitz, and L. B. Tremblay, Eds., Amer. Geophys. Union, 63-76.
- Bitz, C. M., J. K. Ridley, M. M. Holland, and H. Cattle, 2012: 20th and 21st century Arctic climate in global climate models. *Arctic Climate Change – The ACSYS Decade and Beyond*, P. Lemke, Ed.
- Boberg, F., P. Berg, P. Thejll, W. Gutowski, and J. Christensen, 2010: Improved confidence in climate change projections of precipitation evaluated using daily statistics from the PRUDENCE ensemble. *Climate Dynamics*, **35**, 1097-1106.
- Boe, J., and L. Terray, 2008: Uncertainties in summer evapotranspiration changes over Europe and implications for regional climate change. *Geophysical Research Letters*, **35**, L05702.
- Boe, J., A. Hall, and X. Qu, 2009a: September sea-ice cover in the Arctic Ocean projected to vanish by 2100. *Nat. Geosci.*, **2**, 341-343.
- Boe, J., A. Hall, and X. Qu, 2009b: Current GCMs' Unrealistic Negative Feedback in the Arctic. *Journal of Climate*, **22**, 4682-4695.
- Boer, G., and B. Yu, 2003: Climate sensitivity and response. *Climate Dynamics*, **20**, 415-429.
- Boer, G., K. Hamilton, and W. Zhu, 2005: Climate sensitivity and climate change under strong forcing. *Climate Dynamics*, **24**, 685-700.
- Boer, G. J., 1993: Climate change and the regulation of the surface moisture and energy budgets. *Climate Dynamics*, **8**, 225-239.
- , 2011: The ratio of land to ocean temperature change under global warming. *Climate Dynamics*, **37**, 2253-2270.
- Bombardi, R., and L. Carvalho, 2009: IPCC global coupled model simulations of the South America monsoon system. *Climate Dynamics*, **33**, 893-916.
- Böning, C., A. Dispert, M. Visbeck, S. Rintoul, and F. Schwarzkopf, 2008: The response of the Antarctic Circumpolar Current to recent climate change. *Nat. Geosci.*, **1**, 864-869.
- Bony, S., and J. L. Dufresne, 2005: Marine boundary layer clouds at the heart of tropical cloud feedback uncertainties in climate models. *Geophysical Research Letters*, **32**, L20806.
- Bony, S., G. Bellon, D. Klocke, S. Fermepin, S. Sherwood, and S. Denvil, 2012: Direct effect of carbon dioxide on tropical atmospheric circulation and regional rainfall. *Nat. Geosci.*, **submitted**.
- Bony, S., et al., 2006: How well do we understand and evaluate climate change feedback processes? *Journal of Climate*, **19**, 3445-3482.

- 1 Booth, B. B. B., et al., 2012: High sensitivity of future global warming to land carbon cycle processes. *Environ. Res. Lett.*, **7**, 024002.
- 2
- 3 Boucher, O., et al., 2012: Reversibility in an Earth System model in response to CO₂ concentration changes. *Environ. Res. Lett.*, **7**, 024013.
- 4
- 5 Bowerman, N., D. Frame, C. Huntingford, J. Lowe, and M. Allen, 2011: Cumulative carbon emissions, emissions floors and short-term rates of warming: implications for policy. *Philosophical Transactions of the Royal Society A-Mathematical Physical and Engineering Sciences*, **369**, 45-66.
- 6
- 7 Bracegirdle, T., and D. Stephenson, 2012a: Higher precision estimates of regional polar warming by ensemble regression of climate model projections. *Climate Dynamics*. doi:10.1007/s00382-012-1330-3, online first.
- 8
- 9 Bracegirdle, T., W. Connolley, and J. Turner, 2008: Antarctic climate change over the twenty first century. *Journal of Geophysical Research-Atmospheres*, **113**, D03103.
- 10
- 11 Bracegirdle, T. J., and D. B. Stephenson, 2012b: On the robustness of emergent constraints used in multi-model climate change projections of Arctic warming. *Journal of Climate*. submitted.
- 12
- 13 Bracegirdle, T. J., et al., 2012: Assessment of surface winds over the Atlantic, Indian and Pacific Ocean sectors of the Southern Hemisphere in CMIP5 models: historical bias, forcing response, and state dependence. *Journal of Geophysical Research - Atmospheres*. submitted.
- 14
- 15 Brasseur, G., and E. Roeckner, 2005: Impact of improved air quality on the future evolution of climate. *Geophysical Research Letters*, **32**, L23704.
- 16
- 17 Brient, F., and S. Bony, 2012: Interpretation of the positive low-cloud feedback predicted by a climate model under global warming. *Climate Dynamics*, **On-line first**, submitted.
- 18
- 19 Brierley, C. M., M. Collins, and A. J. Thorpe, 2010: The impact of perturbations to ocean-model parameters on climate and climate change in a coupled model. *Climate Dynamics*, **34**, 325-343.
- 20
- 21 Brooke, E., D. Archer, E. Dlugokencky, S. Frolking, and D. Lawrence, 2008: Potential for abrupt changes in atmospheric methane. U.S. Geological Survey, 163-201 pp.
- 22
- 23 Brovkin, V., et al., 2012: Effect of anthropogenic land-use and land cover changes on climate and land carbon storage in CMIP5 projections for the 21st century. *Journal of Climate*. submitted.
- 24
- 25 Brown, R., and P. Mote, 2009: The Response of Northern Hemisphere Snow Cover to a Changing Climate. *Journal of Climate*, **22**, 2124-2145.
- 26
- 27 Brutel-Vuilmet, C., M. Menegoz, and G. Krinner, 2012: An analysis of present and future seasonal Northern Hemisphere land snow cover simulated by CMIP5 coupled climate models. *The Cryosphere Discussions*, **6**, 3317-3348.
- 28
- 29 Burke, E., and S. Brown, 2008: Evaluating uncertainties in the projection of future drought. *Journal of Hydrometeorology*, **9**, 292-299.
- 30
- 31 Buser, C. M., H. R. Kunsch, D. Luthi, M. Wild, and C. Schar, 2009: Bayesian multi-model projection of climate: bias assumptions and interannual variability. *Climate Dynamics*, **33**, 849-868.
- 32
- 33 Butchart, N., et al., 2006: Simulations of anthropogenic change in the strength of the Brewer-Dobson circulation. *Climate Dynamics*, **27**, 727-741.
- 34
- 35 Butchart, N., et al., 2010: Chemistry-Climate Model Simulations of Twenty-First Century Stratospheric Climate and Circulation Changes. *Journal of Climate*, **23**, 5349-5374.
- 36
- 37 Butler, A. H., D. W. J. Thompson, and R. Heikes, 2010: The Steady-State Atmospheric Circulation Response to Climate Change-like Thermal Forcings in a Simple General Circulation Model. *Journal of Climate*, **23**, 3474-3496.
- 38
- 39 Cabre, M. F., S. A. Solman, and M. N. Nunez, 2010: Creating regional climate change scenarios over southern South America for the 2020's and 2050's using the pattern scaling technique: validity and limitations. *Climatic Change*, **98**, 449-469.
- 40
- 41 Caesar, J., and J. A. Lowe, 2012: Comparing the impacts of mitigation versus non-intervention scenarios on future temperature and precipitation extremes in the HadGEM2 climate model. *Journal of Geophysical Research*, **117**, D15109.
- 42
- 43 Cagnazzo, C., E. Manzini, P. G. Fogli, M. Vichi, and P. Davini, 2012: Role of Stratospheric Dynamics in the Ozone-Carbon connection in the Southern Hemisphere. *Climate Dynamics*, **submitted**.
- 44
- 45 Caldeira, K., and J. F. Kasting, 1993: Insensitivity of global warming potentials to carbon-dioxide emission scenarios. *Nature*, **366**, 251-253.
- 46
- 47 Caldwell, P., and C. S. Bretherton, 2009: Response of a Subtropical Stratocumulus-Capped Mixed Layer to Climate and Aerosol Changes. *Journal of Climate*, **22**, 20-38.
- 48
- 49 Cao, L., and K. Caldeira, 2010: Atmospheric carbon dioxide removal: long-term consequences and commitment. *Environmental Research Letters*, **5**, 024011.
- 50
- 51 Capotondi, A., M. Alexander, N. Bond, E. Curchitser, and J. Scott, 2012: Enhanced upper ocean stratification with climate change in the CMIP3 models. *Journal of Geophysical Research-Oceans*, **117**, C04031.
- 52
- 53 Cariolle, D., and H. Teyssedre, 2007: A revised linear ozone photochemistry parameterization for use in transport and general circulation models: multi-annual simulations. *Atmospheric Chemistry and Physics*, **7**, 2183-2196.
- 54
- 55 Carslaw, K., O. Boucher, D. Spracklen, G. Mann, J. Rae, S. Woodward, and M. Kulmala, 2010: A review of natural aerosol interactions and feedbacks within the Earth system. *Atmospheric Chemistry and Physics*, **10**, 1701-1737.
- 56
- 57
- 58
- 59
- 60
- 61
- 62

- Catto, J. L., L. C. Shaffrey, and K. I. Hodges, 2011: Northern Hemisphere Extratropical Cyclones in a Warming Climate in the HiGEM High-Resolution Climate Model. *Journal of Climate*, **24**, 5336-5352.
- CCSP, 2008: Abrupt Climate Change. A Report by the U.S. Climate Change Science Program and the Subcommittee on Global Change Research. [Clark, P.U., A.J. Weaver (coordinating lead authors), E. Brook, E.R. Cook, T.L. Delworth, and K. Steffen (chapter lead authors)]. U.S. Geological Survey, 459 pp.
- CCSP_3.3, 2008: Weather and Climate Extremes in a Changing Climate. Department of Commerce, NOAA's National Climatic Data Center, 164 pp pp.
- Cess, R., et al., 1990: Intercomparison and interpretation of climate feedback processes in 19 atmospheric general-circulation models. *Journal of Geophysical Research-Atmospheres*, **95**, 16601-16615.
- Chang, E. K. M., Y. Guo, and X. Xia, 2012a: CMIP5 Multi-Model Ensemble Projection of Storm Track Change Under Global Warming. *Journal of Geophysical Research - Atmospheres*, (**submitted**).
- Chang, E. K. M., Y. Guo, X. Xia, and M. Zheng, 2012b: Storm Track Activity in IPCC AR4/CMIP3 Model Simulations. *Journal of Climate*, (**In press**).
- Chapin, F., et al., 2005: Role of land-surface changes in Arctic summer warming. *Science*, **310**, 657-660.
- Charbit, S., D. Paillard, and G. Ramstein, 2008: Amount of CO₂ emissions irreversibly leading to the total melting of Greenland. *Geophysical Research Letters*, **35**, L12503.
- Chen, C. T., and T. Knutson, 2008: On the verification and comparison of extreme rainfall indices from climate models. *Journal of Climate*, **21**, 1605-1621.
- Chen, G., J. Lu, and D. M. W. Frierson, 2008: Phase Speed Spectra and the Latitude of Surface Westerlies: Interannual Variability and Global Warming Trend. *Journal of Climate*, **21**, 5942-5959.
- Cherchi, A., A. Alessandri, S. Masina, and A. Navarra, 2010: Effect of increasing CO₂ levels on monsoons. *Climate Dynamics*, **37**, 83-101.
- Choi, D. H., J. S. Kug, W. T. Kwon, F. F. Jin, H. J. Baek, and S. K. Min, 2010: Arctic Oscillation responses to greenhouse warming and role of synoptic eddy feedback. *Journal of Geophysical Research-Atmospheres*, **115**, D17103.
- Chou, C., and J. D. Neelin, 2004: Mechanisms of global warming impacts on regional tropical precipitation. *Journal of Climate*, **17**, 2688-2701.
- Chou, C., and C. Chen, 2010: Depth of Convection and the Weakening of Tropical Circulation in Global Warming. *Journal of Climate*, **23**, 3019-3030.
- Chou, C., J. D. Neelin, J. Y. Tu, and C. T. Chen, 2006: Regional tropical precipitation change mechanisms in ECHAM4/OPYC3 under global warming. *Journal of Climate*, **19**, 4207-4223.
- Chou, C., J. D. Neelin, C. A. Chen, and J. Y. Tu, 2009: Evaluating the "Rich-Get-Richer" Mechanism in Tropical Precipitation Change under Global Warming. *Journal of Climate*, **22**, 1982-2005.
- Chou, C., C. Chen, P.-H. Tan, and K.-T. Chen, 2012: Mechanisms for global warming impacts on precipitation frequency and intensity. *Journal of Climate*, **25**, 3291-3306.
- Christensen, J. H., F. Boberg, O. B. Christensen, and P. Lucas-Picher, 2008: On the need for bias correction of regional climate change projections of temperature and precipitation. *Geophysical Research Letters*, **35**, L20709.
- Christensen, J. H., et al., 2007: Regional Climate Projections. *Climate Change 2007: The Physical Science Basis. Contribution of Working Group I to the Fourth Assessment Report of the Intergovernmental Panel on Climate Change*, Cambridge University Press.
- Christensen, N., and D. Lettenmaier, 2007: A multimodel ensemble approach to assessment of climate change impacts on the hydrology and water resources of the Colorado River Basin. *Hydrology and Earth System Sciences*, **11**, 1417-1434.
- Cionni, I., et al., 2011: Ozone database in support of CMIP5 simulations: results and corresponding radiative forcing. *Atmospheric Chemistry and Physics*, **11**, 11267-11292.
- Clark, R. T., S. J. Brown, and J. M. Murphy, 2006: Modeling northern hemisphere summer heat extreme changes and their uncertainties using a physics ensemble of climate sensitivity experiments. *Journal of Climate*, **19**, 4418-4435.
- Clark, R. T., J. M. Murphy, and S. J. Brown, 2010: Do global warming targets limit heatwave risk? *Geophysical Research Letters*, **37**, L17703.
- Claussen, M., V. Brovkin, A. Ganopolski, C. Kubatzki, and V. Petoukhov, 2003: Climate change in northern Africa: The past is not the future. *Climatic Change*, **57**, 99-118.
- Colle, B. A., Z. Zhang, K. A. Lombardo, E. Chang, P. Liu, M. Zhang, and S. Hameed, 2012: Historical and Future Predictions of Eastern North America and Western Atlantic Extratropical Cyclones in CMIP5 During the Cool Season. *Journal of Climate*, (**submitted**).
- Collier, J., and G. Zhang, 2009: Aerosol direct forcing of the summer Indian monsoon as simulated by the NCAR CAM3. *Climate Dynamics*, **32**, 313-332.
- Collins, M., C. M. Brierley, M. MacVean, B. B. B. Booth, and G. R. Harris, 2007: The sensitivity of the rate of transient climate change to ocean physics perturbations. *Journal of Climate*, **20**, 2315-2320.
- Collins, M., B. B. B. Booth, G. R. Harris, J. M. Murphy, D. M. H. Sexton, and M. J. Webb, 2006a: Towards quantifying uncertainty in transient climate change. *Climate Dynamics*, **27**, 127-147, doi:110.1007/s00382-00006-00121-00380.

- Collins, M., R. E. Chandler, P. M. Cox, J. M. Huthnance, J. Rougier, and D. B. Stephenson, 2012: Quantifying future climate change, **2**, 403-409.
- Collins, M., B. Booth, B. Bhaskaran, G. Harris, J. Murphy, D. Sexton, and M. Webb, 2011: Climate model errors, feedbacks and forcings: a comparison of perturbed physics and multi-model ensembles. *Climate Dynamics*, **36**, 1737-1766.
- Collins, M., et al., 2010: The impact of global warming on the tropical Pacific ocean and El Nino. *Nat. Geosci.*, **3**, 391-397.
- Collins, W., et al., 2006b: Radiative forcing by well-mixed greenhouse gases: Estimates from climate models in the Intergovernmental Panel on Climate Change (IPCC) Fourth Assessment Report (AR4). *Journal of Geophysical Research-Atmospheres*, **111**, D14317.
- Colman, R., and B. McAvaney, 2009: Climate feedbacks under a very broad range of forcing. *Geophysical Research Letters*, **36**.
- Colman, R., and S. Power, 2010: Atmospheric radiative feedbacks associated with transient climate change and climate variability. *Climate Dynamics*, **34**, 919-933.
- Comiso, J. C., and F. Nishio, 2008: Trends in the sea ice cover using enhanced and compatible AMSR-E, SSM/I, and SMMR data. *J. Geophys. Res.*, **113**, C02S07.
- Cook, K., and E. Vizy, 2008: Effects of twenty-first-century climate change on the Amazon rain forest. *Journal of Climate*, **21**, 542-560.
- Costa, M., and G. Pires, 2010: Effects of Amazon and Central Brazil deforestation scenarios on the duration of the dry season in the arc of deforestation. *International Journal of Climatology*, **30**, 1970-1979.
- Crook, J. A., P. M. Forster, and N. Stuber, 2011: Spatial Patterns of Modeled Climate Feedback and Contributions to Temperature Response and Polar Amplification. *Journal of Climate*, **24**, 3575-3592.
- Crucifix, M., 2006: Does the Last Glacial Maximum constrain climate sensitivity? *Geophysical Research Letters*, **33**, L18701.
- Cruz, F. T., A. J. Pitman, J. L. McGregor, and J. P. Evans, 2010: Contrasting Regional Responses to Increasing Leaf-Level Atmospheric Carbon Dioxide over Australia. *Journal of Hydrometeorology*, **11**, 296-314.
- Dai, A., 2011: Drought under global warming: a review. *Wiley Interdisciplinary Reviews: Climate Change*, **2**, 45-65.
- Danabasoglu, G., and P. Gent, 2009: Equilibrium Climate Sensitivity: Is It Accurate to Use a Slab Ocean Model? *Journal of Climate*, **22**, 2494-2499.
- Davin, E., N. de Noblet-Ducoudre, and P. Friedlingstein, 2007: Impact of land cover change on surface climate: Relevance of the radiative forcing concept. *Geophysical Research Letters*, **34**, L13702, doi:10.1029/2007GL029678.
- Davini, P., C. Cagnazzo, P. G. Fogli, E. Manzini, S. Gualdi, and A. Navarra, 2012: European Blocking and Atlantic Jet Stream Variability in the NCEP/NCAR Reanalysis and the CMCC climate model. *Journal of Climate*, **submitted**.
- Davis, S., K. Caldeira, and H. Matthews, 2010: Future CO2 Emissions and Climate Change from Existing Energy Infrastructure. *Science*, **329**, 1330-1333.
- De Angelis, H., and P. Skvarca, 2003: Glacier surge after ice shelf collapse. *Science*, **299**, 1560-1562.
- de Vries, P., and S. Weber, 2005: The Atlantic freshwater budget as a diagnostic for the existence of a stable shut down of the meridional overturning circulation. *Geophysical Research Letters*, **32**.
- Delisle, G., 2007: Near-surface permafrost degradation: How severe during the 21st century? *Geophysical Research Letters*, **34**, L09503.
- Delworth, T. L., et al., 2008: The potential for abrupt change in the Atlantic Meridional Overturning Circulation. *Abrupt Climate Change. A report by the U.S. Climate Change Science Program and the Subcommittee on Global Change Research*, 258-359.
- deMenocal, P., J. Ortiz, T. Guilderson, J. Adkins, M. Sarnthein, L. Baker, and M. Yarusinsky, 2000: Abrupt onset and termination of the African Humid Period: rapid climate responses to gradual insolation forcing. *Quaternary Science Reviews*, **19**, 347-361.
- Deser, C., A. Phillips, V. Bourdette, and H. Teng, 2012a: Uncertainty in climate change projections: the role of internal variability. *Climate Dynamics*, **38**, 527-546.
- Deser, C., R. Knutti, S. Solomon, and A. S. Phillips, 2012b: Communication of the role of natural variability in future North American climate. *Nature Climate Change*, **In press**.
- Dessai, S., X. F. Lu, and M. Hulme, 2005: Limited sensitivity analysis of regional climate change probabilities for the 21st century. *Journal of Geophysical Research-Atmospheres*, **110**, D19108.
- Diffenbaugh, N. S., and M. Ashfaq, 2010: Intensification of hot extremes in the United States. *Geophysical Research Letters*, **37**, L15701.
- Diffenbaugh, N. S., J. S. Pal, F. Giorgi, and X. J. Gao, 2007: Heat stress intensification in the Mediterranean climate change hotspot. *Geophysical Research Letters*, **34**, L11706.
- Dijkstra, H., 2007: Characterization of the multiple equilibria regime in a global ocean model. *Tellus Series a-Dynamic Meteorology and Oceanography*, **59**, 695-705.
- DiNezio, P. N., A. C. Clement, G. A. Vecchi, B. J. Soden, and B. P. Kirtman, 2009: Climate Response of the Equatorial Pacific to Global Warming. *Journal of Climate*, **22**, 4873-4892.

- Dix, M., et al., 2012: The ACCESS Coupled Model: Documentation of core CMIP5 simulations and initial results. *Australian Meteorological and Oceanographic Journal*, **submitted**.
- Dole, R., et al., 2011: Was there a basis for anticipating the 2010 Russian heat wave? *Geophysical Research Letters*, **38**, L06702.
- Dolman, A., G. van der Werf, M. van der Molen, G. Ganssen, J. Erisman, and B. Strengers, 2010: A Carbon Cycle Science Update Since IPCC AR-4. *Ambio*, **39**, 402-412.
- Donat, M. G., et al., 2012: Updated analyses of temperature and precipitation extreme indices since the beginning of the twentieth century: The HadEX2 dataset. *Journal of Geophysical Research*. submitted.
- Dong, B. W., J. M. Gregory, and R. T. Sutton, 2009: Understanding Land-Sea Warming Contrast in Response to Increasing Greenhouse Gases. Part I: Transient Adjustment. *Journal of Climate*, **22**, 3079-3097.
- Dorrepaal, E., S. Toet, R. van Logtestijn, E. Swart, M. van de Weg, T. Callaghan, and R. Aerts, 2009: Carbon respiration from subsurface peat accelerated by climate warming in the subarctic. *Nature*, **460**, 616-619.
- Döscher, R., and T. Koenigk, 2012: Arctic rapid sea ice loss events in regional coupled climate scenario experiments. *Ocean Science*. submitted.
- Doutriaux-Boucher, M., M. J. Webb, J. M. Gregory, and O. Boucher, 2009: Carbon dioxide induced stomatal closure increases radiative forcing via a rapid reduction in low cloud. *Geophysical Research Letters*, **36**, L02703.
- Douville, H., J. Royer, J. Polcher, P. Cox, N. Gedney, D. Stephenson, and P. Valdes, 2000: Impact of CO2 doubling on the Asian summer monsoon: Robust versus model-dependent responses. *Journal of the Meteorological Society of Japan*, **78**, 421-439.
- Downes, S., A. Budnick, J. Sarmiento, and R. Farneti, 2011: Impacts of wind stress on the Antarctic Circumpolar Current fronts and associated subduction. *Geophysical Research Letters*, **38**, L11605.
- Downes, S. M., N. L. Bindoff, and S. R. Rintoul, 2010: Changes in the Subduction of Southern Ocean Water Masses at the End of the Twenty-First Century in Eight IPCC Models. *Journal of Climate*, **23**, 6526-6541.
- Driesschaert, E., et al., 2007: Modeling the influence of Greenland ice sheet melting on the Atlantic meridional overturning circulation during the next millennia. *Geophysical Research Letters*, **34**, L10707.
- Drijfhout, S. S., S. Weber, and E. van der Waluw, 2010: The stability of the MOC as diagnosed from the model projections for the pre-industrial, present and future climate. *Climate Dynamics*. doi:10.1007/s00382-010-0930-z, online first.
- Dufresne, J.-L., et al., 2011: Climate change projections using the IPSL-CM5 Earth System Model: from CMIP3 to CMIP5. *Climate Dynamics*. submitted.
- Dufresne, J., J. Quaas, O. Boucher, S. Denvil, and L. Fairhead, 2005: Contrasts in the effects on climate of anthropogenic sulfate aerosols between the 20th and the 21st century. *Geophysical Research Letters*, **32**.
- Dufresne, J. L., and S. Bony, 2008: An assessment of the primary sources of spread of global warming estimates from coupled atmosphere-ocean models. *Journal of Climate*, **21**, 5135-5144.
- Dulamsuren, C., M. Hauck, and M. Muhlenberg, 2008: Insect and small mammal herbivores limit tree establishment in northern Mongolian steppe. *Plant Ecology*, **195**, 143-156.
- Dulamsuren, C., M. Hauck, and C. Leuschner, 2010: Recent drought stress leads to growth reductions in *Larix sibirica* in the western Khentey, Mongolia. *Global Change Biology*, **16**, 3024-3035.
- Dulamsuren, C., et al., 2009: Water relations and photosynthetic performance in *Larix sibirica* growing in the forest-steppe ecotone of northern Mongolia. *Tree Physiology*, **29**, 99-110.
- Durack, P., and S. Wijffels, 2010: Fifty-Year Trends in Global Ocean Salinities and Their Relationship to Broad-Scale Warming. *Journal of Climate*, **23**, 4342-4362.
- Eby, M., K. Zickfeld, A. Montenegro, D. Archer, K. Meissner, and A. Weaver, 2009: Lifetime of Anthropogenic Climate Change: Millennial Time Scales of Potential CO2 and Surface Temperature Perturbations. *Journal of Climate*, **22**, 2501-2511.
- Eby, M., et al., 2012: Historical and Idealized Climate Model Experiments: An EMIC Intercomparison., submitted.
- Edwards, T., M. Crucifix, and S. Harrison, 2007: Using the past to constrain the future: how the palaeorecord can improve estimates of global warming. *Progress in Physical Geography*, **31**, 481-500.
- Eglin, T., et al., 2010: Historical and future perspectives of global soil carbon response to climate and land-use changes. *Tellus Series B-Chemical and Physical Meteorology*, **62**, 700-718.
- Eisenman, I., 2012: Factors controlling the bifurcation structure of sea ice retreat. *J. Geophys. Res.*, **117**, D01111.
- Eisenman, I., and J. Wettlaufer, 2009: Nonlinear threshold behavior during the loss of Arctic sea ice. *Proc. Natl. Acad. Sci. U. S. A.*, **106**, 28-32.
- Eisenman, I., T. Schneider, D. S. Battisti, and C. M. Bitz, 2011: Consistent changes in the sea ice seasonal cycle in response to global warming. *Journal of Climate*, **24**, 5325-5335.
- Emori, S., and S. Brown, 2005: Dynamic and thermodynamic changes in mean and extreme precipitation under changed climate. *Geophysical Research Letters*, **32**.
- Eyring, V., et al., 2012: Long-term changes in tropospheric and stratospheric ozone and associated climate impacts in CMIP5 simulations. *Journal of Geophysical Research*, **submitted**.
- Farneti, R., and P. Gent, 2011: The effects of the eddy-induced advection coefficient in a coarse-resolution coupled climate model. *Ocean Modelling*, **39**, 135-145.
- Farneti, R., T. Delworth, A. Rosati, S. Griffies, and F. Zeng, 2010: The Role of Mesoscale Eddies in the Rectification of the Southern Ocean Response to Climate Change. *Journal of Physical Oceanography*, **40**, 1539-1557.

- 1 Fasullo, J. T., 2010: Robust Land-Ocean Contrasts in Energy and Water Cycle Feedbacks. *Journal of Climate*, **23**,
2 4677-4693.
- 3 Favre, A., and A. Gershunov, 2009: North Pacific cyclonic and anticyclonic transients in a global warming context:
4 possible consequences for Western North American daily precipitation and temperature extremes. *Climate*
5 *Dynamics*, **32**, 969-987.
- 6 Finnis, J., M. M. Holland, M. C. Serreze, and J. J. Cassano, 2007: Response of Northern Hemisphere extratropical
7 cyclone activity and associated precipitation to climate change, as represented by the Community Climate
8 System Model. *Journal of Geophysical Research-Biogeosciences*, **112**, G04S42.
- 9 Fischer, E. M., and C. Schar, 2009: Future changes in daily summer temperature variability: driving processes and role
10 for temperature extremes. *Climate Dynamics*, **33**, 917-935.
- 11 ———, 2010: Consistent geographical patterns of changes in high-impact European heatwaves. *Nat. Geosci.*, **3**, 398-403.
- 12 Fischer, E. M., and R. Knutti, 2012: Robust joint projections for humidity and temperature extremes. *Nature Climate*
13 *Change*. submitted.
- 14 Fischer, E. M., D. M. Lawrence, and B. M. Sanderson, 2011: Quantifying uncertainties in projections of extremes-a
15 perturbed land surface parameter experiment. *Climate Dynamics*, **37**, 1381-1398.
- 16 Fischer, E. M., K. W. Oleson, and D. M. Lawrence, 2012a: Contrasting urban and rural heat stress responses to climate
17 change. *Geophysical Research Letters*, **39**, L03705.
- 18 Fischer, E. M., J. Rajczak, and C. Schär, 2012b: Changes in European summer temperature variability revisited.
19 *Geophysical Research Letters*. submitted.
- 20 Forest, C. E., P. H. Stone, and A. P. Sokolov, 2008: Constraining climate model parameters from observed 20th century
21 changes. *Tellus Series a-Dynamic Meteorology and Oceanography*, **60**, 911-920, doi:10.1111/j.1600-
22 0870.2008.00346.x.
- 23 Forster, P., and K. Taylor, 2006: Climate forcings and climate sensitivities diagnosed from coupled climate model
24 integrations. *Journal of Climate*, **19**, 6181-6194.
- 25 Forster, P. M., T. Andrews, P. Good, J. M. Gregory, L. S. Jackson, and M. Zelinka, 2012: Evaluating adjusted forcing
26 and model spread for historical and future scenarios in the CMIP5 generation of climate models. *Journal of*
27 *Geophysical Research*, **submitted**.
- 28 Fowler, H., M. Ekstrom, S. Blenkinsop, and A. Smith, 2007a: Estimating change in extreme European precipitation
29 using a multimodel ensemble. *Journal of Geophysical Research-Atmospheres*, **112**, D18104.
- 30 Fowler, H. J., S. Blenkinsop, and C. Tebaldi, 2007b: Linking climate change modelling to impacts studies: recent
31 advances in downscaling techniques for hydrological modelling. *International Journal of Climatology*, **27**, 1547-
32 1578.
- 33 Frame, D., B. Booth, J. Kettleborough, D. Stainforth, J. Gregory, M. Collins, and M. Allen, 2005: Constraining climate
34 forecasts: The role of prior assumptions. *Geophysical Research Letters*, **32**, L09702.
- 35 Friedlingstein, P., and S. Solomon, 2005: Contributions of past and present human generations to committed warming
36 caused by carbon dioxide. *Proc. Natl. Acad. Sci. U. S. A.*, **102**, 10832-10836.
- 37 Friedlingstein, P., S. Solomon, G. Plattner, R. Knutti, P. Ciais, and M. Raupach, 2011: Long-term climate implications
38 of twenty-first century options for carbon dioxide emission mitigation. *Nature Climate Change*, **1**, 457-461.
- 39 Friedlingstein, P., M. Meinshausen, V. K. Arora, C. D. Jones, S. K. Liddicoat, and R. Knutti, 2012: CMIP5 climate
40 projections and uncertainties due to carbon cycle feedbacks. *Journal of Climate*. submitted.
- 41 Friedlingstein, P., et al., 2006: Climate-carbon cycle feedback analysis: Results from the C4MIP model
42 intercomparison. *Journal of Climate*, **19**, 3337-3353.
- 43 Frieler, K., M. Meinshausen, T. Schneider von Deimling, T. Andrews, and P. Forster, 2011: Changes in global-mean
44 precipitation in response to warming, greenhouse gas forcing and black carbon. *Geophysical Research Letters*,
45 **38**, L04702.
- 46 Frieler, K., M. Meinshausen, M. Mengel, N. Braun, and W. Hare, 2012: A scaling approach to probabilistic assessment
47 of regional climate. *Journal of Climate*, **25**, 3117-3144.
- 48 Frierson, D., J. Lu, and G. Chen, 2007: Width of the Hadley cell in simple and comprehensive general circulation
49 models. *Geophysical Research Letters*, **34**, L18804.
- 50 Frolicher, T., and F. Joos, 2010: Reversible and irreversible impacts of greenhouse gas emissions in multi-century
51 projections with the NCAR global coupled carbon cycle-climate model. *Climate Dynamics*, **35**, 1439-1459.
- 52 Fu, Q., C. M. Johanson, J. M. Wallace, and T. Reichler, 2006: Enhanced mid-latitude tropospheric warming in satellite
53 measurements. *Science*, **312**, 1179-1179.
- 54 Fyfe, J., O. Saenko, K. Zickfeld, M. Eby, and A. Weaver, 2007: The role of poleward-intensifying winds on Southern
55 Ocean warming. *Journal of Climate*, **20**, 5391-5400.
- 56 Fyke, J., and A. Weaver, 2006: The effect of potential future climate change on the marine methane hydrate stability
57 zone. *Journal of Climate*, **19**, 5903-5917.
- 58 Gastineau, G., and B. J. Soden, 2009: Model projected changes of extreme wind events in response to global warming.
59 *Geophysical Research Letters*, **36**, L10810.
- 60 Gastineau, G., H. Le Treut, and L. Li, 2008: Hadley circulation changes under global warming conditions indicated by
61 coupled climate models. *Tellus Series a-Dynamic Meteorology and Oceanography*, **60**, 863-884.
- 62 Gastineau, G., L. Li, and H. Le Treut, 2009: The Hadley and Walker Circulation Changes in Global Warming
63 Conditions Described by Idealized Atmospheric Simulations. *Journal of Climate*, **22**, 3993-4013.

- Georgescu, M., D. Lobell, and C. Field, 2011: Direct climate effects of perennial bioenergy crops in the United States. *Proc Natl Acad Sci USA*, **109**, 4307–4312.
- Gerber, E. P., et al., 2012: ASSESSING AND UNDERSTANDING THE IMPACT OF STRATOSPHERIC DYNAMICS AND VARIABILITY ON THE EARTH SYSTEM. *Bulletin of the American Meteorological Society*, **93**, 845-859.
- Gillett, N., M. Wehner, S. Tett, and A. Weaver, 2004: Testing the linearity of the response to combined greenhouse gas and sulfate aerosol forcing. *Geophysical Research Letters*, **31**.
- Gillett, N. P., and P. A. Stott, 2009: Attribution of anthropogenic influence on seasonal sea level pressure. *Geophys. Res. Lett.*, **36**, L23709.
- Gillett, N. P., V. K. Arora, D. Matthews, and M. R. Allen, 2012: Constraining the ratio of global warming to cumulative CO₂ emissions using CMIP5 simulations. *Journal of Climate*. submitted.
- Gillett, N. P., V. K. Arora, K. Zickfeld, S. J. Marshall, and A. J. Merryfield, 2011: Ongoing climate change following a complete cessation of carbon dioxide emissions. *Nat. Geosci.*, **4**, 83-87.
- Giorgetta, M. A., et al., 2012: Climate change from 1850 to 2100 in MPI-ESM simulations for the Coupled Model Intercomparison Project 5. *Journal of Advances in Modeling Earth Systems*, **submitted**.
- Giorgi, F., 2008: A simple equation for regional climate change and associated uncertainty. *Journal of Climate*, **21**, 1589-1604.
- Goelzer, H., P. Huybrechts, M. Loutre, H. Goosse, T. Fichefet, and A. Mouchet, 2011: Impact of Greenland and Antarctic ice sheet interactions on climate sensitivity. *Climate Dynamics*, **37**, 1005-1018.
- Good, P., J. M. Gregory, and J. A. Lowe, 2011a: A step-response simple climate model to reconstruct and interpret AOGCM projections. *Geophysical Research Letters*, **38**, L01703.
- Good, P., J. M. Gregory, J. A. Lowe, and T. Andrews, 2011b: Predicting and understanding CMIP5 representative concentration pathway projections using the response to abrupt CO₂ change. *Climate Dynamics*. submitted.
- Good, P., C. Jones, J. Lowe, R. Betts, B. Booth, and C. Huntingford, 2011c: Quantifying Environmental Drivers of Future Tropical Forest Extent. *Journal of Climate*, **24**, 1337-1349.
- Good, P., et al., 2011d: A review of recent developments in climate change science. Part I: Understanding of future change in the large-scale climate system. *Progress in Physical Geography*, **35**, 281-296.
- Goodwin, P., R. Williams, A. Ridgwell, and M. Follows, 2009: Climate sensitivity to the carbon cycle modulated by past and future changes in ocean chemistry. *Nat. Geosci.*, **2**, 145-150.
- Goosse, H., O. Arzel, C. Bitz, A. de Montety, and M. Vancoppenolle, 2009: Increased variability of the Arctic summer ice extent in a warmer climate. *Geophysical Research Letters*, **36**, L23702.
- Goubanova, K., and L. Li, 2007: Extremes in temperature and precipitation around the Mediterranean basin in an ensemble of future climate scenario simulations. *Global and Planetary Change*, **57**, 27-42.
- Gouttevin, I., G. Krinner, P. Ciais, J. Polcher, and C. Legout, 2012: Multi-scale validation of a new soil freezing scheme for a land-surface model with physically-based hydrology. *Cryosphere*, **6**, 407-430.
- Granier, C., et al., 2011: Evolution of anthropogenic and biomass burning emissions at global and regional scales during the 1980-2010 period. *Climatic Change*, **109**, 163-190.
- Grant, A., S. Brönnimann, and L. Haimberger, 2008: Recent Arctic warming vertical structure contested. *Nature*, **455**, E2-E3.
- Graversen, R., and M. Wang, 2009: Polar amplification in a coupled climate model with locked albedo. *Climate Dynamics*, **33**, 629-643.
- Graversen, R., T. Mauritsen, M. Tjernstrom, E. Kallen, and G. Svensson, 2008: Vertical structure of recent Arctic warming. *Nature*, **541**, 53-56.
- Gregory, J., and M. Webb, 2008: Tropospheric adjustment induces a cloud component in CO₂ forcing. *Journal of Climate*, **21**, 58-71.
- Gregory, J., and P. Forster, 2008: Transient climate response estimated from radiative forcing and observed temperature change. *Journal of Geophysical Research-Atmospheres*, **113**, D23105.
- Gregory, J., et al., 2004: A new method for diagnosing radiative forcing and climate sensitivity. *Geophysical Research Letters*, **31**, L03205.
- Gregory, J., et al., 2005: A model intercomparison of changes in the Atlantic thermohaline circulation in response to increasing atmospheric CO₂ concentration. *Geophysical Research Letters*, **32**, L12703.
- Gregory, J. M., and J. F. B. Mitchell, 1995: Simulation of daily variability of surface-temperature and precipitation over Europe in the current and 2xCO₂ climates using the UKMO climate model. *Quarterly Journal of the Royal Meteorological Society*, **121**, 1451-1476.
- Grubb, M., 1997: Technologies, energy systems and the timing of CO₂ emissions abatement - An overview of economic issues. *Energy Policy*, **25**, 159-172.
- Gutowski, W., K. Kozak, R. Arritt, J. Christensen, J. Patton, and E. Takle, 2007: A possible constraint on regional precipitation intensity changes under global warming. *Journal of Hydrometeorology*, **8**, 1382-1396.
- Haarsma, R. J., F. Selten, and G. J. van Oldenborgh, 2012: Anthropogenic changes of the thermal and zonal flow structure over Western Europe and Eastern North Atlantic in CMIP3 and CMIP5 models. *Climate Dynamics*, **(submitted)**.

- Haarsma, R. J., F. Selten, B. V. Hurk, W. Hazeleger, and X. L. Wang, 2009: Drier Mediterranean soils due to greenhouse warming bring easterly winds over summertime central Europe. *Geophysical Research Letters*, **36**, L04705.
- Hall, A., 2004: The role of surface albedo feedback in climate. *Journal of Climate*, **17**, 1550-1568.
- Hall, A., X. Qu, and J. Neelin, 2008: Improving predictions of summer climate change in the United States. *Geophysical Research Letters*, **35**.
- Hansen, J., M. Sato, P. Kharecha, and K. von Schuckmann, 2011: Earth's energy imbalance and implications. *Atmospheric Chemistry and Physics*, **11**, 13421-13449.
- Hansen, J., G. Ruessell, A. Lacis, I. Fung, D. Rind, and P. Stone, 1985: Climate response-times - dependence on climate sensitivity and ocean mixing. *Science*, **229**, 857-859.
- Hansen, J., M. Sato, P. Kharecha, G. Russell, D. Lea, and M. Siddall, 2007: Climate change and trace gases. *Philosophical Transactions of the Royal Society a-Mathematical Physical and Engineering Sciences*, **365**, 1925-1954.
- Hansen, J., et al., 1984: Climate sensitivity: Analysis of feedback mechanisms. *Climate Processes and Climate Sensitivity*, J. Hansen, and T. Takahashi, Eds., American Geophysical Union, 130-163.
- Hansen, J., et al., 2008: Target Atmospheric CO₂: Where Should Humanity Aim? *The Open Atmospheric Science Journal*, **2**, 217-231.
- Hansen, J., et al., 2005a: Earth's energy imbalance: Confirmation and implications. *Science*, **308**, 1431-1435.
- Hansen, J., et al., 2005b: Efficacy of climate forcings. *Journal of Geophysical Research-Atmospheres*, **110**, D18104.
- Hardiman, S., N. Butchart, T. Hinton, S. Osprey, and L. Gray, 2012: The effect of a well resolved stratosphere on surface climate: Differences between CMIP5 simulations with high and low top versions of the Met Office climate model. *Journal of Climate*, **In press**.
- Hare, B., and M. Meinshausen, 2006: How much warming are we committed to and how much can be avoided? *Climatic Change*, **75**, 111-149.
- Hargreaves, J., A. Abe-Ouchi, and J. Annan, 2007: Linking glacial and future climates through an ensemble of GCM simulations. *Climate of the Past*, **3**, 77-87.
- Harris, G. R., M. Collins, D. M. H. Sexton, J. M. Murphy, and B. B. B. Booth, 2010: Probabilistic projections for 21st century European climate. *Natural Hazards and Earth System Sciences*, **10**, 2009-2020, doi:2010.5194/nhess-2010-2009-2010.
- Harris, G. R., D. M. H. Sexton, B. B. B. Booth, M. Collins, J. M. Murphy, and M. J. Webb, 2006: Frequency distributions of transient regional climate change from perturbed physics ensembles of general circulation model simulations. *Climate Dynamics*, **27**, 357-375.
- Hartmann, D. L., and K. Larson, 2002: An important constraint on tropical cloud - climate feedback. *Geophysical Research Letters*, **29**, 1951.
- Harvey, B. J., L. C. Shaffrey, T. J. Woollings, G. Zappa, and K. I. Hodges, 2012: How large are projected 21st century storm track changes? *Geophysical Research Letters*, **(submitted)**.
- Haugen, J., and T. Iversen, 2008: Response in extremes of daily precipitation and wind from a downscaled multi-model ensemble of anthropogenic global climate change scenarios. *Tellus Series a-Dynamic Meteorology and Oceanography*, **60**, 411-426.
- Hawkins, E., and R. Sutton, 2011: The potential to narrow uncertainty in projections of regional precipitation change. *Climate Dynamics*, **37**, 407-418.
- Hawkins, E., R. Smith, L. Allison, J. Gregory, T. Woollings, H. Pohlmann, and B. de Cuevas, 2011: Bistability of the Atlantic overturning circulation in a global climate model and links to ocean freshwater transport. *Geophysical Research Letters*, **38**.
- Hazeleger, W., et al., 2012: Multiyear climate predictions using two initialisation strategies. *Geophysical Research Letters*, **submitted**.
- Hegerl, G., T. Crowley, W. Hyde, and D. Frame, 2006: Climate sensitivity constrained by temperature reconstructions over the past seven centuries. *Nature*, **440**, 1029-1032.
- Hegerl, G. C., F. W. Zwiers, P. A. Stott, and V. V. Kharin, 2004: Detectability of anthropogenic changes in annual temperature and precipitation extremes. *Journal of Climate*, **17**, 3683-3700.
- Held, I., and B. Soden, 2006: Robust responses of the hydrological cycle to global warming. *Journal of Climate*, **19**, 5686-5699.
- Held, I. M., M. Winton, K. Takahashi, T. Delworth, F. R. Zeng, and G. K. Vallis, 2010: Probing the Fast and Slow Components of Global Warming by Returning Abruptly to Preindustrial Forcing. *Journal of Climate*, **23**, 2418-2427.
- Hellmer, H. H., F. Kauker, R. Timmermann, J. Determann, and J. Rae, 2012: Twenty-first-century warming of a large Antarctic ice-shelf cavity by a redirected coastal current. *Nature*, **484**, 225-228.
- Henderson-Sellers, A., P. Irannejad, and K. McGuffie, 2008: Future desertification and climate change: The need for land-surface system evaluation improvement. *Global and Planetary Change*, **64**, 129-138.
- Hibbard, K. A., G. A. Meehl, P. A. Cox, and P. Friedlingstein, 2007: A strategy for climate change stabilization experiments. *EOS Transactions AGU*, **88**, 217-221.
- Hirschi, M., et al., 2011: Observational evidence for soil-moisture impact on hot extremes in southeastern Europe. *Nat. Geosci.*, **4**, 17-21.

- Hoelzmann, P., D. Jolly, S. Harrison, F. Laarif, R. Bonnefille, and H. Pachur, 1998: Mid-Holocene land-surface conditions in northern Africa and the Arabian Peninsula: A data set for the analysis of biogeophysical feedbacks in the climate system. *Global Biogeochemical Cycles*, **12**, 35-51.
- Hoerling, M., J. Eischeid, and J. Perlwitz, 2010: Regional Precipitation Trends: Distinguishing Natural Variability from Anthropogenic Forcing. *Journal of Climate*, **23**, 2131-2145.
- Hofmann, M., and S. Rahmstorf, 2009: On the stability of the Atlantic meridional overturning circulation. *Proc. Natl. Acad. Sci. U. S. A.*, **106**, 20584-20589.
- Hogg, E., and A. Schwarz, 1997: Regeneration of planted conifers across climatic moisture gradients on the Canadian prairies: implications for distribution and climate change. *Journal of Biogeography*, **24**, 527-534.
- Holden, P. B., and N. R. Edwards, 2010: Dimensionally reduced emulation of an AOGCM for application to integrated assessment modelling. *Geophysical Research Letters*, **37**, L21707.
- Holland, M., C. Bitz, and B. Tremblay, 2006: Future abrupt reductions in the summer Arctic sea ice. *Geophysical Research Letters*, **33**, L23503.
- Holland, M., M. Serreze, and J. Stroeve, 2010: The sea ice mass budget of the Arctic and its future change as simulated by coupled climate models. *Climate Dynamics*, **34**, 185-200.
- Holland, M. M., and C. M. Bitz, 2003: Polar amplification of climate change in coupled models. *Climate Dynamics*, **21**, 221-232.
- Holland, M. M., C. M. Bitz, B. Tremblay, and D. A. Bailey, 2008: The role of natural versus forced change in future rapid summer Arctic ice loss. *Arctic Sea Ice Decline: Observations, Projections, Mechanisms, and Implications*, E. T. DeWeaver, C. M. Bitz, and L. B. Tremblay, Eds., Amer. Geophys. Union, 133-150.
- Hu, A., G. Meehl, W. Han, and J. Yin, 2009: Transient response of the MOC and climate to potential melting of the Greenland Ice Sheet in the 21st century. *Geophysical Research Letters*, **36**, L10707.
- Hu, Z., M. Latif, E. Roeckner, and L. Bengtsson, 2000: Intensified Asian summer monsoon and its variability in a coupled model forced by increasing greenhouse gas concentrations. *Geophysical Research Letters*, **27**, 2681-2684.
- Huisman, S., M. den Toom, H. Dijkstra, and S. Drijfhout, 2010: An Indicator of the Multiple Equilibria Regime of the Atlantic Meridional Overturning Circulation. *Journal of Physical Oceanography*, **40**, 551-567.
- Huntingford, C., J. Lowe, B. Booth, C. Jones, G. Harris, L. Gohar, and P. Meir, 2009: Contributions of carbon cycle uncertainty to future climate projection spread. *Tellus Series B-Chemical and Physical Meteorology*, **61**, 355-360.
- Huntingford, C., et al., 2008: Towards quantifying uncertainty in predictions of Amazon 'dieback'. *Philosophical Transactions of the Royal Society B-Biological Sciences*, **363**, 1857-1864.
- Hurt, G., et al., 2011: Harmonization of land-use scenarios for the period 1500-2100: 600 years of global gridded annual land-use transitions, wood harvest, and resulting secondary lands. *Climatic Change*, **109**, 117-161.
- Hwang, Y.-T., D. M. W. D.M.W. Frierson, B. J. Soden, and I. M. Held, 2011: The corrigendum for Held and Soden (2006). *Journal of Climate*, **24**, 1559-1560.
- IPCC, 2000: *IPCC Special Report on Emissions Scenarios. Prepared by Working Group III of the Intergovernmental Panel on Climate Change*. Cambridge University Press.
- , 2007: *Climate Change 2007: The Physical Science Basis. Contribution of Working Group I to the Fourth Assessment Report of the Intergovernmental Panel on Climate Change (IPCC)*. Cambridge University Press, 996 pp pp.
- Ishizaki, Y., et al., 2012: Temperature scaling pattern dependence on representative concentration pathway emission scenarios. *Climatic Change*, **112**, 535-546.
- Iversen, T., et al., 2012: The Norwegian Earth System Model, NorESM1-M. Part 2: Climate Response and Scenario Projections. *Geoscientific Model Development*, **submitted**.
- Jackson, C. S., M. K. Sen, G. Huerta, Y. Deng, and K. P. Bowman, 2008: Error Reduction and Convergence in Climate Prediction. *Journal of Climate*, **21**, 6698-6709.
- Jaeger, C., and J. Jaeger, 2011: Three views of two degrees. *Regional Environmental Change*, **11**, S15-S26.
- Johanson, C. M., and Q. Fu, 2009: Hadley Cell Widening: Model Simulations versus Observations. *Journal of Climate*, **22**, 2713-2725.
- Johns, T. C., et al., 2011: Climate change under aggressive mitigation: the ENSEMBLES multi-model experiment. *Climate Dynamics*, **37**, 1975-2003.
- Jones, A., J. Haywood, and O. Boucher, 2007: Aerosol forcing, climate response and climate sensitivity in the Hadley Centre climate model. *Journal of Geophysical Research-Atmospheres*, **112**, D20211.
- Jones, C., P. Cox, and C. Huntingford, 2006: Climate-carbon cycle feedbacks under stabilization: uncertainty and observational constraints. *Tellus Series B-Chemical and Physical Meteorology*, **58**, 603-613.
- Jones, C., J. Lowe, S. Liddicoat, and R. Betts, 2009: Committed terrestrial ecosystem changes due to climate change. *Nat. Geosci.*, **2**, 484-487.
- Jones, C. D., et al., 2012: 21st Century compatible CO2 emissions and airborne fraction simulated by CMIP5 Earth System models under 4 Representative Concentration Pathways. *Journal of Climate*. submitted.
- Jones, C. D., et al., 2011: The HadGEM2-ES implementation of CMIP5 centennial simulations. *Geoscientific Model Development*, **4**, 543-570.

- Joshi, M., E. Hawkins, R. Sutton, J. Lowe, and D. Frame, 2011: Projections of when temperature change will exceed 2 degrees C above pre-industrial levels. *Nature Climate Change*, **1**, 407-412.
- Joshi, M., K. Shine, M. Ponater, N. Stuber, R. Sausen, and L. Li, 2003: A comparison of climate response to different radiative forcings in three general circulation models: towards an improved metric of climate change. *Climate Dynamics*, **20**, 843-854.
- Joshi, M. M., F. H. Lambert, and M. J. Webb, 2012: Explaining the differences between 20th and 21st century land-sea warming ratio. *Climate Dynamics*. submitted.
- Joshi, M. M., J. M. Gregory, M. J. Webb, D. M. H. Sexton, and T. C. Johns, 2008: Mechanisms for the land/sea warming contrast exhibited by simulations of climate change. *Climate Dynamics*, **30**, 455-465.
- Jungclauss, J., H. Haak, M. Esch, E. Roeckner, and J. Marotzke, 2006: Will Greenland melting halt the thermohaline circulation? *Geophysical Research Letters*, **33**, L17708.
- Kamiguchi, K., A. Kitoh, T. Uchiyama, R. Mizuta, and A. Noda, 2006: Changes in Precipitation-based Extremes Indices Due to Global Warming Projected by a Global 20-km-mesh Atmospheric Model. *SOLA*, **2**, 64-67.
- Karpechko, A. Y., and E. Manzini, 2012: Stratospheric influence on tropospheric climate change in the Northern Hemisphere. *Journal of Geophysical Research-Atmospheres*, **117**, D05133.
- Kattenberg, A., et al., 1996: Climate Models - Projections of Future Climate. *Climate Change 1995 - The Science of Climate Change. Contribution of WGI to the Second Assessment Report of the Intergovernmental Panel on Climate Change*, Cambridge University Press.
- Kawase, H., T. Nagashima, K. Sudo, and T. Nozawa, 2011: Future changes in tropospheric ozone under Representative Concentration Pathways (RCPs). *Geophys. Res. Lett.*, **38**, L05801.
- Kay, J., M. Holland, and A. Jahn, 2011: Inter-annual to multi-decadal Arctic sea ice extent trends in a warming world. *Geophysical Research Letters*, **38**.
- Kay, J. E., M. M. Holland, C. Bitz, E. Blanchard-Wrigglesworth, A. Gettelman, A. Conley, and D. Bailey, 2012: The influence of local feedbacks and northward heat transport on the equilibrium Arctic climate response to increased greenhouse gas forcing in coupled climate models. *Journal of Climate*. published online.
- Kaye, N., A. Hartley, and D. Hemming, 2012: Mapping the climate: guidance on appropriate techniques to map climate variables and their uncertainty. *Geoscientific Model Development*, **5**, 245-256.
- Kellomaki, S., M. Maajarvi, H. Strandman, A. Kilpelainen, and H. Peltola, 2010: Model Computations on the Climate Change Effects on Snow Cover, Soil Moisture and Soil Frost in the Boreal Conditions over Finland. *Silva Fennica*, **44**, 213-233.
- Kendon, E., D. Rowell, and R. Jones, 2010: Mechanisms and reliability of future projected changes in daily precipitation. *Climate Dynamics*, **35**, 489-509.
- Kendon, E., D. Rowell, R. Jones, and E. Buonomo, 2008: Robustness of future changes in local precipitation extremes. *Journal of Climate*, **17**, 4280-4297.
- Kharin, V. V., F. W. Zwiers, X. B. Zhang, and G. C. Hegerl, 2007: Changes in temperature and precipitation extremes in the IPCC ensemble of global coupled model simulations. *Journal of Climate*, **20**, 1419-1444.
- Kharin, V. V., F. W. Zwiers, X. Zhang, and M. Wehner, 2012: Changes in temperature and precipitation extremes in the CMIP5 ensemble. *Climatic Change*. submitted.
- Khvorostyanov, D., P. Ciaia, G. Krinner, and S. Zimov, 2008: Vulnerability of east Siberia's frozen carbon stores to future warming. *Geophysical Research Letters*, **35**, L10703.
- Kidston, J., and E. P. Gerber, 2010: Intermodel variability of the poleward shift of the austral jet stream in the CMIP3 integrations linked to biases in 20th century climatology. *Geophysical Research Letters*, **37**, L09708.
- Kienzle, S., M. Nemeth, J. Byrne, and R. MacDonald, 2012: Simulating the hydrological impacts of climate change in the upper North Saskatchewan River basin, Alberta, Canada. *Journal of Hydrology*, **412**, 76-89.
- Kinne, S., et al., 2012: A new global aerosol climatology for climate studies. *Journal of Advances in Modeling Earth Systems*, **submitted**.
- Kirkevåg, K., et al., 2012: Aerosol-climate interactions in the Norwegian Earth System Model – NorESM. *Geoscientific Model Development*, **submitted**.
- Kitoh, A., S. Yukimoto, A. Noda, and T. Motoi, 1997: Simulated changes in the Asian summer monsoon at times of increased atmospheric CO₂. *Journal of the Meteorological Society of Japan*, **75**, 1019-1031.
- Kjellstrom, E., L. Barring, D. Jacob, R. Jones, G. Lenderink, and C. Schar, 2007: Modelling daily temperature extremes: recent climate and future changes over Europe. *Climatic Change*, **81**, 249-265.
- Knutti, R., 2010: The end of model democracy? *Climatic Change*, **102**, 395-404.
- Knutti, R., and G. C. Hegerl, 2008: The equilibrium sensitivity of the Earth's temperature to radiation changes. *Nat. Geosci.*, **1**, 735-743.
- Knutti, R., and G.-K. Plattner, 2011: Comment on 'Why Hasn't Earth Warmed as Much as Expected?' by Schwartz et al. 2010. *Journal of Climate*. in press.
- Knutti, R., and J. Sedláček, 2012: Robustness and uncertainties in the new CMIP5 climate model projections. *Nature Climate Change*. submitted.
- Knutti, R., S. Krahenmann, D. Frame, and M. Allen, 2008a: Comment on "Heat capacity, time constant, and sensitivity of Earth's climate system" by S. E. Schwartz. *Journal of Geophysical Research-Atmospheres*, **113**, D15103.
- Knutti, R., F. Joos, S. Muller, G. Plattner, and T. Stocker, 2005: Probabilistic climate change projections for CO₂ stabilization profiles. *Geophysical Research Letters*, **32**, L20707.

- Knutti, R., R. Furrer, C. Tebaldi, J. Cermak, and G. A. Meehl, 2010a: Challenges in Combining Projections from Multiple Climate Models. *Journal of Climate*, **23**, 2739-2758.
- Knutti, R., G. Abramowitz, M. Collins, V. Eyring, P. J. Gleckler, B. Hewitson, and L. Mearns, 2010b: Good Practice Guidance Paper on Assessing and Combining Multi Model Climate Projections. IPCC Working Group I Technical Support Unit, University of Bern, Bern, Switzerland.
- Knutti, R., et al., 2008b: A review of uncertainties in global temperature projections over the twenty-first century. *Journal of Climate*, **21**, 2651-2663.
- Kodra, E., K. Steinhaeuser, and A. R. Ganguly, 2011: Persisting cold extremes under 21st-century warming scenarios. *Geophysical Research Letters*, **38**, L08705.
- Kolomyts, E., and N. Surova, 2010: Predicting the Impact of Global Warming on Soil Water Resources in Marginal Forests of the Middle Volga Region. *Water Resources*, **37**, 89-101.
- Komuro, Y., et al., 2012: Sea-Ice in Twentieth-Century Simulations by New MIROC Coupled Models: A Comparison between Models with High Resolution and with Ice Thickness Distribution. *Journal of the Meteorological Society of Japan*, **90A**, 213-232.
- Körper, J., et al., 2012: The effect of aggressive mitigation on sea level rise and sea ice changes. *Climate Dynamics*, submitted.
- Koster, R., Z. Guo, R. Yang, P. Dirmeyer, K. Mitchell, and M. Puma, 2009a: On the Nature of Soil Moisture in Land Surface Models. *Journal of Climate*, **22**, 4322-4335.
- Koster, R., et al., 2006: GLACE: The Global Land-Atmosphere Coupling Experiment. Part I: Overview. *Journal of Hydrometeorology*, **7**, 590-610.
- Koster, R. D., S. D. Schubert, and M. J. Suarez, 2009b: Analyzing the Concurrence of Meteorological Droughts and Warm Periods, with Implications for the Determination of Evaporative Regime. *Journal of Climate*, **22**, 3331-3341.
- Koster, R. D., H. L. Wang, S. D. Schubert, M. J. Suarez, and S. Mahanama, 2009c: Drought-Induced Warming in the Continental United States under Different SST Regimes. *Journal of Climate*, **22**, 5385-5400.
- Koven, C., P. Friedlingstein, P. Ciais, D. Khvorostyanov, G. Krinner, and C. Tarnocai, 2009: On the formation of high-latitude soil carbon stocks: Effects of cryoturbation and insulation by organic matter in a land surface model. *Geophysical Research Letters*, **36**, L21501.
- Koven, C. D., and W. J. Riley, 2012: Analysis of permafrost thermal dynamics and response to climate change in the CMIP5 Earth System Models. *J. Climate*, **submitted**.
- Koven, C. D., et al., 2011: Permafrost carbon-climate feedbacks accelerate global warming. *Proc. Natl. Acad. Sci. U. S. A.*, **108**, 14769-14774.
- Kripalani, R., J. Oh, A. Kulkarni, S. Sabade, and H. Chaudhari, 2007: South Asian summer monsoon precipitation variability: Coupled climate model simulations and projections under IPCC AR4. *Theoretical and Applied Climatology*, **90**, 133-159.
- Kug, J., D. Choi, F. Jin, W. Kwon, and H. Ren, 2010: Role of synoptic eddy feedback on polar climate responses to the anthropogenic forcing. *Geophysical Research Letters*, **37**, L14704.
- Kuhry, P., E. Dorrepaal, G. Hugelius, E. Schuur, and C. Tarnocai, 2010: Potential Remobilization of Belowground Permafrost Carbon under Future Global Warming. *Permafrost and Periglacial Processes*, **21**, 208-214.
- Kunkel, K. E., T. R. Karl, D. R. Easterling, K. Redmond, J. Young, X. Yin, and P. Hennon, 2012: Probable Maximum Precipitation (PMP) and Climate Change. *Geophysical Research Letters*.
- Kysely, J., and R. Beranova, 2009: Climate-change effects on extreme precipitation in central Europe: uncertainties of scenarios based on regional climate models. *Theoretical and Applied Climatology*, **95**, 361-374.
- Lamarque, J.-F., et al., 2011: Global and regional evolution of short-lived radiatively-active gases and aerosols in the Representative Concentration Pathways. *Climatic Change*, **109**, 191-212.
- Lamarque, J., 2008: Estimating the potential for methane clathrate instability in the 1%-CO₂ IPCC AR-4 simulations. *Geophysical Research Letters*, **35**, L19806.
- Lamarque, J., et al., 2010: Historical (1850-2000) gridded anthropogenic and biomass burning emissions of reactive gases and aerosols: methodology and application. *Atmospheric Chemistry and Physics*, **10**, 7017-7039.
- Lambert, F., and M. Webb, 2008: Dependency of global mean precipitation on surface temperature. *Geophysical Research Letters*, **35**, L16706.
- Lambert, F. H., and J. C. H. Chiang, 2007: Control of land-ocean temperature contrast by ocean heat uptake. *Geophysical Research Letters*, **34**, L13704.
- Lambert, F. H., M. J. Webb, and M. J. Joshi, 2011: The relationship between land-ocean surface temperature contrast and radiative forcing. *Journal of Climate*, **24**, 3239-3256.
- Landrum, L., M. M. Holland, D. P. Schneider, and E. Hunke, 2012: Antarctic sea ice climatology, variability and late 20th century change in CCSM4. *Journal of Climate*, in press.
- Lau, K., M. Kim, and K. Kim, 2006: Asian summer monsoon anomalies induced by aerosol direct forcing: the role of the Tibetan Plateau. *Climate Dynamics*, **26**, 855-864.
- Lawrence, D., and A. Slater, 2010: The contribution of snow condition trends to future ground climate. *Climate Dynamics*, **34**, 969-981.
- Lawrence, D., A. Slater, and S. Swenson, 2012: Simulation of Present-day and Future Permafrost and Seasonally Frozen Ground Conditions in CCSM4. *Journal of Climate*, **25**, 2207-2225.

- Lawrence, D., A. Slater, V. Romanovsky, and D. Nicolsky, 2008a: Sensitivity of a model projection of near-surface permafrost degradation to soil column depth and representation of soil organic matter. *Journal of Geophysical Research-Earth Surface*, **113**, F02011.
- Lawrence, D., A. Slater, R. Tomas, M. Holland, and C. Deser, 2008b: Accelerated Arctic land warming and permafrost degradation during rapid sea ice loss. *Geophysical Research Letters*, **35**, L11506.
- Lean, J., and D. Rind, 2009: How will Earth's surface temperature change in future decades? *Geophysical Research Letters*, **36**, L15708.
- Lefebvre, W., and H. Goosse, 2008: Analysis of the projected regional sea-ice changes in the Southern Ocean during the twenty-first century. *Climate Dynamics*, **30**, 59-76.
- Lemoine, D. M., 2010: Climate Sensitivity Distributions Dependence on the Possibility that Models Share Biases. *Journal of Climate*, **23**, 4395-4415.
- Lenderink, G., and E. Van Meijgaard, 2008: Increase in hourly precipitation extremes beyond expectations from temperature changes. *Nat. Geosci.*, **1**, 511-514.
- Lenderink, G., A. van Ulden, B. van den Hurk, and E. van Meijgaard, 2007: Summertime inter-annual temperature variability in an ensemble of regional model simulations: analysis of the surface energy budget. *Climatic Change*, **81**, 233-247.
- Lenton, T., H. Held, E. Kriegler, J. Hall, W. Lucht, S. Rahmstorf, and H. Schellnhuber, 2008: Tipping elements in the Earth's climate system. *Proc. Natl. Acad. Sci. U. S. A.*, **105**, 1786-1793.
- Levermann, A., J. Schewe, V. Petoukhov, and H. Held, 2009: Basic mechanism for abrupt monsoon transitions. *Proc. Natl. Acad. Sci. U. S. A.*, **106**, 20572-20577.
- Levitus, S., J. Antonov, and T. Boyer, 2005: Warming of the world ocean, 1955-2003. *Geophysical Research Letters*, **32**, L02604.
- Levitus, S., J. Antonov, T. Boyer, R. Locarnini, H. Garcia, and A. Mishonov, 2009: Global ocean heat content 1955-2008 in light of recently revealed instrumentation problems. *Geophysical Research Letters*, **36**, L07608.
- Levy II, H., L. W. Horowitz, M. D. Schwarzkopf, Y. Ming, J.-C. Golaz, V. Naik, and V. Ramaswamy, 2012: The Roles of Aerosol Direct and Indirect Effects in Past and Future Climate Change. *Journal of Geophysical Research*, **submitted**.
- Li, C., J.-S. von Storch, and J. Marotzke, 2012a: Deep-ocean heat uptake and equilibrium climate response. *Climate Dynamics*. doi:10.1007/s00382-012-1350-z, published online.
- Li, C., D. Notz, S. Tietsche, and J. Marotzke, 2012b: The transient versus the equilibrium response of sea ice to global warming. *Journal of Climate*. submitted.
- Li, F., J. Austin, and J. Wilson, 2008: The strength of the Brewer-Dobson circulation in a changing climate: Coupled chemistry-climate model simulations. *Journal of Climate*, **21**, 40-57.
- Li, F., W. Collins, M. Wehner, D. Williamson, J. Olson, and C. Algieri, 2011a: Impact of horizontal resolution on simulation of precipitation extremes in an aqua-planet version of Community Atmospheric Model (CAM3). *Tellus*, **63**, 884-892.
- Li, L., X. Jiang, M. Chahine, E. Olsen, E. Fetzer, L. Chen, and Y. Yung, 2011b: The recycling rate of atmospheric moisture over the past two decades (1988-2009). *Environmental Research Letters*, **6**, 034018.
- Li, L. J., et al., 2012c: The Flexible Global Ocean-Atmosphere-Land System Model version g2. *Advances in Atmospheric Sciences*, **submitted**.
- Lim, E. P., and I. Simmonds, 2009: Effect of tropospheric temperature change on the zonal mean circulation and SH winter extratropical cyclones. *Climate Dynamics*, **33**, 19-32.
- Lindsay, K., et al., 2012: Preindustrial Control and 20th Century Carbon Cycle Experiments with the Earth System Model CESM1-(BGC). *Journal of Climate*, **submitted**.
- Lindsay, R., and J. Zhang, 2005: The thinning of Arctic sea ice, 1988-2003: Have we passed a tipping point? *Journal of Climate*, **18**, 4879-4894.
- Livina, V. N., and T. M. Lenton, 2012: A recent bifurcation in Arctic sea-ice cover. *The Cryosphere*. submitted.
- Loarie, S. R., D. B. Lobell, G. P. Asner, Q. Z. Mu, and C. B. Field, 2011: Direct impacts on local climate of sugar-cane expansion in Brazil. *Nature Climate Change*, **1**, 105-109.
- Loeb, N. G., et al., 2009: Toward Optimal Closure of the Earth's Top-of-Atmosphere Radiation Budget. *Journal of Climate*, **22**, 748-766.
- Lorenz, A., B. J. Todd, N. Bowerman, D. J. Frame, and M. R. Allen, 2012: Climate system properties determining the social cost of emissions. *Nature Climate Change*. submitted.
- Lorenz, D. J., and E. T. DeWeaver, 2007: Tropopause height and zonal wind response to global warming in the IPCC scenario integrations. *Journal of Geophysical Research-Atmospheres*, **112**, D10119.
- Lowe, J., C. Huntingford, S. Raper, C. Jones, S. Liddicoat, and L. Gohar, 2009: How difficult is it to recover from dangerous levels of global warming? *Environmental Research Letters*, **4**, 014012.
- Lu, J., and M. Cai, 2009: Seasonality of polar surface warming amplification in climate simulations. *Geophysical Research Letters*, **36**, L16704.
- Lu, J., G. Vecchi, and T. Reichler, 2007: Expansion of the Hadley cell under global warming. *Geophysical Research Letters*, **34**, L06805.
- Lu, J., G. Chen, and D. Frierson, 2008: Response of the Zonal Mean Atmospheric Circulation to El Nino versus Global Warming. *Journal of Climate*, **21**, 5835-5851.

- Lucht, W., S. Schaphoff, T. Ebrecht, U. Heyder, and W. Cramer, 2006: Terrestrial vegetation redistribution and carbon balance under climate change. *Carbon Balance and Management*, **1**.
- Lunt, D., A. Haywood, G. Schmidt, U. Salzmann, P. Valdes, and H. Dowsett, 2010: Earth system sensitivity inferred from Pliocene modelling and data. *Nat. Geosci.*, **3**, 60-64.
- MacDougall, A. H., C. A. Avis, and A. J. Weaver, 2012: Significant existing commitment to warming from the permafrost carbon feedback. *Nat. Geosci.*, **submitted**.
- Mahlstein, I., and R. Knutti, 2011: Ocean Heat Transport as a Cause for Model Uncertainty in Projected Arctic Warming. *Journal of Climate*, **24**, 1451-1460.
- Mahlstein, I., and R. Knutti, 2012: September Arctic sea ice predicted to disappear near 2°C global warming above present. *J. Geophys. Res.*, **117**, D06104.
- Mahlstein, I., P. R. Gent, and S. Solomon, 2012: Historical Antarctic mean sea ice area, sea ice trends, and winds in CMIP5 simulations. *Journal of Climate*. submitted.
- Malhi, Y., et al., 2009: Exploring the likelihood and mechanism of a climate-change-induced dieback of the Amazon rainforest. *Proc. Natl. Acad. Sci. U. S. A.*, **106**, 20610-20615.
- Manabe, S., and R. T. Wetherald, 1980: Distribution of climate change resulting from an increase in CO₂ content of the atmosphere. *Journal of the Atmospheric Sciences*, **37**, 99-118.
- Manabe, S., and R. Stouffer, 1980: Sensitivity of a global climate model to an increase of CO₂ concentration in the atmosphere. *Journal of Geophysical Research-Oceans and Atmospheres*, **85**, 5529-5554.
- , 1994: Multiple-century response of a coupled ocean-atmosphere model to an increase of atmospheric carbon-dioxide. *Journal of Climate*, **7**, 5-23.
- Manabe, S., K. Bryan, and M. J. Spelman, 1990: Transient-response of a global ocean atmosphere model to a doubling of atmospheric carbon-dioxide. *Journal of Physical Oceanography*, **20**, 722-749.
- Manabe, S., R. J. Stouffer, M. J. Spelman, and K. Bryan, 1991: TRANSIENT RESPONSES OF A COUPLED OCEAN ATMOSPHERE MODEL TO GRADUAL CHANGES OF ATMOSPHERIC CO₂. 1. ANNUAL MEAN RESPONSE. *Journal of Climate*, **4**, 785-818.
- Manzini, E., et al., 2012: Role of the stratosphere in Northern winter climate change as simulated by the CMIP5 models. *Journal of Geophysical Research*. submitted.
- Massonnet, F., T. Fichefet, H. Goosse, C. M. Bitz, G. Philippon-Berthier, M. Holland, and P. Y. Barriat, 2012: Constraining projections of summer Arctic sea ice. *The Cryosphere*. submitted.
- Matthews, H., and K. Caldeira, 2008: Stabilizing climate requires near-zero emissions. *Geophysical Research Letters*, **35**, L04705.
- Matthews, H., N. Gillett, P. Stott, and K. Zickfeld, 2009: The proportionality of global warming to cumulative carbon emissions. *Nature*, **459**, 829-832.
- Matthews, H. D., S. Solomon, and R. Pierrehumbert, 2011: Cumulative carbon as a policy framework for achieving climate stabilization. *Philosophical Transactions of the Royal Society*. in press.
- May, W., 2002: Simulated changes of the Indian summer monsoon under enhanced greenhouse gas conditions in a global time-slice experiment. *Geophysical Research Letters*, **29**, 1118.
- May, W., 2008a: Climatic changes associated with a global "2 degrees C-stabilization" scenario simulated by the ECHAM5/MPI-OM coupled climate model. *Climate Dynamics*, **31**, 283-313.
- May, W., 2008b: Potential future changes in the characteristics of daily precipitation in Europe simulated by the HIRHAM regional climate model. *Climate Dynamics*, **30**, 581-603.
- May, W., 2012: Assessing the strength of regional changes in near-surface climate associated with a global warming of 2 degrees C. *Climatic Change*, **110**, 619-644.
- McCabe, G., and D. Wolock, 2007: Warming may create substantial water supply shortages in the Colorado River basin. *Geophysical Research Letters*, **34**, L22708.
- McLandress, C., and T. G. Shepherd, 2009: Simulated Anthropogenic Changes in the Brewer-Dobson Circulation, Including Its Extension to High Latitudes. *Journal of Climate*, **22**, 1516-1540.
- McLandress, C., T. G. Shepherd, J. F. Scinocca, D. A. Plummer, M. Sigmond, A. I. Jonsson, and M. C. Reader, 2011: Separating the Dynamical Effects of Climate Change and Ozone Depletion. Part II Southern Hemisphere Troposphere. *Journal of Climate*, **24**, 1850-1868.
- McSweeney, C. F., and R. G. Jones, 2012: No consensus on consensus: The challenge of finding a universal approach to measuring and mapping ensemble consistency in GCM projections. *Climatic Change*. submitted.
- Meehl, G., and W. Washington, 1993: South Asian summer monsoon variability in a model with doubled atmospheric carbon-dioxide concentration. *Science*, **260**, 1101-1104.
- Meehl, G., J. Arblaster, and C. Tebaldi, 2005a: Understanding future patterns of increased precipitation intensity in climate model simulations. *Geophysical Research Letters*, **32**, L18719.
- Meehl, G., J. Arblaster, and W. Collins, 2008: Effects of black carbon aerosols on the Indian monsoon. *Journal of Climate*, **21**, 2869-2882.
- Meehl, G., G. Boer, C. Covey, M. Latif, and R. Stouffer, 2000: The Coupled Model Intercomparison Project (CMIP). *Bull. Amer. Meteorol. Soc.*, **81**, 313-318.
- Meehl, G., W. Washington, C. Ammann, J. Arblaster, T. Wigley, and C. Tebaldi, 2004: Combinations of natural and anthropogenic forcings in twentieth-century climate. *Journal of Climate*, **17**, 3721-3727.
- Meehl, G., et al., 2005b: How much more global warming and sea level rise? *Science*, **307**, 1769-1772.

- Meehl, G., et al., 2006: Climate change projections for the twenty-first century and climate change commitment in the CCSM3. *Journal of Climate*, **19**, 2597-2616.
- Meehl, G., et al., 2012a: Climate System Response to External Forcings and Climate Change Projections in CCSM4. *Journal of Climate*, **25**, 3661-3683.
- Meehl, G. A., and C. Tebaldi, 2004: More intense, more frequent, and longer lasting heat waves in the 21st century. *Science*, **305**, 994-997.
- Meehl, G. A., C. Tebaldi, G. Walton, D. Easterling, and L. McDaniel, 2009: Relative increase of record high maximum temperatures compared to record low minimum temperatures in the U. S. *Geophysical Research Letters*, **36**, L23701.
- Meehl, G. A., et al., 2007a: The WCRP CMIP3 multimodel dataset - A new era in climate change research. *Bulletin of the American Meteorological Society*, **88**, 1383-1394.
- Meehl, G. A., et al., 2012b: Climate change projections in CESM1(CAM5). *Journal of Climate*, **submitted**.
- Meehl, G. A., et al., 2007b: Global Climate Projections. *Climate Change 2007: The Physical Science Basis. Contribution of Working Group I to the Fourth Assessment Report of the Intergovernmental Panel on Climate Change*, Cambridge University Press.
- Meijers, A. J. S., E. Shuckburgh, N. Bruneau, J.-B. Sallee, T. J. Bracegirdle, and Z. Wang, 2012: Representation of the Antarctic Circumpolar Current in the CMIP5 climate models and future changes under warming scenarios. *Journal of Geophysical Research*. submitted.
- Meinshausen, M., T. Wigley, and S. Raper, 2011a: Emulating atmosphere-ocean and carbon cycle models with a simpler model, MAGICC6-Part 2: Applications. *Atmospheric Chemistry and Physics*, **11**, 1457-1471.
- Meinshausen, M., S. Raper, and T. Wigley, 2011b: Emulating coupled atmosphere-ocean and carbon cycle models with a simpler model, MAGICC6-Part 1: Model description and calibration. *Atmospheric Chemistry and Physics*, **11**, 1417-1456.
- Meinshausen, M., B. Hare, T. Wigley, D. Van Vuuren, M. Den Elzen, and R. Swart, 2006: Multi-gas emissions pathways to meet climate targets. *Climatic Change*, **75**, 151-194.
- Meinshausen, M., et al., 2009: Greenhouse-gas emission targets for limiting global warming to 2 degrees C. *Nature*, **458**, 1158-1162.
- Meinshausen, M., et al., 2011c: The RCP Greenhouse Gas Concentrations and their Extensions from 1765 to 2300. *Climatic Change*, **109**, 213-241.
- Merryfield, W. J., M. M. Holland, and A. H. Monahan, 2008: Multiple equilibria and abrupt transitions in Arctic summer sea ice extent. *Arctic Sea Ice Decline: Observations, Projections, Mechanisms, and Implications*, AGU, 151-174.
- Mignone, B., R. Socolow, J. Sarmiento, and M. Oppenheimer, 2008: Atmospheric stabilization and the timing of carbon mitigation. *Climatic Change*, **88**, 251-265.
- Mikolajewicz, U., M. Vizcaino, J. Jungclaus, and G. Schurgers, 2007: Effect of ice sheet interactions in anthropogenic climate change simulations. *Geophysical Research Letters*, **34**, L18706.
- Milly, P., J. Betancourt, M. Falkenmark, R. Hirsch, Z. Kundzewicz, D. Lettenmaier, and R. Stouffer, 2008: Climate change - Stationarity is dead: Whither water management? *Science*, **319**, 573-574.
- Min, S., X. Zhang, F. Zwiers, and G. Hegerl, 2011: Human contribution to more-intense precipitation extremes. *Nature*, **470**, 378-381.
- Ming, Y., V. Ramaswamy, and G. Persad, 2010: Two opposing effects of absorbing aerosols on global-mean precipitation. *Geophysical Research Letters*, **37**, L13701.
- Mitas, C., and A. Clement, 2006: Recent behavior of the Hadley cell and tropical thermodynamics in climate models and reanalyses. *Geophysical Research Letters*, **33**, L01810.
- Mitchell, J., T. Johns, W. Ingram, and J. Lowe, 2000: The effect of stabilising atmospheric carbon dioxide concentrations on global and regional climate change. *Geophysical Research Letters*, **27**, 2977-2980.
- Mitchell, J. F. B., 1983: The seasonal response of a general-circulation model to changes in CO₂ and sea temperatures. *Quarterly Journal of the Royal Meteorological Society*, **109**, 113-152.
- , 1990: Is the Holocene a good analogue for greenhouse warming? *Journal of Climate*, **3**, 1177-1192.
- Mitchell, J. F. B., T. C. Johns, M. Eagles, W. J. Ingram, and R. A. Davis, 1999: Towards the construction of climate change scenarios. *Climatic Change*, **41**, 547-581.
- Mitchell, T. D., 2003: Pattern scaling - An examination of the accuracy of the technique for describing future climates. *Climatic Change*, **60**, 217-242.
- Mizuta, R., 2012: Intensification of extratropical cyclones associated with the polar jet change in the CMIP5 global warming projections. *Geophysical Research Letters*, **(submitted)**.
- Monaghan, A., D. Bromwich, and D. Schneider, 2008: Twentieth century Antarctic air temperature and snowfall simulations by IPCC climate models. *Geophysical Research Letters*, **35**, L07502.
- Montenegro, A., V. Brovkin, M. Eby, D. Archer, and A. Weaver, 2007: Long term fate of anthropogenic carbon. *Geophysical Research Letters*, **34**, L19707.
- Moss, R. H., et al., 2010: The next generation of scenarios for climate change research and assessment. *Nature*, **463**, 747-756.
- Moss, R. H., et al., 2008: Towards New Scenarios for Analysis of Emissions, Climate Change, Impacts, and Response Strategies. Intergovernmental Panel on Climate Change, 132 pp.

- Murphy, D. M., S. Solomon, R. W. Portmann, K. H. Rosenlof, P. M. Forster, and T. Wong, 2009: An observationally based energy balance for the Earth since 1950. *Journal of Geophysical Research-Atmospheres*, **114**, D17107.
- Murphy, J., D. Sexton, D. Barnett, G. Jones, M. Webb, and M. Collins, 2004: Quantification of modelling uncertainties in a large ensemble of climate change simulations. *Nature*, **430**, 768-772.
- Murphy, J. M., B. B. Booth, M. Collins, G. R. Harris, D. M. H. Sexton, and M. J. Webb, 2007: A methodology for probabilistic predictions of regional climate change from perturbed physics ensembles. *Philosophical Transactions of the Royal Society a-Mathematical Physical and Engineering Sciences*, **365**, 1993-2028.
- Myhre, G., E. Highwood, K. Shine, and F. Stordal, 1998: New estimates of radiative forcing due to well mixed greenhouse gases. *Geophysical Research Letters*, **25**, 2715-2718.
- Nakicenovic, N., et al., 2000: Special Report on Emissions Scenarios: A special report of Working Group III of the Intergovernmental Panel on Climate Change. C. U. Press, Ed., 599 pp.
- Neelin, J. D., C. Chou, and H. Su, 2003: Tropical drought regions in global warming and El Nino teleconnections. *Geophysical Research Letters*, **30**, doi:10.1029/2003GL018625.
- Neelin, J. D., M. Munnich, H. Su, J. E. Meyerson, and C. E. Holloway, 2006: Tropical drying trends in global warming models and observations. *Proc. Natl. Acad. Sci. U. S. A.*, **103**, 6110-6115.
- Nelson, F., and S. Outcalt, 1987: A computational method for prediction and regionalization of permafrost. *Arctic and Alpine Research*, **19**, 279-288.
- Nicolsky, D., V. Romanovsky, V. Alexeev, and D. Lawrence, 2007: Improved modeling of permafrost dynamics in a GCM land-surface scheme. *Geophysical Research Letters*, **34**, L08501.
- Niinemets, U., 2010: Responses of forest trees to single and multiple environmental stresses from seedlings to mature plants: Past stress history, stress interactions, tolerance and acclimation. *Forest Ecology and Management*, **260**, 1623-1639.
- Nikulin, G., E. Kjellstrom, U. Hansson, G. Strandberg, and A. Ullerstig, 2011: Evaluation and future projections of temperature, precipitation and wind extremes over Europe in an ensemble of regional climate simulations. *Tellus Series a-Dynamic Meteorology and Oceanography*, **63**, 41-55.
- Nobre, C., and L. Borma, 2009: 'Tipping points' for the Amazon forest. *Current Opinion in Environmental Sustainability*, **1**, 28-36.
- North, G., 1984: The small ice cap instability in diffuse climate models. *Journal of the Atmospheric Sciences*, **41**, 3390-3395.
- Notaro, M., 2008: Statistical identification of global hot spots in soil moisture feedbacks among IPCC AR4 models. *Journal of Geophysical Research-Atmospheres*, **113**, D09101.
- Notz, D., 2009: The future of ice sheets and sea ice: Between reversible retreat and unstoppable loss. *Proc. Natl. Acad. Sci. U. S. A.*, **106**, 20590-20595.
- Notz, D., 2012: Sea-ice extent provides a limited metric of model performance. *Journal of Geophysical Research*. submitted.
- NRC, 2011: *Climate Stabilization Targets: Emissions, Concentrations, and Impacts over Decades to Millennia*. National Academies Press, 298 pp.
- O'Connor, F., et al., 2010: Possible role of wetlands, permafrost, and methane hydrates in the methane cycle under future climate change: A review. *Reviews of Geophysics*, **48**, RG4005.
- O'Gorman, P., and T. Schneider, 2009a: Scaling of Precipitation Extremes over a Wide Range of Climates Simulated with an Idealized GCM. *Journal of Climate*, **22**, 5676-5685.
- , 2009b: The physical basis for increases in precipitation extremes in simulations of 21st-century climate change. *Proc. Natl. Acad. Sci. U. S. A.*, **106**, 14773-14777.
- O'Gorman, P. A., 2010: Understanding the varied response of the extratropical storm tracks to climate change. *Proc. Natl. Acad. Sci. U. S. A.*, **107**, 19176-19180.
- O'Gorman, P. A., and C. J. Muller, 2010: How closely do changes in surface and column water vapor follow Clausius-Clapeyron scaling in climate change simulations? *Environmental Research Letters*, **5**, 025207.
- O'Gorman, P., R. Allan, M. Byrne, and M. Previdi, 2012: Energetic Constraints on Precipitation Under Climate Change. *Surveys in Geophysics*, **33**, 585-608.
- Olson, R., R. Sriver, M. Goes, N. Urban, H. Matthews, M. Haran, and K. Keller, 2012: A climate sensitivity estimate using Bayesian fusion of instrumental observations and an Earth System model. *Journal of Geophysical Research-Atmospheres*, **117**.
- Orlowsky, B., and S. I. Seneviratne, 2012: Global changes in extreme events: regional and seasonal dimension. *Climatic Change*, **110**, 669-696.
- Overland, J. E., M. Wang, N. A. Bond, J. E. Walsh, V. M. Kattsov, and W. L. Chapman, 2011: Considerations in the selection of global climate models for regional climate projections: The Arctic as a case study. *Journal of Climate*, **24**, 1583-1597.
- Padilla, L., G. Vallis, and C. Rowley, 2011: Probabilistic Estimates of Transient Climate Sensitivity Subject to Uncertainty in Forcing and Natural Variability. *Journal of Climate*, **24**, 5521-5537.
- Paeth, H., and F. Pollinger, 2010: Enhanced evidence in climate models for changes in extratropical atmospheric circulation. *Tellus Series a-Dynamic Meteorology and Oceanography*, **62**, 647-660.
- Pagani, M., Z. Liu, J. LaRiviere, and A. Ravelo, 2010: High Earth-system climate sensitivity determined from Pliocene carbon dioxide concentrations. *Nat. Geosci.*, **3**, 27-30.

- 1 Pall, P., M. Allen, and D. Stone, 2007: Testing the Clausius-Clapeyron constraint on changes in extreme precipitation
2 under CO₂ warming. *Climate Dynamics*, **28**, 351-363.
- 3 Perrie, W., Y. H. Yao, and W. Q. Zhang, 2010: On the impacts of climate change and the upper ocean on midlatitude
4 northwest Atlantic landfalling cyclones. *Journal of Geophysical Research-Atmospheres*, **115**, D23110.
- 5 Piani, C., D. J. Frame, D. A. Stainforth, and M. R. Allen, 2005: Constraints on climate change from a multi-thousand
6 member ensemble of simulations. *Geophysical Research Letters*, **32**, L23825.
- 7 Pierce, D., et al., 2008: Attribution of Declining Western US Snowpack to Human Effects. *Journal of Climate*, **21**,
8 6425-6444.
- 9 Pitman, A., et al., 2009: Uncertainties in climate responses to past land cover change: First results from the LUCID
10 intercomparison study. *Geophys. Res. Lett.*, **36**, L14814.
- 11 Plattner, G., et al., 2008: Long-term climate commitments projected with climate-carbon cycle models. *Journal of*
12 *Climate*, **21**, 2721-2751.
- 13 Polvani, L. M., M. Previdi, and C. Deser, 2011: Large cancellation, due to ozone recovery, of future Southern
14 Hemisphere atmospheric circulation trends. *Geophysical Research Letters*, **38**, L04707.
- 15 Pongratz, J., C. Reick, T. Raddatz, and M. Claussen, 2010: Biogeophysical versus biogeochemical climate response to
16 historical anthropogenic land cover change. *Geophys. Res. Lett.*, **37**, L08702.
- 17 Power, S., and G. Kociuba, 2011a: The impact of global warming on the Southern Oscillation Index. *Climate*
18 *Dynamics*, **37**, 1745-1754.
- 19 Power, S., F. Delage, R. Colman, and A. Moise, 2012: Consensus on Twenty-First-Century Rainfall Projections in
20 Climate Models More Widespread than Previously Thought. *Journal of Climate*, **25**, 3792-3809.
- 21 Power, S. B., and G. Kociuba, 2011b: What Caused the Observed Twentieth-Century Weakening of the Walker
22 Circulation? *Journal of Climate*, **24**, 6501-6514.
- 23 Power, S. B., and F. P. Delage, 2012: What won't change in response to global warming? *Geophysical Research*
24 *Letters*. submitted.
- 25 Previdi, M., 2010: Radiative feedbacks on global precipitation. *Environmental Research Letters*, **5**.
- 26 Rahmstorf, S., et al., 2005: Thermohaline circulation hysteresis: A model intercomparison. *Geophysical Research*
27 *Letters*, **32**, L23605.
- 28 Raisanen, J., 2007: How reliable are climate models? *Tellus Series a-Dynamic Meteorology and Oceanography*, **59**, 2-
29 29.
- 30 Raisanen, J., 2008: Warmer climate: less or more snow? *Climate Dynamics*, **30**, 307-319.
- 31 Raisanen, J., and L. Ruokolainen, 2006: Probabilistic forecasts of near-term climate change based on a resampling
32 ensemble technique. *Tellus Series a-Dynamic Meteorology and Oceanography*, **58**, 461-472.
- 33 Raisanen, J., and J. S. Ylhäisi, 2011: Cold months in a warming climate. *Geophysical Research Letters*, **38**.
- 34 Ramaswamy, V., et al., 2001: Radiative Forcing of Climate Change. *Climate Change 2001: The Scientific Basis.*
35 *Contribution of Working Group I to the Third Assessment Report of the Intergovernmental Panel on Climate*
36 *Change*, Cambridge University Press.
- 37 Rammig, A., et al., 2010: Estimating the risk of Amazonian forest dieback. *New Phytologist*, **187**, 694-706.
- 38 Randall, D. A., et al., 2007: Climate Models and Their Evaluation. *Climate Change 2007: The Physical Science Basis.*
39 *Contribution of Working Group I to the Fourth Assessment Report of the Intergovernmental Panel on Climate*
40 *Change*, Cambridge University Press.
- 41 Randalls, S., 2010: History of the 2°C climate target. *Wiley Interdisciplinary Reviews: Climate Change*, **1**, 598-605.
- 42 Randel, W., and F. Wu, 2007: A stratospheric ozone profile data set for 1979-2005: Variability, trends, and
43 comparisons with column ozone data. *Journal of Geophysical Research-Atmospheres*, **112**.
- 44 Randles, C., and V. Ramaswamy, 2008: Absorbing aerosols over Asia: A Geophysical Fluid Dynamics Laboratory
45 general circulation model sensitivity study of model response to aerosol optical depth and aerosol absorption.
46 *Journal of Geophysical Research-Atmospheres*, **113**, D21203.
- 47 Reagan, M., and G. Moridis, 2007: Oceanic gas hydrate instability and dissociation under climate change scenarios.
48 *Geophysical Research Letters*, **34**, L22709.
- 49 —, 2009: Large-scale simulation of methane hydrate dissociation along the West Spitsbergen Margin. *Geophysical*
50 *Research Letters*, **36**, L23612.
- 51 Ridley, J., J. Lowe, and D. Simonin, 2008: The demise of Arctic sea ice during stabilisation at high greenhouse gas
52 concentrations. *Climate Dynamics*, **30**, 333-341.
- 53 Ridley, J., J. Lowe, C. Brierley, and G. Harris, 2007: Uncertainty in the sensitivity of Arctic sea ice to global warming
54 in a perturbed parameter climate model ensemble. *Geophysical Research Letters*, **34**, L19704.
- 55 Ridley, J., J. Gregory, P. Huybrechts, and J. Lowe, 2010: Thresholds for irreversible decline of the Greenland ice sheet.
56 *Climate Dynamics*, **35**, 1049-1057.
- 57 Ridley, J. K., J. A. Lowe, and H. T. Hewitt, 2012a: How reversible is sea ice loss? *The Cryosphere*, **6**, 193-198.
- 58 Ridley, J. K., H. T. Hewitt, A. J. McLaren, A. B. Keen, and A. E. West, 2012b: Understanding the climate response of
59 sea ice in an Earth System model. *Journal of Climate*. submitted.
- 60 Riley, W. J., Z. M. Subin, M. S. Torn, L. Meng, M. Mahowald, P. G. Hess, and D. M. Lawrence, 2011: Barriers to
61 predicting changes in global terrestrial methane fluxes: Analyses using CLM4ME, a methane biogeochemistry
62 model integrated in CESM. *Biogeosciences*. submitted.

- Rind, D., 1987: The doubled CO₂ climate - impact of the sea-surface temperature-gradient. *Journal of the Atmospheric Sciences*, **44**, 3235-3268.
- Rinke, A., P. Kuhry, and K. Dethloff, 2008: Importance of a soil organic layer for Arctic climate: A sensitivity study with an Arctic RCM. *Geophysical Research Letters*, **35**, L13709.
- Rive, N., A. Torvanger, T. Berntsen, and S. Kallbekken, 2007: To what extent can a long-term temperature target guide near-term climate change commitments? *Climatic Change*, **82**, 373-391.
- Robinson, A., R. Calov, and A. Ganopolski, 2012: Multistability and critical thresholds of the Greenland ice sheet. *Nature Climate Change*, **2**, 429-432.
- Roehrig, R., D. Bouniol, F. Guichard, F. Hourdin, and J.-L. Redelsperger, 2012: The present and future of the West African monsoon: a process-oriented assessment of CMIP5 simulations along the AMMA transect. *J. of Climate*, **submitted**.
- Roesch, A., 2006: Evaluation of surface albedo and snow cover in AR4 coupled climate models. *Journal of Geophysical Research-Atmospheres*, **111**, D15111.
- Rogelj, J., M. Meinshausen, and R. Knutti, 2012: Global warming under old and new scenarios using IPCC climate sensitivity range estimates. *Nature Climate Change*, **2**, 248-253.
- Rogelj, J., et al., 2011: Emission pathways consistent with a 2°C global temperature limit. *Nature Climate Change*, **1**, 413-418.
- Rohling, E., and P. P. Members, 2012: Making sense of palaeoclimate sensitivity. *Nature*. submitted.
- Rohling, E., K. Grant, M. Bolshaw, A. Roberts, M. Siddall, C. Hemleben, and M. Kucera, 2009: Antarctic temperature and global sea level closely coupled over the past five glacial cycles. *Nat. Geosci.*, **2**, 500-504.
- Rotstayn, L. D., S. J. Jeffrey, M. A. Collier, S. M. Dravitzki, A. C. Hirst, J. I. Syktus, and K. K. Wong, 2012: Aerosol- and greenhouse gas-induced changes in summer rainfall and circulation in the Australasian region: a study using single-forcing climate simulations. *Atmospheric Chemistry and Physics*, **12**, 6377-6404.
- Rougier, J., 2007: Probabilistic inference for future climate using an ensemble of climate model evaluations. *Climatic Change*, **81**, 247-264.
- Rougier, J., D. M. H. Sexton, J. M. Murphy, and D. Stainforth, 2009: Analyzing the Climate Sensitivity of the HadSM3 Climate Model Using Ensembles from Different but Related Experiments. *Journal of Climate*, **22**, 3540-3557.
- Rowell, D. P., 2012: Sources of Uncertainty in Future Changes in Local Precipitation. *Climate Dynamics*. doi:DOI 10.1007/s00382-011-1210-2, on-line first.
- Ruosteenoja, K., H. Tuomenvirta, and K. Jylha, 2007: GCM-based regional temperature and precipitation change estimates for Europe under four SRES scenarios applying a super-ensemble pattern-scaling method. *Climatic Change*, **81**, 193-208.
- Saenko, O. A., A. S. Gupta, and P. Spence, 2012: On Challenges in Predicting Bottom Water Transport in the Southern Ocean. *Journal of Climate*, **25**, 1349-1356.
- Saito, K., M. Kimoto, T. Zhang, K. Takata, and S. Emori, 2007: Evaluating a high-resolution climate model: Simulated hydrothermal regimes in frozen ground regions and their change under the global warming scenario. *Journal of Geophysical Research-Earth Surface*, **112**, F02S11.
- Sallée, J. B., E. Shuckburgh, N. Bruneau, A. Meijers, Z. Wang, and T. Bracegirdle, 2012a: Assessment of Southern Ocean water mass circulation and characteristics in CMIP5 models: Historical bias and forcing response. *Journal of Geophysical Research*. submitted.
- Sallée, J. B., E. Shuckburgh, N. Bruneau, A. Meijers, Z. Wang, and T. Bracegirdle, 2012b: Assessment of Southern Ocean mixed layer depths in CMIP5 models: Historical bias and forcing response. *Journal of Geophysical Research*. submitted.
- Samanta, A., B. Anderson, S. Ganguly, Y. Knyazikhin, R. Nemani, and R. Myneni, 2010: Physical Climate Response to a Reduction of Anthropogenic Climate Forcing. *Earth Interactions*, **14**.
- Sanderson, B. M., 2011: A Multimodel Study of Parametric Uncertainty in Predictions of Climate Response to Rising Greenhouse Gas Concentrations. *Journal of Climate*, **25**, 1362-1377.
- , 2012: On the estimation of systematic error in regression-based predictions of climate sensitivity. *Climatic Change*. in press.
- Sanderson, B. M., and R. Knutti, 2012: On the interpretation of constrained climate model ensembles. *Geophysical Research Letters*. in press.
- Sanderson, B. M., K. M. Shell, and W. Ingram, 2010: Climate feedbacks determined using radiative kernels in a multi-thousand member ensemble of AOGCMs. *Climate Dynamics*, **35**, 1219-1236.
- Sanderson, B. M., et al., 2008: Constraints on model response to greenhouse gas forcing and the role of subgrid-scale processes. *Journal of Climate*, **21**, 2384-2400.
- Sanderson, M. G., D. L. Hemming, and R. A. Betts, 2011: Regional temperature and precipitation changes under high-end (≥ 4 degrees C) global warming. *Philosophical Transactions of the Royal Society a-Mathematical Physical and Engineering Sciences*, **369**, 85-98.
- Sanso, B., and C. Forest, 2009: Statistical calibration of climate system properties. *Journal of the Royal Statistical Society Series C-Applied Statistics*, **58**, 485-503, doi:10.1111/j.1467-9876.2009.00669.x.
- Sanso, B., C. E. Forest, and D. Zantedeschi, 2008: Inferring Climate System Properties Using a Computer Model. *Bayesian Analysis*, **3**, 1-37.

- Sansom, P. G., D. B. Stephenson, C. A. T. Ferro, G. Zappa, and L. C. Shaffrey, 2012: A simple framework for weighting climate change projections in multi-model ensembles. *Journal of Climate*. submitted.
- Santer, B. D., T. M. L. Wigley, M. E. Schlesinger, and J. F. B. Mitchell, 1990: Developing climate scenarios from equilibrium GCM results. Max-Planck-Institut-für-Meteorologie, 29 pp. pp.
- Sato, T., F. Kimura, and A. Kitoh, 2007: Projection of global warming onto regional precipitation over Mongolia using a regional climate model. *Journal of Hydrology*, **333**, 144-154.
- Scaife, A. A., et al., 2012: Climate change projections and stratosphere-troposphere interaction. *Climate Dynamics*, **38**, 2089-2097.
- Schaefer, K., T. Zhang, L. Bruhwiler, and A. Barrett, 2011: Amount and timing of permafrost carbon release in response to climate warming. *Tellus Series B-Chemical and Physical Meteorology*, **63**, 165-180.
- Schaller, N., J. Cermak, M. Wild, and R. Knutti, 2012: The sensitivity of the energy budget and hydrological cycle to CO₂ and solar forcing. *Climate Dynamics*. submitted.
- Schar, C., P. L. Vidale, D. Luthi, C. Frei, C. Haberli, M. A. Liniger, and C. Appenzeller, 2004: The role of increasing temperature variability in European summer heatwaves. *Nature*, **427**, 332-336.
- Scheff, J., and D. M. W. Frierson, 2012: Robust future precipitation declines in CMIP5 largely reflect the poleward expansion of model subtropical dry zones. *Geophysical Research Letters*, **(submitted)**.
- Schlesinger, M., 1986: Equilibrium and transient climatic warming induced by increased atmospheric CO₂. *Climate Dynamics*, **1**, 35-51.
- Schlesinger, M., et al., 2000: Geographical distributions of temperature change for scenarios of greenhouse gas and sulfur dioxide emissions. *Technological Forecasting and Social Change*, **65**, 167-193.
- Schmidt, M. W. I., et al., 2011: Persistence of soil organic matter as an ecosystem property. *Nature*, **478**, 49-56.
- Schmittner, A., et al., 2011: Climate Sensitivity Estimated from Temperature Reconstructions of the Last Glacial Maximum. *Science*, **334**, 1385-1388.
- Schneider von Deimling, T., H. Held, A. Ganopolski, and S. Rahmstorf, 2006: Climate sensitivity estimated from ensemble simulations of glacial climate. *Climate Dynamics*, **27**, 149-163.
- Schneider von Deimling, T., M. Meinshausen, A. Levermann, V. Huber, K. Frieler, D. Lawrence, and V. Brovkin, 2011: Estimating the permafrost-carbon feedback on global warming. *Biogeosciences Discussions*, **8**, 4727-4761.
- Schoof, C., 2007: Ice sheet grounding line dynamics: Steady states, stability, and hysteresis. *Journal of Geophysical Research-Earth Surface*, **112**, F03S28.
- Schröder, D., and W. M. Connolley, 2007: Impact of instantaneous sea ice removal in a coupled general circulation model. *Geophys. Res. Lett.*, **34**, L14502.
- Schuenemann, K. C., and J. J. Cassano, 2010: Changes in synoptic weather patterns and Greenland precipitation in the 20th and 21st centuries: 2. Analysis of 21st century atmospheric changes using self-organizing maps. *Journal of Geophysical Research-Atmospheres*, **115**, D05108.
- Schuur, E., J. Vogel, K. Crummer, H. Lee, J. Sickman, and T. Osterkamp, 2009: The effect of permafrost thaw on old carbon release and net carbon exchange from tundra. *Nature*, **459**, 556-559.
- Schwartz, S., R. Charlson, R. Kahn, J. Ogren, and H. Rodhe, 2010: Why Hasn't Earth Warmed as Much as Expected? *Journal of Climate*, **23**, 2453-2464.
- , 2012: Reply to "Comments on 'Why Hasn't Earth Warmed as Much as Expected?'". *Journal of Climate*, **25**, 2200-2204.
- Schwartz, S. E., 2012: Determination of Earth's Transient and Equilibrium Climate Sensitivities from Observations Over the Twentieth Century: Strong Dependence on Assumed Forcing. *Surveys of Geophysics*, **33**, 745-777.
- Screen, J., and I. Simmonds, 2010: The central role of diminishing sea ice in recent Arctic temperature amplification. *Nature*, **464**, 1334-1337.
- Screen, J. A., N. P. Gillett, A. Y. Karpechko, and D. P. Stevens, 2010: Mixed Layer Temperature Response to the Southern Annular Mode: Mechanisms and Model Representation. *Journal of Climate*, **23**, 664-678.
- Seager, R., and G. A. Vecchi, 2010: Greenhouse warming and the 21st century hydroclimate of the southwestern North America. *Proc. Nat. Acad. Sci.*, **107**, 21277-21282.
- Seager, R., and N. Naik, 2012: A Mechanisms-Based Approach to Detecting Recent Anthropogenic Hydroclimate Change. *Journal of Climate*, **25**, 236-261.
- Seager, R., et al., 2007: Model projections of an imminent transition to a more arid climate in southwestern North America. *Science*, **316**, 1181-1184.
- Sedláček, J., R. Knutti, O. Martius, and U. Beyerle, 2011: Impact of a Reduced Arctic Sea Ice Cover on Ocean and Atmospheric Properties. *Journal of Climate*, **25**, 307-319.
- Seidel, D., and W. Randel, 2007: Recent widening of the tropical belt: Evidence from tropopause observations. *Journal of Geophysical Research-Atmospheres*, **112**, D20113.
- Seidel, D. J., Q. Fu, W. J. Randel, and T. J. Reichler, 2008: Widening of the tropical belt in a changing climate. *Nat. Geosci.*, **1**, 21-24.
- Sen Gupta, A., A. Santoso, A. Taschetto, C. Ummenhofer, J. Trevena, and M. England, 2009: Projected Changes to the Southern Hemisphere Ocean and Sea Ice in the IPCC AR4 Climate Models. *Journal of Climate*, **22**, 3047-3078.

- Seneviratne, S., and N. Nicholls, 2012: Comparing IPCC Assessments: How do the AR4 and SREX assessments of changes in extremes differ? *Climatic Change*. submitted.
- Seneviratne, S. I., D. Luthi, M. Litschi, and C. Schar, 2006: Land-atmosphere coupling and climate change in Europe. *Nature*, **443**, 205-209.
- Seneviratne, S. I., et al., 2010: Investigating soil moisture-climate interactions in a changing climate: A review. *Earth-Science Reviews*, **99**, 125-161.
- Seneviratne, S. I., et al., 2012: Changes in climate extremes and their impacts on the natural physical environment. *Managing the Risks of Extreme Events and Disasters to Advance Climate Change Adaptation. A Special Report of Working Groups I and II of the Intergovernmental Panel on Climate Change (IPCC)*, C. B. Field, et al., Eds., Cambridge University Press, pp. 109-230.
- Senior, C., and J. Mitchell, 2000: The time-dependence of climate sensitivity. *Geophysical Research Letters*, **27**, 2685-2688.
- Serreze, M., A. Barrett, J. Stroeve, D. Kindig, and M. Holland, 2009: The emergence of surface-based Arctic amplification. *Cryosphere*, **3**, 11-19.
- Serreze, M. C., 2011: Climate change: Rethinking the sea-ice tipping point. *Nature*, **471**, 47-48.
- Serreze, M. C., and J. A. Francis, 2006: The arctic amplification debate. *Climatic Change*, **76**, 241-264.
- Sexton, D., H. Grubb, K. Shine, and C. Folland, 2003: Design and analysis of climate model experiments for the efficient estimation of anthropogenic signals. *Journal of Climate*, **16**, 1320-1336.
- Sexton, D. M. H., and J. M. Murphy, 2012: Multivariate probabilistic projections using imperfect climate models. Part II: robustness of methodological choices and consequences for climate sensitivity. *Climate Dynamics*, 2543-2558.
- Sexton, D. M. H., J. M. Murphy, M. Collins, and M. J. Webb, 2012: Multivariate probabilistic projections using imperfect climate models part I: outline of methodology. *Climate Dynamics*, 2513-2542.
- Shepherd, T. G., and C. McLandress, 2011: A Robust Mechanism for Strengthening of the Brewer-Dobson Circulation in Response to Climate Change: Critical-Layer Control of Subtropical Wave Breaking. *Journal of the Atmospheric Sciences*, **68**, 784-797.
- Sherwood, S. C., 2010: Direct versus indirect effects of tropospheric humidity changes on the hydrologic cycle. *Environmental Research Letters*, **5**, 025206.
- Sherwood, S. C., and M. Huber, 2010: An adaptability limit to climate change due to heat stress. *Proc. Natl. Acad. Sci. U. S. A.*, **107**, 9552-9555.
- Sherwood, S. C., W. Ingram, Y. Tsushima, M. Satoh, M. Roberts, P. L. Vidale, and P. A. O'Gorman, 2010: Relative humidity changes in a warmer climate. *Journal of Geophysical Research-Atmospheres*, **115**, D09104.
- Shindell, D. T., et al., 2012a: Interactive ozone and methane chemistry in GISS-E2 historical and future climate simulations. *Atmospheric Chemistry and Physics*, **submitted**.
- Shindell, D. T., et al., 2012b: Radiative forcing in the ACCMIP historical and future climate simulations. *Atmospheric Chemistry and Physics*, **submitted**.
- Shine, K., J. Cook, E. Highwood, and M. Joshi, 2003: An alternative to radiative forcing for estimating the relative importance of climate change mechanisms. *Geophysical Research Letters*, **30**, 2047.
- Shiogama, H., S. Emori, K. Takahashi, T. Nagashima, T. Ogura, T. Nozawa, and T. Takemura, 2010a: Emission Scenario Dependency of Precipitation on Global Warming in the MIROC3.2 Model. *Journal of Climate*, **23**, 2404-2417.
- Shiogama, H., et al., 2010b: Emission scenario dependencies in climate change assessments of the hydrological cycle. *Climatic Change*, **99**, 321-329.
- Shkolnik, I., E. Nadyozhina, T. Pavlova, E. Molkentin, and A. Semioshina, 2010: Snow cover and permafrost evolution in Siberia as simulated by the MGO regional climate model in the 20th and 21st centuries. *Environmental Research Letters*, **5**, 015005.
- Shongwe, M. E., G. J. van Oldenborgh, B. van den Hurk, and M. van Aalst, 2011: Projected Changes in Mean and Extreme Precipitation in Africa under Global Warming. Part II: East Africa. *Journal of Climate*, **24**, 3718-3733.
- Siegenthaler, U., and H. Oeschger, 1984: Transient temperature changes due to increasing CO₂ using simple models. *Annals of Glaciology*, 153-159.
- Sigmond, M., P. C. Siegmund, E. Manzini, and H. Kelder, 2004: A simulation of the separate climate effects of middle-atmospheric and tropospheric CO₂ doubling. *Journal of Climate*, **17**, 2352-2367.
- Sillmann, J., and E. Roeckner, 2008: Indices for extreme events in projections of anthropogenic climate change. *Climatic Change*, **86**, 83-104.
- Sillmann, J., and M. Croci-Maspoli, 2009: Present and future atmospheric blocking and its impact on European mean and extreme climate. *Geophysical Research Letters*, **36**, L10702.
- Sillmann, J., V. V. Kharin, F. W. Zwiers, and X. Zhang, 2012: Climate extreme indices in the CMIP5 multi-model ensemble. Part 2: Future climate projections. *Journal of Geophysical Research*. submitted.
- Simpkins, G. R., and A. Y. Karpechko, 2012: Sensitivity of the southern annular mode to greenhouse gas emission scenarios. *Climate Dynamics*, **38**, 563-572.
- Skeie, R., J. Fuglestad, T. Berntsen, M. Lund, G. Myhre, and K. Rypdal, 2009: Global temperature change from the transport sectors: Historical development and future scenarios. *Atmospheric Environment*, **43**, 6260-6270.

- Slater, A. G., and D. M. Lawrence, 2012: Diagnosing Present and Future Permafrost from Climate Models. *J. Climate*, **submitted**.
- Smith, L., Y. Sheng, G. MacDonald, and L. Hinzman, 2005: Disappearing Arctic lakes. *Science*, **308**, 1429-1429.
- Smith, L., et al., 2004: Siberian peatlands a net carbon sink and global methane source since the early Holocene. *Science*, **303**, 353-356.
- Smith, R. L., C. Tebaldi, D. Nychka, and L. O. Mearns, 2009: Bayesian Modeling of Uncertainty in Ensembles of Climate Models. *Journal of the American Statistical Association*, **104**, 97-116, doi:10.1198/jasa.2009.0007.
- Smith, S. J., J. van Aardenne, Z. Klimont, R. J. Andres, A. Volke, and S. Delgado Arias, 2011: Anthropogenic sulfur dioxide emissions: 1850-2005. *Atmos. Chem. Phys.*, **11**, 1101-1116.
- Soden, B., I. Held, R. Colman, K. Shell, J. Kiehl, and C. Shields, 2008: Quantifying climate feedbacks using radiative kernels. *Journal of Climate*, **21**, 3504-3520.
- Soden, B. J., and I. M. Held, 2006: An assessment of climate feedbacks in coupled ocean-atmosphere models. *Journal of Climate*, **19**, 3354-3360.
- Soden, B. J., and G. A. Vecchi, 2011: The vertical distribution of cloud feedback in coupled ocean-atmosphere models. *Geophysical Research Letters*, **38**, L12704.
- Sokolov, A., C. Forest, and P. Stone, 2010a: Sensitivity of climate change projections to uncertainties in the estimates of observed changes in deep-ocean heat content. *Climate Dynamics*, **34**, 735-745.
- Sokolov, A. P., et al., 2010b: Probabilistic forecast for twenty-first-century climate based on uncertainties in emissions (without policy) and climate parameters. *Journal of Climate*, **23**, 2230-2231, doi:2210.1175/2009jcli3566.2231.
- Solomon, S., G. Plattner, R. Knutti, and P. Friedlingstein, 2009: Irreversible climate change due to carbon dioxide emissions. *Proc. Natl. Acad. Sci. U. S. A.*, **106**, 1704-1709.
- Solomon, S., J. Daniel, T. Sanford, D. Murphy, G. Plattner, R. Knutti, and P. Friedlingstein, 2010: Persistence of climate changes due to a range of greenhouse gases. *Proc. Natl. Acad. Sci. U. S. A.*, **107**, 18354-18359.
- Solomon, S., et al., 2007: Technical Summary. *Climate Change 2007: The Physical Science Basis. Contribution of Working Group I to the Fourth Assessment Report of the Intergovernmental Panel on Climate Change*, Cambridge University Press.
- Son, S. W., et al., 2010: Impact of stratospheric ozone on Southern Hemisphere circulation change: A multimodel assessment. *Journal of Geophysical Research-Atmospheres*, **115**, D00M07.
- Sorensson, A., C. Menendez, R. Ruscica, P. Alexander, P. Samuelsson, and U. Willen, 2010: Projected precipitation changes in South America: a dynamical downscaling within CLARIS. *Meteorologische Zeitschrift*, **19**, 347-355.
- Stott, P., G. Jones, and J. Mitchell, 2003: Do models underestimate the solar contribution to recent climate change? *Journal of Climate*, **16**, 4079-4093.
- Stouffer, R., 2004: Time scales of climate response. *Journal of Climate*, **17**, 209-217.
- Stowasser, M., H. Annamalai, and J. Hafner, 2009: Response of the South Asian Summer Monsoon to Global Warming: Mean and Synoptic Systems. *Journal of Climate*, **22**, 1014-1036.
- Stroeve, J., M. Holland, W. Meier, T. Scambos, and M. Serreze, 2007: Arctic sea ice decline: Faster than forecast. *Geophysical Research Letters*, **34**, L09501.
- Stroeve, J. C., V. Kattsov, A. Barrett, M. Serreze, T. Pavlova, M. Holland, and W. N. Meier, 2012: Trends in Arctic sea ice extent from CMIP5, CMIP3 and observations. *Geophysical Research Letters*. accepted.
- Stuber, N., M. Ponater, and R. Sausen, 2005: Why radiative forcing might fail as a predictor of climate change. *Climate Dynamics*, **24**, 497-510.
- Sudo, K., M. Takahashi, and H. Akimoto, 2003: Future changes in stratosphere-troposphere exchange and their impacts on future tropospheric ozone simulations. *Geophysical Research Letters*, **30**.
- Sugiyama, M., H. Shiogama, and S. Emori, 2010: Precipitation extreme changes exceeding moisture content increases in MIROC and IPCC climate models. *Proc. Natl. Acad. Sci. U. S. A.*, **107**, 571-575.
- Sun, Y., S. Solomon, A. Dai, and R. W. Portmann, 2007: How often will it rain? *Journal of Climate*, **20**, 4801-4818.
- Sutton, R. T., B. W. Dong, and J. M. Gregory, 2007: Land/sea warming ratio in response to climate change: IPCC AR4 model results and comparison with observations. *Geophysical Research Letters*, **34**, L02701.
- Swart, N. C., and J. C. Fyfe, 2012: Observed and simulated changes in the Southern Hemisphere surface westerly wind-stress. *Geophysical Research Letters*. accepted.
- Swingedouw, D., P. Braconnot, P. Delecluse, E. Guilyardi, and O. Marti, 2007: Quantifying the AMOC feedbacks during a 2xCO₂ stabilization experiment with land-ice melting. *Climate Dynamics*, **29**, 521-534.
- Swingedouw, D., T. Fichefet, P. Huybrechts, H. Goosse, E. Driesschaert, and M. Loutre, 2008: Antarctic ice-sheet melting provides negative feedbacks on future climate warming. *Geophysical Research Letters*, **35**, L17705.
- Szopa, S., et al., 2012: Aerosol and Ozone changes as forcing for Climate Evolution between 1850 and 2100. *Climate Dynamics*. doi:10.1007/s00382-012-1408-y, accepted.
- Takahashi, K., 2009a: The Global Hydrological Cycle and Atmospheric Shortwave Absorption in Climate Models under CO₂ Forcing. *Journal of Climate*, **22**, 5667-5675.
- Takahashi, K., 2009b: Radiative Constraints on the Hydrological Cycle in an Idealized Radiative-Convective Equilibrium Model. *Journal of the Atmospheric Sciences*, **66**, 77-91.
- Tanaka, K., and T. Raddatz, 2011: Correlation between climate sensitivity and aerosol forcing and its implication for the "climate trap" A Letter. *Climatic Change*, **109**, 815-825.

- Tarnocai, C., J. Canadell, E. Schuur, P. Kuhry, G. Mazhitova, and S. Zimov, 2009: Soil organic carbon pools in the northern circumpolar permafrost region. *Global Biogeochemical Cycles*, **23**, GB2023.
- Taylor, K. E., R. J. Stouffer, and G. A. Meehl, 2012: A Summary of the CMIP5 Experiment Design. *Bull. Amer. Meteor. Soc.*, **93**, 485–498.
- Tebaldi, C., and R. Knutti, 2007: The use of the multi-model ensemble in probabilistic climate projections. *Philosophical Transactions of the Royal Society A-Mathematical Physical and Engineering Sciences*, **365**, 2053–2075.
- Tebaldi, C., and D. B. Lobell, 2008: Towards probabilistic projections of climate change impacts on global crop yields. *Geophysical Research Letters*, **35**, L08705.
- Tebaldi, C., and B. Sanso, 2009: Joint projections of temperature and precipitation change from multiple climate models: a hierarchical Bayesian approach. *Journal of the Royal Statistical Society Series A-Statistics in Society*, **172**, 83–106.
- Tebaldi, C., J. M. Arblaster, and R. Knutti, 2011: Mapping model agreement on future climate projections. *Geophysical Research Letters*, **38**, L23701.
- Tebaldi, C., K. Hayhoe, J. M. Arblaster, and G. A. Meehl, 2006: Going to the extremes. *Climatic Change*, **79**, 185–211.
- Terray, L., L. Corre, S. Cravatte, T. Delcroix, G. Reverdin, and A. Ribes, 2012: Near-Surface Salinity as Nature's Rain Gauge to Detect Human Influence on the Tropical Water Cycle. *Journal of Climate*, **25**, 958–977.
- Thorne, P., 2008: Arctic tropospheric warming amplification? *Nature*, **455**, E1–E2.
- Tietsche, S., D. Notz, J. H. Jungclauss, and J. Marotzke, 2011: Recovery mechanisms of Arctic summer sea ice. *Geophys. Res. Lett.*, **38**, L02707.
- Tjiputra, J. F., et al., 2012: Evaluation of the carbon cycle components in the Norwegian Earth System Model (NorESM). *Geoscientific Model Development*, **submitted**.
- Tomassini, L., P. Reichert, R. Knutti, T. F. Stocker, and M. E. Borsuk, 2007: Robust Bayesian uncertainty analysis of climate system properties using Markov chain Monte Carlo methods. *Journal of Climate*, **20**, 1239–1254.
- Trenberth, K. E., and D. J. Shea, 2005: Relationships between precipitation and surface temperature. *Geophysical Research Letters*, **32**, L14703.
- Trenberth, K. E., and J. T. Fasullo, 2009: Global warming due to increasing absorbed solar radiation. *Geophysical Research Letters*, **36**, L07706.
- , 2010: Simulation of Present-Day and Twenty-First-Century Energy Budgets of the Southern Oceans. *Journal of Climate*, **23**, 440–454.
- Ueda, H., A. Iwai, K. Kuwako, and M. Hori, 2006: Impact of anthropogenic forcing on the Asian summer monsoon as simulated by eight GCMs. *Geophysical Research Letters*, **33**, L06703.
- Ulbrich, U., G. C. Leckebusch, and J. G. Pinto, 2009: Extra-tropical cyclones in the present and future climate: a review. *Theoretical and Applied Climatology*, **96**, 117–131.
- Ulbrich, U., J. G. Pinto, H. Kupfer, G. C. Leckebusch, T. Spanghel, and M. Meyers, 2008: Changing northern hemisphere storm tracks in an ensemble of IPCC climate change simulations. *Journal of Climate*, **21**, 1669–1679.
- UNEP, 2010: The emissions gap report: Are the Copenhagen Accord pledges sufficient to limit global warming to 2°C or 1.5°C?, 55 pp., <http://www.unep.org/publications/ebooks/emissionsgapreport/> pp.
- Urban, N., and K. Keller, 2009: Complementary observational constraints on climate sensitivity. *Geophysical Research Letters*, **36**, L04708.
- van Vuuren, D. P., et al., 2011: RCP3-PD: Exploring the possibilities to limit global mean temperature change to less than 2°C. *Climatic Change*, **109**, 95–116.
- Vavrus, S., M. Holland, and D. Bailey, 2011: Changes in Arctic clouds during intervals of rapid sea ice loss. *Climate Dynamics*, **36**, 1475–1489.
- Vecchi, G. A., and B. J. Soden, 2007: Global warming and the weakening of the tropical circulation. *Bulletin of the American Meteorological Society*, **88**, 1529–1530.
- Vedantham, A., and M. Oppenheimer, 1998: Long-term scenarios for aviation: Demand and emissions of CO₂ and NO_x. *Energy Policy*, **26**, 625–641.
- Vidale, P. L., D. Luthi, R. Wegmann, and C. Schar, 2007: European summer climate variability in a heterogeneous multi-model ensemble. *Climatic Change*, **81**, 209–232.
- Volz, A., et al., 2012: The CNRM-CM5.1 global climate model: Description and basic evaluation. *Climate Dynamics*, **Online First**, DOI: 10.1007/s00382-00011-01259-y.
- Voss, R., and U. Mikolajewicz, 2001: Long-term climate changes due to increased CO₂ concentration in the coupled atmosphere-ocean general circulation model ECHAM3/LSG. *Climate Dynamics*, **17**, 45–60.
- Walker, R., et al., 2009: Protecting the Amazon with protected areas. *Proc. Natl. Acad. Sci. U. S. A.*, **106**, 10582–10586.
- Wang, M., and J. Overland, 2009: A sea ice free summer Arctic within 30 years? *Geophysical Research Letters*, **36**, L07502.
- Wang, M., and J. E. Overland, 2012: Summer Arctic sea ice will be gone sooner or later - an update from CMIP5 models. *Geophysical Research Letters*. accepted.
- Wania, R., I. Ross, and I. Prentice, 2009: Integrating peatlands and permafrost into a dynamic global vegetation model: 2. Evaluation and sensitivity of vegetation and carbon cycle processes. *Global Biogeochemical Cycles*, **23**, GB3015.

- Washington, W., et al., 2009: How much climate change can be avoided by mitigation? *Geophysical Research Letters*, **36**, L08703.
- Watanabe, S., et al., 2011: MIROC-ESM 2010: model description and basic results of CMIP5-20c3m experiments. *Geoscientific Model Development*, **4**, 845-872.
- Watterson, I. G., 2008: Calculation of probability density functions for temperature and precipitation change under global warming. *Journal of Geophysical Research-Atmospheres*, **113**, D12106, doi:12110.11029/12007JD009254.
- , 2011: Calculation of joint PDFs for climate change with properties matching Australian projections. *Australian Meteorological and Oceanographic Journal*, **61**, 211-219.
- Watterson, I. G., and P. H. Whetton, 2011: Joint PDFs for Australian climate in future decades and an idealized application to wheat crop yield. *Australian Meteorological and Oceanographic Journal*, **61**, 221-230.
- Watterson, I. G., J. L. McGregor, and K. C. Nguyen, 2008: Changes in extreme temperatures of Australasian summer simulated by CCAM under global warming, and the roles of winds and land-sea contrasts. *Australian Meteorological Magazine*, **57**, 195-212.
- WBGU, 2009: Solving the climate dilemma: The budget approach. German Advisory Council on Global Change, 59 pp., ISBN 53-936191-936127-936191 pp.
- Weaver, A., K. Zickfeld, A. Montenegro, and M. Eby, 2007: Long term climate implications of 2050 emission reduction targets. *Geophysical Research Letters*, **34**, L19703.
- Weaver, A. J., et al., 2012: Stability of the Atlantic meridional overturning circulation: A model intercomparison. *Geophysical Research Letters*. submitted.
- Webb, M., et al., 2006: On the contribution of local feedback mechanisms to the range of climate sensitivity in two GCM ensembles. *Climate Dynamics*, **27**, 17-38.
- Weber, S., et al., 2007: The modern and glacial overturning circulation in the Atlantic Ocean in PMIP coupled model simulations. *Climate of the Past*, **3**, 51-64.
- Weertman, J., 1974: Stability of the junction of an ice sheet and an ice shelf. 3-11.
- Wehner, M., D. Easterling, J. Lawrimore, R. Heim, R. Vose, and B. Santer, 2011: Projections of Future Drought in the Continental United States and Mexico. *Journal of Hydrometeorology*, **12**, 1359-1377.
- Weigel, A., R. Knutti, M. Liniger, and C. Appenzeller, 2010: Risks of Model Weighting in Multimodel Climate Projections. *Journal of Climate*, **23**, 4175-4191.
- Wentz, F., L. Ricciardulli, K. Hilburn, and C. Mears, 2007: How much more rain will global warming bring? *Science*, **317**, 233-235.
- Wetherald, R., and S. Manabe, 1988: Cloud Feedback processes in a General-Circulation Model. *Journal of the Atmospheric Sciences*, **45**, 1397-1415.
- Wetherald, R., R. Stouffer, and K. Dixon, 2001: Committed warming and its implications for climate change. *Geophysical Research Letters*, **28**, 1535-1538.
- Wigley, T., 2005: The climate change commitment. *Science*, **307**, 1766-1769.
- Wilcox, L. J., A. J. Charlton-Perez, and L. J. Gray, 2012: Trends in Austral jet position in ensembles of high- and low-top CMIP5 models. *Journal of Geophysical Research*, (submitted).
- Willett, K., and S. Sherwood, 2012: Exceedance of heat index thresholds for 15 regions under a warming climate using the wet-bulb globe temperature. *International Journal of Climatology*, **32**, 161-177.
- Williams, J. W., S. T. Jackson, and J. E. Kutzbach, 2007: Projected distributions of novel and disappearing climates by 2100 AD. *Proc. Natl. Acad. Sci. U. S. A.*, **104**, 5738-5742.
- Winton, M., 2006a: Does the Arctic sea ice have a tipping point? *Geophysical Research Letters*, **33**, L23504.
- , 2006b: Amplified Arctic climate change: What does surface albedo feedback have to do with it? *Geophysical Research Letters*, **33**, L03701.
- Winton, M., 2008: Sea ice-albedo feedback and nonlinear Arctic climate change. *Arctic Sea Ice Decline: Observations, Projections, Mechanisms, and Implications*, E. T. DeWeaver, C. M. Bitz, and L. B. Tremblay, Eds., Amer. Geophys. Union, 111-131.
- Winton, M., 2011: Do Climate Models Underestimate the Sensitivity of Northern Hemisphere Sea Ice Cover? *Journal of Climate*, **24**, 3924-3934.
- WMO, 2007: Scientific Assessment of Ozone Depletion. World Meteorological Organization.
- Wood, R., A. Keen, J. Mitchell, and J. Gregory, 1999: Changing spatial structure of the thermohaline circulation in response to atmospheric CO₂ forcing in a climate model. *Nature*, **399**, 572-575.
- Woollings, T., 2008: Vertical structure of anthropogenic zonal-mean atmospheric circulation change. *Geophys. Res. Lett.*, **35**, L19702.
- Woollings, T., and M. Blackburn, 2012: The North Atlantic Jet Stream under Climate Change and Its Relation to the NAO and EA Patterns. *Journal of Climate*, **25**, 886-902.
- Woollings, T., J. M. Gregory, J. G. Pinto, M. Reyers, and D. J. Brayshaw, 2012: Response of the North Atlantic storm track to climate change shaped by ocean-atmosphere coupling. *Nat. Geosci.*, **5**, 313-317.
- Wu, P., R. Wood, J. Ridley, and J. Lowe, 2010: Temporary acceleration of the hydrological cycle in response to a CO₂ rampdown. *Geophysical Research Letters*, **37**, L12705.
- Wu, P., L. Jackson, A. Pardaens, and N. Schaller, 2011: Extended warming of the northern high latitudes due to an overshoot of the Atlantic meridional overturning circulation. *Geophysical Research Letters*, **38**.

- 1 Wu, T., et al., 2012: Global carbon budgets simulated by the Beijing Climate Center Climate System Model for the last
2 century. *Journal of Climate*, **submitted**.
- 3 Wyant, M. C., et al., 2006: A comparison of low-latitude cloud properties and their response to climate change in three
4 AGCMs sorted into regimes using mid-tropospheric vertical velocity. *Climate Dynamics*, **27**, 261-279.
- 5 Xie, S. P., C. Deser, G. A. Vecchi, J. Ma, H. Y. Teng, and A. T. Wittenberg, 2010: Global Warming Pattern Formation:
6 Sea Surface Temperature and Rainfall. *Journal of Climate*, **23**, 966-986.
- 7 Xin, X., L. Zhang, J. Zhang, T. Wu, and Y. Fang, 2012a: Climate change projections over East Asia with
8 BCC_CSM1.1 under RCP scenarios. *Journal of the Meteorological Society of Japan*, **submitted**.
- 9 Xin, X., T. Wu, J. Li, Z. Wang, W. Li, and F. Wu, 2012b: How well does BCC_CSM1.1 reproduce the 20th century
10 climate change in China? *Atmospheric and Oceanic Science Letters*, **in press**.
- 11 Yin, J., J. Overpeck, S. Griffies, A. Hu, J. Russell, and R. Stouffer, 2011: Different magnitudes of projected subsurface
12 ocean warming around Greenland and Antarctica. *Nat. Geosci.*, **4**, 524-528.
- 13 Yokohata, T., M. Webb, M. Collins, K. Williams, M. Yoshimori, J. Hargreaves, and J. Annan, 2010: Structural
14 Similarities and Differences in Climate Responses to CO₂ Increase between Two Perturbed Physics Ensembles.
15 *Journal of Climate*, **23**, 1392-1410.
- 16 Yokohata, T., J. D. Annan, J. C. Hargreaves, C. S. Jackson, M. Tobis, M. Webb, and M. Collins, 2012: Reliability of
17 multi-model and structurally different single-model ensembles. *Climate Dynamics*. doi:10.1007/s00382-011-
18 1203-1, published online.
- 19 Yukimoto, S., et al., 2012: A New Global Climate Model of the Meteorological Research Institute: MRI-CGCM3-
20 Model Description and Basic Performance. *Journal of the Meteorological Society of Japan*, **90A**, 23-64.
- 21 Zappa, G., L. C. Shaffrey, K. I. Hodges, P. G. Sansom, and D. B. Stephenson, 2012: A Multi-Model Assessment of
22 Future Projections of North Atlantic and European extratropical cyclones in the CMIP5. *Journal of Climate*,
23 **(submitted)**.
- 24 Zelazowski, P., Y. Malhi, C. Huntingford, S. Sitch, and J. Fisher, 2011: Changes in the potential distribution of humid
25 tropical forests on a warmer planet. *Philosophical Transactions of the Royal Society a-Mathematical Physical
26 and Engineering Sciences*, **369**, 137-160.
- 27 Zelinka, M., and D. Hartmann, 2010: Why is longwave cloud feedback positive? *Journal of Geophysical Research-
28 Atmospheres*, **115**, D16117.
- 29 Zelinka, M., S. Klein, and D. Hartmann, 2012: Computing and Partitioning Cloud Feedbacks Using Cloud Property
30 Histograms. Part II: Attribution to Changes in Cloud Amount, Altitude, and Optical Depth. *Journal of Climate*,
31 **25**, 3736-3754.
- 32 Zhang, M., and H. Song, 2006: Evidence of deceleration of atmospheric vertical overturning circulation over the
33 tropical Pacific. *Geophysical Research Letters*, **33**, L12701.
- 34 Zhang, M. H., and C. Bretherton, 2008: Mechanisms of low cloud-climate feedback in idealized single-column
35 simulations with the Community Atmospheric Model, version 3 (CAM3). *Journal of Climate*, **21**, 4859-4878.
- 36 Zhang, R., 2010a: Northward intensification of anthropogenically forced changes in the Atlantic meridional overturning
37 circulation (AMOC). *Geophysical Research Letters*, **37**, L24603.
- 38 Zhang, T., 2005: Influence of the seasonal snow cover on the ground thermal regime: An overview. *Reviews of
39 Geophysics*, **43**, RG4002.
- 40 Zhang, X., 2010b: Sensitivity of arctic summer sea ice coverage to global warming forcing: towards reducing
41 uncertainty in arctic climate change projections. *Tellus Series a-Dynamic Meteorology and Oceanography*, **62**,
42 220-227.
- 43 Zhang, X., and J. Walsh, 2006: Toward a seasonally ice-covered Arctic Ocean: Scenarios from the IPCC AR4 model
44 simulations. *Journal of Climate*, **19**, 1730-1747.
- 45 Zhang, X. B., et al., 2007: Detection of human influence on twentieth-century precipitation trends. *Nature*, **448**, 461-
46 U464.
- 47 Zhou, L. M., R. E. Dickinson, P. Dirmeyer, A. Dai, and S. K. Min, 2009: Spatiotemporal patterns of changes in
48 maximum and minimum temperatures in multi-model simulations. *Geophysical Research Letters*, **36**, L02702.
- 49 Zhuang, Q., et al., 2004: Methane fluxes between terrestrial ecosystems and the atmosphere at northern high latitudes
50 during the past century: A retrospective analysis with a process-based biogeochemistry model. *Global
51 Biogeochemical Cycles*, **18**, GB3010.
- 52 Zickfeld, K., B. Knopf, V. Petoukhov, and H. Schellnhuber, 2005: Is the Indian summer monsoon stable against global
53 change? *Geophysical Research Letters*, **32**, L15707.
- 54 Zickfeld, K., M. Eby, H. Matthews, and A. Weaver, 2009: Setting cumulative emissions targets to reduce the risk of
55 dangerous climate change. *Proc. Natl. Acad. Sci. U. S. A.*, **106**, 16129-16134.
- 56 Zickfeld, K., M. Morgan, D. Frame, and D. Keith, 2010: Expert judgments about transient climate response to
57 alternative future trajectories of radiative forcing. *Proc. Natl. Acad. Sci. U. S. A.*, **107**, 12451-12456.
- 58 Zickfeld, K., et al., 2012: Long-term Climate Change Commitment and Reversibility: An EMIC Intercomparison. J.
59 Climate, **submitted**.
- 60 Zimov, S., S. Davydov, G. Zimova, A. Davydova, E. Schuur, K. Dutta, and F. Chapin, 2006: Permafrost carbon: Stock
61 and decomposability of a globally significant carbon pool. *Geophysical Research Letters*, **33**, L20502.
- 62 Zunz, V., H. Goosse, and F. Massonnet, 2012: How does internal variability influence the ability of CMIP5 models to
63 reproduce the recent trend in Southern Ocean sea ice extent. *The Cryosphere*. **submitted**.

Tables

Table 12.1: Radiative forcing agents in the CMIP5 multi-model global climate projections. See Table 9.1 for descriptions of the models and main model references. ESMs are highlighted in bold. Numeric superscripts indicate model-specific references that document forcing implementations. Forcing agents are mostly implemented in close conformance with standard prescriptions (Taylor et al., 2012) and recommended datasets (Cionni et al., 2011; Lamarque et al., 2011; Lamarque et al., 2010; Meinshausen et al., 2011c) provided for CMIP5. Variations in forcing implementations are highlighted with superscripts and expanded in the table footnotes. Entries mean: n.a.: Forcing agent is not included in either the historical or future scenario simulations; Y: Forcing agent included (via prescribed concentrations, distributions or time series data); E: Concentrations of forcing agent calculated interactively driven by prescribed emissions or precursor emissions; Es: Concentrations of forcing agent calculated interactively driven by prescribed surface concentrations. For a more detailed classification of ozone chemistry and ozone forcing implementations in CMIP5 models see Eyring et al. (2012).

Model	Forcing Agents																
	Greenhouse Gases						Aerosols									Other	
	CO ₂ ^{ce}	CH ₄	N ₂ O	Trop O ₃	Strat O ₃	CFCs	SO ₄	Black carbon	Organic carbon	Nitrate	Cloud albedo effect	Cloud lifetime effect	Dust	Volcanic	Sea salt	Land use	Solar
ACCESS-1.0 ¹	Y ^p	Y	Y	Y ^b	Y ^b	Y	E	E	E	n.a.	Y	Y	Y ^{pd}	Y ^{v5}	Y ^{pd}	n.a.	Y
ACCESS-1.3 ¹	Y ^p	Y	Y	Y ^b	Y ^b	Y	E	E	E	n.a.	Y	Y	n.a.	Y ^{v5}	Y ^{pd}	n.a.	Y
BCC-CSM1.1 ²	Y/E ^p	Y	Y	Y ^b	Y ^b	Y	Y ^a	Y ^a	Y ^a	n.a.	n.a.	n.a.	Y ^a	Y ^{v0}	Y ^a	n.a.	Y
BCC-CSM1.1-m ²	Y/E ^p	Y	Y	Y ^b	Y ^b	Y	Y ^a	Y ^a	Y ^a	n.a.	n.a.	n.a.	Y ^a	Y ^{v0}	Y ^a	n.a.	Y
BNU-ESM	Y/E ^p	Y	Y	Y ^a	Y ^a	Y	Y ^a	Y ^a	Y ^a	n.a.	n.a.	n.a.	Y ^a	Y ^{v5}	Y ^a	n.a.	Y
CanCM4	Y ^p	Y	Y	Y ^b	Y ^b	Y	E	E	E	n.a.	Y ^{so}	n.a.	Y ^{pd}	Y/E st ^{v0}	Y ^{pd}	n.a.	Y
CanESM2	Y/E ^p	Y	Y	Y ^b	Y ^b	Y	E	E	E	n.a.	Y ^{so}	n.a.	Y ^{pd}	Y/E st ^{v0}	Y ^{pd}	Y ^{cr}	Y
CCSM4 ³	Y ^p	Y	Y	Y ^a	Y ^a	Y	Y ^a	Y ^a	Y ^a	n.a.	n.a.	n.a.	Y ^a	Y ^{v0}	Y ^a	Y	Y
CESM1(BGC) ^{4,5}	Y/E ^p	Y	Y	Y ^a	Y ^a	Y	Y ^a	Y ^a	Y ^a	n.a.	n.a.	n.a.	Y ^a	Y ^{v0}	Y ^a	Y	Y
CESM1(CAM5) ⁴	Y ^p	Y	Y	Y ^a	Y ^a	Y	E	E	E	n.a.	Y	Y	E	Y ^{v0}	E	Y	Y
CESM1(CAM5.1,FV2) ⁴	Y ^p	Y	Y	Y ^a	Y ^a	Y	E	E	E	n.a.	Y	Y	E	Y ^{v0}	E	Y	Y
CESM1(FASTCHEM) ⁴	Y ^p	Y ^a	Y	E	E	Y	E	Y ^a	Y ^a	n.a.	n.a.	n.a.	Y ^a	Y ^{v0}	Y ^a	Y	Y
CESM1(WACCM) ⁴	Es ^p	Es	Es	E/Es ^{op}	E/Es ^{op}	Es	Y	Y	Y	n.a.	n.a.	n.a.	Y ^a	Y ^{v0}	Y ^a	Y	Y
CMCC-CESM ⁶	Y	Y	Y	Y ^b	Y ^b	Y	Y ^a	n.a.	n.a.	n.a.	Y ^{so}	n.a.	Y ^{fx}	n.a.	n.a.	n.a.	Y
CMCC-CM	Y	Y	Y	Y ^b	Y ^b	Y	Y ^a	n.a.	n.a.	n.a.	Y ^{so,ic}	n.a.	Y ^{fx}	n.a.	n.a.	n.a.	Y
CMCC-CMS ⁷	Y	Y	Y	Y ^b	Y ^b	Y	Y ^a	n.a.	n.a.	n.a.	Y ^{so,ic}	n.a.	Y ^{fx}	n.a.	n.a.	n.a.	Y
CNRM-CM5 ⁸	Y	Y	Y	Y ^c	Y ^c	Y	Y ^c	Y ^c	Y ^c	n.a.	Y ^{so,ic}	n.a.	Y ^c	Y ^{v1}	Y ^c	n.a.	Y
CSIRO-Mk3.6 ⁹	Y	Y	Y	Y ^b	Y ^b	Y	E	E	E	n.a.	Y	Y	Y ^{pd}	Y ^{v0}	Y ^{pd}	n.a.	Y

EC-EARTH ¹⁰	Y	Y	Y	Y ^b	Y ^b	Y	Y ^a	Y ^a	Y ^a	n.a.	n.a.	n.a.	Y ^a	Y ^{v1}	Y ^a	Y	Y
FGOALS-g2 ¹¹	Y	Y	Y	Y ^b	Y ^b	Y	Y ^a	Y ^a	Y ^a	n.a.	Y	Y	Y ^a	Y ^{v0}	Y ^a	n.a.	Y
FGOALS-s2 ¹²	Y/E	Y	Y	Y ^b	Y ^b	Y	Y ^a	Y ^a	Y ^a	n.a.	n.a.	n.a.	Y ^a	Y ^{v0}	Y ^a	n.a.	Y
FIO-ESM	Y/E	Y	Y	Y ^b	Y ^b	Y	Y ^a	Y ^a	Y ^a	n.a.	n.a.	n.a.	Y ^a	Y ^{v0}	Y ^a	n.a.	Y
GFDL-CM3 ¹³	Y ^p	Y/Es ^{rc}	Y/Es ^{rc}	E	E	Y/Es ^{rc}	E	E	E	n.a.	Y	Y	E ^{pd}	Y/E st ^{v0}	E ^{pd}	Y	Y
GFDL-ESM2G	Y/E ^p	Y	Y	Y ^b	Y ^b	Y	Y ^a	Y ^a	Y ^a	n.a.	n.a.	n.a.	Y ^{fx}	Y ^{v0}	Y ^{fx}	Y	Y
GFDL-ESM2M	Y/E ^p	Y	Y	Y ^b	Y ^b	Y	Y ^a	Y ^a	Y ^a	n.a.	n.a.	n.a.	Y ^{fx}	Y ^{v0}	Y ^{fx}	Y	Y
GISS-E2(NINT) ¹⁴	Y	Y	Y	Y ^d	Y ^d	Y	Y	Y	Y	Y	Y	n.a.	Y ^{fx}	Y ^{v4}	Y ^{fx}	Y	Y ^{or}
GISS-E2(TCAD) ¹⁴	Y	Es/E ^{hf}	Es	E	E	Es/E ^{hf}	E	E	E	E	Y	n.a.	Y ^{pd}	Y ^{v4}	Y ^{pd}	Y	Y ^{or}
GISS-E2(TCADI) ¹⁴	Y	Es/E ^{hf}	Es	E	E	Es/E ^{hf}	E	E	E	E	Y	n.a.	Y ^{pd}	Y ^{v4}	Y ^{pd}	Y	Y ^{or}
HadCM3	Y ^p	Y	Y	Y ^b	Y ^b	Y	E	n.a.	n.a.	n.a.	Y ^{so}	n.a.	n.a.	Y ^{v2}	n.a.	n.a.	Y
HadGEM2-AO ¹⁵	Y ^p	Y	Y	Y ^b	Y ^b	Y	E	E	E	n.a.	Y	Y	Y ^{pd}	Y ^{v2}	Y ^{pd}	Y	Y
HadGEM2-CC ^{16,17}	Y ^p	Es	Y	Y ^b	Y ^b	Y	E	E	E	n.a.	Y	Y	Y ^{pd}	Y ^{v2}	Y ^{pd}	Y	Y
HadGEM2-ES ¹⁶	Y/E ^p	Es	Y	E	Y ^b	Y	E	E	E	n.a.	Y	Y	Y ^{pd}	Y ^{v2}	Y ^{pd}	Y	Y
INM-CM4	Y/E	Y	Y	Y ^b	Y ^b	n.a.	Y ^{fx}	n.a.	n.a.	n.a.	Y ^{so}	n.a.	n.a.	Y ^{v0}	n.a.	Y	Y
IPSL-CM5A-LR ¹⁸	Y/E ^p	Y	Y	Y ^e	Y ^e	Y	Y ^e	Y ^e	Y ^e	n.a.	Y	n.a.	Y ^e	Y ^{v1}	Y ^e	Y	Y
IPSL-CM5A-MR ¹⁸	Y/E ^p	Y	Y	Y ^e	Y ^e	Y	Y ^e	Y ^e	Y ^e	n.a.	Y	n.a.	Y ^e	Y ^{v1}	Y ^e	Y	Y
IPSL-CM5B-LR ¹⁸	Y ^p	Y	Y	Y ^e	Y ^e	Y	Y ^e	Y ^e	Y ^e	n.a.	Y	n.a.	Y ^e	Y ^{v1}	Y ^e	Y	Y
MIROC-ESM ¹⁹	Y/E ^p	Y	Y	Y ^f	Y ^f	Y	E	E	E	n.a.	Y ^{ic}	Y ^{ic}	Y ^{pd}	Y ^{v3}	Y ^{pd}	Y	Y
MIROC-ESM-CHEM ¹⁹	Y ^p	Y	Y	E	E	Y	E	E	E	n.a.	Y ^{ic}	Y ^{ic}	Y ^{pd}	Y ^{v3}	Y ^{pd}	Y	Y
MIROC4h ²⁰	Y ^p	Y	Y	Y ^g	Y ^g	Y	E	E	E	n.a.	Y	Y	Y ^{pd}	Y ^{v3}	Y ^{pd}	Y ^{cr}	Y
MIROC5 ²⁰	Y ^p	Y	Y	Y ^f	Y ^f	Y	E	E	E	n.a.	Y ^{ic}	Y ^{ic}	Y ^{pd}	Y ^{v3}	Y ^{pd}	Y ^{cr}	Y
MPI-ESM-LR ²¹	Y/E ^p	Y	Y	Y ^b	Y ^b	Y	Y ^h	Y ^h	Y ^h	Y ^h	n.a.	n.a.	Y ^h	Y ^{v0}	Y ^h	Y	Y ^{or}
MPI-ESM-MR ²¹	Y ^p	Y	Y	Y ^b	Y ^b	Y	Y ^h	Y ^h	Y ^h	Y ^h	n.a.	n.a.	Y ^h	Y ^{v0}	Y ^h	Y	Y ^{or}
MPI-ESM-P ²¹	Y ^p	Y	Y	Y ^b	Y ^b	Y	Y ^h	Y ^h	Y ^h	Y ^h	n.a.	n.a.	Y ^h	Y ^{v0}	Y ^h	Y	Y ^{or}
MRI-CGCM3 ²²	Y	Y	Y	Y ^b	Y ^b	Y	E	E	E	n.a.	Y ^{ic}	Y ^{ic}	E ^{pd}	E ^{v0}	E ^{pd}	Y	Y
MRI-ESM1	E	Y	Y	E	E	Es	E	E	E	n.a.	Y ^{ic}	Y ^{ic}	E ^{pd}	E ^{v0}	E ^{pd}	Y	Y
NorESM1-M ²³	Y ^p	Y	Y	Y ^a	Y ^a	Y	E	E	E	n.a.	Y	Y	E ^{pd}	E ^{v0}	E ^{pd}	Y	Y

NorESM1-ME ²³	Y/E ^p	Y	Y	Y ^a	Y ^a	Y	E	E	E	n.a.	Y	Y	E ^{pd}	E ^{v0}	E ^{pd}	Y	Y
---------------------------------	------------------	---	---	----------------	----------------	---	---	---	---	------	---	---	-----------------	-----------------	-----------------	---	---

Notes:

Model-specific references relating to forcing implementations:

¹ Dix et al. (2012)

² Wu et al. (2012); Xin et al. (2012a; 2012b)

³ Meehl et al. (2012a)

⁴ Meehl et al. (2012b)

⁵ Lindsay et al. (2012)

⁶ Cagnazzo et al. (2012)

⁷ Davini et al. (2012)

⁸ Voldoire et al. (2012)

⁹ Rotstayn et al. (2012)

¹⁰ Hazeleger et al. (2012)

¹¹ Li et al. (2012c)

¹² Bao et al. (2012)

¹³ Levy et al. (2012)

¹⁴ Shindell et al. (2012a). GISS-E2-R and GISS-E2-H models are forced similarly and both represented here as GISS-E2. Both -R and -H model versions have three variants: in the NINT variant (physics version 1) aerosols and ozone are specified from pre-computed transient aerosol and ozone fields, in the TCAD variant (physics version 2) aerosols and atmospheric chemistry are calculated online as a function of atmospheric state and transient emissions inventories, while in the TCADI variant (physics version 3) atmospheric composition is calculated as for TCAD but the aerosol impacts on clouds (and hence the aerosol indirect effect) is calculated interactively. In NINT and TCAD variants the aerosol indirect effect is parameterized following Hansen et al. (2005b).

¹⁵ HadGEM2-AO is forced in a similar way to HadGEM2-ES and HadGEM2-CC, following Jones et al. (2011), but tropospheric and stratospheric ozone are prescribed.

¹⁶ Jones et al. (2011)

¹⁷ Hardiman et al. (2012)

¹⁸ Dufresne et al. (2011)

¹⁹ Watanabe et al. (2011)

²⁰ Komuro et al. (2012)

²¹ Giorgetta et al. (2012)

²² Yukimoto et al. (2012)

²³ Bentsen et al. (2012); Iversen et al. (2012); Kirkevåg et al. (2012); Tjiputra et al. (2012)

Additional notes:

^{ce} Separate entries for CO₂ denote “concentrations-driven” and “emissions-driven” experiments as indicated.

^p Physiological forcing effect of CO₂ via plant stomatal response and evapotranspiration (Betts et al., 2007) included.

^{rc} Separate entries for different treatments used for radiation and chemistry respectively.

^{hf} Separate entries denote historical and future (RCPs) respectively.

^a Three-dimensional tropospheric ozone, stratospheric ozone and/or aerosol distributions specified as monthly 10-year mean concentrations, computed off-line using CAM-Chem – a modified version of CAM3.5 with interactive chemistry – driven with specified emissions for the historical period (Lamarque et al., 2010) and RCPs (Lamarque et al., 2011) with sea surface temperature and sea ice boundary conditions based on CCSM3's projections for the closest corresponding AR4 scenarios.

^b Ozone prescribed using the original or slightly modified IGAC/SPARC ozone dataset (Cionni et al., 2011); in some models this dataset is modified to add a future solar cycle and in some models tropospheric ozone is zonally averaged.

^c Linearized 2D ozone chemistry scheme (Cariolle and Teyssedre, 2007) including transport and photochemistry, reactive to stratospheric chlorine concentrations but not tropospheric chemical emissions.

^d Ozone prescribed using the dataset described in (Hansen et al., 2007), with historical tropospheric ozone being calculated by a CCM and stratospheric ozone taken from Randel and Wu (2007) in the past. Tropospheric ozone is held constant from 1990 onwards, while stratospheric ozone is constant from 1997 to 2003 and then returned linearly to its 1979 value over the period 2004 to 2050.

^e For IPSL-CM5 model versions, ozone and aerosol concentrations are calculated semi-offline with the atmospheric general circulation model including interactive chemistry and aerosol, following the four RCPs in the future (Dufresne et al., 2011; Szopa et al., 2012). The same aerosol concentration fields (but not ozone) are also prescribed for the CNRM-CM5 model.

^f Ozone concentrations computed off-line by Kawase et al. (2011) using a CCM forced with CMIP5 emissions.

^g Ozone concentrations computed off-line by Sudo et al. (2003) for the historical period and Kawase et al. (2011) for the future.

^h Time dependent climatology based on simulations and observations (Kinne et al., 2012); aerosols are distinguished only with respect to coarse and fine mode, and anthropogenic and natural origins, not with respect to composition.

^{op} Separate entries denote different ozone chemistry precursors.

^{so} First indirect effect from sulphate aerosol only.

st Separate entries denote stratosphere and troposphere respectively.

^{ic} Radiative effects of aerosols on ice clouds are represented.

^{pd} Prognostic or diagnostic scheme for dust/sea salt aerosol with emissions/concentrations determined by the model state rather than externally prescribed.

^{fx} Fixed prescribed climatology of dust/sea salt aerosol concentrations with no year-to-year variability.

^{v0} Explosive volcanic aerosol returns rapidly in future to zero (or near-zero) background, like that in the pre-industrial control experiment.

^{v1} Explosive volcanic aerosol returns rapidly in future to a constant (average volcano) background, same as in the pre-industrial control experiment.

^{v2} Explosive volcanic aerosol returns slowly in future (over several decades) to a constant background like that in the pre-industrial control experiment.

^{v3} Explosive volcanic aerosol returns rapidly in future to near-zero background, below that in the pre-industrial control experiment.

^{v4} Explosive volcanic aerosol set to zero in future, but constant (average volcano) background used in the pre-industrial control experiment.

^{v5} Explosive volcanic aerosol set to a non-zero constant value in future that differs substantially from the constant background in the pre-industrial control experiment.

^{cr} Land use change represented via crop change only.

^{or} Realistic time-varying orbital parameters for solar forcing (in historical period only for GISS-E2).

Chapter 12: Long-term Climate Change: Projections, Commitments and Irreversibility

Coordinating Lead Authors: Matthew Collins (UK), Reto Knutti (Switzerland)

Lead Authors: Julie Arblaster (Australia), Jean-Louis Dufresne (France), Thierry Fichefet (Belgium), Pierre Friedlingstein (UK), Xuejie Gao (China), William Gutowski (USA), Tim Johns (UK), Gerhard Krinner (France), Mxolisi Shongwe (South Africa), Claudia Tebaldi (USA), Andrew Weaver (Canada), Michael Wehner (USA)

Contributing Authors: Myles R. Allen, Tim Andrews, Urs Beyerle, Cecilia Bitz, Sandrine Bony, Ben Booth, Oliver Brown, Victor Brovkin, Claire Brutel-Vuilmet, Mark Cane, Robin Chadwick, Ed Cook, Kerry H. Cook, Sébastien Denvil, Michael Eby, John Fasullo, Erich M. Fischer, Piers Forster, Peter Good, Hugues Goosse, Kevin I. Hodges, Marika Holland, Philippe Huybrechts, Manoj Joshi, Viatcheslav Kharin, Yochanan Kushnir, David Lawrence, Robert W. Lee, Spencer Liddicoat, Wolfgang Lucht, Damon Matthews, François Massonnet, Malte Meinshausen, Christina M. Patricola, Gwenaëlle Philippon-Berthier, Prabhat, Stefan Rahmstorf, William J. Riley, Joeri Rogelj, Oleg Saenko, Richard Seager, Jan Sedlacek, Len Shaffrey, Drew Shindell, Jana Sillmann, Andrew Slater, Robert Webb, Giuseppe Zappa, Kirsten Zickfeld

Review Editors: Sylvie Joussaume (France), Abdalah Mokssit (Morocco), Karl Taylor (USA), Simon Tett (UK)

Date of Draft: 5 October 2012

Notes: TSU Compiled Version

Figures

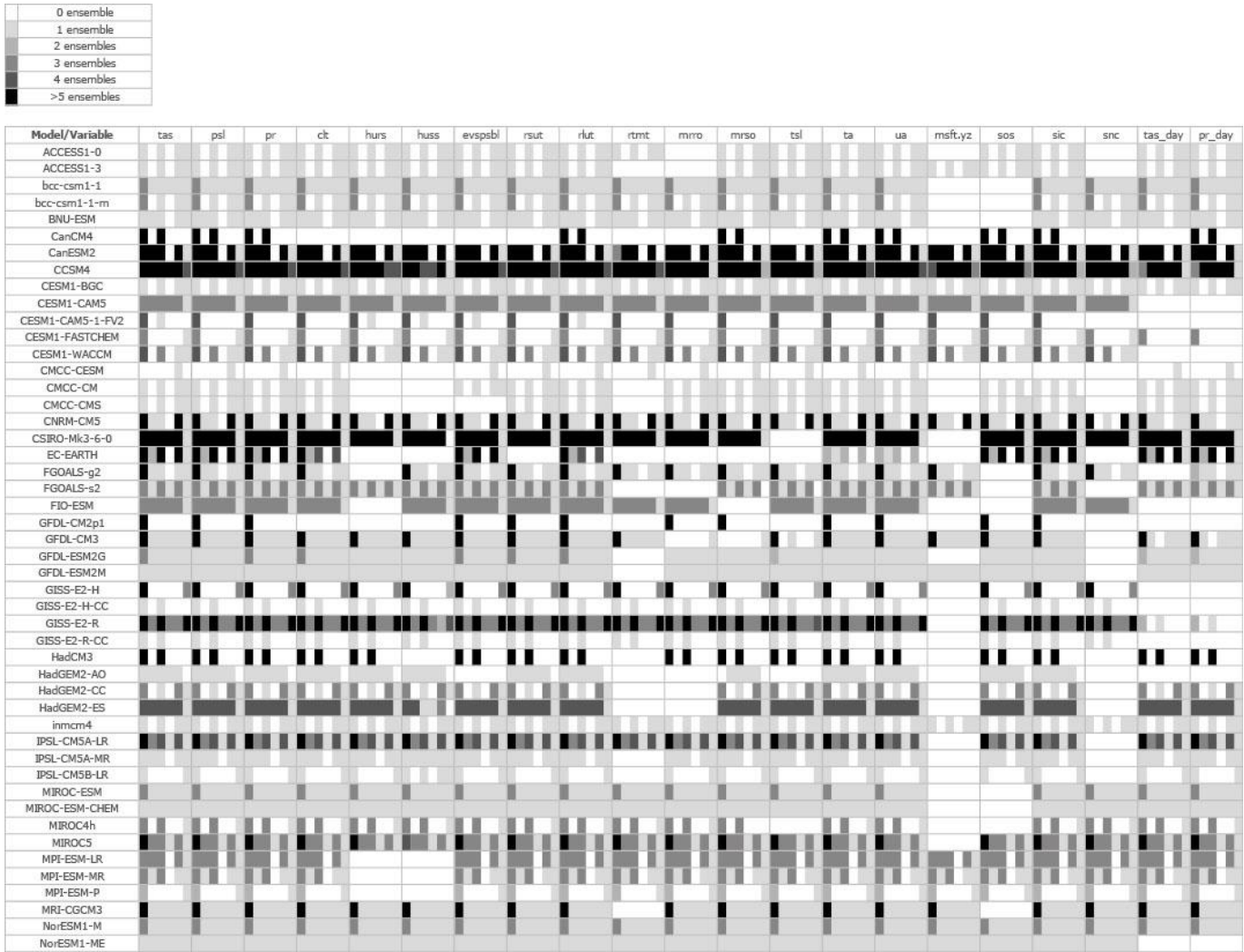


Figure 12.1: A summary of the output used to make the CMIP5 figures in this chapter (and some figures in Chapter 11). The climate variable names run along the horizontal axis and use the standard abbreviations. The climate model names run along the vertical axis. In each box the shading indicates the number of ensemble members available for historical, RCP2.6, RCP4.5, RCP6.0, RCP8.5 and pre-industrial control experiments, although only one ensemble member per model is used in the relevant figures.

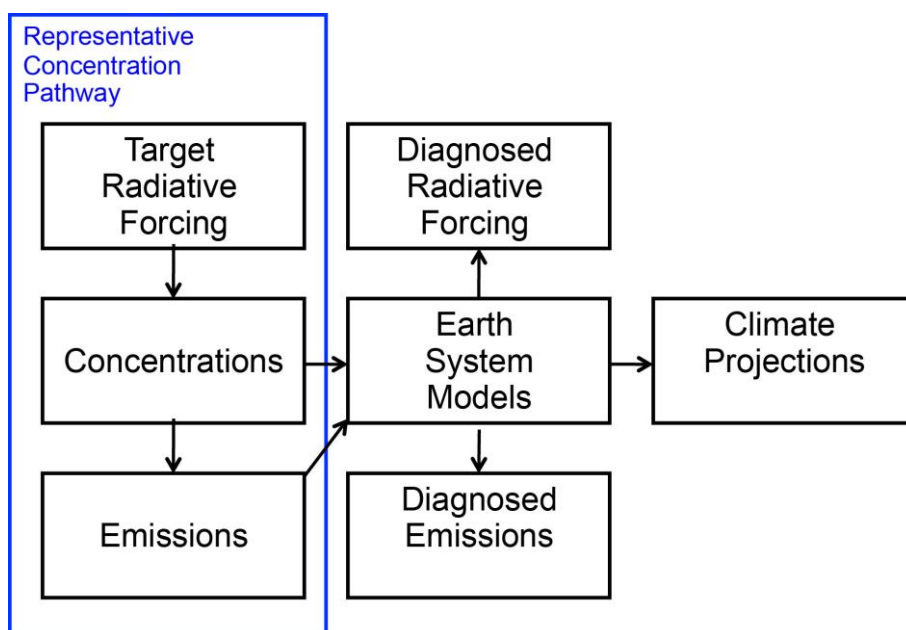
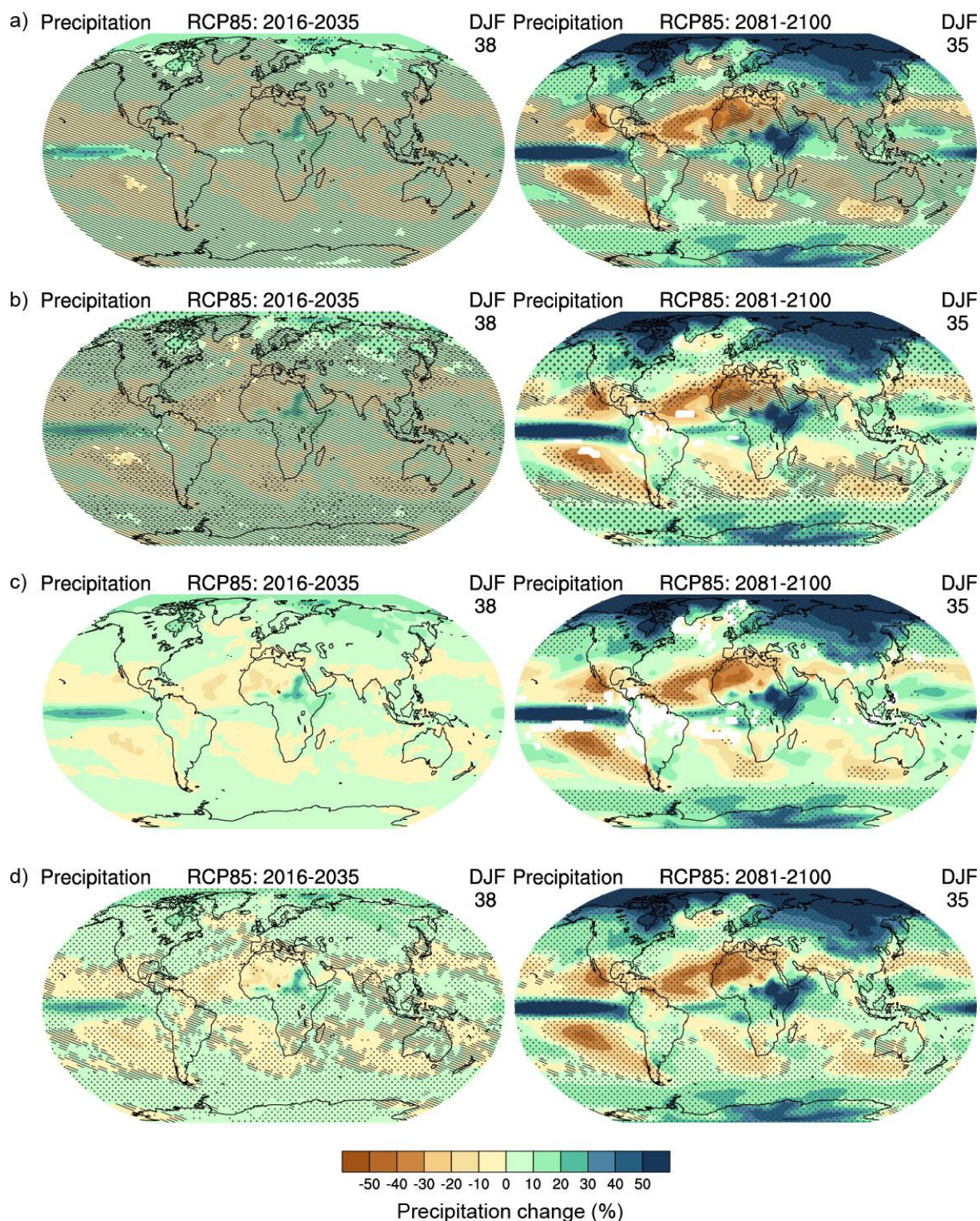


Figure 12.2: Links in the chain from scenarios, through models to climate projections. The Representative Concentration Pathways (RCPs) are designed to sample a range of radiative forcing of the climate system at 2100. The RCPs are translated into both concentrations and emissions of greenhouse gases using Integrated Assessment Models (IAMs). These are then used as inputs to dynamical Earth System Models (ESMs) in simulations that are either concentration-driven (the majority of projection experiments) or emissions-driven (only run for RCP8.5). Aerosols and other forcing factors are implemented in subtly different ways in each ESM. The ESM projections each have a potentially different radiative forcing, which may be viewed as an output of the model and which may not correspond to precisely the level of radiative forcing indicated by the RCP nomenclature. Similarly, for concentration-driven experiments, the emissions consistent with those concentrations diagnosed from the ESM may be different from those specified in the RCP (diagnosed from the IAM). Different models would produce different responses even under the same radiative forcing. Uncertainty propagates through the chain and results in a spread of ESM projections. This spread is only one way of assessing uncertainty in projections and alternative methods, which combine information from simple and complex models and observations through statistical models or expert judgment are also used to quantify that uncertainty.



2
3
4 **Box 12.1, Figure 1:** Projected relative change in December to February precipitation for 2016–2035 and 2081–2100,
5 relative to 1986–2005 from CMIP5. The choice of the variable is just for illustration on how the different methods
6 compare in cases with low and high signal-to-noise situations (left and right column, respectively). The color maps are
7 identical in all cases. Stippling and hatching are shown as determined a) from relating the model mean to internal
8 variability, b) as a but hatching indicating high agreement for “small change” (see text), c) the robustness measure by
9 Knutti and Sedlacek (2012), d) the method proposed by Tebaldi et al. (2011) and e) the method by Power et al.(2012)
10 and Power and Delage (2012) (but using 66% rather than 95% for the hatched area). Detailed technical explanations for
11 each method are given in the text. The number of CMIP5 models used is indicated in the upper right corner of each
12 panel.
13
14

1

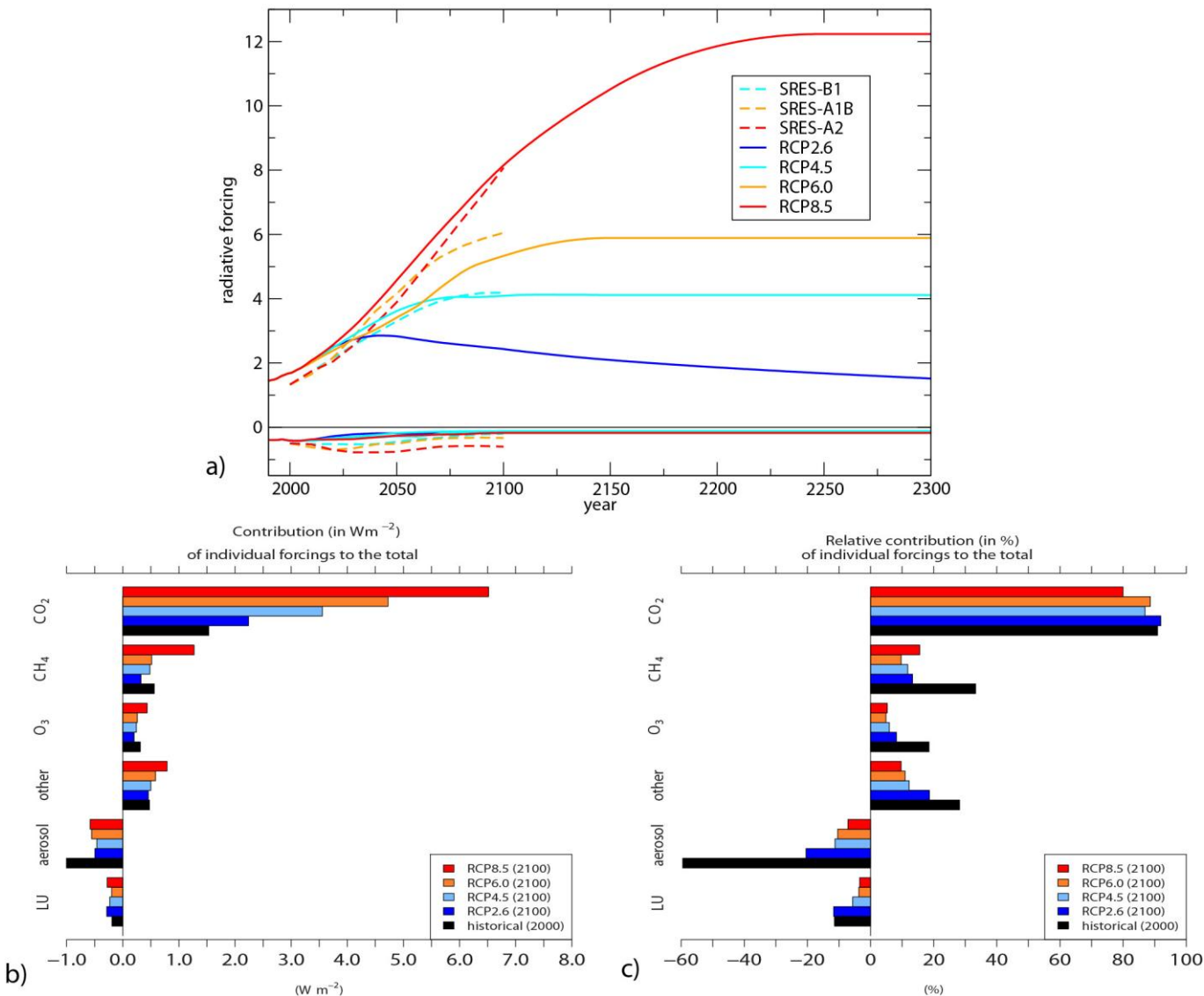


Figure 12.3: (a) Time evolution of the total anthropogenic and anthropogenic aerosol radiative forcing relative to preindustrial (~1765) between 2000 and 2300 for RCP scenarios and their extensions (continuous lines), and SRES scenarios (dashed lines) as computed by the integrated assessment models (IAMs) used to develop those scenarios. The four RCP scenarios used in CMIP5 are: RCP2.6 (dark blue), RCP4.5 (light blue), RCP6.0 (orange) and RCP8.5 (red). The three SRES scenarios used in CMIP3 are: B1 (light blue, dashed), A1B (orange, dashed) and A2 (red, dashed). Positive values correspond to the total anthropogenic radiative forcing. Negative values correspond to the forcing from all anthropogenic aerosol-radiation interactions. (b) Contribution of the individual anthropogenic forcings to the total radiative forcing in year 2100 for the four RCP scenarios. The individual forcings are gathered into five groups: CO_2 , CH_4 , ozone, other GHGs, aerosol (all effects, i.e. aerosols-radiation and aerosol-cloud interactions, aerosol deposition on snow, unlike in (a)) and land use. (c) As in b, but the individual forcings are relative to the total radiative forcing (i.e., $\text{RF}_x/\text{RF}_{\text{tot}}$, in %, with RF_x individual radiative forcings and RF_{tot} total radiative forcing). The total radiative forcing of the two families of scenarios, SRES and RCP, differ in 2000 as the number of forcings and our knowledge about them have changed since the TAR. The values shown here are summarised in Annex II.

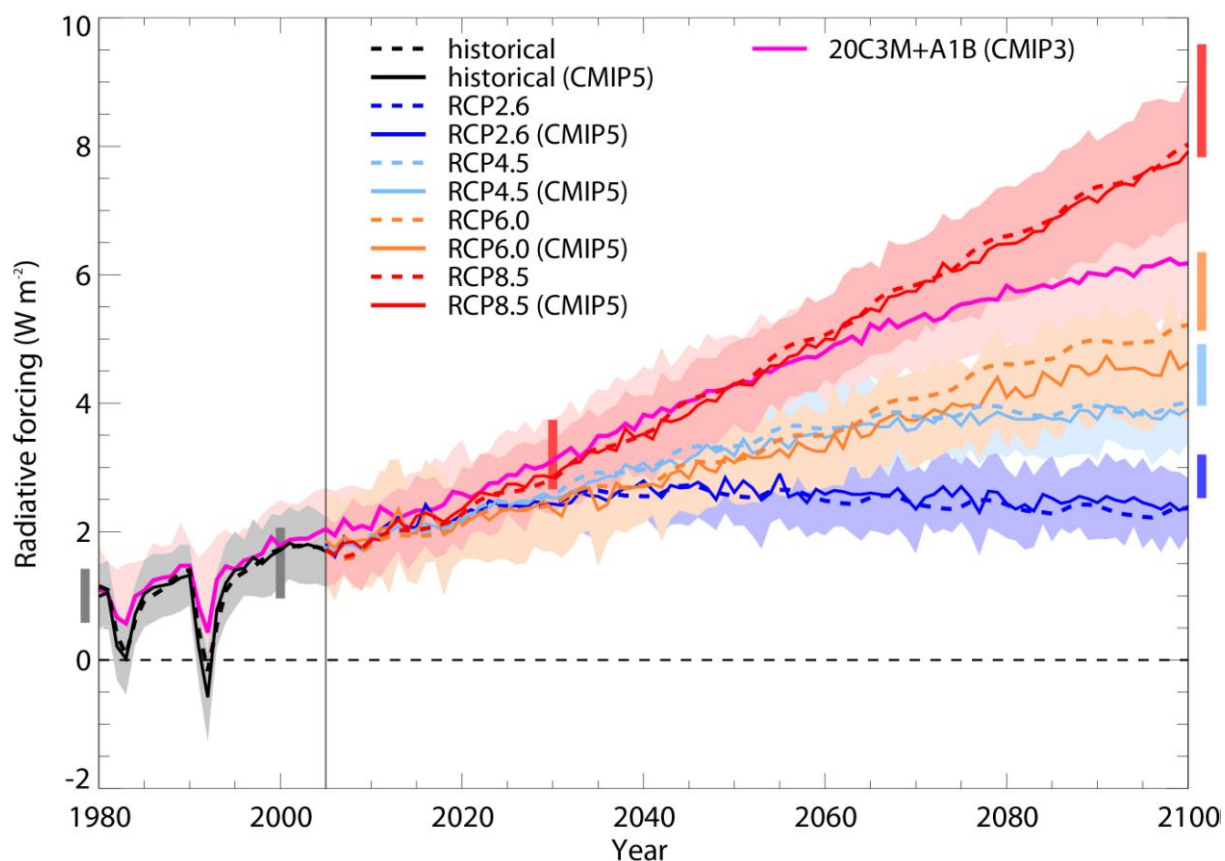


Figure 12.4: Global mean radiative forcing (W m^{-2}) between 1980 and 2100, relative to 1850, estimated by alternative methods. Dashed lines indicate the indicative total anthropogenic plus natural forcing from Meinshausen et al. (2011b), using adjusted forcing values for anthropogenic combined with solar and volcanic RF, normalised by the mean between 1850 and 1859. Solid lines are multi-model mean adjusted forcing relative to the pre-industrial control simulations realised in a subset of CMIP5 models for the historical experiment and RCP scenarios (Forster et al., 2012) driven by concentrations, with a 1-sigma uncertainty range about each line shaded in light colour. This assumes each model has an invariant climate feedback parameter, calculated from abrupt $4 \times \text{CO}_2$ experiments using the method of Gregory et al. (2004). Grey or coloured vertical bars illustrate the 5–95% uncertainty range of anthropogenic forcing estimated in ACCMIP models (Shindell et al., 2012) for time slice experiments at 1980, 2000, 2030 (RCP8.5 only) and 2100 (all RCPs). Note that the ACCMIP bars at 1980 and 2100 are shifted slightly to aid clarity. The mean adjusted forcing diagnosed from 21 CMIP3 models for the SRES A1B scenario, as in Forster and Taylor (2006), is also shown with a 1-sigma uncertainty range.

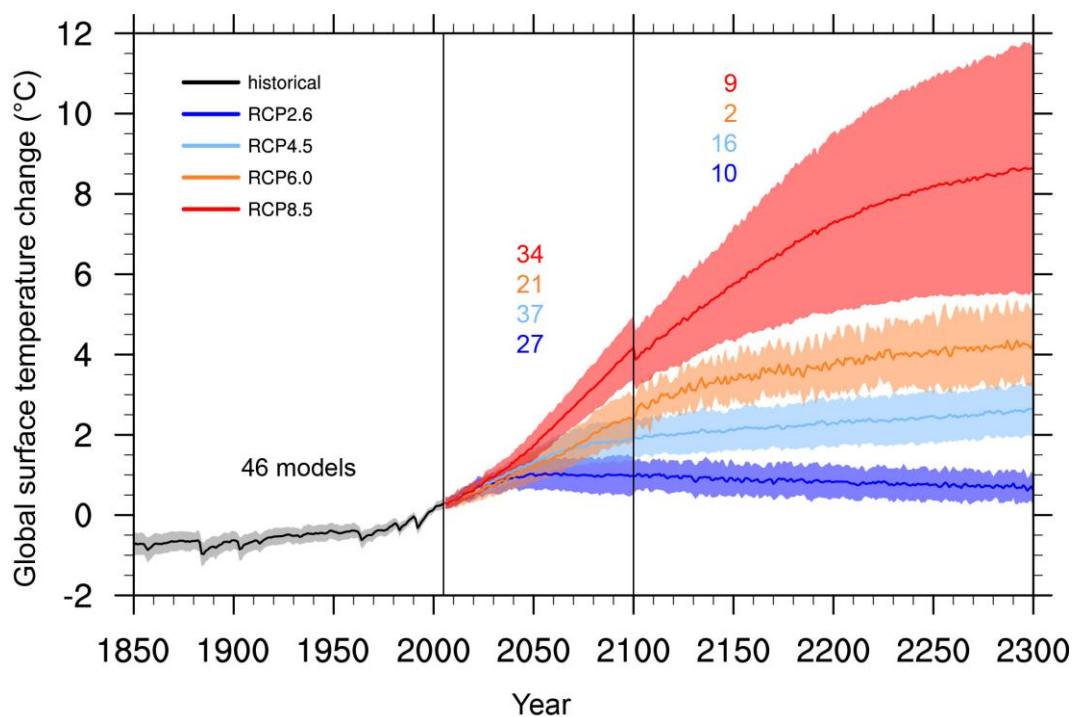


Figure 12.5: Time series of global and annual mean surface air temperature anomalies (relative to 1986–2005) from CMIP5 concentration-driven experiments. Projections are shown for each RCP for the multimodel mean (solid lines) and ± 1 standard deviation across the distribution of individual models (shading). Discontinuities at 2100 are due to different numbers of models performing the extension runs beyond the 21st century and have no physical meaning. Numbers in the figure indicate the number of different models contributing to the different time periods.

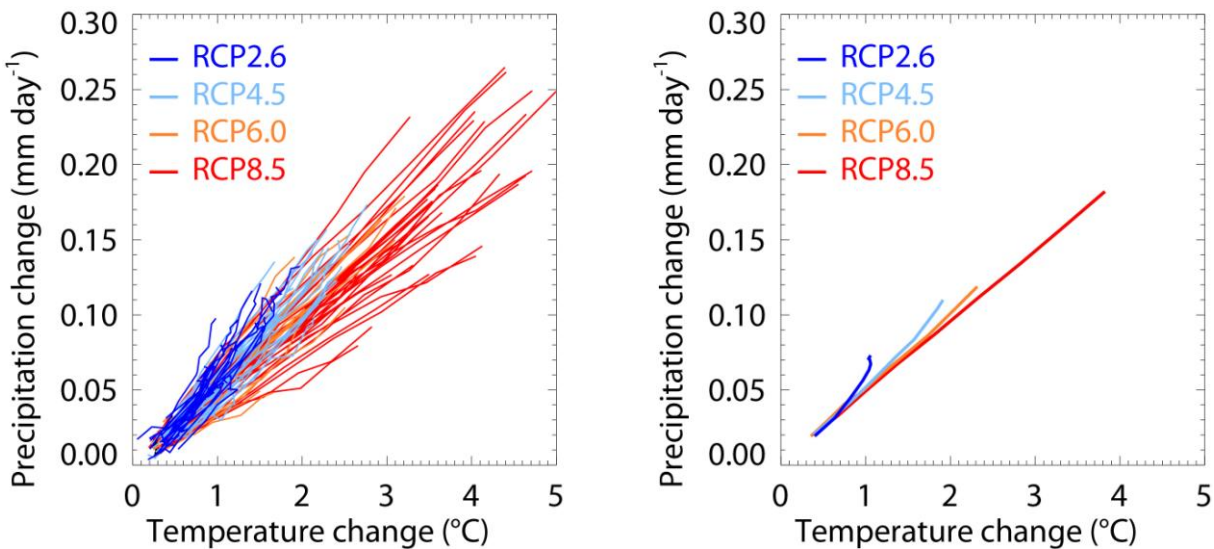


Figure 12.6: Global mean precipitation (mm day⁻¹) versus temperature (°C) changes relative to 1986–2005 for CMIP5 model projections for the four RCPs scenarios. a) Ensemble means for individual models averaged over successive decadal periods (2006–2015 up to 2086–2095), each line representing a different model. b) The corresponding multi-model means for each RCP.

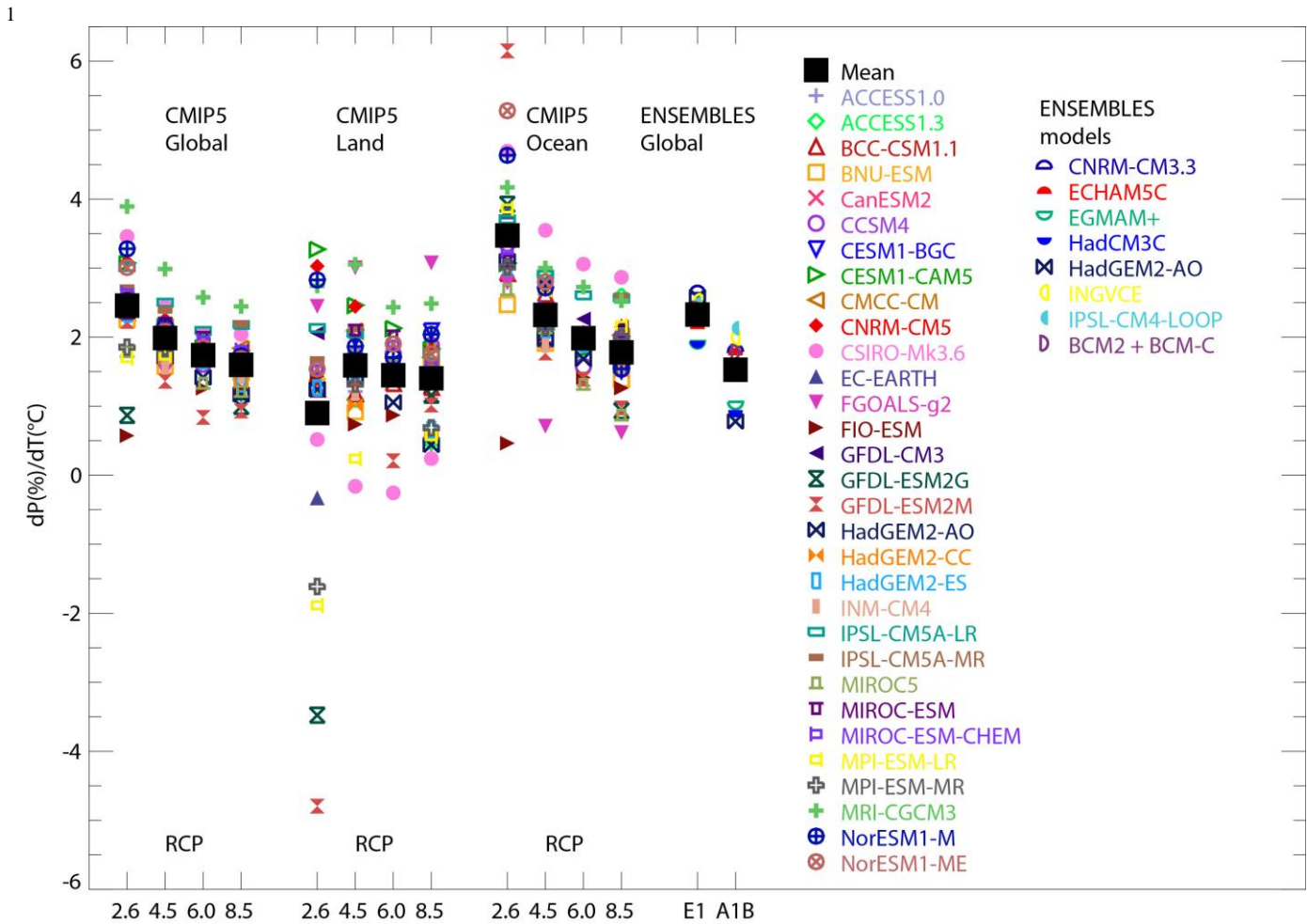
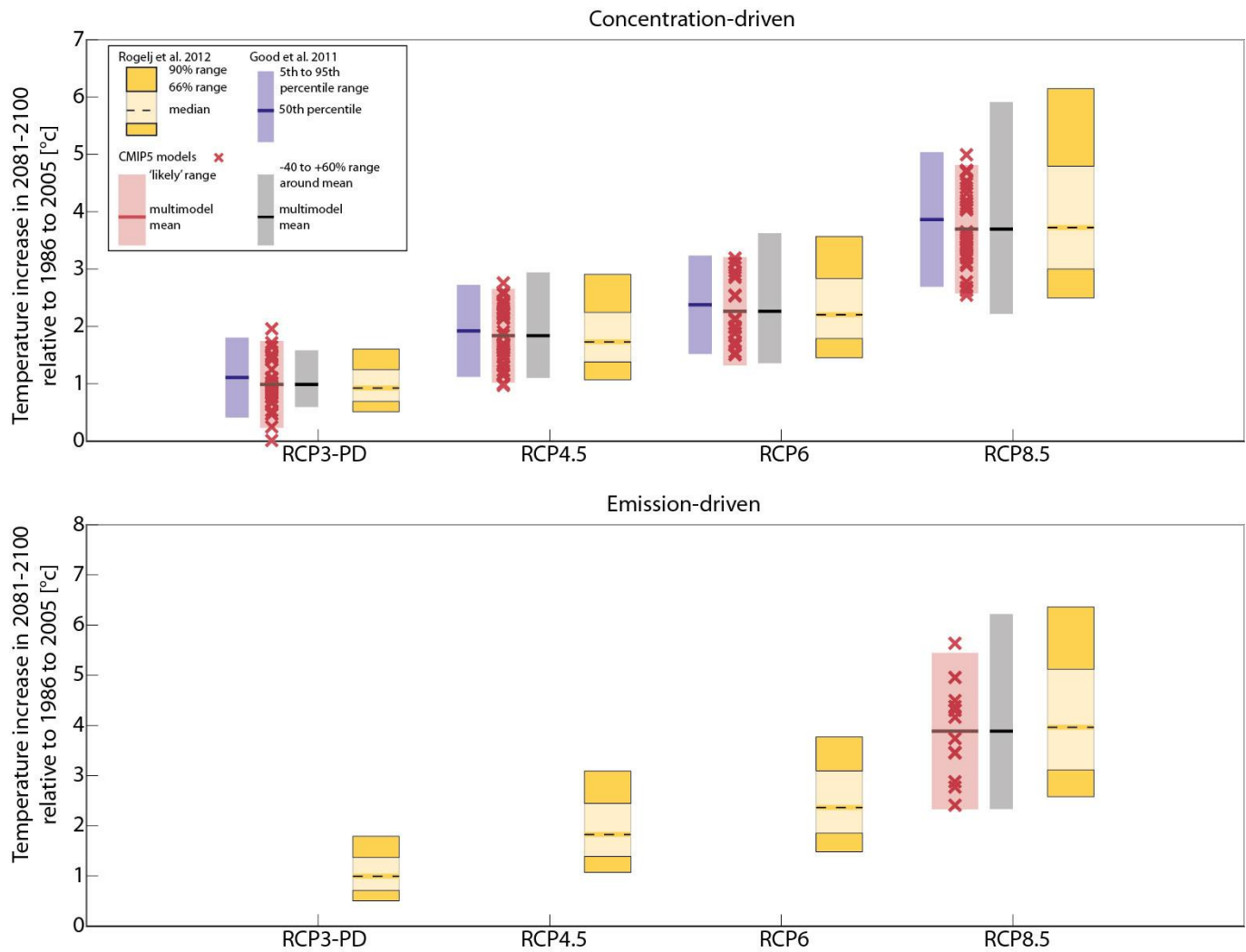


Figure 12.7: Percentage changes in global, land and ocean precipitation per °C of global warming for CMIP5 model projections for the four RCPs, over the period 2006–2100. Changes are calculated relative to the mean precipitation and temperature for 1986–2005 and the gradient of a least-squares fit through annual mean data for each model ensemble mean is computed. Land and ocean values use global mean temperature in the denominator. Each coloured symbol represents the ensemble mean for a single model, and black squares are multi-model means. Also shown are corresponding results for ENSEMBLES model projections for the E1 and A1B scenarios (Johns et al., 2011), in this case using a least-squares fit calculated over the period 2000–2099 and for percentage change relative to the period 1980–1999. The change of precipitation over land and ocean are discussed in Section 12.4.5.2.

1



2

3

4

5

6

7

8

9

10

11

Figure 12.8: Uncertainty estimates for global mean temperature change in 2081–2100 with respect to 1986–2005. Red crosses mark projections from individual CMIP5 models. Red bars indicate mean and 5–95% ranges based on CMIP5 (1.64 standard deviations), which are considered as a *likely range*. Blue bars indicate 5–95% ranges from the pulse response emulation of 23 models (Good et al., 2011a). Grey bars mark the range from the mean of CMIP5 minus 40% mean to the mean +60%, assessed as *likely* in AR4 for the SRES scenarios. The yellow bars show the median, 33–66% range and 10–90% range based on Rogelj et al. (2012).

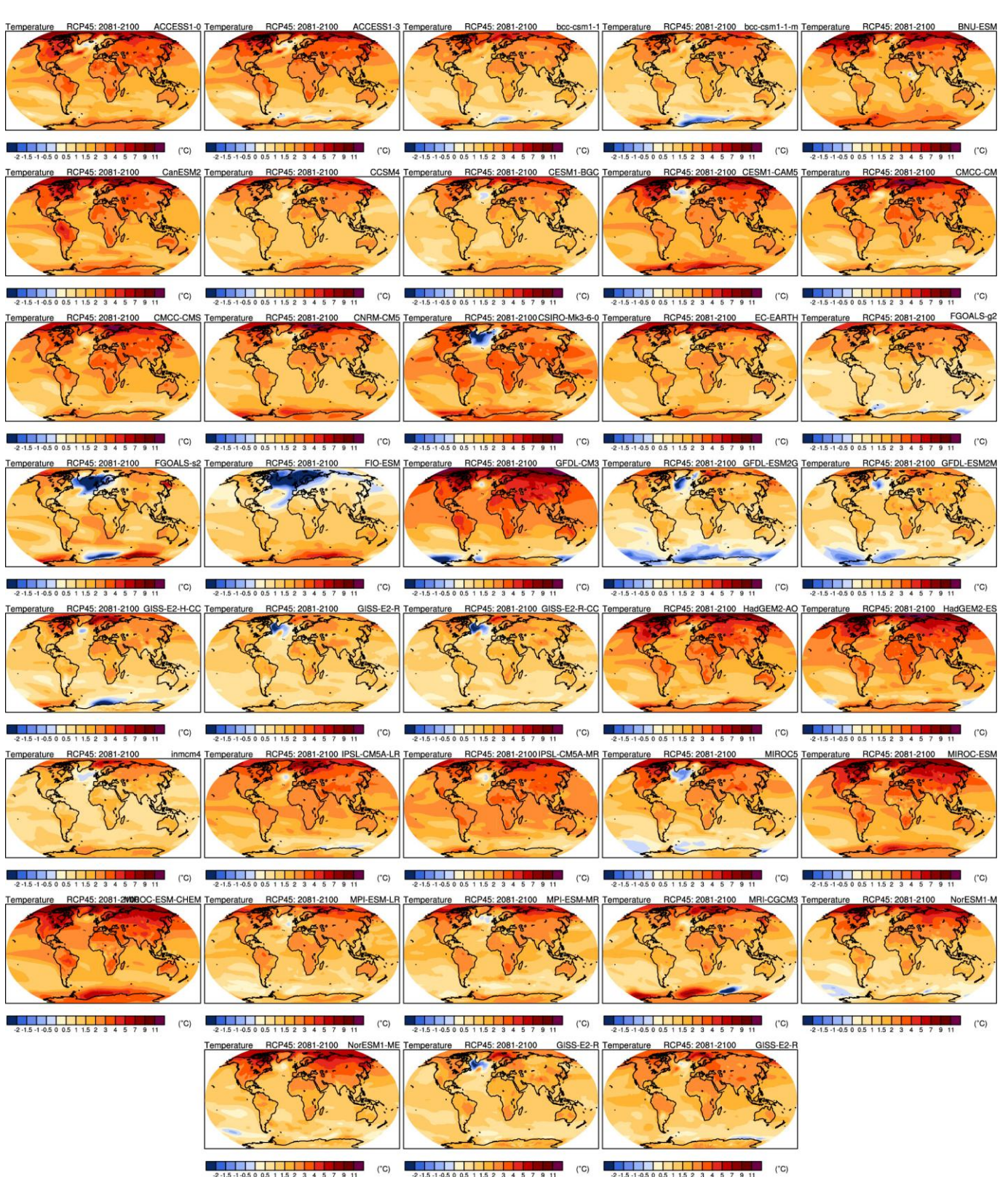


Figure 12.9: Surface air temperature change in 2081–2100 displayed as anomalies with respect to 1986–2005 for RCP4.5 from one ensemble member of each of the concentration-driven models available in the CMIP5 archive.

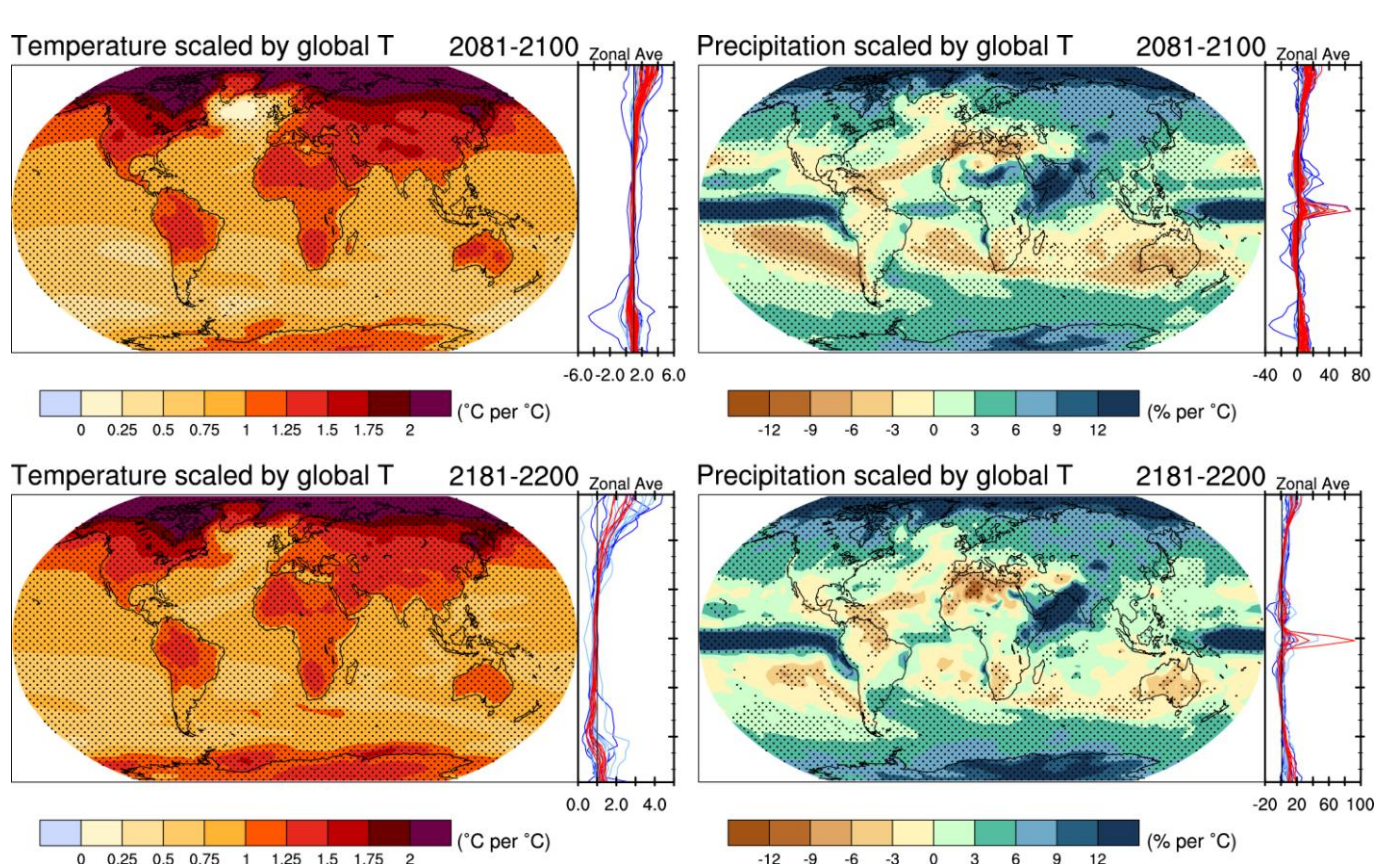
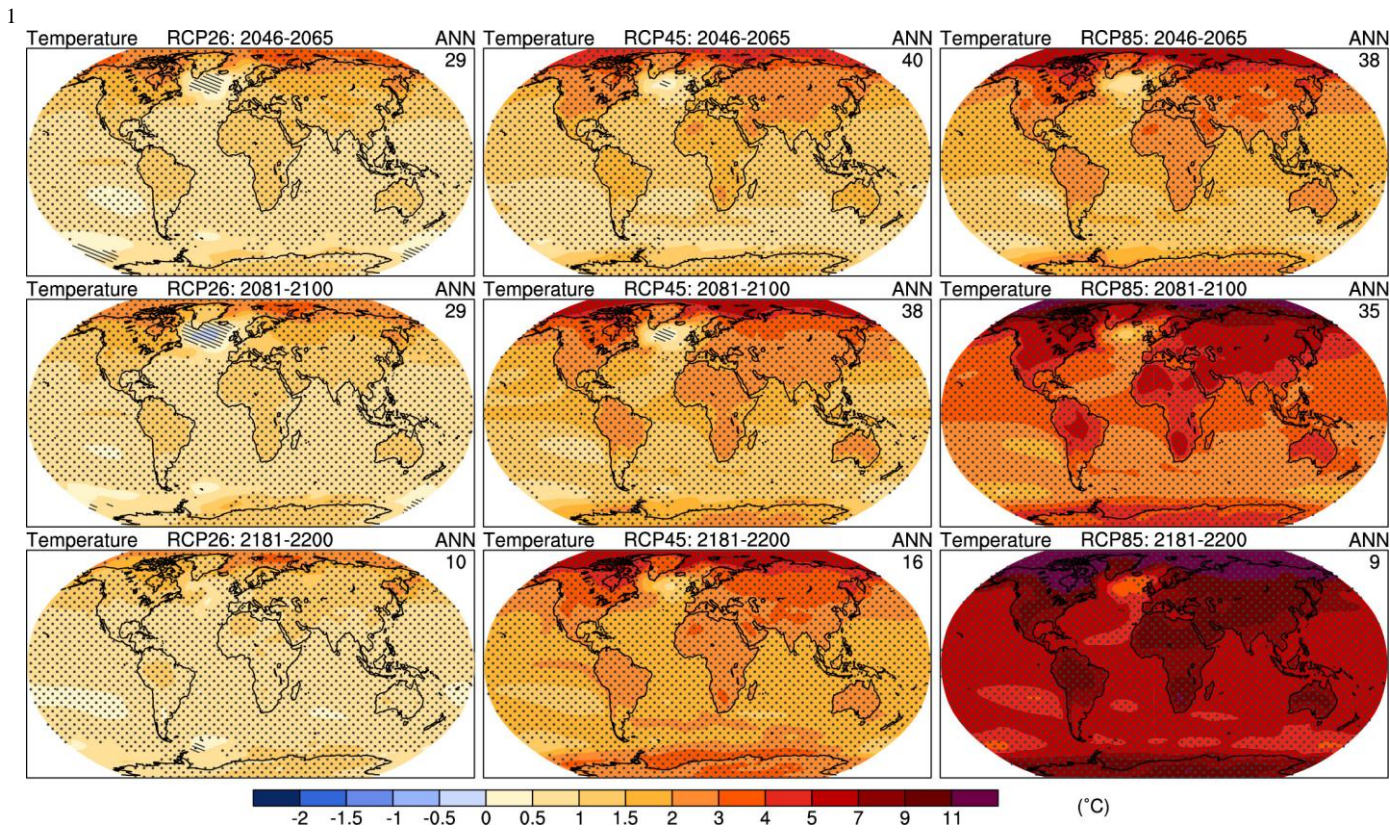


Figure 12.10: Temperature (left) and precipitation (right) change patterns derived from transient simulations from the CMIP5 ensembles, scaled to 1°C of global average warming. The patterns have been calculated by computing 20-year averages at the end of the 21st (top) and 22nd (bottom) Century and over the period 1986–2005 for the available simulations under all RCPs, taking their difference (percentage difference in the case of precipitation) and normalizing it, grid-point by grid-point, by the corresponding value of global average temperature change for each model and scenario. The normalized patterns have then been averaged across models and scenarios. The colour scale represents °C (in the case of temperature) and % (in the case of precipitation) per 1°C of global average warming and stippling indicates the mean change averaged over all realisations is larger than the 95% percentile of the distribution of models. Zonal means of the geographical patterns are shown for each individual model for RCP2.6 (blue), 4.5 (light blue), 6.0 (orange) and 8.5 (red). RCP8.5 is excluded from the stabilisation figures.



2

3

4 **Figure 12.11:** Multimodel ensemble average of surface air temperature change (compared to 1986–2005 base period)

5 for 2046–2065, 2081–2100, 2181–2200 for RCP2.6, 4.5 and 8.5. Hatching indicates regions where the multi model

6 mean is less than one standard deviation of internal variability. Stippling indicates regions where the multi model mean

7 is greater than two standard deviations of internal variability and where 90% of the models agree on the sign of change

8 (see Box 12.1). The number of CMIP5 models used is indicated in the upper right corner of each panel.

9

10

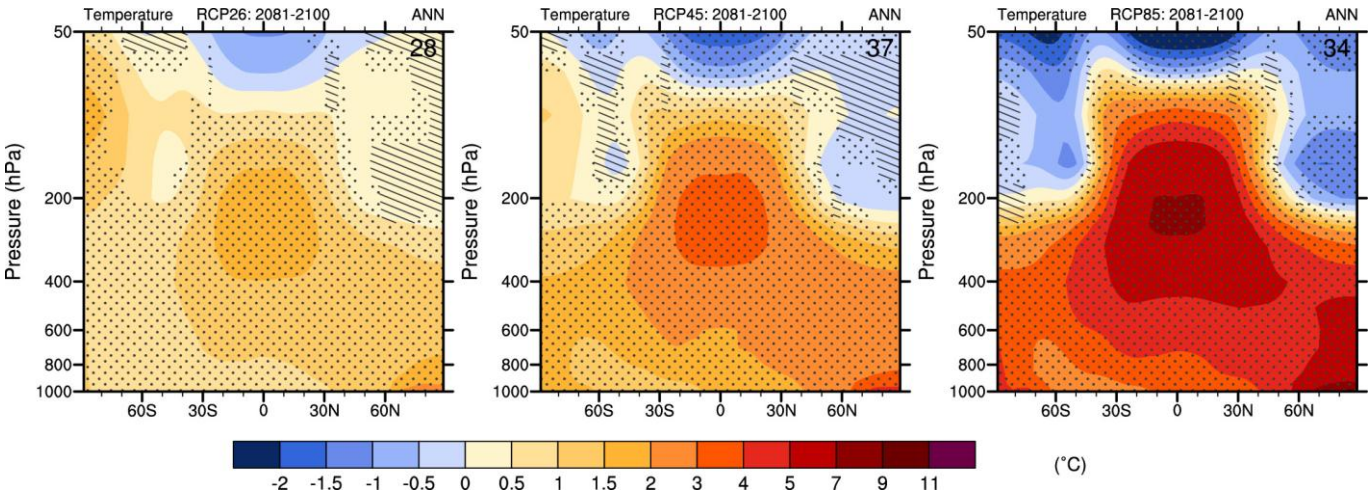


Figure 12.12: CMIP5 multi-model changes in annual mean zonal mean temperature relative to 1986–2005 for 2081–2100 under the RCP2.6 (left), RCP4.5 (centre) and RCP8.5 (right) forcing scenarios. Hatching indicates regions where the multi model mean is less than one standard deviation of internal variability. Stippling indicates regions where the multi model mean is greater than two standard deviations of internal variability and where 90% of the models agree on the sign of change (see Box 12.1).

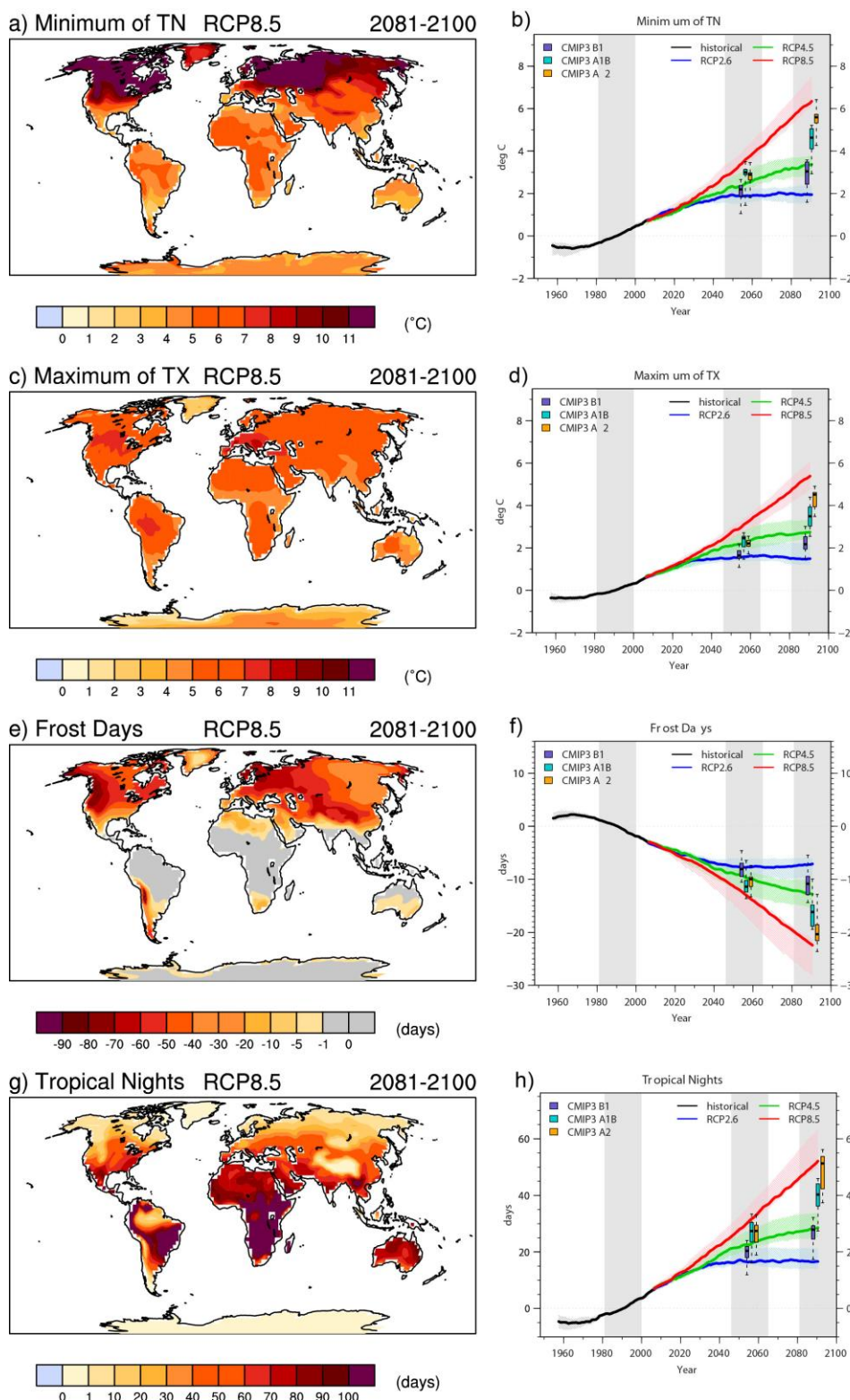


Figure 12.13: CMIP5 multimodel mean geographical changes at RCP8.5 and 20-year smoothed timeseries for RCP2.6, RCP4.5 and RCP8.5 in the (a,b) annual minimum of minimum daily temperature, (c,d) annual maximum of maximum daily temperature, (e,f) frost days (number of days below 0°C) and (g,h) tropical nights (number of days above 20°C). Shading in the timeseries represents the interquartile ensemble spread (25th and 75th quantiles). The box-and-whisker plots show the interquartile ensemble spread (box) and outliers (whiskers) for 11 CMIP3 model simulations of the SRES scenarios A2 (orange), A1B (cyan), and B1 (purple) globally averaged over the respective future time periods (2046–2065 and 2081–2100) as anomalies from the CMIP3 reference period 1981–2000. Stippling indicates grid points with changes that are significant at the 5% level. Adapted from Sillmann et al. (2012).

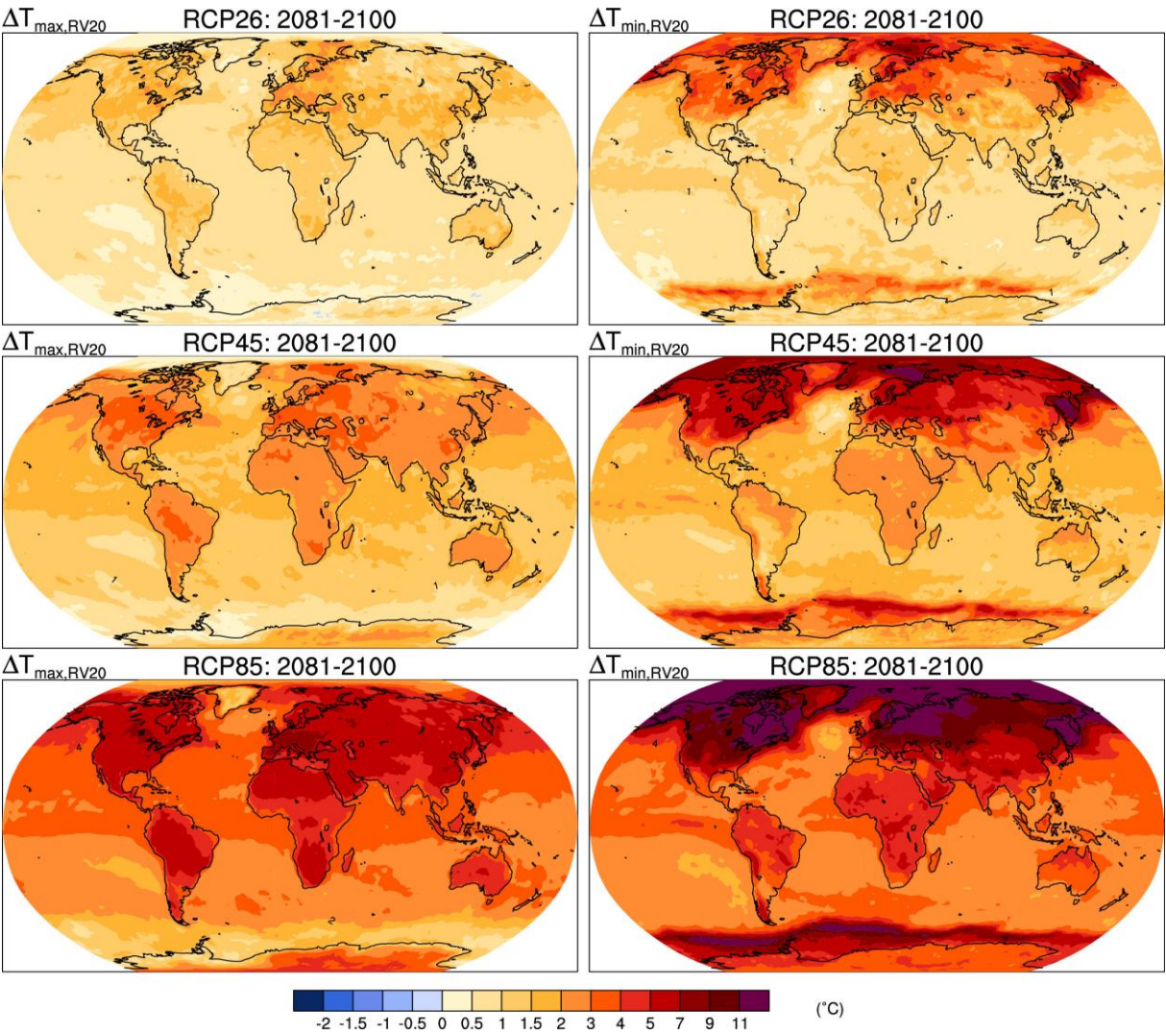


Figure 12.14: The CMIP5 multi-model median change in 20-year return values of annual warm temperature extremes (left hand panels) and cold temperature extremes (right hand panels) as simulated by CMIP5 models in 2081–2100 relative to 1986–2005 in the RCP2.6 (top panels), RCP4.5 (middle panels), and RCP8.5 (bottom panels) experiments.

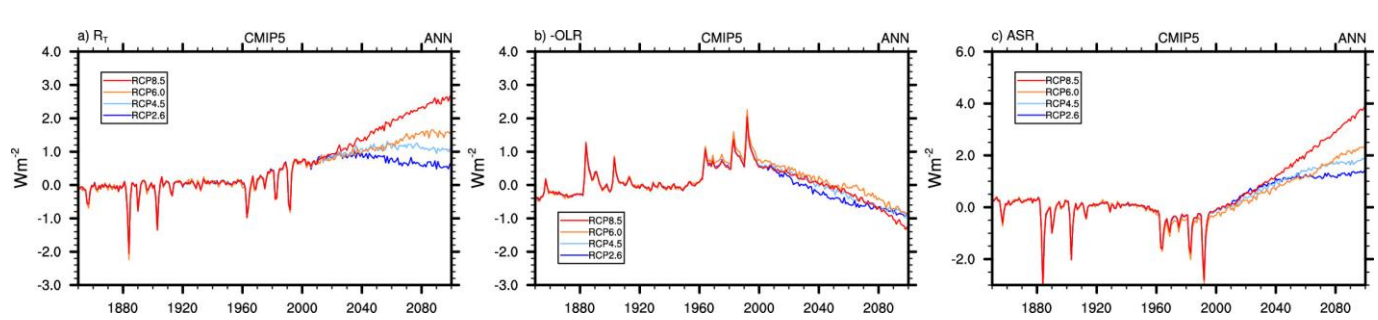
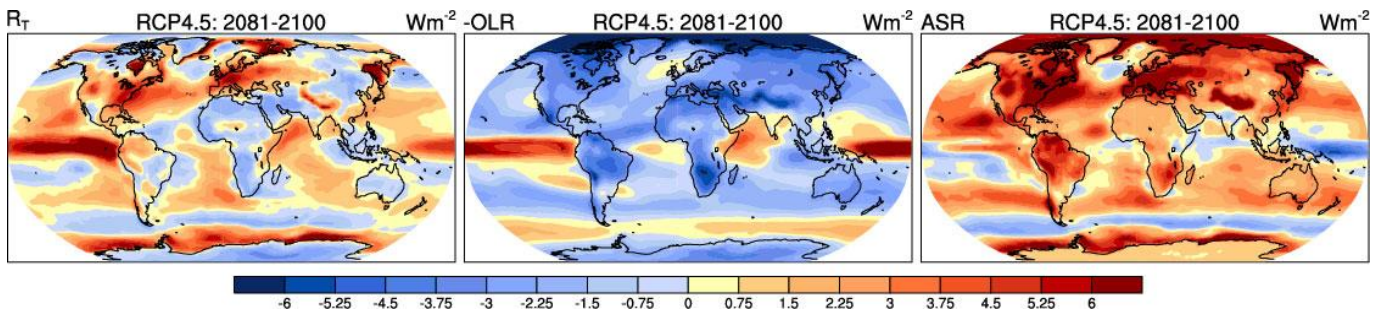


Figure 12.15: Time evolution of the global mean (a) net total radiation anomaly at the TOA, (b) net longwave radiation anomaly at the TOA and (c) net shortwave radiation anomaly at the TOA for the historical period and three RCP scenarios from available models. All the fluxes are positive downward and units are W m^{-2} . The anomalies are computed with respect to the 1900–1950 base period.



2
3
4 **Figure 12.16:** CMIP multi-model changes in annual mean net radiation (R_T , left) net longwave radiation ($-\text{OLR}$, centre)
5 and absorbed solar radiation (ASR, bottom) at the TOA for the RCP4.5 scenario from the available models. All fluxes
6 are positive downward, units are W m^{-2} and $R_T = \text{ASR} - \text{OLR}$. The net radiation anomalies are computed with respect to
7 the 1900–1950 base period.
8
9

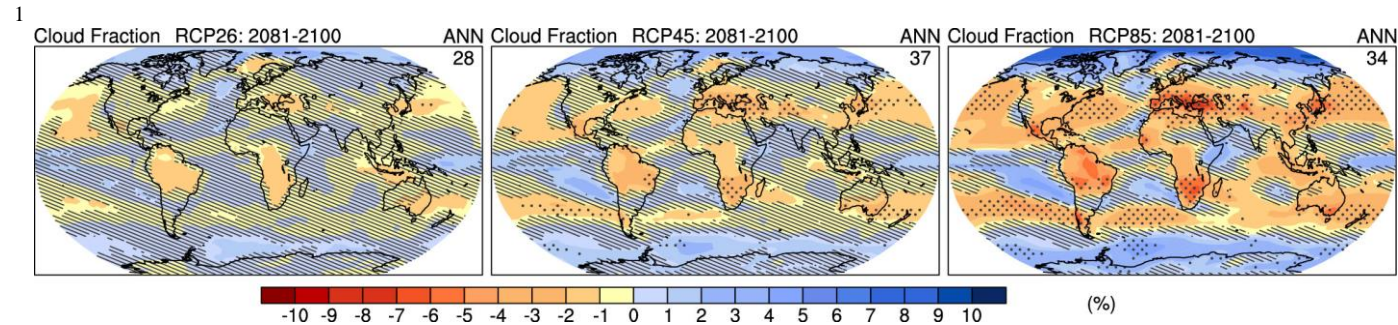


Figure 12.17: CMIP5 multi-model changes in annual mean total cloud amount relative to 1986–2005 for 2081–2100 under the RCP2.6 (left), RCP4.5 (centre) and RCP8.5 (right) forcing scenarios. Hatching indicates regions where the multi model mean is less than one standard deviation of internal variability. Stippling indicates regions where the multi model mean is greater than two standard deviations of internal variability and where 90% of the models agree on the sign of change (see Box 12.1). The number of CMIP5 models used is indicated in the upper right corner of each panel.

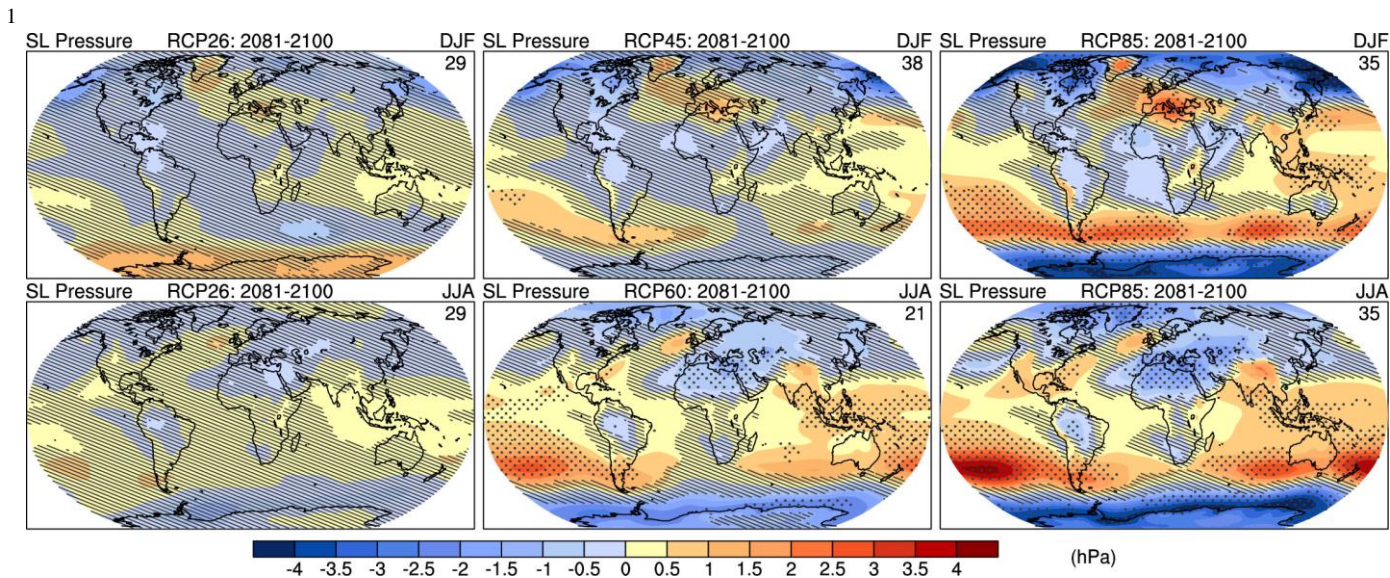


Figure 12.18: CMIP5 multimodel ensemble average of DJF and JJA mean sea level pressure change (2081–2100 minus 1986–2005) for RCP2.6, 4.5 and 8.5. Hatching indicates regions where the multi model mean is less than one standard deviation of internal. Stippling indicates regions where the multi model mean is greater than two standard deviations of internal variability and where 90% of models agree on the sign of change (see Box 12.1). The number of CMIP5 models used is indicated in the upper right corner of each panel.

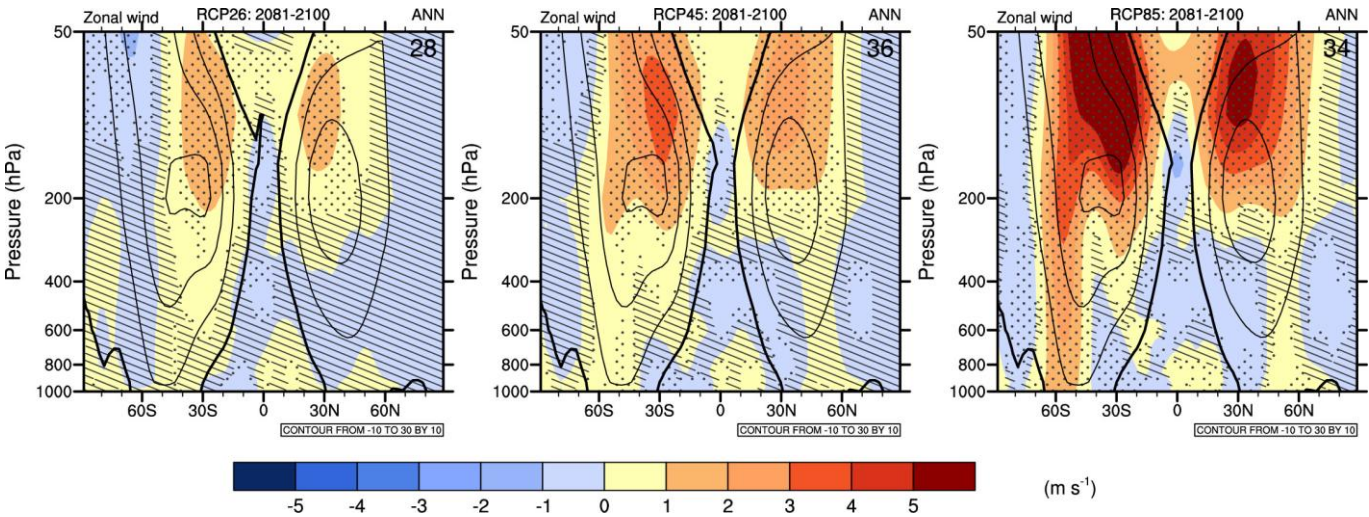
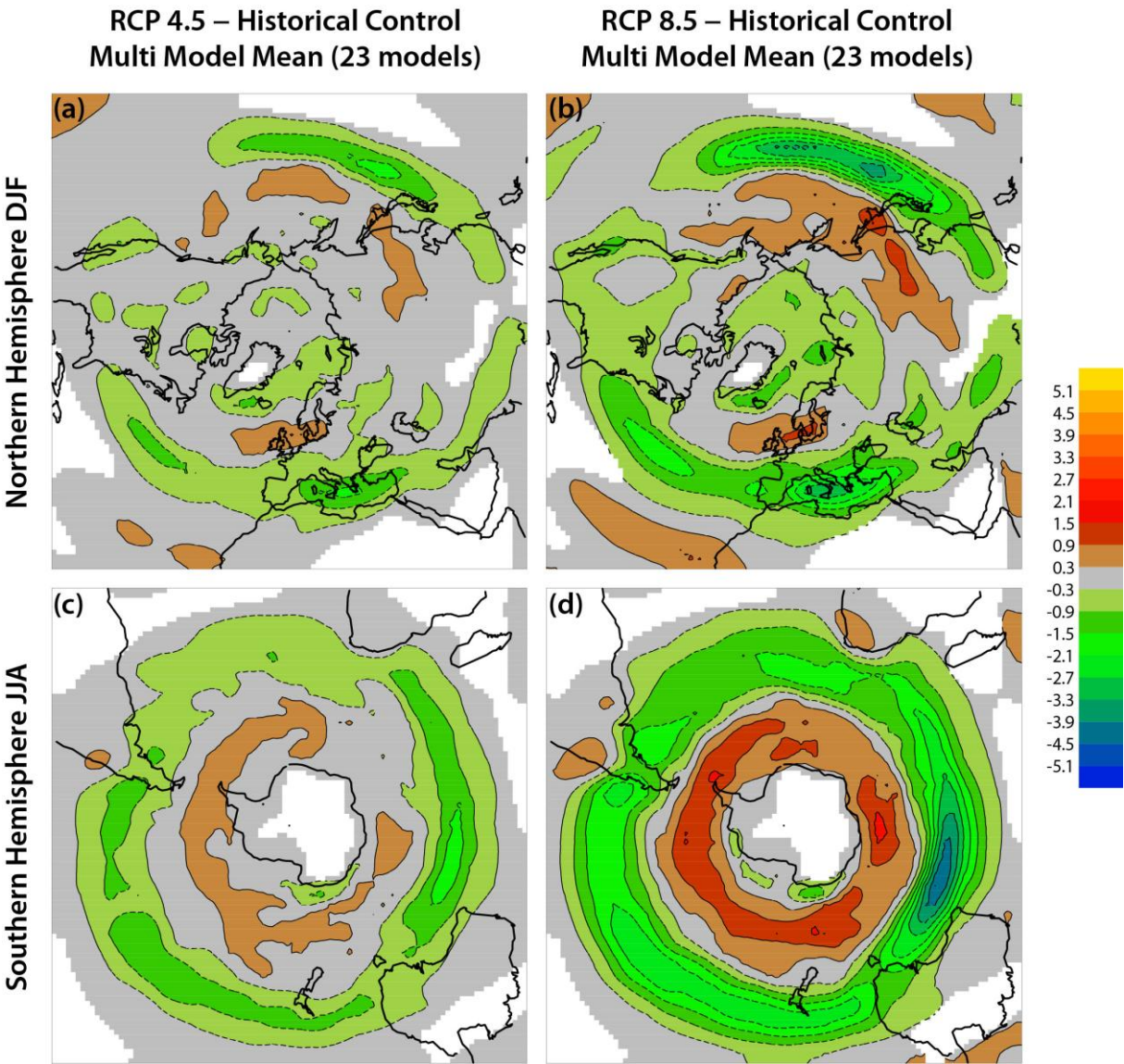


Figure 12.19: CMIP5 multimodel ensemble average of zonal and annual mean wind change (2081–2100 minus 1986–2005) for RCP2.6, 4.5 and 8.5. Black contours represent the multimodel mean average for the 1986–2005 base period. Hatching indicates regions where the multi model mean is less than one standard deviation of internal variability. Stippling indicates regions where the multi model mean is greater than two standard deviations of internal variability and where 90% of model agree on the sign of change (see Box 12.1).

Climate Change: Winter Season



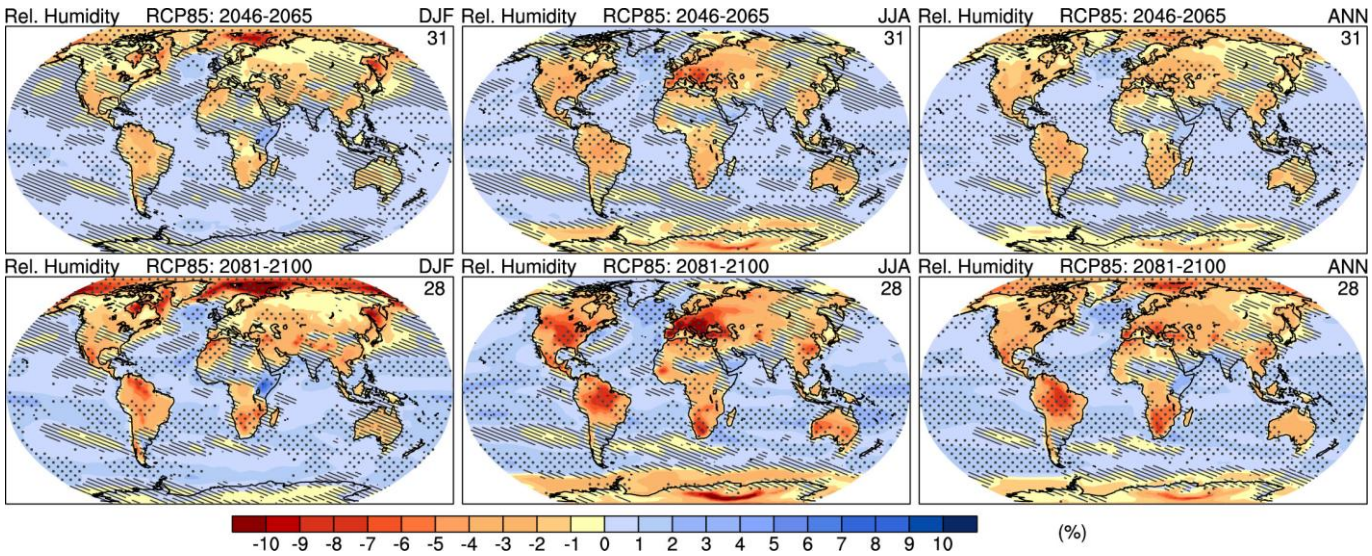


Figure 12.21: Projected changes in near-surface relative humidity from the CMIP5 models under RCP8.5 for the DJF (left), JJA (middle) and annual mean (left) averages relative to 1986–2005 for the periods 2046–2065 (top row), 2081–2100 (bottom row). Hatching indicates regions where the multi model mean is less than one standard deviation of internal variability. Stippling indicates regions where the multi model mean is greater than two standard deviations of internal variability and where 90% of models agree on the sign of change (see Box 12.1). The number of CMIP5 models used is indicated in the upper right corner of each panel.

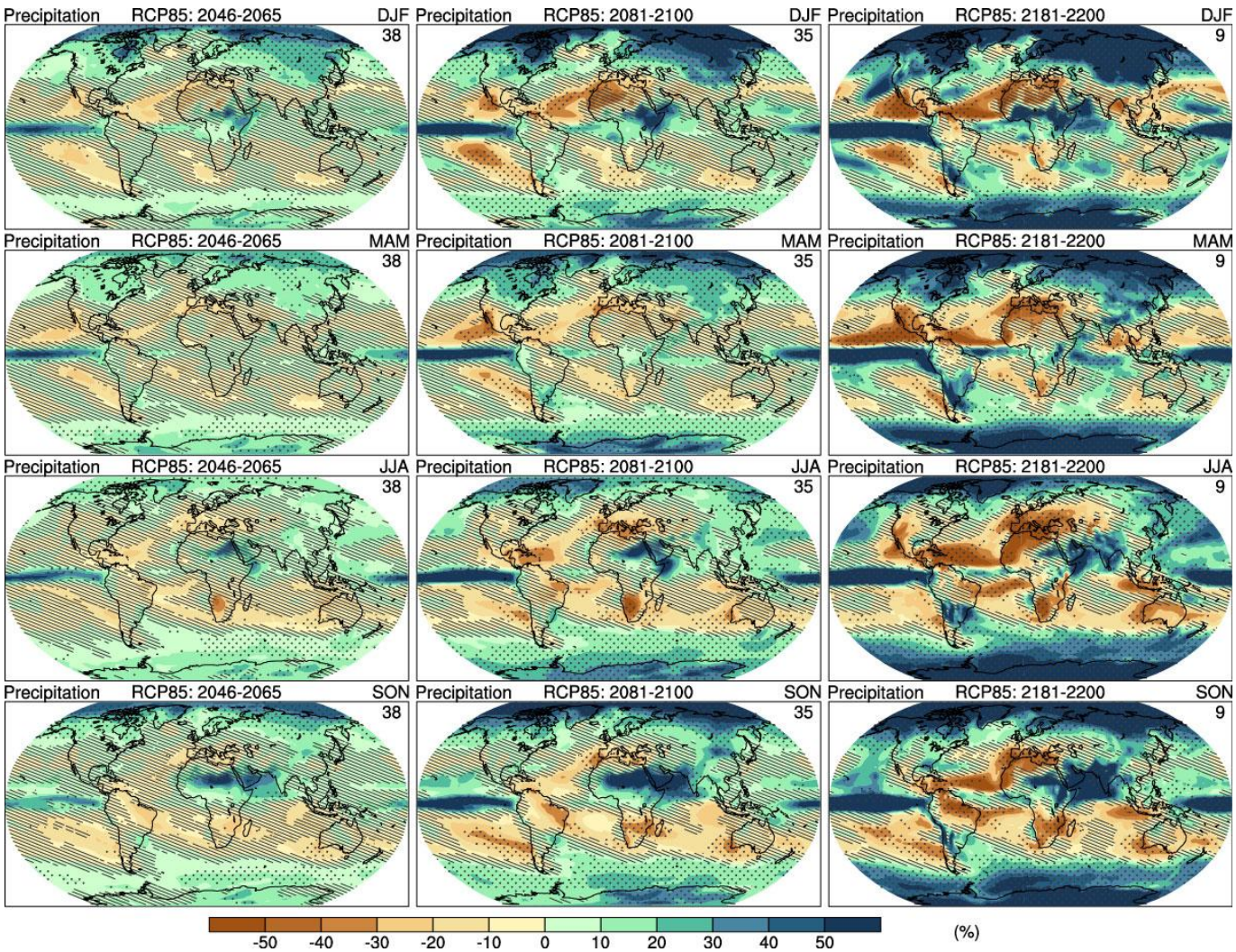


Figure 12.22: Multi-model CMIP5 average percent change in seasonal mean precipitation relative to the reference period 1985–2005 averaged over the periods 2045–2065, 2081–2100 and 2181–2200 under the RCP8.5 forcing scenarios. Hatching indicates regions where the multi model mean is less than one standard deviation of internal variability. Stippling indicates regions where the multi model mean is greater than two standard deviations of internal variability and where 90% of models agree on the sign of change (see Box 12.1).

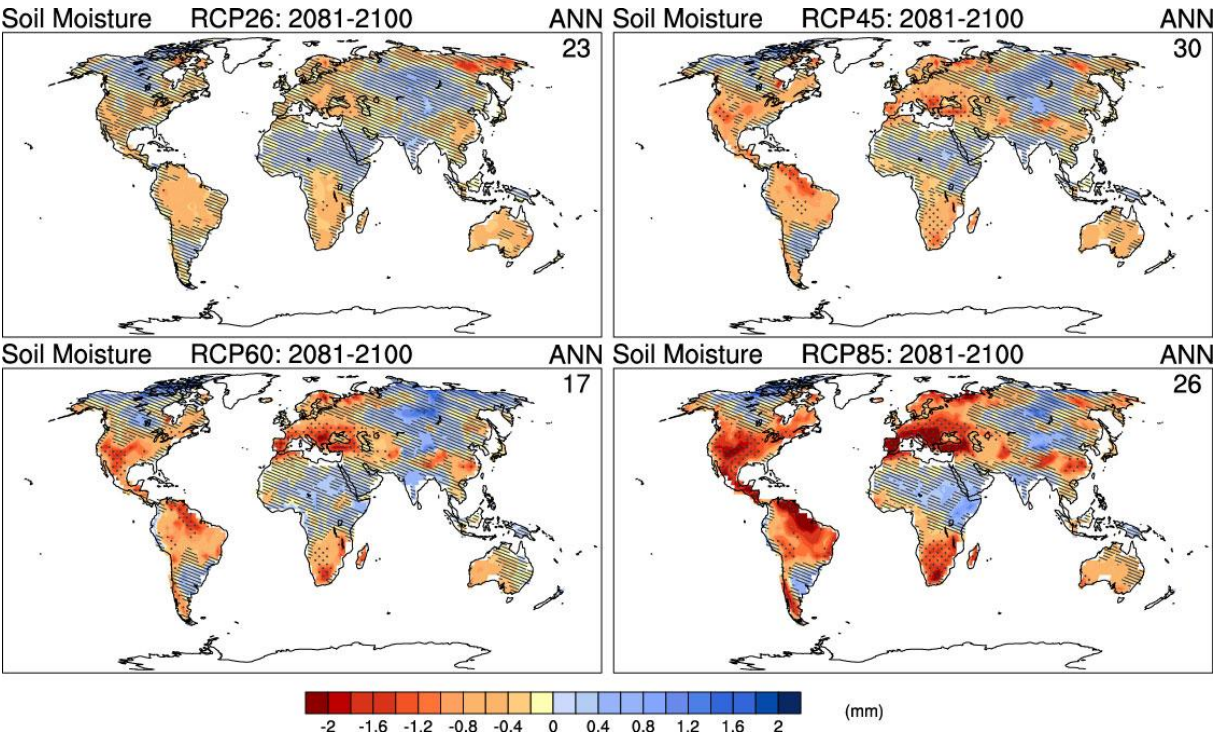


Figure 12.23: Change in annual mean soil moisture (mass of water in all phases in the uppermost 10 cm of the soil) (mm) relative to the reference period 1985–2005 projected for 2081–2100 from the CMIP5 ensemble for (a) RCP2.6, (b) RCP4.5, (c) RCP6.0 and (d) RCP8.5. Hatching indicates regions where the multi model mean is less than one standard deviation of internal variability. Stippling indicates regions where the multi model mean is greater than two standard deviations of internal variability and where 90% of models agree on the sign of change (see Box 12.1). The number of CMIP5 models used is indicated in the upper right corner of each panel.

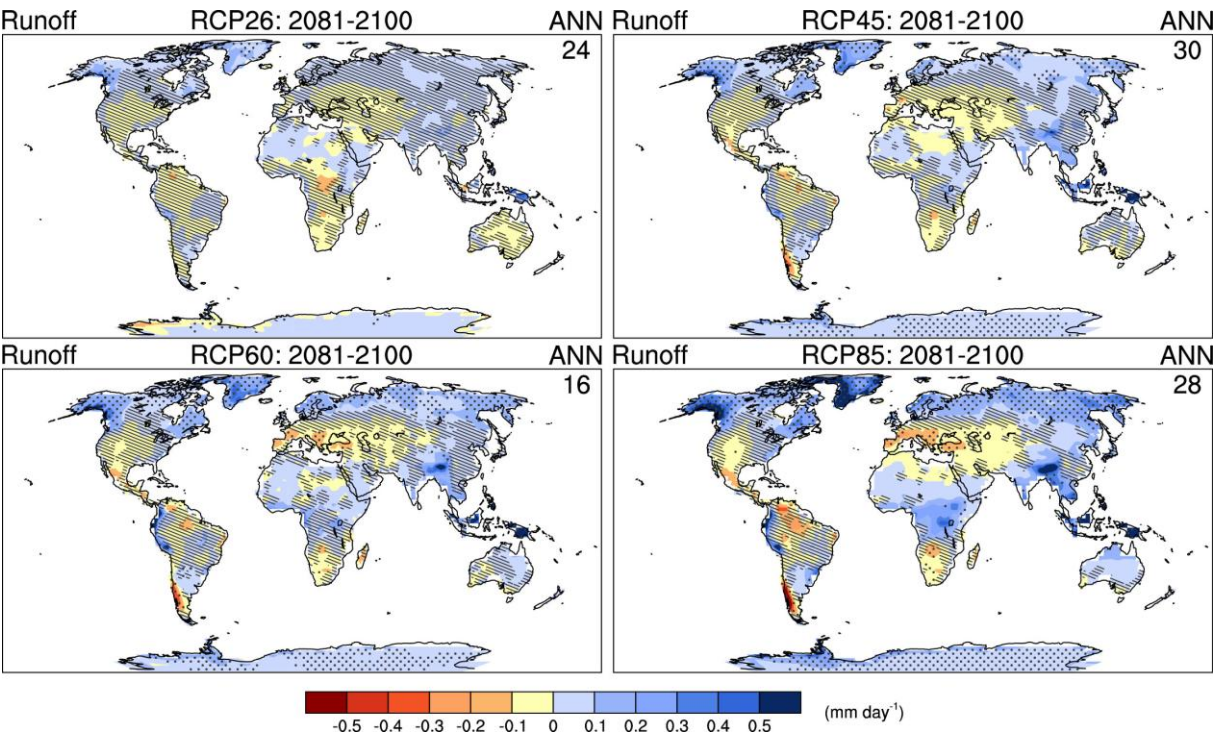


Figure 12.24: Change in annual mean runoff (mm) relative to the reference period 1985–2005 projected for 2081–2100 from the CMIP5 ensemble for (a) RCP2.6, (b) RCP4.5, and (c) RCP6.0 and (d) RCP8.5. Hatching indicates regions where the multi model mean is less than one standard deviation of internal variability. Stippling indicates regions where the multi model mean is greater than two standard deviations of internal variability and where 90% of models agree on the sign of change (see Box 12.1). The number of CMIP5 models used is indicated in the upper right corner of each panel.

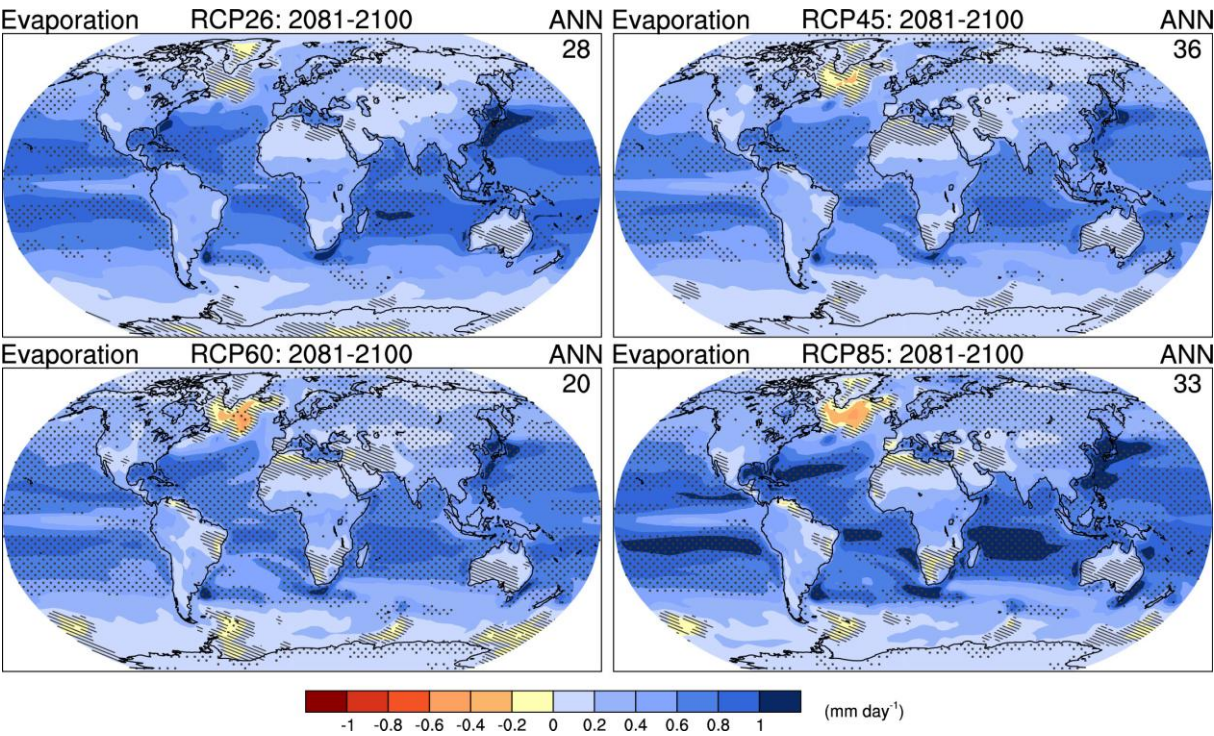


Figure 12.25: Change in annual mean evaporation (mm) relative to the reference period 1985–2005 projected for 2081–2100 from the CMIP5 ensemble for (a) RCP2.6, (b) RCP4.5, and (c) RCP6.0 and (d) RCP8.5. Hatching indicates regions where the multi model mean is less than one standard deviation of internal variability. Stippling indicates regions where the multi model mean is greater than two standard deviations of internal variability and where 90% of models agree on the sign of change (see Box 12.1). The number of CMIP5 models used is indicated in the upper right corner of each panel.

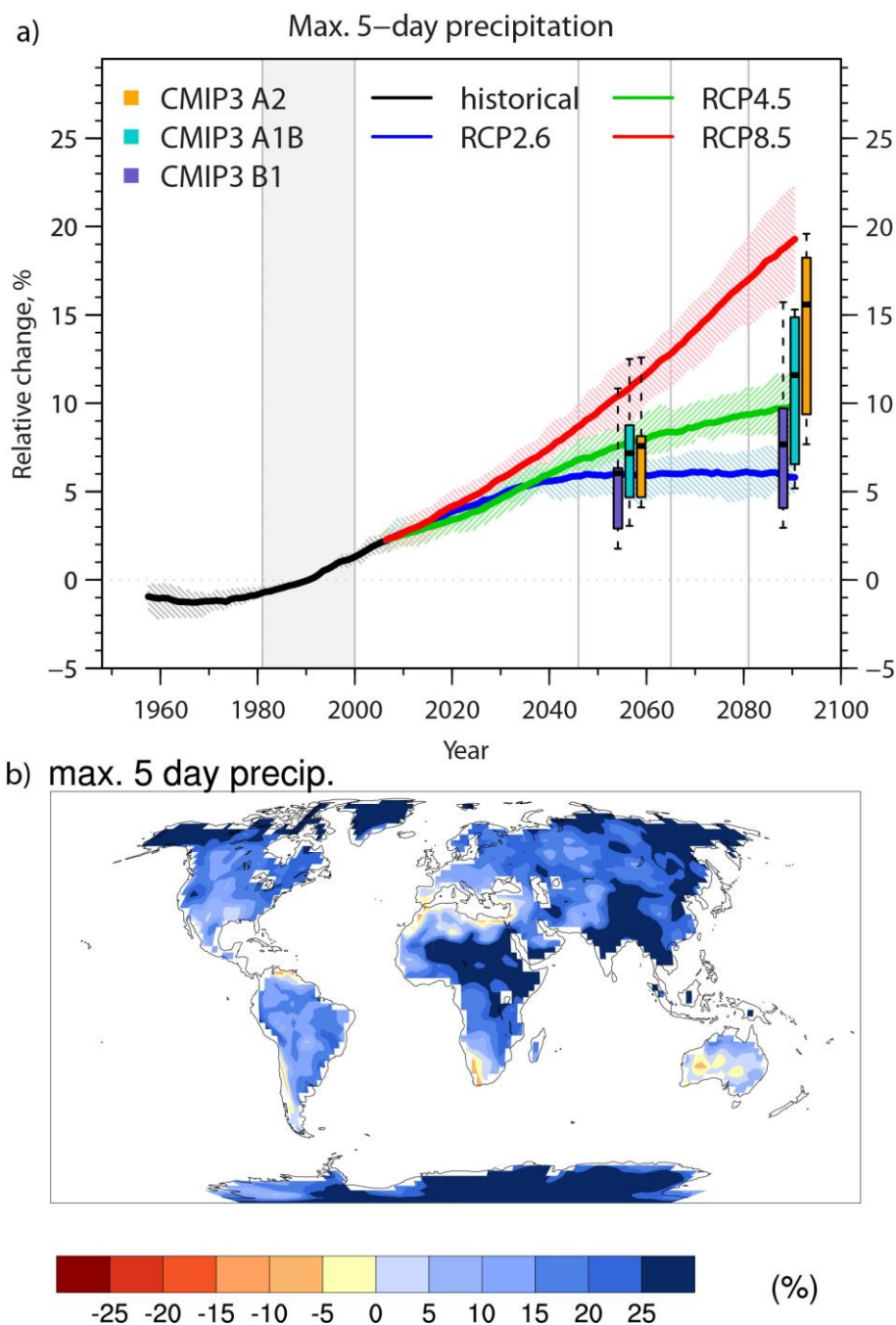


Figure 12.26: Projected percent changes (relative to the AR4 1981–2000 baseline period) from the CMIP5 models in R5dmax, the annual maximum five-day precipitation accumulation a) Global average percent change over land regions for the RCP2.6, 4.5 and 8.5 scenarios. b) Percent change over the 2081–2100 period in the RCP8.5. Equal model weighting.

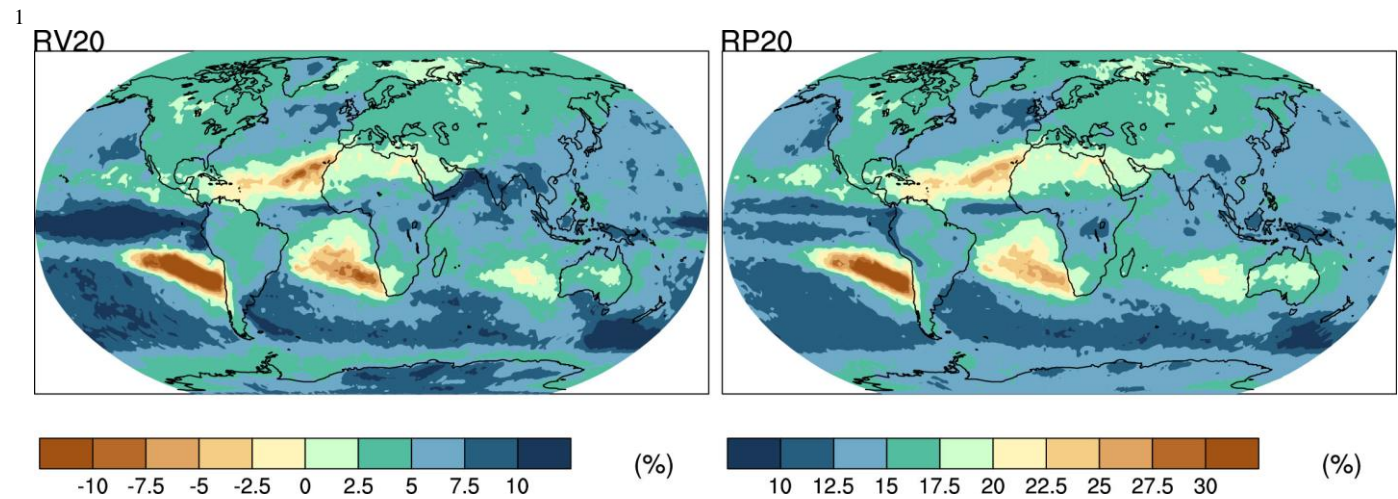
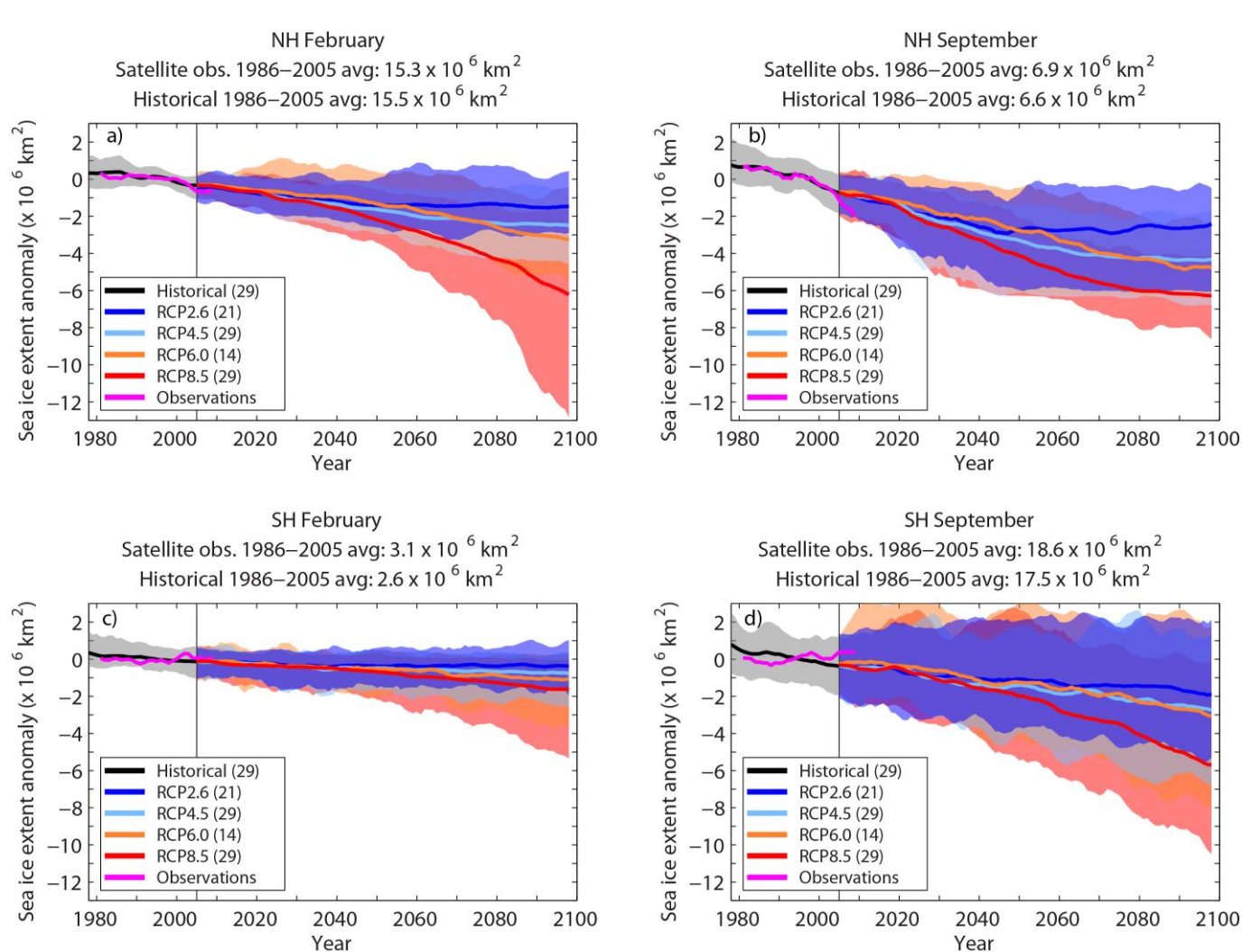
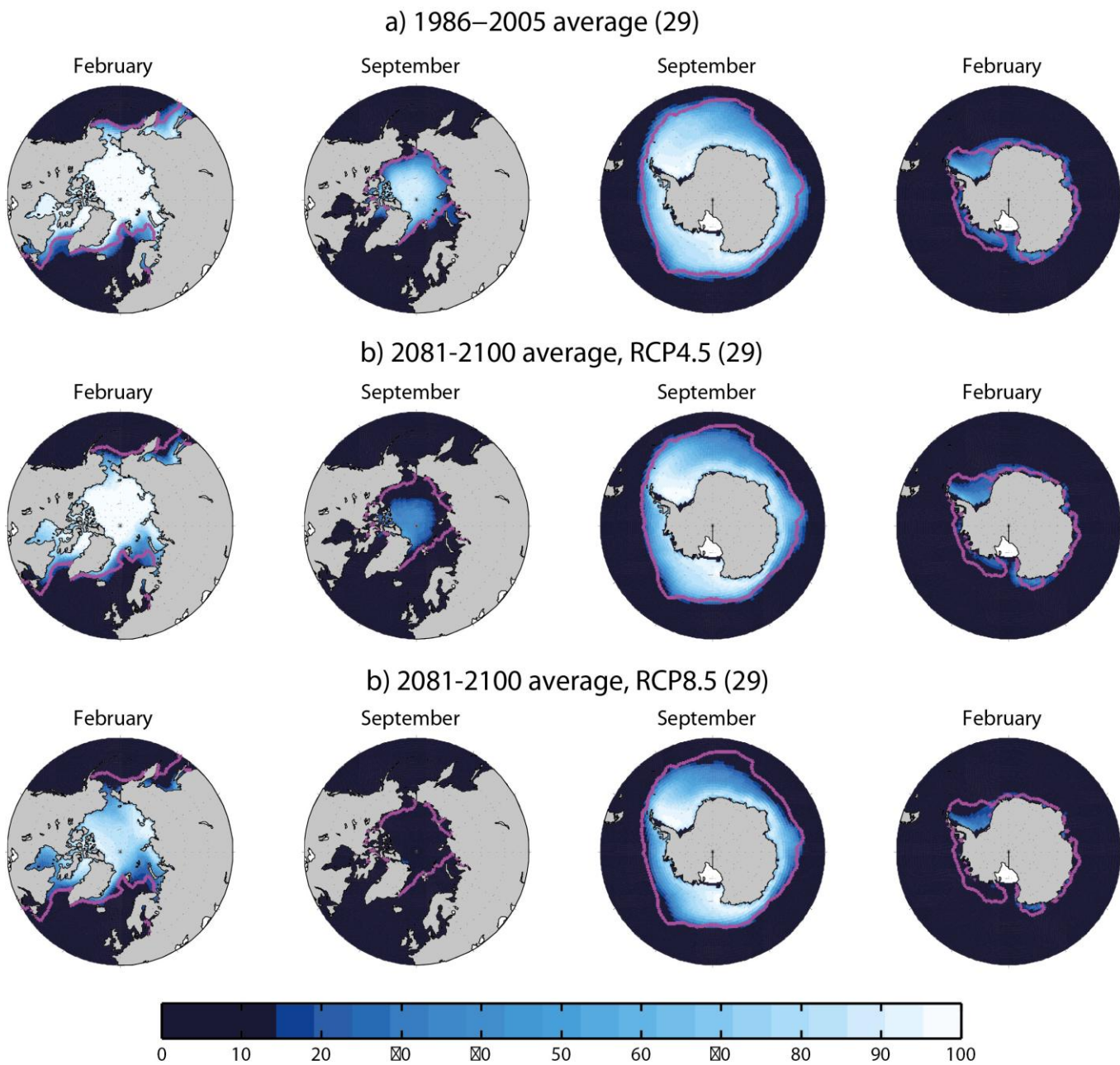


Figure 10.27: Left: The average 2081–2100 CMIP5 multi-model ensemble median percent change in twenty year return values of annual maximum daily precipitation per 1 K of local warming relative to the 1986–2005 reference period. Right: The average 2081–2100 CMIP5 multi-model ensemble median of the return periods (years) of 1986–2005 twenty year return values of annual maximum daily precipitation corresponding to 1 K of local warming. Regions of no change would have return periods of twenty years.



2
3
4 **Figure 12.28:** Anomalies in sea ice extent (5-year running mean) as simulated by CMIP5 models over the late 20th
5 century and the whole 21st century under RCP2.6, RCP4.5, RCP6.0 and RCP8.5 for (a) Northern Hemisphere February,
6 (b) Northern Hemisphere September, (c) Southern Hemisphere February and (d) Southern Hemisphere September. The
7 solid curves show the multi-model means and the shading denotes the 5–95% range of the ensemble. The vertical bar
8 marks the end of CMIP5 historical climate change simulations. One ensemble member per model is taken into account
9 in the analysis. Sea ice extent is defined as the total oceanic area where sea ice concentration exceeds 15% and is
10 calculated on the original model grids. Anomalies are relative to the reference period 1986–2005. The number of
11 models is given in the legend. Also plotted (solid pink curves) are the satellite data of Comiso and Nishio (2008) over
12 1979–2011.
13
14

1



2
3
4
5
6
7
8
9
10

Figure 12.29: February and September CMIP5 multi-model mean sea ice concentrations (%) in the Northern and Southern Hemispheres for the periods (a) 1986–2005, (b) 2081–2100 under RCP4.5 and (c) 2081–2100 under RCP8.5. The model ice concentrations are interpolated onto a $1^{\circ} \times 1^{\circ}$ regular grid. One ensemble member per model is taken into account in the analysis. The number of models is given in parentheses. The pink lines show the observed 15% sea ice concentration limits averaged over 1986–2005 (Comiso and Nishio, 2008).

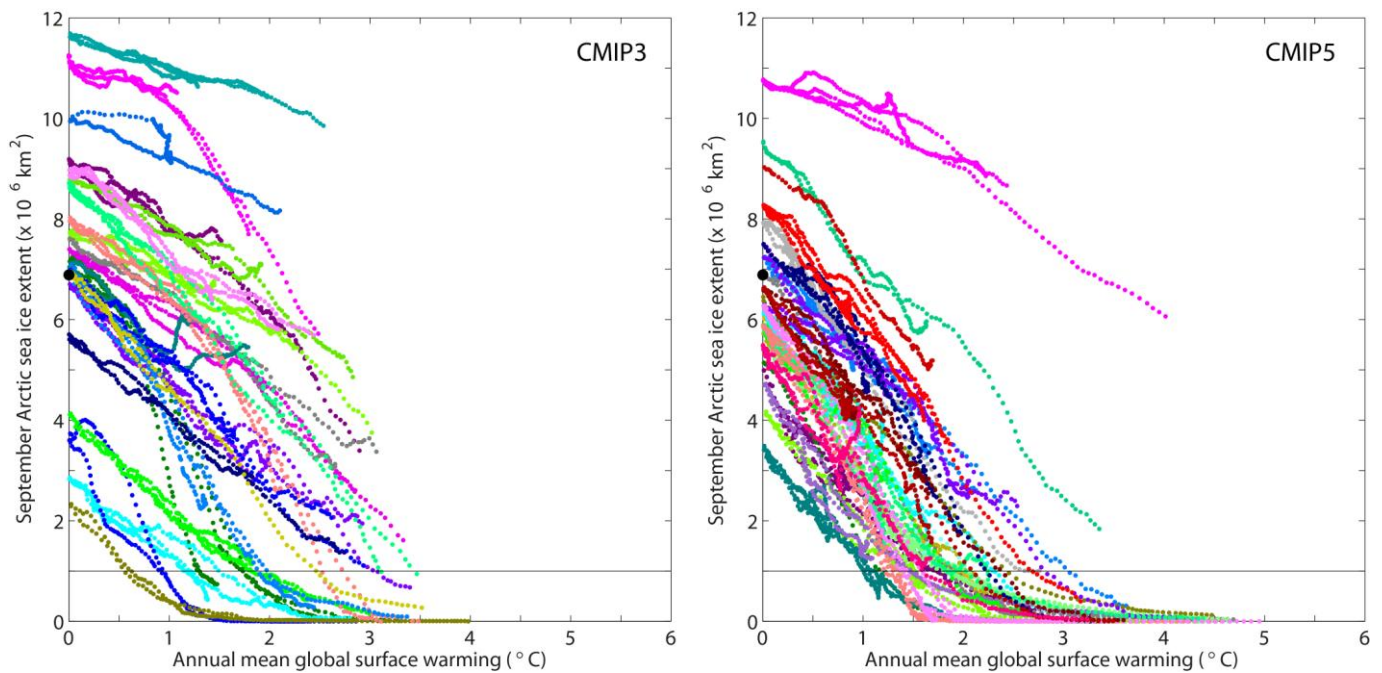


Figure 12.30: September Arctic sea ice extent as a function of the annual mean global surface temperature change with respect to the period 1986–2005 for (left) CMIP3 models (all SRES scenarios) and (right) CMIP5 models (all RCPs). The ice extents and global temperatures are computed on a common latitude-longitude grid for CMIP3 and on the original model grids for CMIP5. One ensemble member per model is taken into account in the analysis. A 21-year running mean is applied to the model output. The black circle on the y-axis shows the mean observed September Arctic sea ice extent over 1986–2005 (Comiso and Nishio, 2008).

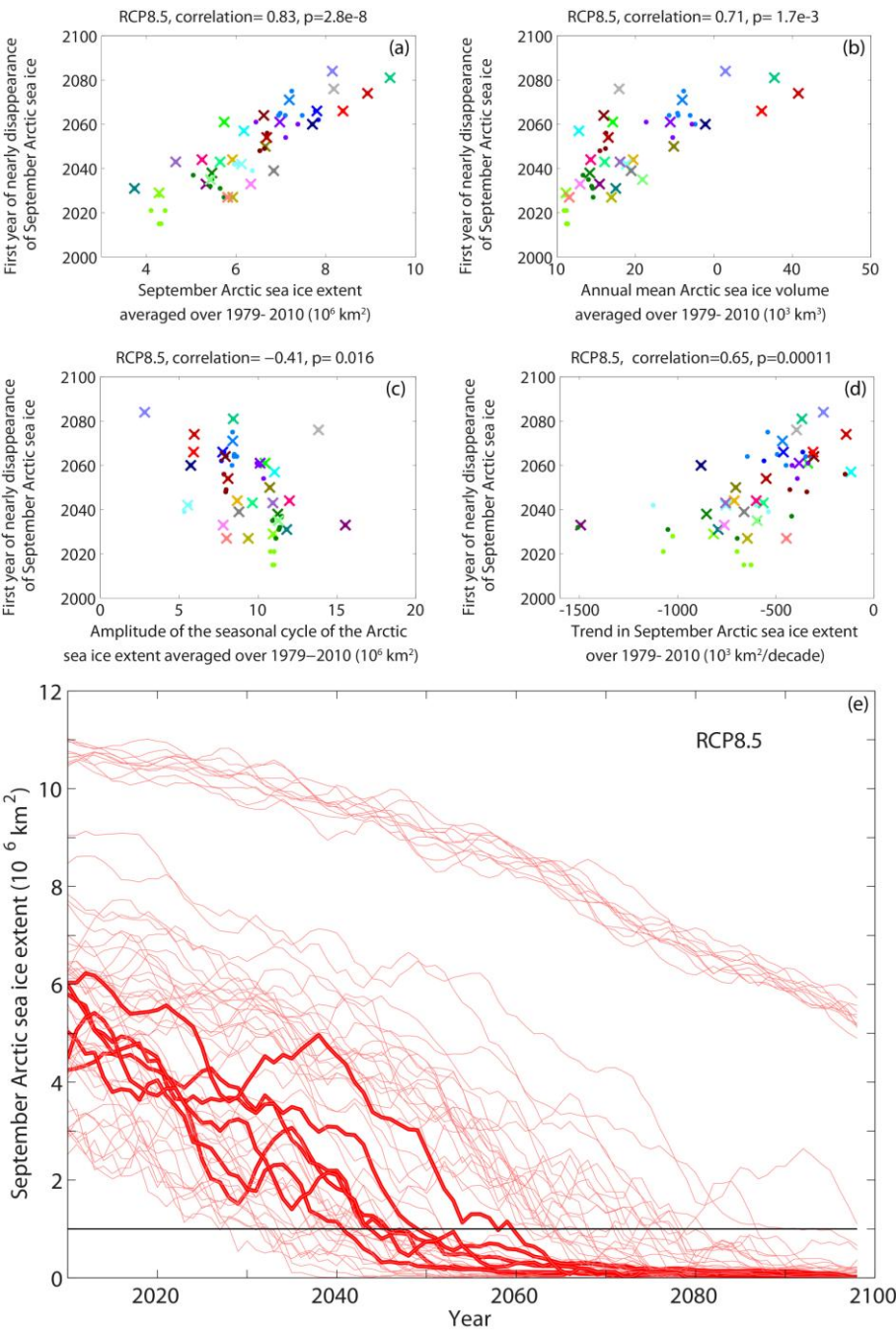


Figure 12.31: (a-d) First year during which the September Arctic sea ice extent falls below $1 \times 10^6 \text{ km}^2$ in CMIP5 climate projections (29 models, RCP8.5) as a function of (a) the September Arctic sea ice extent averaged over 1979–2010, (b) the annual mean Arctic sea ice volume averaged over 1979–2010, (c) the amplitude of the seasonal cycle of Arctic sea ice extent averaged over 1979–2010 and (d) the trend in September Arctic sea ice extent over 1979–2010. The sea ice variables shown are calculated on the original model grids. The correlations and one-tailed p -values are computed from the multi-member means for models with several ensemble members (coloured crosses), but the ensemble members of individual models are also depicted (coloured dots). (e) Time series of September Arctic sea ice extent (5-year running mean) as simulated by all CMIP5 models and their ensemble members under RCP8.5 (thin curves). The thick curves correspond to a subset of six CMIP5 models that meet criteria based on panels a-d and defined in Massonnet et al. (2012). Note that each of these selected models only provides one ensemble member.

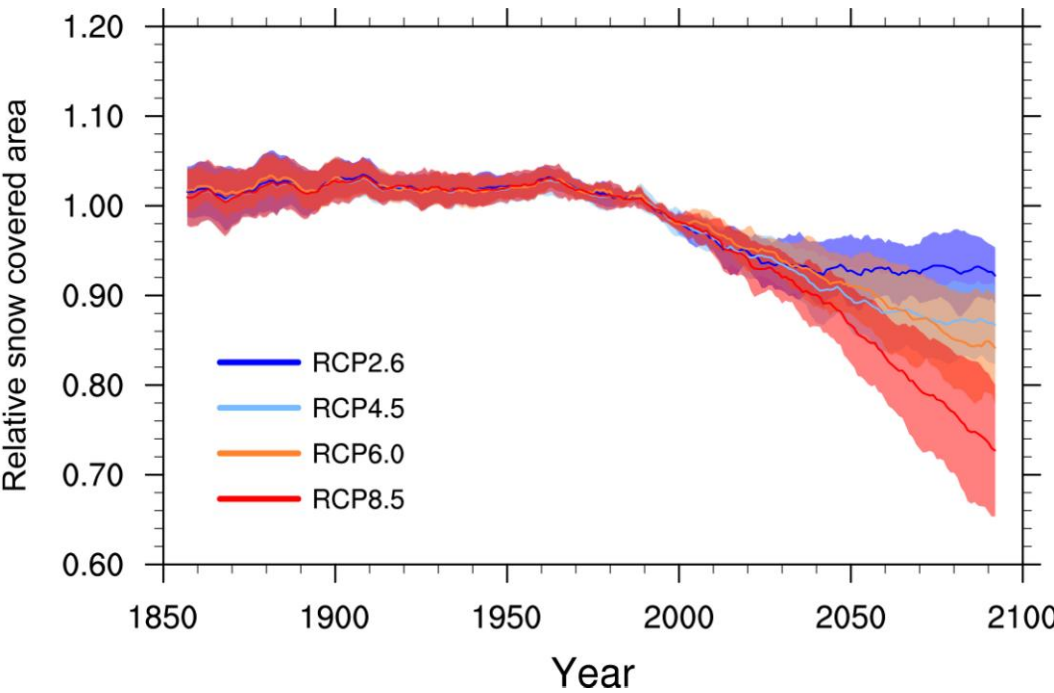


Figure 12.32: Northern Hemisphere spring (March to April average) relative snow covered area (RSCA) in the CMIP5 MMD, obtained through dividing the simulated 5-year box smoothed spring snow covered area (SCA) by the simulated average spring SCA of 1986–2005 reference period. Blue: RCP2.6; Light blue: RCP4.5; Orange: RCP6.0; Red: RCP8.5. Thick lines: MMD average. Shading and thin dotted lines indicate the inter-model spread (one standard deviation).

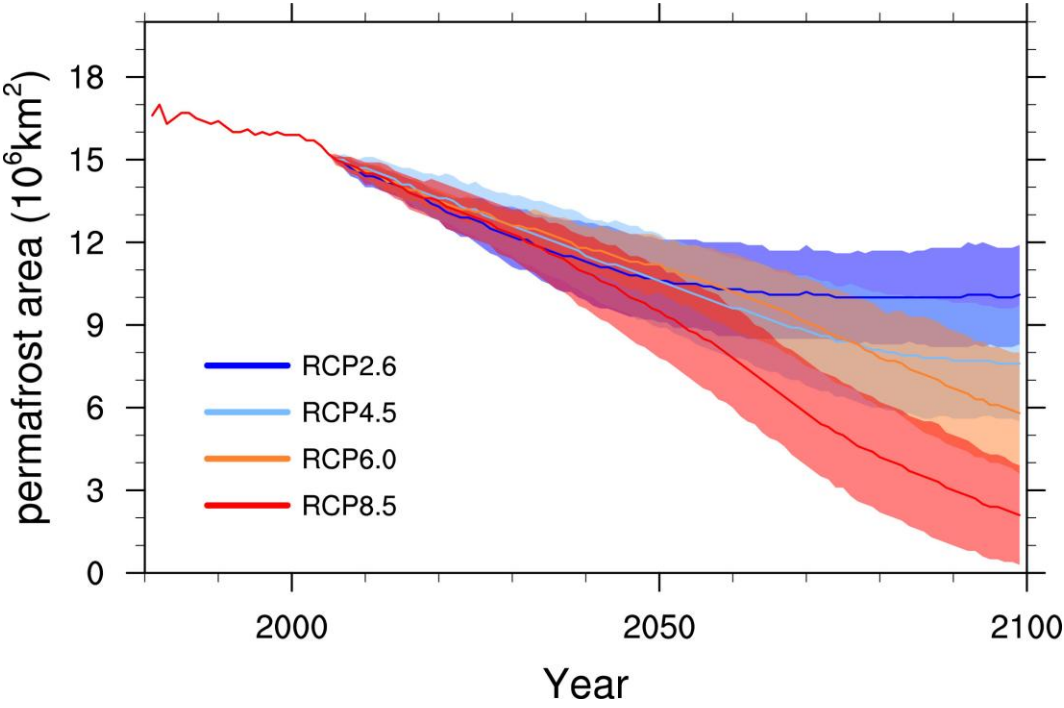


Figure 12.33: Northern hemisphere diagnosed near-surface permafrost area in the CMIP5 MMD following Nelson and Outcalt (1987) and using 20-year average monthly surface air temperatures and snow depths. Blue: RCP2.6; Light blue: RCP4.5; Orange: RCP6.0; Red: RCP8.5. Thick lines: MMD average. Shading and thin lines indicate the inter-model spread (one standard deviation).

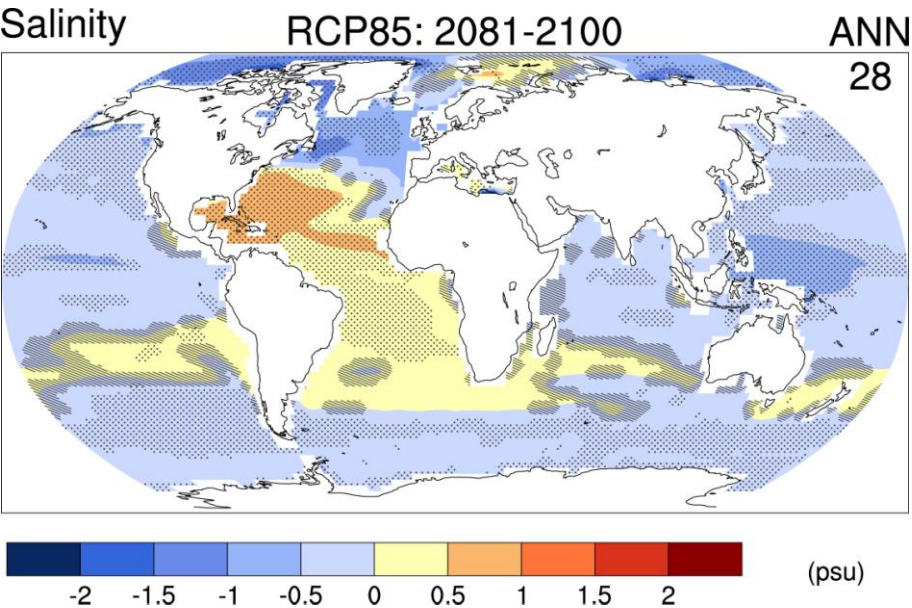


Figure 12.34: Projected sea surface salinity differences 2081–2100 for RCP8.5 relative to 1986–2005 from CMIP5 models. Hatching indicates regions where the multi model mean is less than one standard deviation of internal variability. Stippling indicates regions where the multi model mean is greater than two standard deviations of internal variability and where 90% of the models agree on the sign of change (see Box 12.1). The number of CMIP5 models used is indicated in the upper right corner of each panel.

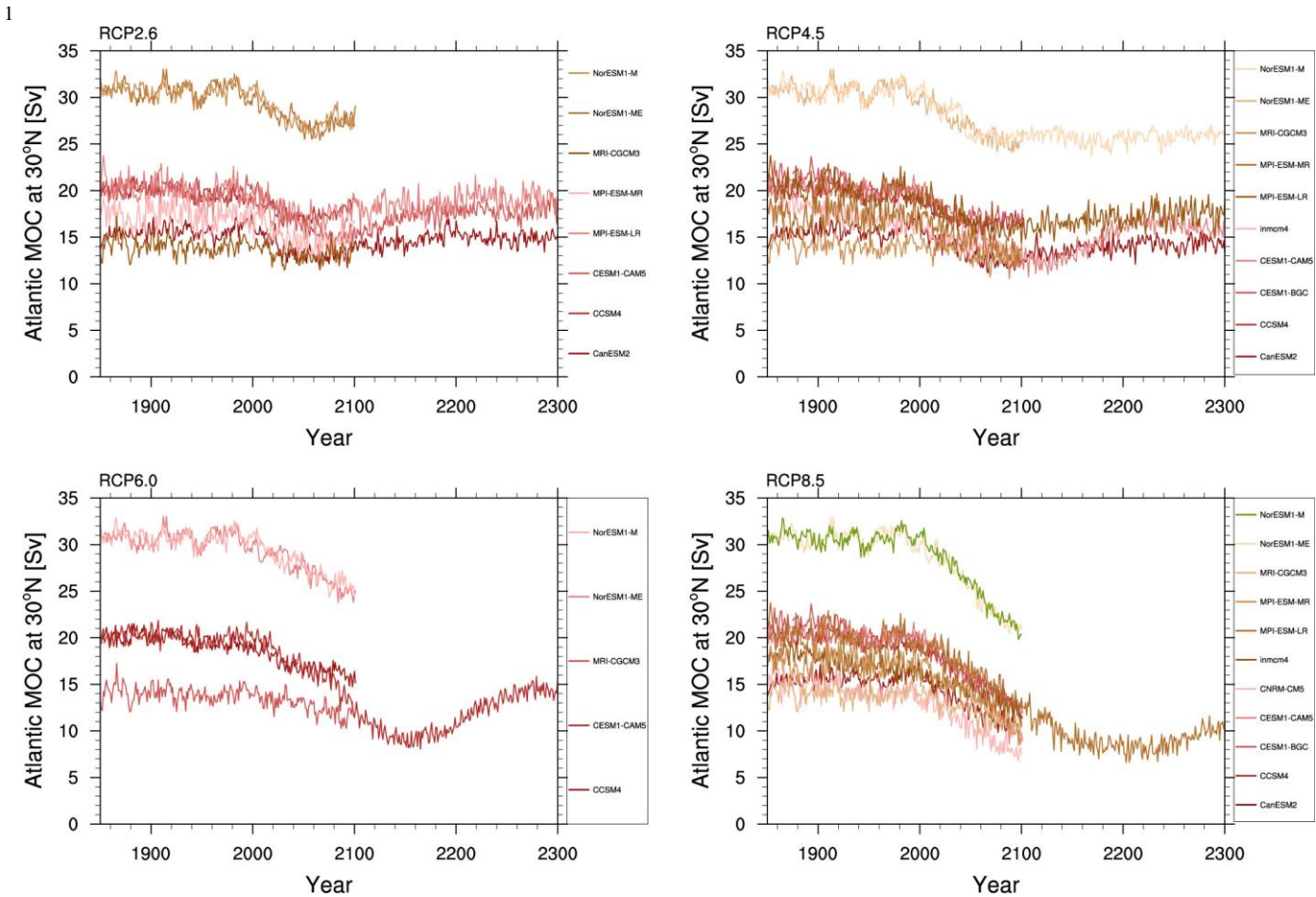


Figure 12.35: Multi model projections of Atlantic meridional overturning circulation (AMOC) strength at 30°N from 1850 through to the end of the RCP extensions. a) RCP2.6; b) RCP4.5; c) RCP6.0; d) RCP8.5. Results are based on a small number of CMIP5 models available. Curves show results from only the first member (r1i1p1) of the submitted ensemble of experiments.

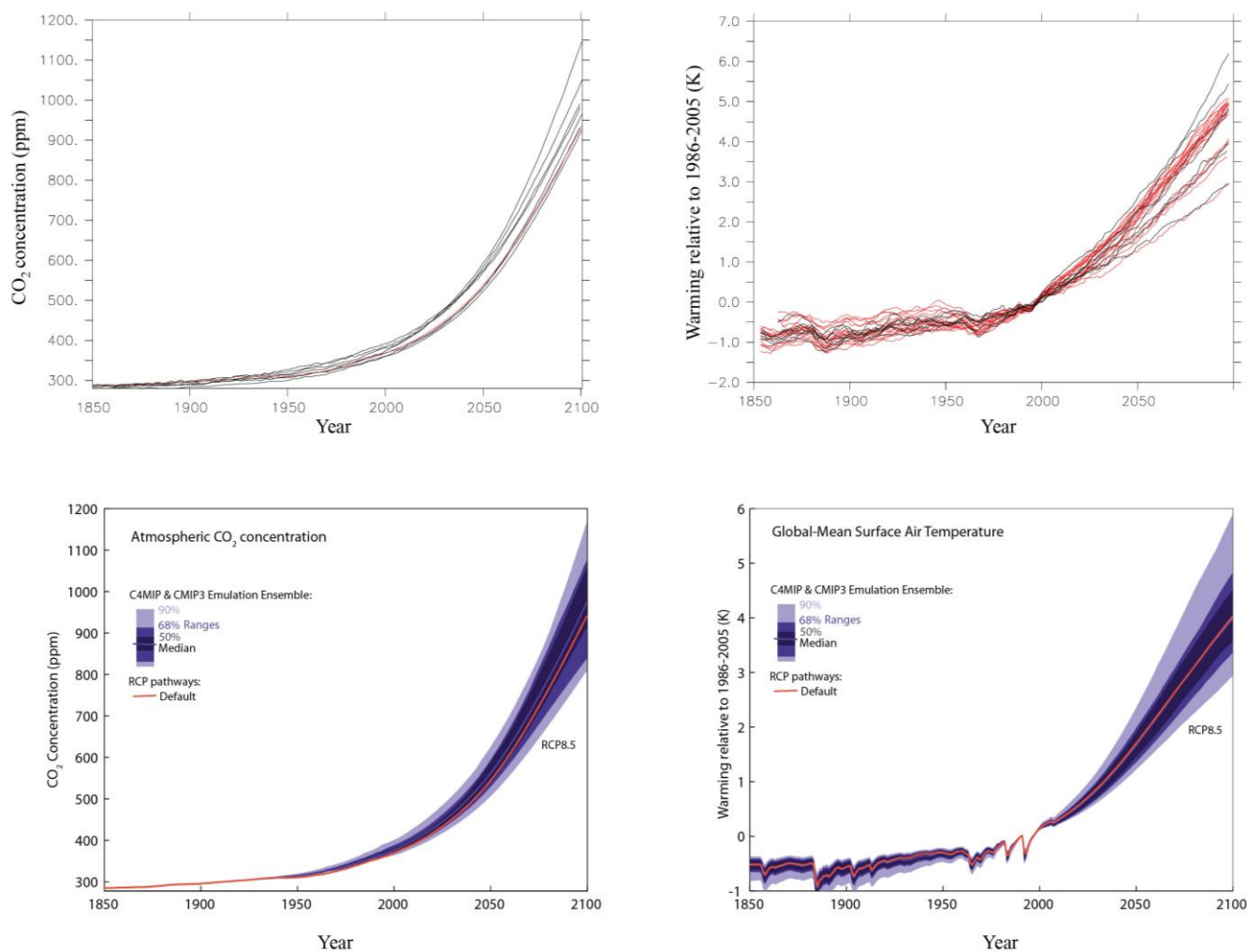


Figure 12.36: Comparison between CMIP5 ESMs simulations for RCP8.5 with CO₂ emissions (black) or CO₂ concentration (red) as external forcing for a) atmospheric CO₂ concentration (ppm), and b) global average surface air temperature difference (°C). Range of c) CO₂ concentrations and d) global average surface air temperature difference (°C) simulated by the MAGICC6 model when emulating the CMIP3 models climate sensitivity range and the C⁴MIP models carbon cycle feedbacks.

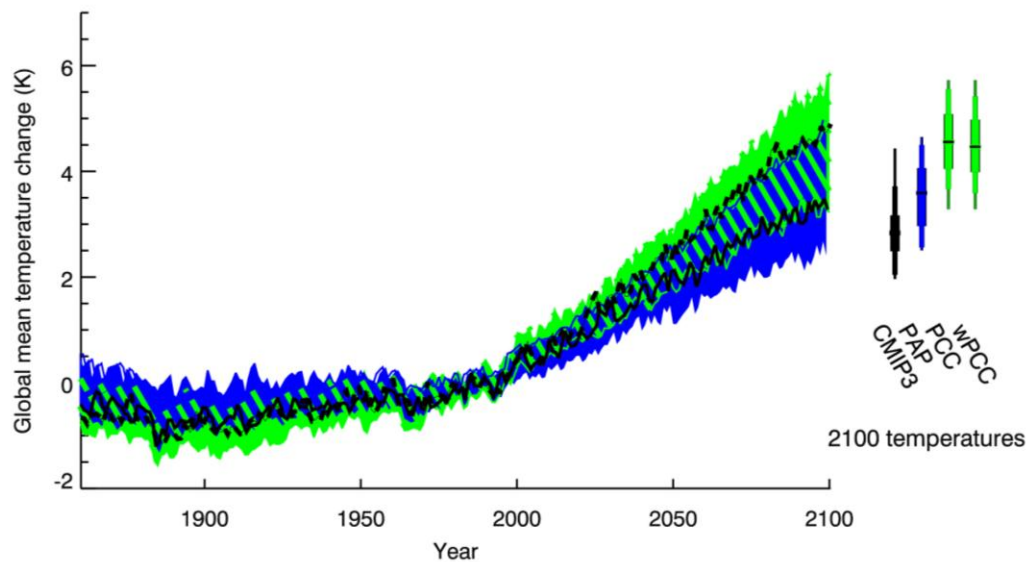


Figure 12.37: Uncertainty in global mean temperature from HadCM3 results exploring atmospheric physics and terrestrial carbon cycle parameter perturbations (Booth et al., 2012; Murphy et al., 2004). Relative uncertainties in the Perturbed Carbon Cycle (PCC, green plume) and Perturbed Atmospheric Processes (PAP, blue) on global mean anomalies of temperature (plotted with respect to the 1980–1999 period). The green/blue hatching illustrates where these two ensembles overlap. The standard simulations from the two ensembles, HadCM3 (black solid) and HadCM3C (black dashed) are also shown. Four bars are shown on the right illustrating the 2100 temperature anomalies associated with the CMIP3/AR4 ensemble (black) the PAP ensemble (blue) the land carbon cycle (PCC) and the weighted land carbon ensemble wPCC (both green). The range (thin line), 10th–90th (medium line) and 25th–75th (thick line) and 50th percentiles (central bar) are all shown.

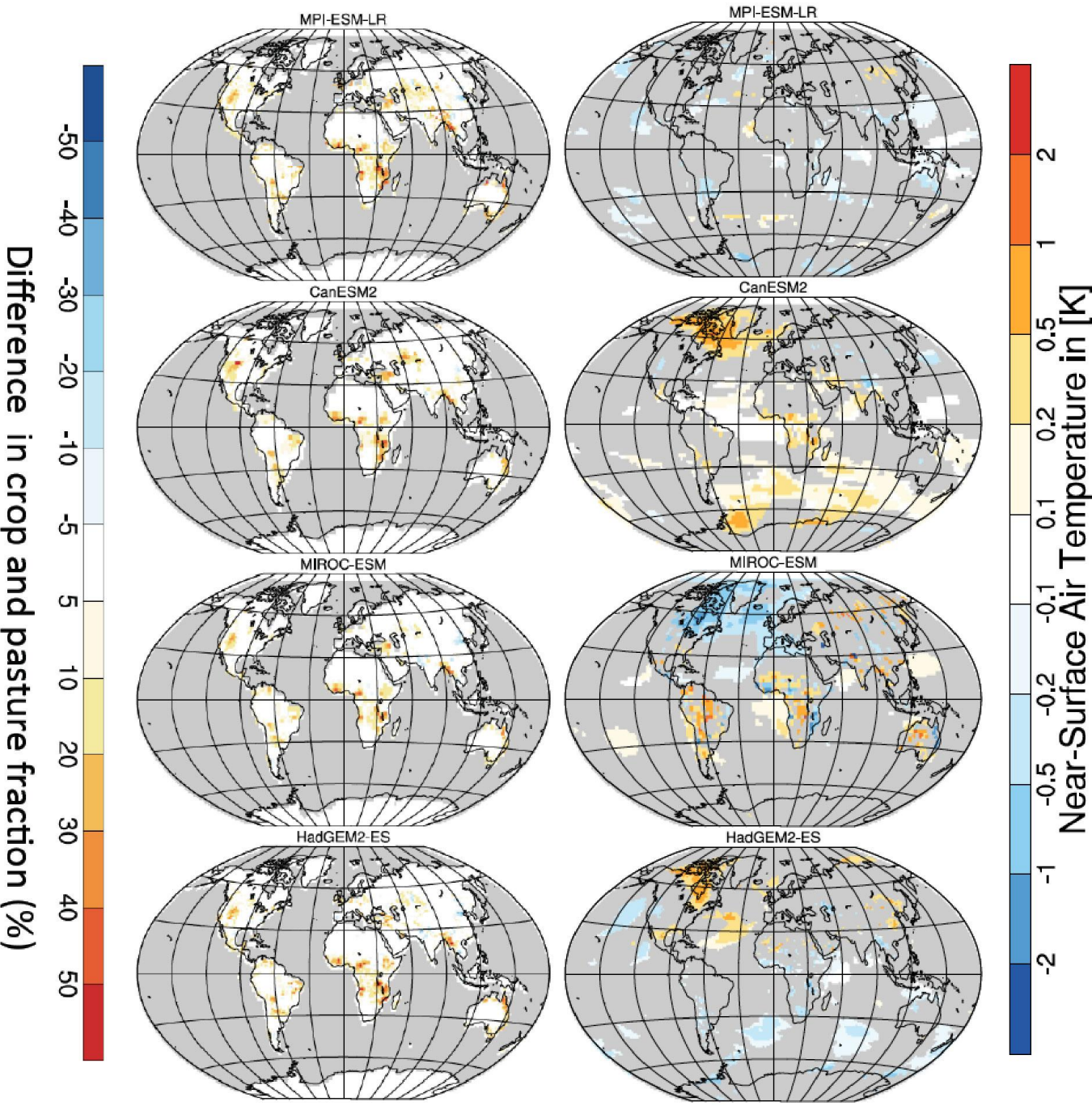


Figure 12.38: Impact of land-use change on surface temperature. LUCID experiments where 4 ESMs (MPI-ESM-LR, CanESM2, MIROC-ESM and HadGEM2-ES) were forced with and without land-use change beyond 2005 under the RCP2.6 scenario. Left maps show the change in crop and pasture fractions due to the absence of future land-use as implemented in the four ESMs. Right maps show the difference in near surface temperature difference between the simulation with- and without land use change beyond 2005 (Brovkin et al., 2012). The differences are averaged for years 2071–2100; only statistically significant changes ($p < 0.05$) are plotted

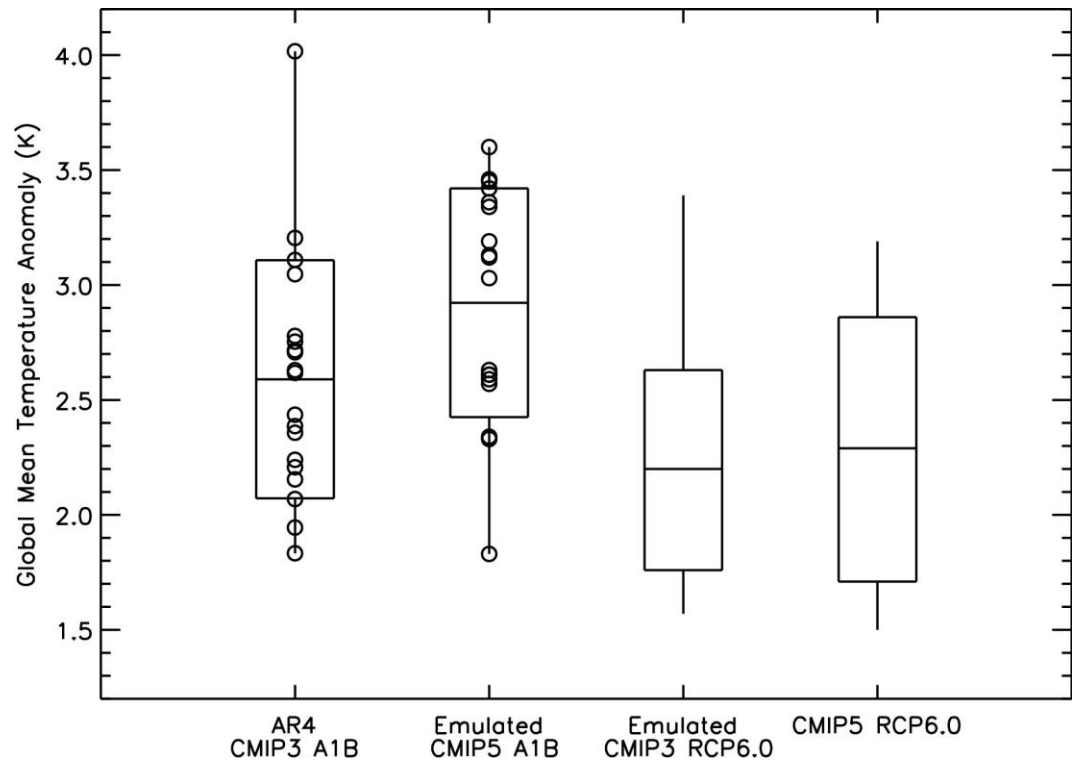


Figure 12.39: Global mean temperature anomalies at the end of the 21st century (2080–2099) from GCM experiments and emulators comparing CMIP3/CMIP5 responses under SRES A1B and RCP6.0. The boxes and whiskers indicate minimum, mean value – 1 standard deviation, mean, mean value + 1 standard deviation and maximum values. The emulated SRES A1B projections of CMIP5 are obtained by the method of (Good et al., 2011b) and are expressed with respect to the AR4 baseline period of 1980–1999. (Because of the method, the subset of CMIP5 that are emulated are restricted to those with preindustrial control, abrupt $4 \times \text{CO}_2$, historical, RCP4.5 and RCP8.5 simulations). The emulated RCP6.0 projections of CMIP3 are from (Knutti and Sedláček, 2012) obtained using the method of Meinshausen et al. (2011b; 2011c) and are expressed with respect to the AR5 baseline period of 1986–2005.

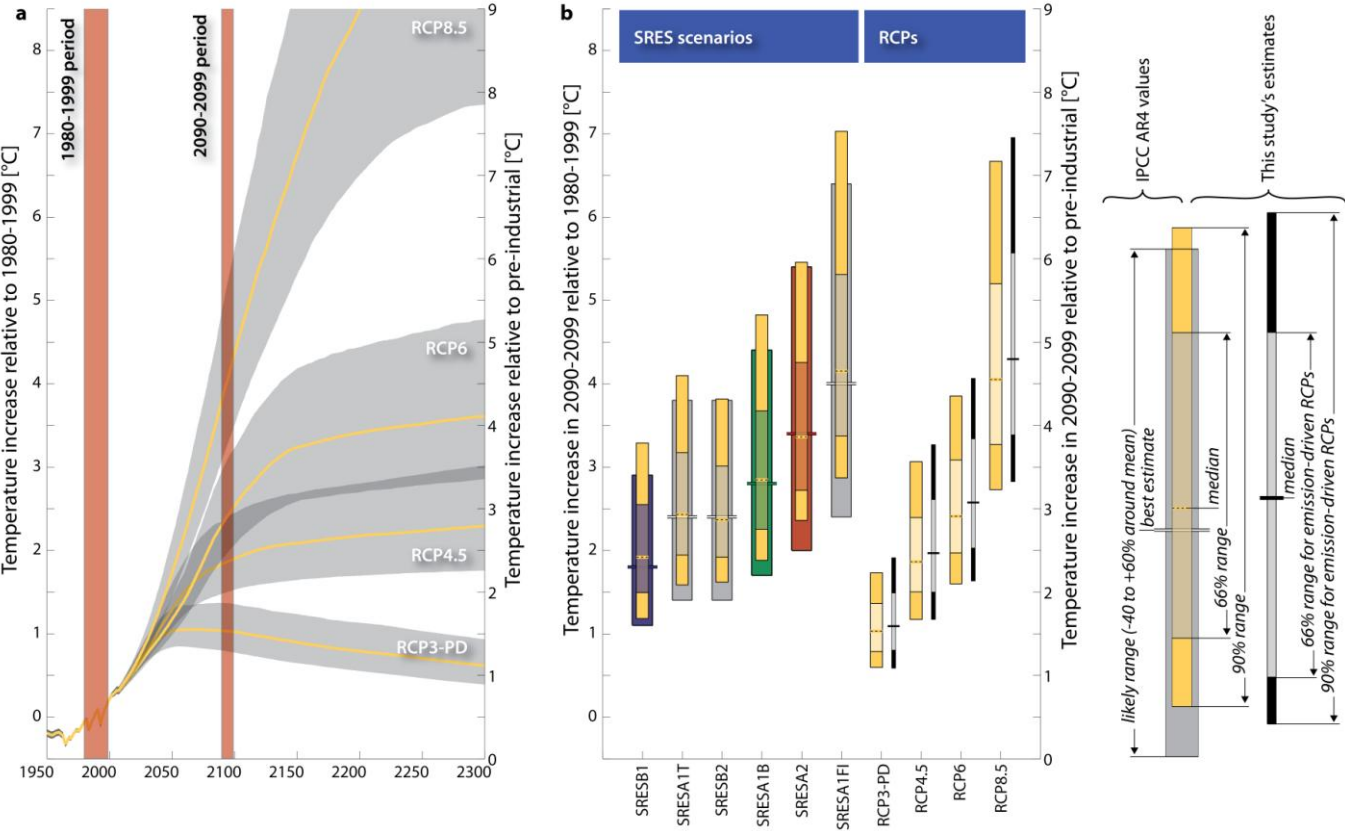


Figure 12.40: Temperature projections for SRES scenarios and the RCPs. (a) Time-evolving temperature distributions (66% range) for the four RCPs computed with this study’s ECS distribution and a model setup representing closely the carbon-cycle and climate system uncertainty estimates of the AR4 (grey areas). Median paths are drawn in yellow. Red shaded areas indicate time periods referred to in panel b. (b) Ranges of estimated average temperature increase between 2090 and 2099 for SRES scenarios and the RCPs respectively. Note that results are given both relative to 1980–1999 (left scale) and relative to pre-industrial (right scale). Yellow ranges indicate results of this study; other ranges show the AR4 estimates. Colour-coding of AR4 ranges is chosen to be consistent with the AR4.

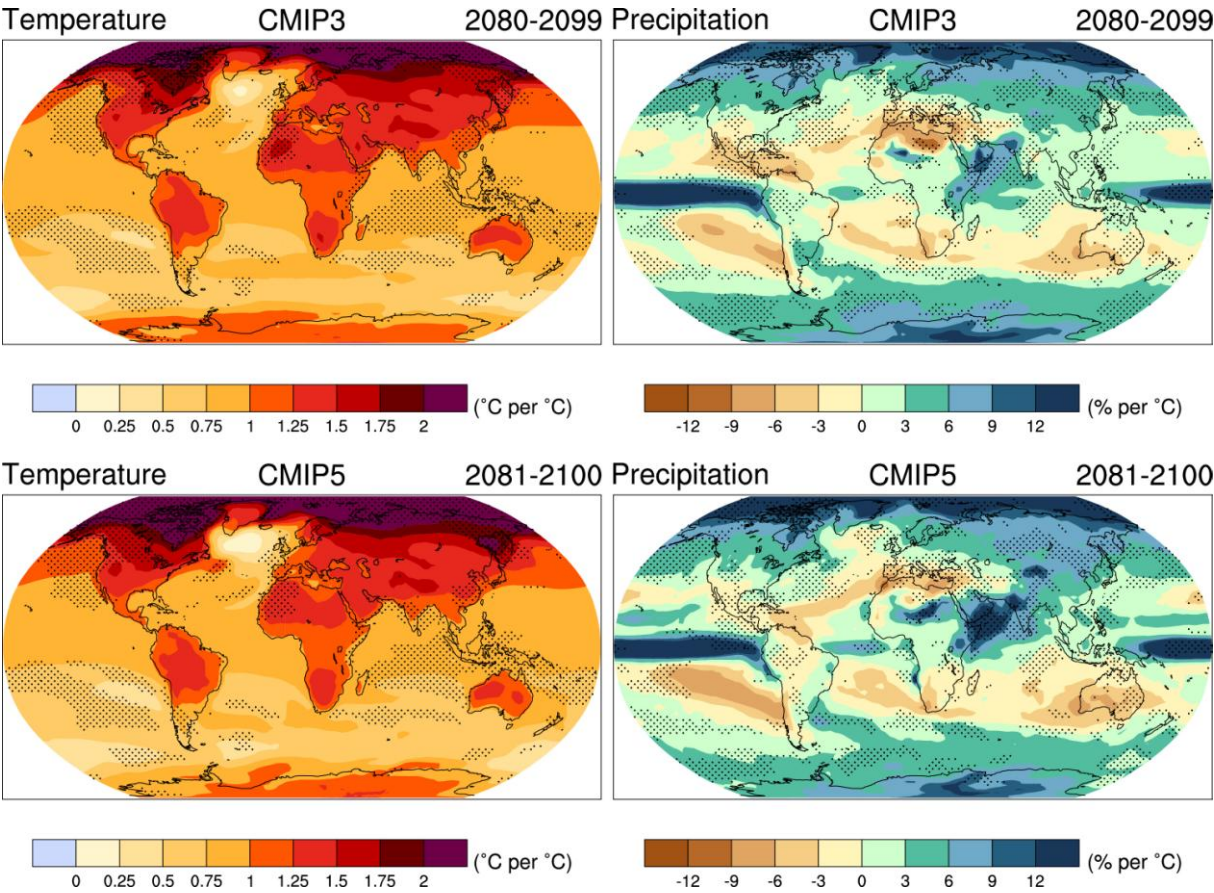


Figure 12.41: Patterns of temperature (left column) and percent precipitation change (right column) by the end of the 21st century (2081–2100 vs 1986–2005), for the CMIP3 models average (first row) and CMIP5 models average (second row), scaled by the corresponding global average temperature changes.

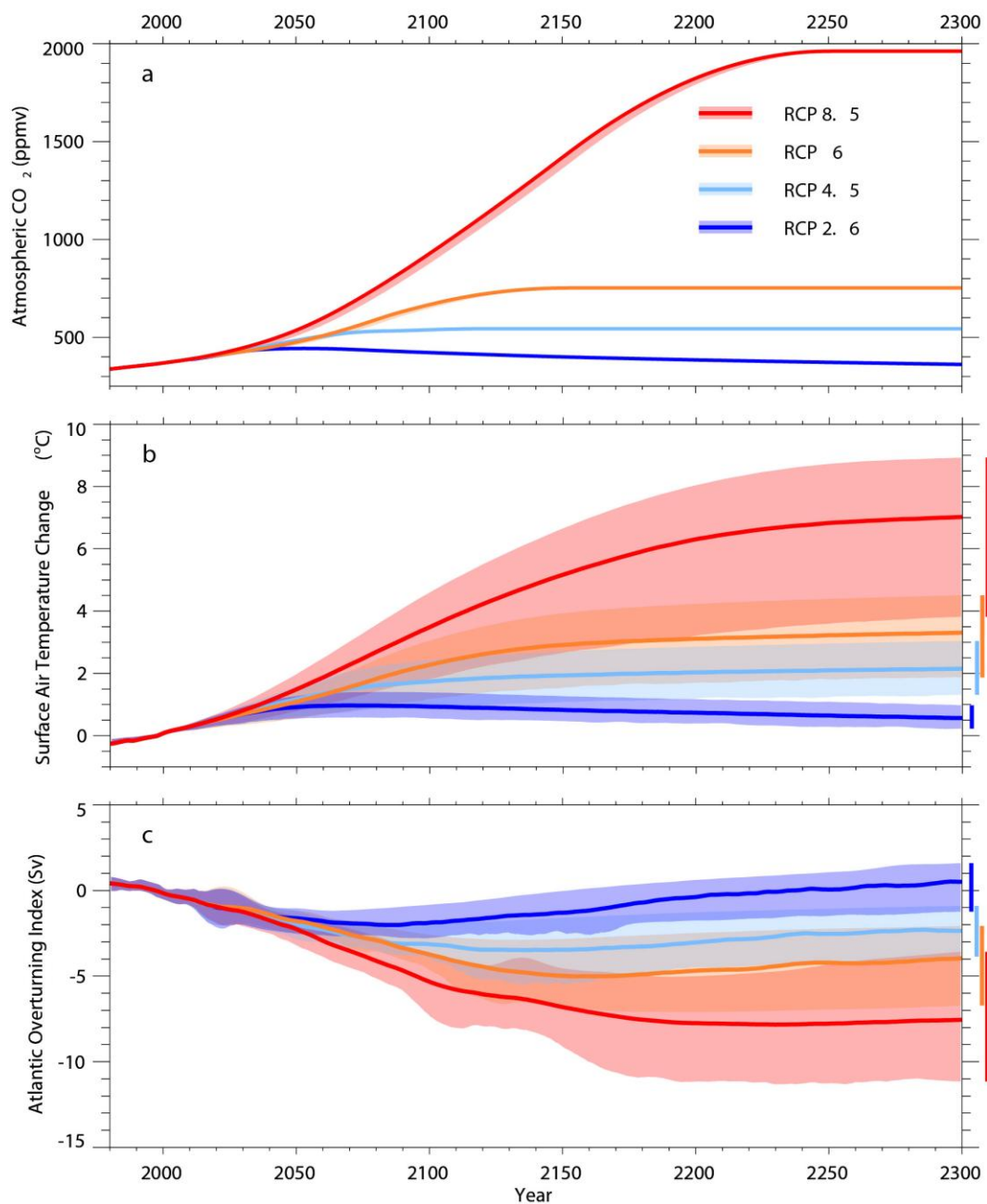


Figure 12.42: Atmospheric CO₂ forcing, b) projected global mean surface temperature warming and c) projected change in meridional overturning circulation, as simulated by 12 EMICs (Bern3D, CLIMBER 2, CLIMBER 3-a, DCESS, GENIE, IAPRASC, IGSM, LOVECLIM, MICOC3-LGM, MESMO, UMD and UVic) for the four RCPs up to 2300 (Zickfeld et al., 2012). A ten-year smoothing was applied.

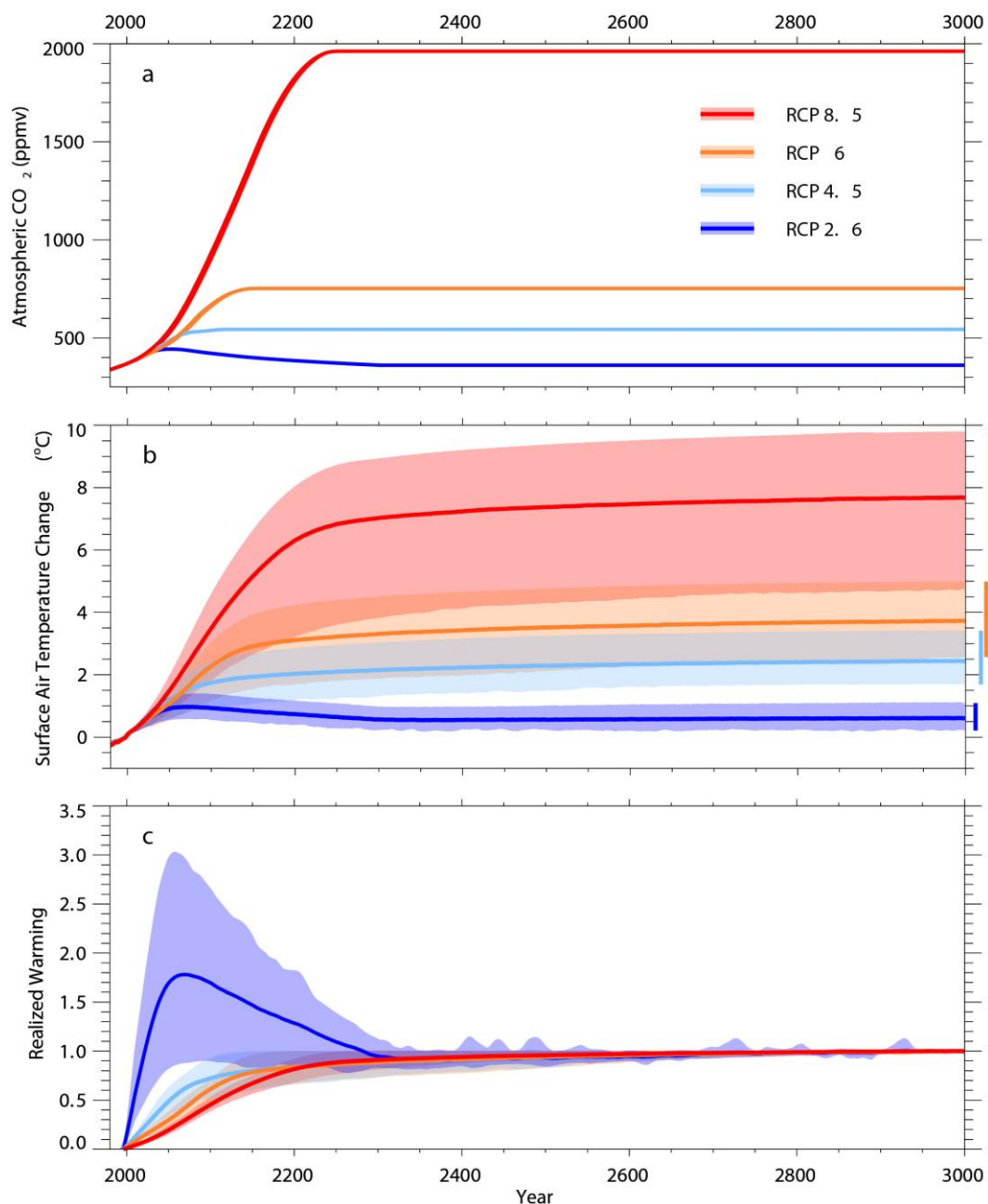


Figure 12.43: Atmospheric CO₂ forcing, b) projected global mean surface temperature warming and c) fraction of realized warming calculate as the ratio of global temperature change at a given time to the change averaged over the 2980–2999 time period, as simulated by 12 EMICs (Bern3D, CLIMBER 2, CLIMBER 3-a, DCESS, GENIE, IAPRASCN, IGSM, LOVECLIM, MICOC3-LGM, MESMO, UMD and UVic) for the 4 RCPs up to 2300 followed by a constant (2300 level) radiative forcing up to the year 3000 (Zickfeld et al., 2012). A ten-year smoothing was applied.

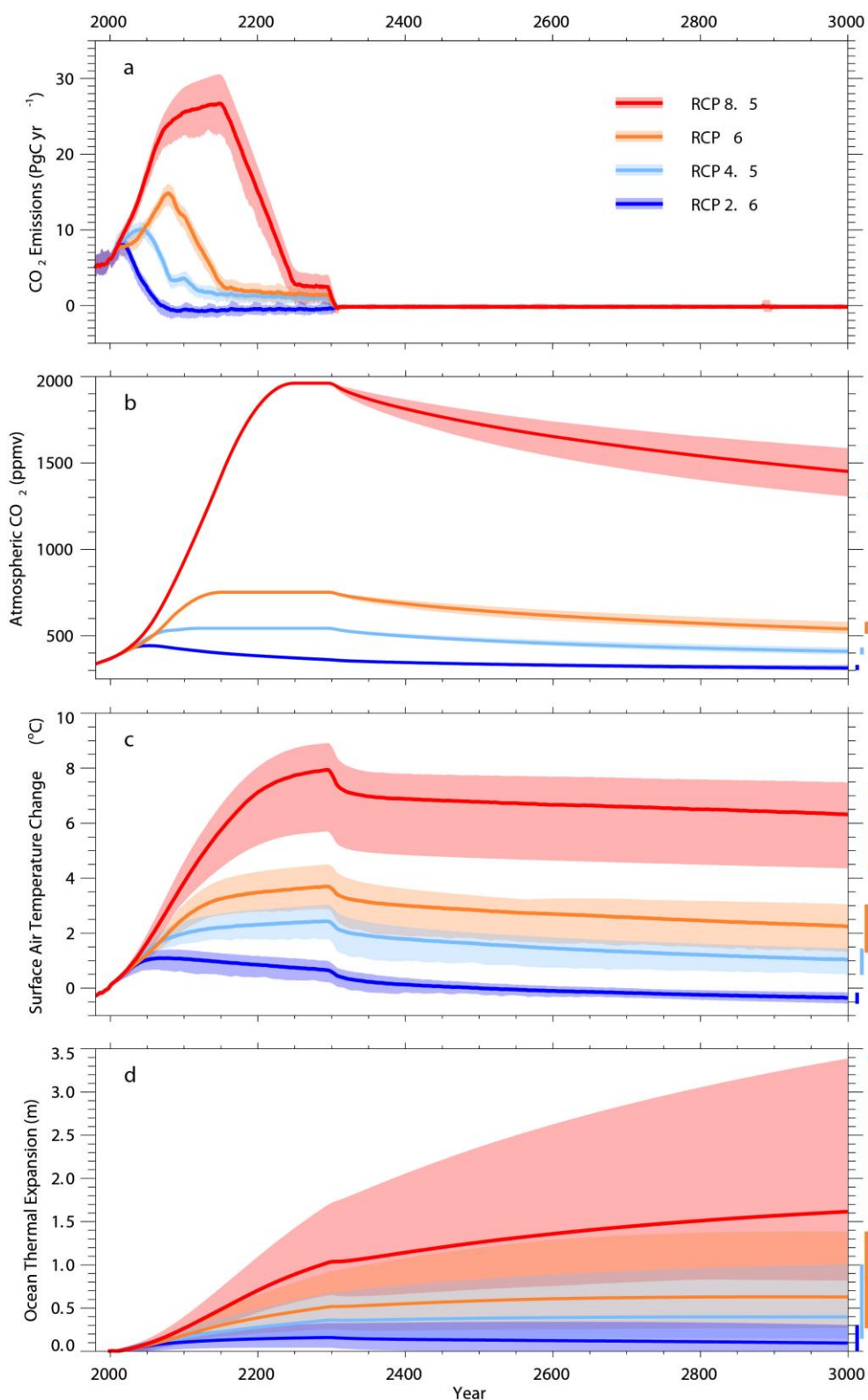


Figure 12.44: a) compatible anthropogenic CO₂ emissions, b) projected atmospheric CO₂ concentration, c) global mean surface temperature change and d) ocean thermal expansion, as simulated by six EMICs (Bern3D, DCESS, GENIE, IGSM, MESMO and UVic) for the four RCPs with all forcings included, assuming zero anthropogenic emissions after 2300 (Zickfeld et al., 2012). A 10-year smoothing was applied. The drop in temperature in 2300 is a result of eliminating short-lived forcings along with CO₂.

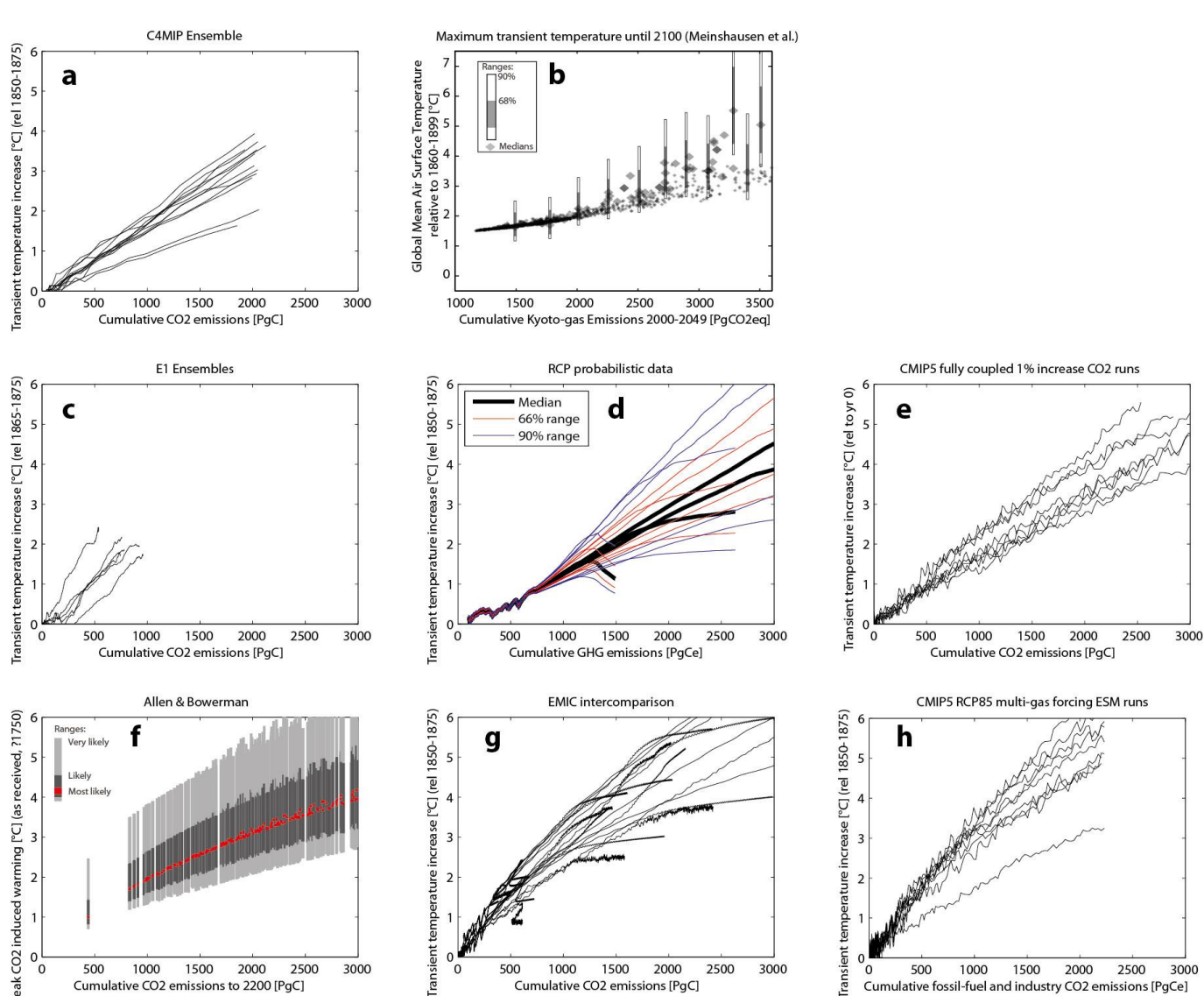
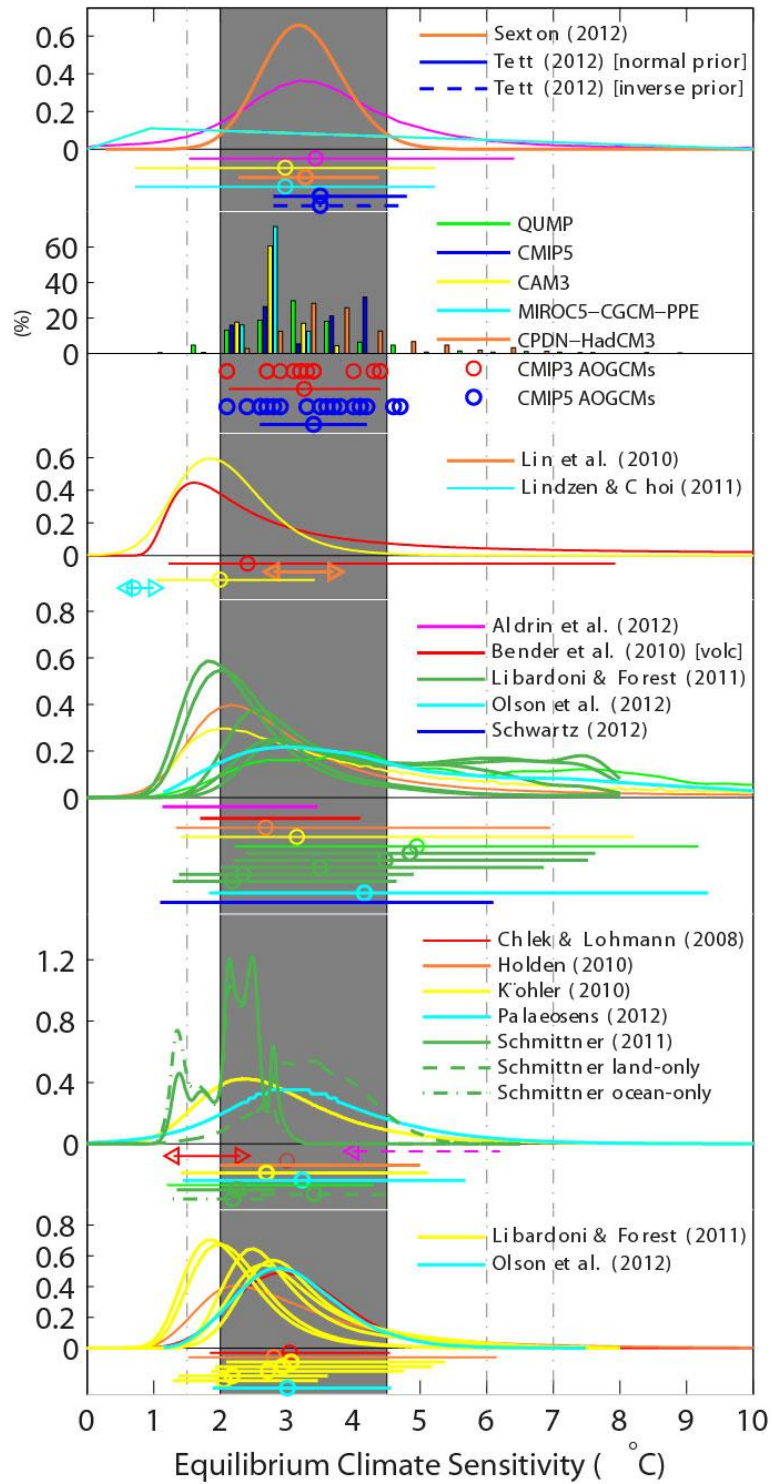
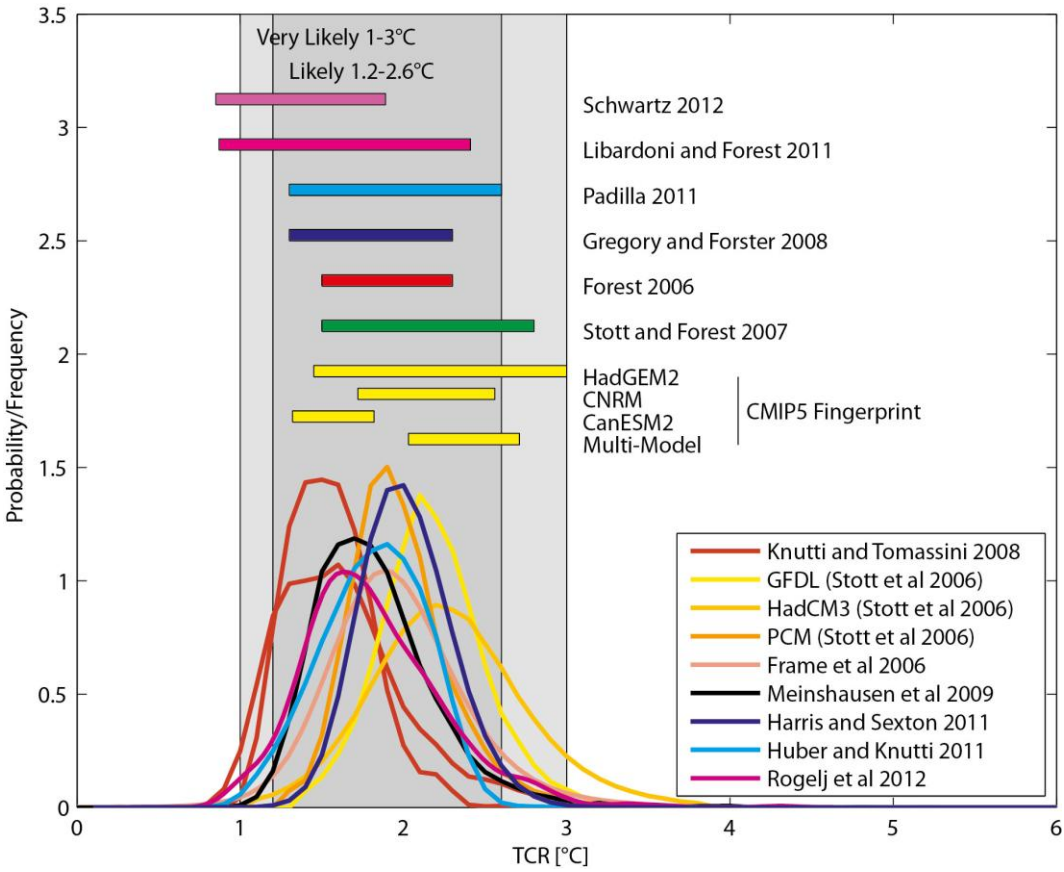


Figure 12.45: Global temperature change vs. cumulative emissions for different scenarios and models. a) Transient global temperature increase vs. cumulative carbon emissions for C⁴MIP (Matthews et al., 2009), b) maximum temperature increase until 2100 vs. cumulative Kyoto-gas emissions (CO₂ equivalent) (Meinshausen et al., 2009), c) as in panel a but for the ENSEMBLES E1 scenario (Johns et al., 2011), d) transient temperature increase for the RCP scenarios based on the MAGICC model constrained to C⁴MIP, observed warming, and the IPCC AR4 climate sensitivity range (Rogelj et al., 2012), e) transient temperature change from the CMIP5 1% yr⁻¹ simulations, f) peak CO₂ induced warming vs. cumulative CO₂ emissions to 2200 (Allen et al., 2009; Bowerman et al., 2011), g) transient temperature increase from the new EMIC simulations (Eby et al., 2012) and g) transient temperature change from the CMIP5 RCP8.5 simulations (note that warming is higher in this case due to other forcings).

1



Box 12.2, Figure 1: Probability density functions, distributions and ranges for equilibrium climate sensitivity, based on Figure 10.19b plus climatological constraints shown in IPCC AR4 Box 12.2 Figure 1. See Figure 10.19b for details.



Box 12.2, Figure 2: Probability density functions, distributions and ranges (5–95%) for the transient climate response from different studies. See Figure 10.19a for details.

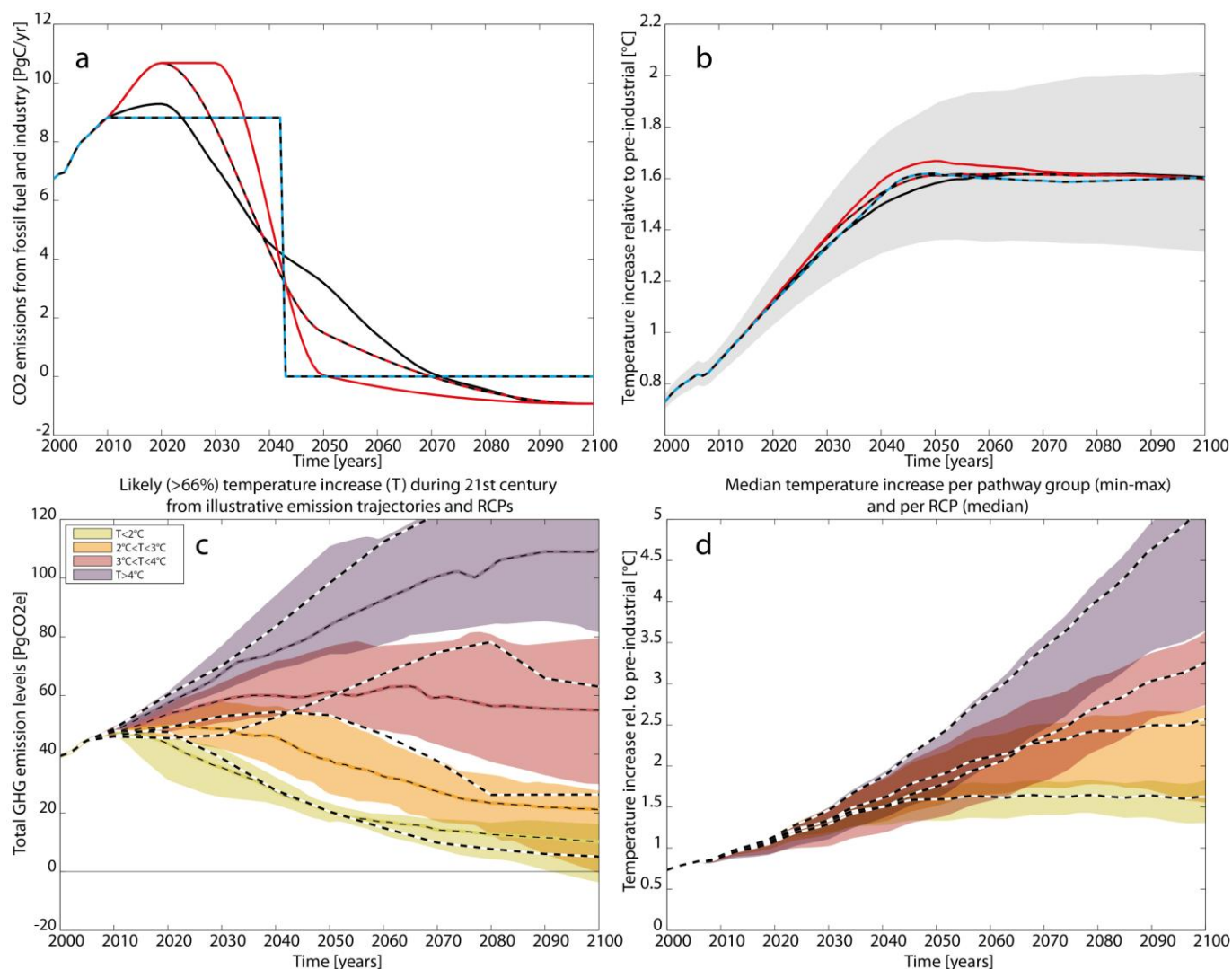
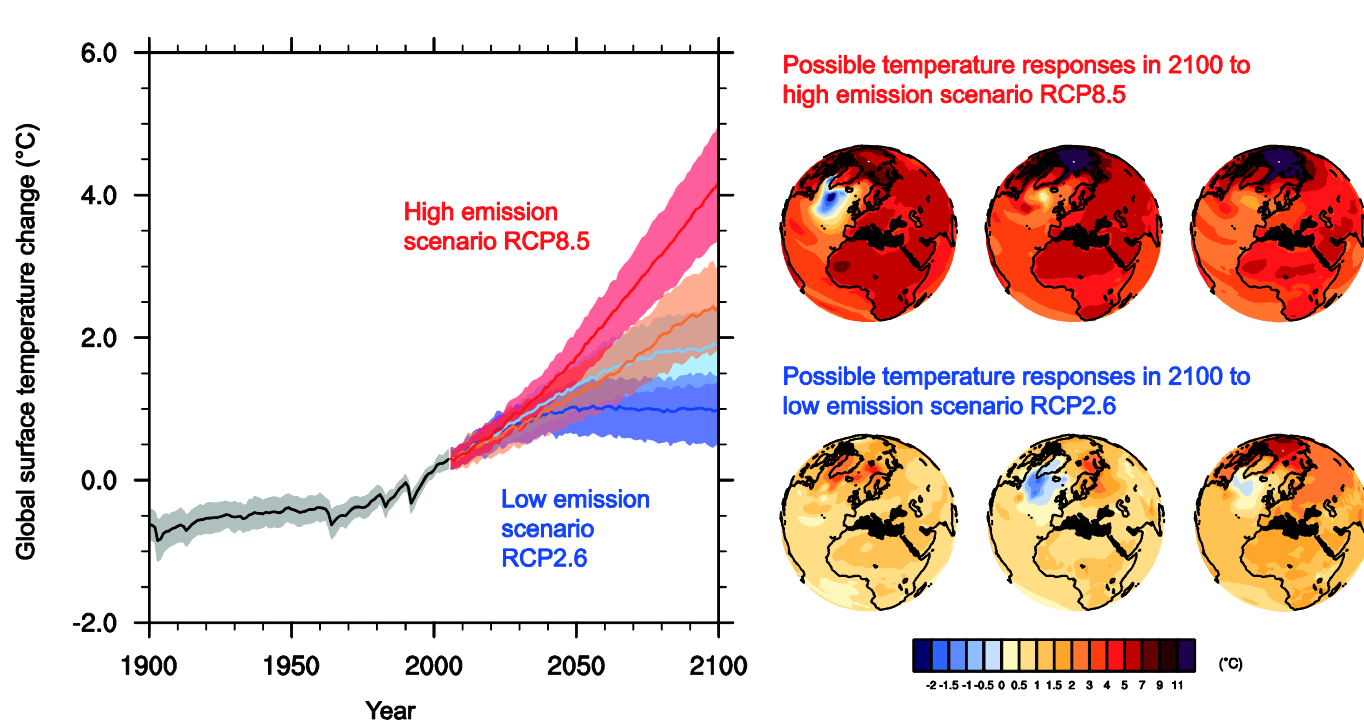
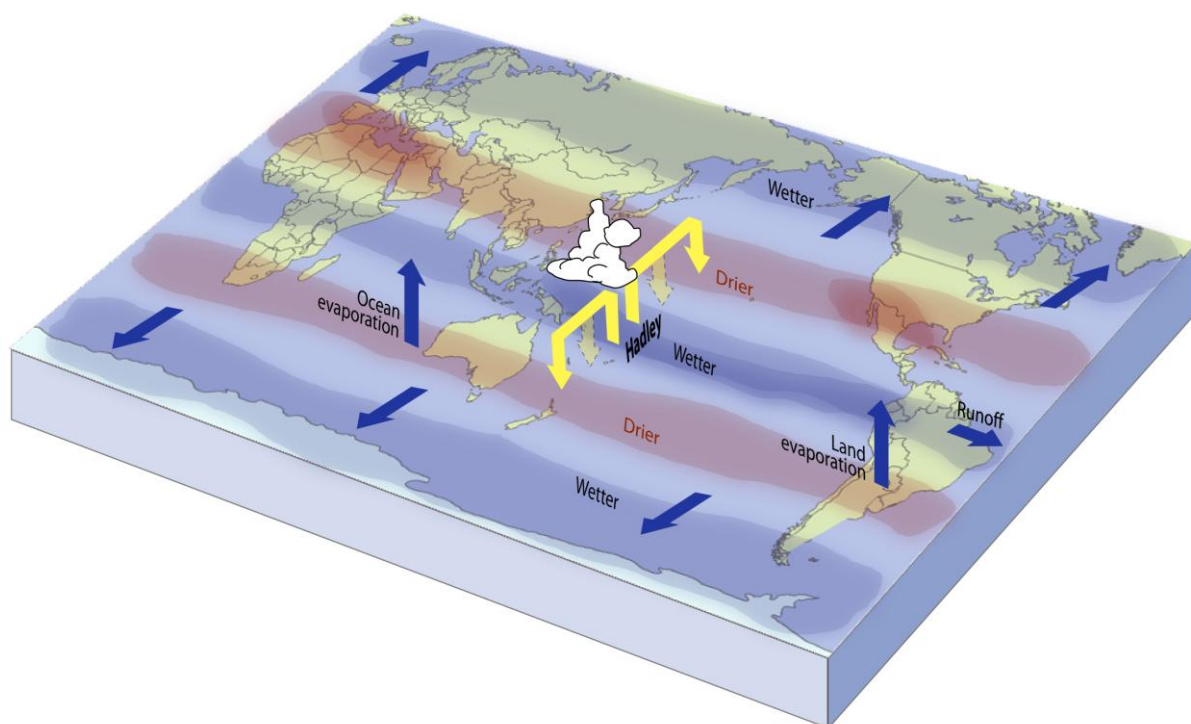


Figure 12.46: a) CO₂ emissions for the RCP3PD scenario (black) and three illustrative modified emission pathways leading to the same warming, b) global temperature change relative to preindustrial for the pathways shown in panel a. c) Coloured bands show IAM emission pathways over the twenty-first century. The pathways were grouped based on ranges of "likely" avoided temperature increase in the 21st century. Pathways in the yellow, orange and red bands likely stay below 2°C, 3°C, 4°C by 2100, respectively, while those in the purple band are higher than that. Emission corridors were defined by, at each year, identifying the 20th to 80th percentile range of emissions and drawing the corresponding coloured bands across the range. Individual scenarios that follow the upper edge of the bands early on tend to follow the lower edge of the band later on, d) global temperature relative to preindustrial for the pathways in panel a. Data in panels c,d based on Rogelj et al. (2011).



FAQ 12.1, Figure 1: Global mean temperature change (mean and one standard deviation, relative to 1986–2005) for the CMIP5 models, and the four RCP scenarios. For the highest (RCP8.5) and lowest (RCP2.6) scenario, illustrative maps of surface temperature change at the end of the 21st century (relative to 1986–2005) are shown for three CMIP5 models. These models are chosen to show a rather broad range of response, but this particular set is not representative of any measure of model response uncertainty.

1



2

3

4

5

6

7

8

9

10

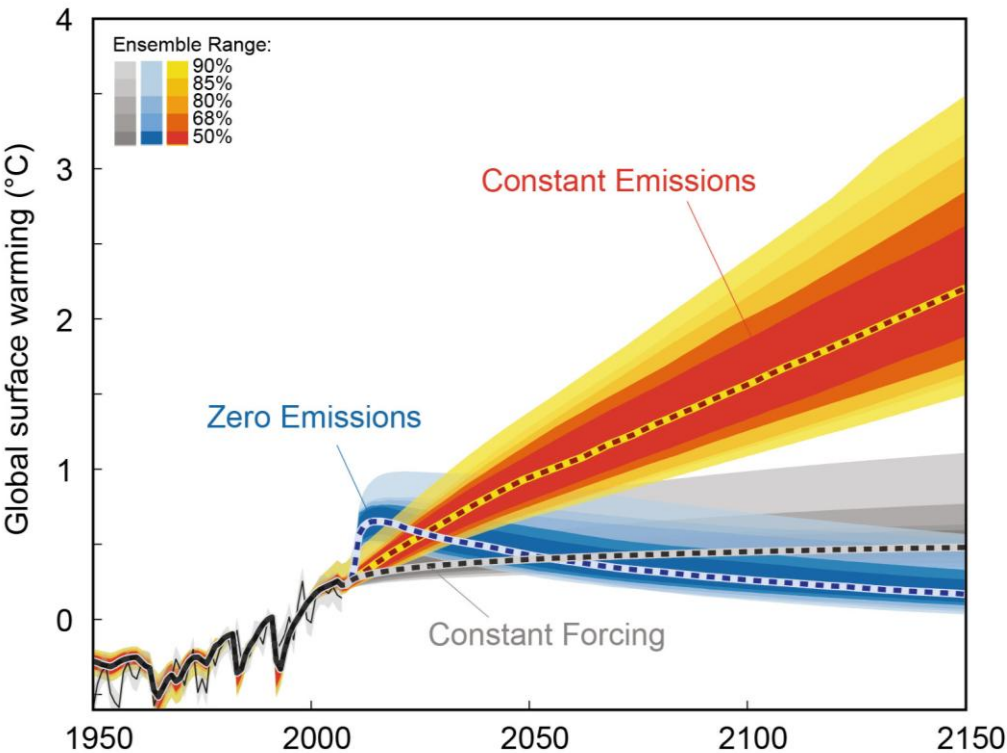
11

12

13

FAQ 12.2, Figure 1: Schematic diagram of projected changes in major components of the water cycle. The blue arrows indicate major types of water movement changes through the Earth's climate system: poleward water transport by extratropical winds, evaporation from the surface and runoff from the land to the oceans. The shaded regions denote areas more likely to become drier or wetter. Yellow arrows indicate an important atmospheric circulation change by the Hadley circulation, whose upward motion promotes tropical rainfall, while suppressing subtropical rainfall. Model projections indicate that the Hadley circulation will shift its downward branch poleward in both the Northern and Southern Hemispheres, with associated drying. Wetter conditions are projected at high latitudes, because a warmer atmosphere will allow greater precipitation, with greater movement of water into these regions.

1



FAQ 12.3, Figure 1: Projections based on the energy balance carbon cycle model MAGICC for constant atmospheric composition (constant forcing, grey), constant emissions (red) and zero future emissions (blue) starting in 2010, with estimates of uncertainty. Figure adapted from Hare and Meinshausen (2006) based on the MAGICC calibration to all CMIP3 and C⁴MIP models (Meinshausen et al., 2011a; Meinshausen et al., 2011c).